PopZ and FtsZ coordinate polar growth termination and cell division in *Agrobacterium tumefaciens*

A Dissertation

presented to

the Faculty of the Graduate School

at the University of Missouri-Columbia

In Partial Fulfillment

of the Requirements for the Degree

Doctor of Philosophy

---

by

Matthew Howell

July 2018

The undersigned, appointed by the dean of the Graduate School, have examined the thesis entitled

PopZ and FtsZ coordinate polar growth termination and cell division in *Agrobacterium tumefaciens*

presented by Matthew Howell,

a candidate for the degree of Doctor of Philosophy,

and hereby certify that, in their opinion, it is worthy of acceptance.

_____

Dr. Pamela Brown, Major Advisor

_____

Dr. Michael Calcutt

_____

Dr. Miriam Golomb

_____

Dr. Patrick Shiu

ACKNOWLEDGEMENTS

A big thank you is deserved to my wife, Lauren. You have been extremely understanding of my late night timepoints and weekend trips to the lab. Thank you for being so supportive through all the stressful times.

Thank you to my advisor, Dr. Pamela Brown for letting me be a part of your lab. Your mentorship has not only built my knowledge and lab techniques but has also given me confidence in so many areas like problem solving and leadership.

I also could not have gotten through grad school without my Brown Lab lab-mates. From troubleshooting protocols, to coffee runs; I'm positive my time as a grad student would not have been nearly as enjoyable without each one of you.

Thank you to my committee members Dr. Calcutt, Dr. Golomb, and Dr. Shiu. I've appreciated your support and different perspectives on my projects.

TABLE OF CONTENTS

LIST OF FIGURES

LIST OF TABLES

PopZ and FtsZ coordinate polar growth termination and cell division in *Agrobacterium tumefaciens*

Matthew Howell

Dr. Pamela Brown, Dissertation Advisor

Abstract

Understanding how bacterial cells expand their cell walls is an important question with relevance to development of antibiotics. While many studies have focused on the regulation of bacterial elongation utilizing lateral cell wall biogenesis, polar growth in bacteria is less well understood. Yet, polar growth has been observed across taxonomically diverse bacteria like Actinobacteria and the alphaproteobacterial clade Rhizobiales (Howell and Brown, 2016). Interestingly, polar-growing bacteria within Rhizobiales lack canonical scaffolding proteins for spatial and temporal regulation of peptidoglycan synthesis during elongation. Here, we dissect the role of two candidate scaffolding proteins in directing cell wall synthesis in the bacterial plant pathogen, *Agrobacterium tumefaciens*.

Since cell wall (peptidoglycan) biosynthesis during elongation and cell division is vital for bacterial survival, we expected many key proteins involved in these processes to be essential for cell survival. Thus, we developed a depletion system for *A. tumefaciens* (Figureroa-Cuilan et al. 2016). We further optimized a suite of target-specific fluorescent labeling techniques which allow us to visualize morphological changes during essential cell processes (Howell, Daniel, and Brown, 2017).

We use these techniques to dissect the contributions of PopZ and FtsZ to polar growth and cell division. Although PopZ is not required for polar growth, it is required for proper coordination of polar growth, chromosome segregation, and cell division. This PopZ-mediated coordination ensures that daughter cells are the proper size and contain a complete complement of genetic material (Howell et al 2017). Next, we find that FtsZ is required for both termination of polar growth and cell division. This finding suggests that FtsZ has at least two important functions in regulation of cell wall biogenesis. First, FtsZ enables cell wall biogenesis machinery to be released or inactivated from the growth pole. Second, FtsZ must recruit additional proteins to mid cell to assemble the divisome, enabling activation of cell wall biogenesis to promote septum formation and cell separation.

While further research is needed to understand how growth is targeted to the pole during elongation, our work provides mechanistic insights about the coordination of polar growth termination, chromosome segregation, and cell division. We hypothesize that our findings will be applicable to other closely related polar growing Rhizobiales, including plant, animal, and human pathogens.

List of Abbreviations:

4-64: N-(3-triethylammoniumpropyl) -4-(6-(4-(diethylamino) phenyl)hexatrienyl)pyridinium dibromide

D-Ala: D-alanine

DAPI: 4,6-diamidino-2-phenylindole

dH_2O: Distilled water

DIC: Differential interference contrast

DMSO: Dimethyl sulfoxide

DNA: Deoxyribonucleic acid

DTT: Dithiothreitol

EMCCD: Electron-multiplying charge-coupled-device

FDAA: Fluorescent D-amino acids

HADA: 7-hydroxycoumarin-3-carboxylic acid-3-amino-D-alanine

h: hours

IPTG: Isopropyl β-d-1-thiogalactopyranoside

KM: Kanamycin

M4: Monomeric muro-tetrapeptide

M5: Monomeric muro-pentapeptide

m-DAP: meso-diamino-pimelic acid

min: minutes

NADA: 4-chloro-7-nitrobenzofurazan-3-amino- D-alanine

OD_{600}: Optical density of the cells at 600 nm

PBPs: Penicillin-binding proteins

PBS: Phosphate buffered saline

PG: Peptidoglycan

PVDF: Polyvinylidene difluoride

SD: Standard deviation

TADA: Tetramethylrhodamine-3-amino-D-alanine

TBS: Tris buffered saline

TBST: Tris buffered saline, 1% tween 20

TRITC: Tetramethylrhodamine isothiocyanate

UPLC: Ultra performance liquid chromotography

UPP: Unipolar polysaccharide

UV: Ultraviolet

WGA-AF488: Wheat germ agglutinin lectin conjugated to AlexaFluor488

WT: wildtype

CHAPTER 1

Building the bacterial cell wall at the pole

Adapted from

Howell, M., & Brown, P. J. B.: Building the bacterial cell wall at the pole. *Curr Opin Microbiol*, 2016, 34:53-59.

Abstract

Polar growth is the predominant mode of cell wall extension in the Actinobacteria and the alphaproteobacterial clade Rhizobiales. The observation of polar elongation in taxonomically diverse bacteria suggests that polar growth may have evolved independently. Indeed, the regulatory mechanisms governing the assembly of cell wall biosynthesis machinery at the pole are distinct in the Actinobacteria and Rhizobiales. Here we highlight recent advances in our understanding of polar growth mechanisms in bacteria, with an emphasis on *Streptomyces* and *Agrobacterium.* This review illustrates that common themes are emerging in the regulation of polar growth in diverse bacteria. Emerging themes include the use of landmark proteins to direct growth to the pole and coordination of polar growth with cell-cycle progression.

Introduction

Across bacteria, an astonishing variety of morphologies have been observed. Bacterial cell shapes range from relatively simple (rods and spheres) to increasingly complex (vibrioid, helical, star-shaped, and branched). Over the last decade, understanding how and why bacteria generate such a diverse range of cell shapes has become an active area of research [1-3]. The bacterial cell wall or peptidoglycan (PG) is a heteropolymer of adjacent glycan strands crosslinked through peptide stems that is required to maintain proper cell shape. While PG is a key shape determinant, it is the precise targeting of cell wall biosynthesis machinery to specific locations that enables the observed myriad of bacterial cell shapes to be formed. Indeed, the use of fluorescent D-amino acids (FDAAs)

for high resolution imaging of patterns of cell wall biogenesis in diverse bacteria has confirmed the presence of many different growth patterns [4-8]. Although the biosynthetic machineries driving cell wall expansion are relatively well conserved among bacteria, the regulatory mechanisms that have allowed diverse growth patterns to emerge are only just beginning to be uncovered.

The regulation of cell wall growth is best-studied in rod-shaped bacteria. Many rod-shaped bacteria such as *Escherichia coli* and *Bacillus subtilis* elongate via insertion of new PG along the lateral sidewall [9,10]. This mode of growth requires precise spatial and temporal regulation of the elongasome, the complex of proteins responsible for PG biosynthesis during elongation. The bacterial actin homolog, MreB, is a major scaffolding protein that interacts with PG biosynthesis machinery and forms mobile patches that move perpendicularly to the long axis of the cell [11-13]. In *E. coli*, MreB promotes local PG insertion in regions of negative curvature, straightening the cell and maintaining the proper cell shape [14]. Remarkably, not all rod-shaped bacteria use an MreB-dependent, dispersed mode of growth for cell extension. Some rod-shaped, budding, and filamentous bacteria, particularly within the Actinomycetales and Rhizobiales, utilize polar elongation as an alternative growth strategy [15-17]. These clades of polar growing bacteria are of specific interest as they contain many symbionts and pathogens. Here, we will highlight recent advances in our understanding of the mechanisms that restrict PG synthesis to the pole during elongation, with an emphasis on *Streptomyces* and *Agrobacterium* species.

Spatial and temporal regulation of polar growth in *Streptomyces*

How is polar growth directed to the proper location?

In order for growth to be restricted to a specific subcellular location, the machinery responsible for PG biosynthesis must be precisely targeted to the pole. A common theme in targeting the PG machinery is the use of polymer-forming landmark proteins. Cytoplasmic polymer-forming landmark proteins self-assemble at a specific location in a cell-cycle dependent manner, enabling the PG biosynthesis to be synchronized with cell cycle progression [18].

The filamentous Actinobacterium, *Streptomyces coelicolor,* utilizes at least three polymer-forming proteins to guide growth at the pole. DivIVA may use negative curvature as a cue to self-assemble into short filaments and form a matrix to establish new growth poles where it recruits or activates PG biosynthetic machinery [19-21]. DivIVA also recruits the paralogous polymer-forming proteins, Scy and FliP, to the growth poles [22,23]. Scy colocalizes with DivIVA at both existing growth poles and sites of future growth pole formation [23]. Scy is proposed to sequester DivIVA, regulating the number of DivIVA foci and promoting the establishment of a limited number of new growth zones [23]. FilP is an intermediate filament-like protein that forms a crosslinked network of fibers and contributes to maintaining rigidity and elasticity of *S. coelicolor* hyphae [22,24]. During polar growth, FilP forms an apical gradient and is most concentrated at the growth pole, where it interacts with both DivIVA and Scy. The increased density of FilP at the cell pole provides a stress-bearing cytoskeletal network which likely compensates for the inherent weakness of the PG at the growth pole [22]. Together, DivIVA, Scy, and FilP form a tip organizing center or polarisome that directs

PG biosynthesis to existing hyphal tips and newly established polarity centers to enable branching (Figure 1.1A).

How are new branch sites selected?

During apical growth, *Streptomyces* cells exhibit a complex branching morphology. Remarkably, polarisome splitting is responsible for the formation of new polarity centers [25]. During elongation, the polarisome continues to remain associated with the growth pole; however, a daughter polarisome is left behind along the lateral hyphal wall and marks the future site of branch formation. The daughter polarisome must recruit additional proteins from the cytoplasm, presumably including Scy and FilP, and pass a critical size threshold before becoming competent to trigger PG biosynthesis and branch formation (Figure 1.1B-C).

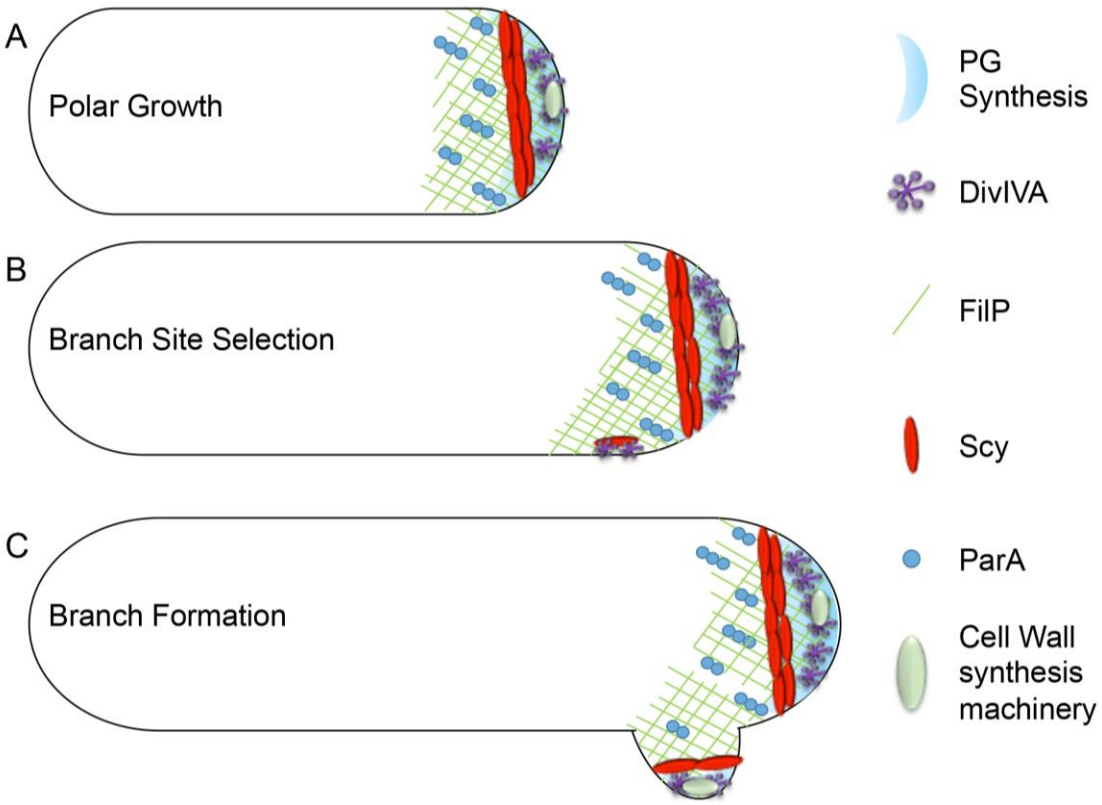

Figure 1.1. Polar growth of *Steptomyces*. A. During polar growth, PG synthesis is restricted to the growth pole. The growth pole is marked by the presence of the polarisome which is comprised of DivIVA, Scy, and FilP. The cell wall synthesis machinery is active at the growth pole. B. In order to initiate branching, the branch site is selected via the spiltting of the polarisome. The small focus of polarisome marks the future site of PG biosynthesis. C. The polarisome matures into a larger protein complex and recruits the cell wall machinery to the initiate branch formation.

Polar growth of *Agrobacterium tumefaciens*

Many species of Alphaproteobacteria, particularly within the clade Rhizobiales, lack both MreB and DivIVA, making it unclear how growth is spatially targeted. Blocking cell division in some of these bacteria results in branching or bulging phenotypes rather than smooth filaments, leading to the hypothesis that these bacteria may exhibit polar growth [26]. Indeed, studies using both amine-reactive dyes and FDAAs have confirmed that *Agrobacterium tumefaciens* and other members of the Rhizobiales elongate from the new pole [4,27,28]. The mechanisms underlying the spatial and temporal regulation of polar elongation in *Agrobacterium tumefaciens* remain relatively poorly resolved (Figure 1.2A); however, this is an exciting area of ongoing research.

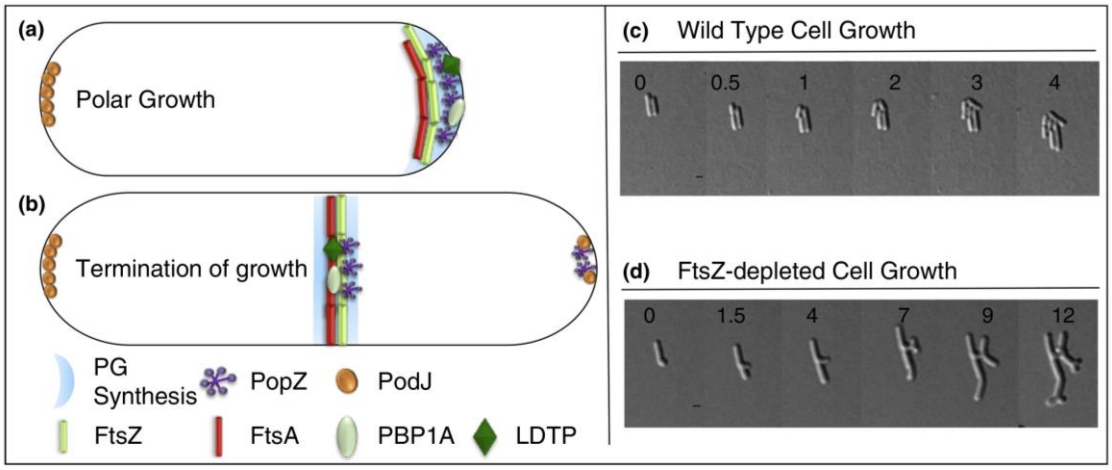

Figure 1.2. Polar growth of *Agrobacterium*. A. During polar growth, PG synthesis is restricted to the growth pole. The growth pole is marked by the presence of a number of polymer-forming proteins including PopZ, FtsA, and FtsZ. The PG biosynthesis machinery is present at the growth pole and likely includes PBP1 and LD-transpeptidases. B. During the termination of polar growth, PodJ appears at the pole and likely functions to release PopZ from the pole. FtsZ, FtsA, and PG synthesis machinery relocate to the mid-cell as part of the transition from polar growth to cell division. C. Time-lapse microscopy of wildtype cells illustrates polar growth and typical cell division. Times of image acquisition are shown in hours on each image. D. Time-lapse microscopy of FtsZ-depleted cells reveals a role for FtsZ in both cell division and the termination of polar growth. When polar growth does not terminate, tip splitting behavior leads to the accumulation of growth poles. Depletion time in hours is shown on each image.

Does A. tumefaciens use a landmark protein to coordinate polar growth?

In order to insert newly synthesized PG at the growth pole, the PG biosynthesis machinery must be targeted to the new cell pole, suggesting the presence of a polarisome-like complex. While the putative polarisome has not yet been defined, localization studies have revealed a number of attractive candidate proteins (Figure 1.2A), including PopZ [29]. *A. tumefaciens* PopZ ($PopZ_{AT}$) shares homology with the well characterized PopZ from *Caulobacter crescentus* ($PopZ_{CC}$). $PopZ_{CC}$ is a polymer forming protein that exhibits a dynamic localization pattern and has key functions in both cell-cycle progression and chromosome segregation [30-34]. In contrast to the unipolar-to-bipolar localization of $PopZ_{CC}$, $PopZ_{AT}$ exclusively marks the growth pole [29]. $PopZ_{AT}$ localizes to the growth pole during elongation and reappears at new growth poles immediately following cell division. The localization pattern of $PopZ_{AT}$ and its sequence similarity to $PopZ_{CC}$ make PopZ an intriguing candidate landmark protein to coordinate polar growth and chromosome segregation in *A. tumefaciens*.

Since *A. tumefaciens* lacks canonical elongation machinery and the growth poles originate from the site of cell division, it has been suggested that cell division machinery may function to regulate polar elongation [28,35]. Remarkably, canonical cell division proteins, FtsZ and FtsA, persist at the growth pole for at least a portion of the cell cycle [16,29,35,36] and are predicted to form polymers suggesting that they may serve as bacterial scaffolds at the growth pole. The recent development of a depletion system for *A. tumefaciens* [37] will open the door for characterizing the role of these proteins in polar growth, cell division, or cell-cycle progression. Here, we show that depletion of FtsZ triggers multipolar growth and tip splitting (Figure 1.2B-C) suggesting that FtsZ is

required not only for cell division but also for the termination of polar growth, highlighting the coordination of polar growth and cell division in *A. tumefaciens*.

Another non-polymer forming landmark protein, PodJ, plays an important role in coordination of polar growth with cell cycle progression [29,38]. PodJ has a complex localization pattern initially marking the old pole and later associating with both poles [29]. The arrival of PodJ at the new pole just before cessation of polar growth makes PodJ an attractive candidate to regulate polar growth. Deletion of PodJ results in multiple morphological defects such as elongated cells, branching, multiple constrictions, bent, and small rounded cells [38]. This phenotype suggests that PodJ is not strictly required for polar growth; however, PodJ may have a direct or indirect role in the transition of the growth pole into a non-growing old pole.

Concluding remarks

While many mechanistic insights remain to be uncovered, it is clear that *Streptomyces* and *Agrobacterium* have evolved distinct mechanisms to drive polar growth. Yet, a number of common themes are emerging among these phylogenetically distant polar-growing bacteria including the use of landmark proteins, tip splitting behavior, and coordination of growth with cell cycle progression. Ongoing and future studies of PG biosynthesis and its regulation in polar growing bacteria will provide insights into a number of outstanding questions.

Is polar growth polar? While many proteins involved in the regulation of polar growth are present at the cell pole, the precise regions of PG insertion have not been well defined in most polar growing bacteria. The combination of metabolic labeling of cell

surface components and super-resolution microscopy is beginning to reveal the sites of PG insertion at higher resolution [6]. This approach revealed that polar DivIVA directs subpolar PG insertion in mycobacteria [39]. Future research should determine if subpolar growth is common among the Actinobacteria or even more distant polar growing bacteria.

Is the growth machinery conserved? The PG composition of polar growing bacteria is distinctive. Both Actinomycetales and Rhizobiales PG are highly crosslinked and enriched in muropeptides containing 3-3 crosslinks [27,40-42] suggesting a potential role for DD-carboxypeptidases and LD-transpeptidases (Figure 1.3). While 3-3 crosslinks are typically found in PG from diverse bacteria, the abundance of muropeptides containing 3-3 crosslinks is much higher in polar growing bacteria. For example, in *E. coli* PG, ~25% of the total muropeptides are crosslinked; however only ~1-5% of crosslinked muropeptides contain 3-3 crosslinks [43]. In contrast ~64% of the muropeptides from *A. tumefaciens* PG are crosslinked and 4-3 and 3-3 crosslinks are equally abundant [27]. During stationary phase, *Mycobacterium* PG is highly crosslinked (~65% of total muropeptides) and 3-3 crosslinks are highly abundant (70-80%)[41,42]. Loss of LD-transpeptidases in mycobacteria results in altered morphology [44,45] and at least one LD-transpeptidases localizes to the growth pole in *A. tumefaciens* [28]. Thus, it is intriguing to speculate that polar growing bacteria may use accessory enzymes including LD-transpeptidases as key components of the polar PG biosynthesis machinery.

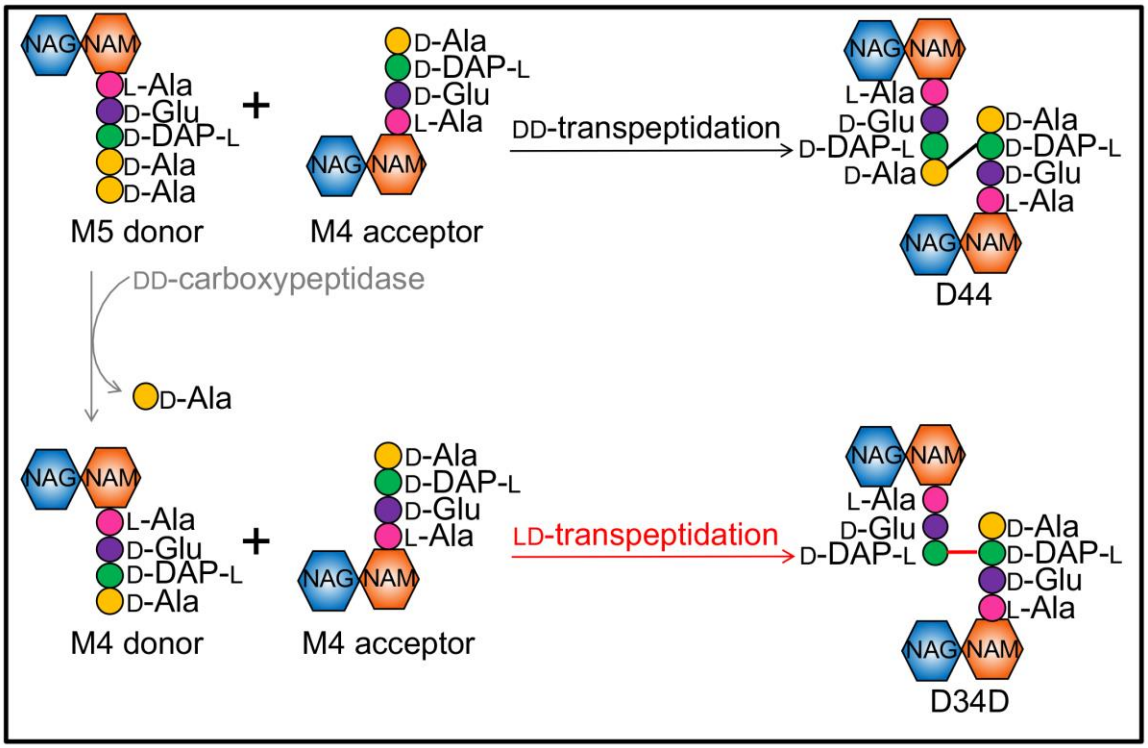

Figure 1.3. Representative PG crosslinking reactions catalyzed by DD- and LD-transpeptidases. Representative reactions were selected because D44 and D34D are the most abundant muropeptide dimers in *A. tumefaciens* PG [27]. PG is crosslinked through peptide stems to connect adjacent glycan strands and provide a mesh-like architecture. Most bacteria utilize the DD-transpeptidase activity associated with penicillin binding proteins to link glycan strands. In Gram negative bacteria, DD-transpeptidases link D-alanine (D-Ala) in position 4 of the peptide stem to the free amino group at the D-center of meso-diamino-pimelic acid (mDAP) at position 3 of the peptide stem, forming a characteristic 4-3 crosslink (black bar). The representative reaction illustrates the linkage of a monomeric muro-pentapeptide (M5) donor and a monomeric muro-tetrapeptide (M4) acceptor to generate a dimeric muropeptide containing a DD-DAla-mDAP crosslink (D44). In contrast, LD-transpeptidases link the carbonyl group at the L-center of mDAP at

position 3 to the amino group at the D-center of mDAP in an adjacent peptide stem to generate 3-3 crosslinks (red bar). The representative reaction illustrates the linkage of a monomeric muro-tetrapeptide (M4) donor and a monomeric muro-tetrapeptide (M4) acceptor to generate a dimeric muropeptide containing a LD-mDAP-mDAP crosslink (D34D). DD-carboxypeptidases are responsible for the conversion of monomeric muro-pentatpeptides (M5) to monomeric muro-tetrapeptides (M4), which are the substrate for LD-transpeptidases. Muropeptide naming conventions were taken from Brown et al [36].

What is the advantage of polar growth? Polar growth and subsequent cell division generates phenotypic variation which can increase fitness in unstable environments [17]. For example, differences in polar growth rates in *Mycobacterium* give rise to a heterogeneous population in which the slowest-growing bacteria exhibit increased resistance to antibiotics [46,47]. In *Agrobacterium*, FDAA labeling experiments show that the area of labeling increases with cell length [28], hinting that the elongation rate may be variable at the population level.

In the following chapters we optimize techniques to thoroughly dissect the spatial and temporal regulation of peptidoglycan synthesis using *A. tumefaciens* as a model for polar growth. First, we show that while not required for polar growth, PopZ plays a key role coordinating chromosome segregation with cell division. Furthermore, we demonstrate that the transition from elongation to cell division occurs in two distinct steps. First, polar elongation must be terminated in an FtsZ dependent manner. Once elongation is terminated and the divisome assembles at mid-cell, there is a divisome activation period required to begin constriction. We hypothesize that many of the mechanisms elucidated in *A. tumefaciens* will be utilized by closely related polar growing species within Rhizobiales.

While the potential advantages of polar growth remain to be elucidated, it is clear that distantly related bacteria have converged on a similar growth pattern. Future studies on diverse bacteria are needed to provide key insights into both unique and conserved mechanisms underpinning polar growth.

References

1. Randich AM, Brun YV: Molecular mechanisms for the evolution of bacterial morphologies and growth modes. *Front Microbiol* 2015, 6:580.
2. Yang DC, Blair KM, Salama NR: Staying in shape: the impact of cell shape on bacterial survival in diverse environments. *Microbiol Mol Biol Rev* 2016, 80:187-203.
3. Young KD: The selective value of bacterial shape. *Microbiol Mol Biol Rev* 2006, 70:660-703.
4. Kuru E, Hughes HV, Brown PJ, Hall E, Tekkam S, Cava F, de Pedro MA, Brun YV, VanNieuwenhze MS: In Situ probing of newly synthesized peptidoglycan in live bacteria with fluorescent D-amino acids. *Angew Chem Int Ed Engl* 2012, 51:12519-12523.
5. Kuru E, Tekkam S, Hall E, Brun YV, Van Nieuwenhze MS: Synthesis of fluorescent D-amino acids and their use for probing peptidoglycan synthesis and bacterial growth in situ. *Nat Protoc* 2015, 10:33-52.
6. Siegrist MS, Swarts BM, Fox DM, Lim SA, Bertozzi CR: Illumination of growth, division and secretion by metabolic labeling of the bacterial cell surface. *FEMS Microbiol Rev* 2015, 39:184-202.
7. Siegrist MS, Whiteside S, Jewett JC, Aditham A, Cava F, Bertozzi CR: (D)-Amino acid chemical reporters reveal peptidoglycan dynamics of an intracellular pathogen. *ACS Chem Biol* 2013, 8:500-505.
8. Cava F, Kuru E, Brun YV, de Pedro MA: Modes of cell wall growth differentiation in rod-shaped bacteria. *Curr Opin Microbiol* 2013, 16:731-737.

9. Daniel RA, Errington J: Control of cell morphogenesis in bacteria: two distinct ways to make a rod-shaped cell. *Cell* 2003, 113:767-776.

10. de Pedro MA, Quintela JC, Holtje JV, Schwarz H: Murein segregation in *Escherichia coli*. *J Bacteriol* 1997, 179:2823-2834.

11. Dominguez-Escobar J, Chastanet A, Crevenna AH, Fromion V, Wedlich-Soldner R, Carballido-Lopez R: Processive movement of MreB-associated cell wall biosynthetic complexes in bacteria. *Science* 2011, 333:225-228.

12. Garner EC, Bernard R, Wang W, Zhuang X, Rudner DZ, Mitchison T: Coupled, circumferential motions of the cell wall synthesis machinery and MreB filaments in *B. subtilis*. *Science* 2011, 333:222-225.

13. van Teeffelen S, Wang S, Furchtgott L, Huang KC, Wingreen NS, Shaevitz JW, Gitai Z: The bacterial actin MreB rotates, and rotation depends on cell-wall assembly. *Proc Natl Acad Sci U S A* 2011, 108:15822-15827.

14. Ursell TS, Nguyen J, Monds RD, Colavin A, Billings G, Ouzounov N, Gitai Z, Shaevitz JW, Huang KC: Rod-like bacterial shape is maintained by feedback between cell curvature and cytoskeletal localization. *Proc Natl Acad Sci U S A* 2014, 111:E1025-1034.

15. Brown PJ, Kysela DT, Brun YV: Polarity and the diversity of growth mechanisms in bacteria. *Semin Cell Dev Biol* 2011, 22:790-798.

16. Cameron TA, Zupan JR, Zambryski PC: The essential features and modes of bacterial polar growth. *Trends Microbiol* 2015, 23:347-353.

17. Kysela DT, Brown PJ, Huang KC, Brun YV: Biological consequences and advantages of asymmetric bacterial growth. *Annu Rev Microbiol* 2013, 67:417-435.

18. Treuner-Lange A, Sogaard-Andersen L: Regulation of cell polarity in bacteria. *J Cell Biol* 2014, 206:7-17.

19. Flardh K, Richards DM, Hempel AM, Howard M, Buttner MJ: Regulation of apical growth and hyphal branching in *Streptomyces*. *Curr Opin Microbiol* 2012, 15:737-743.

20. Wang SB, Cantlay S, Nordberg N, Letek M, Gil JA, Flardh K: Domains involved in the *in vivo* function and oligomerization of apical growth determinant DivIVA in *Streptomyces coelicolor*. *FEMS Microbiol Lett* 2009, 297:101-109.

21. Hempel AM, Wang SB, Letek M, Gil JA, Flardh K: Assemblies of DivIVA mark sites for hyphal branching and can establish new zones of cell wall growth in *Streptomyces coelicolor*. *J Bacteriol* 2008, 190:7579-7583.

22. Fuchino K, Bagchi S, Cantlay S, Sandblad L, Wu D, Bergman J, Kamali-Moghaddam M, Flardh K, Ausmees N: Dynamic gradients of an intermediate filament-like cytoskeleton are recruited by a polarity landmark during apical growth. *Proc Natl Acad Sci U S A* 2013, 110:E1889-1897.

23. Holmes NA, Walshaw J, Leggett RM, Thibessard A, Dalton KA, Gillespie MD, Hemmings AM, Gust B, Kelemen GH: Coiled-coil protein Scy is a key component of a multiprotein assembly controlling polarized growth in *Streptomyces*. *Proc Natl Acad Sci U S A* 2013, 110:E397-406.

24. Bagchi S, Tomenius H, Belova LM, Ausmees N: Intermediate filament-like proteins in bacteria and a cytoskeletal function in *Streptomyces*. *Mol Microbiol* 2008, 70:1037-1050.

25. Richards DM, Hempel AM, Flardh K, Buttner MJ, Howard M: Mechanistic basis of branch-site selection in filamentous bacteria. *PLoS Comput Biol* 2012, 8:e1002423.

26. Margolin W: Sculpting the bacterial cell. *Curr Biol* 2009, 19:R812-822.

27. Brown PJ, de Pedro MA, Kysela DT, Van der Henst C, Kim J, De Bolle X, Fuqua C, Brun YV: Polar growth in the Alphaproteobacterial order Rhizobiales. *Proc Natl Acad Sci U S A* 2012, 109:1697-1701.

28. Cameron TA, Anderson-Furgeson J, Zupan JR, Zik JJ, Zambryski PC: Peptidoglycan synthesis machinery in *Agrobacterium tumefaciens* during unipolar growth and cell division. *MBio* 2014, 5:e01219-01214.

29. Grangeon R, Zupan JR, Anderson-Furgeson J, Zambryski PC: PopZ identifies the new pole, and PodJ identifies the old pole during polar growth in *Agrobacterium tumefaciens*. *Proc Natl Acad Sci U S A* 2015, 112:11666-11671.

30. Bowman GR, Comolli LR, Gaietta GM, Fero M, Hong SH, Jones Y, Lee JH, Downing KH, Ellisman MH, McAdams HH, et al.: *Caulobacter* PopZ forms a polar subdomain dictating sequential changes in pole composition and function. *Mol Microbiol* 2010, 76:173-189.

31. Bowman GR, Comolli LR, Zhu J, Eckart M, Koenig M, Downing KH, Moerner WE, Earnest T, Shapiro L: A polymeric protein anchors the chromosomal origin/ParB complex at a bacterial cell pole. *Cell* 2008, 134:945-955.

32. Ebersbach G, Briegel A, Jensen GJ, Jacobs-Wagner C: A self-associating protein critical for chromosome attachment, division, and polar organization in *Caulobacter*. *Cell* 2008, 134:956-968.

33. Laloux G, Jacobs-Wagner C: Spatiotemporal control of PopZ localization through cell cycle-coupled multimerization. *J Cell Biol* 2013, 201:827-841.

34. Ptacin JL, Gahlmann A, Bowman GR, Perez AM, von Diezmann AR, Eckart MR, Moerner WE, Shapiro L: Bacterial scaffold directs pole-specific centromere segregation. *Proc Natl Acad Sci U S A* 2014, 111:E2046-2055.

35. Zupan JR, Cameron TA, Anderson-Furgeson J, Zambryski PC: Dynamic FtsA and FtsZ localization and outer membrane alterations during polar growth and cell division in *Agrobacterium tumefaciens*. *Proc Natl Acad Sci U S A* 2013, 110:9060-9065.

36. Ma X, Sun Q, Wang R, Singh G, Jonietz EL, Margolin W: Interactions between heterologous FtsA and FtsZ proteins at the FtsZ ring. *J Bacteriol* 1997, 179:6788-6797.

37. Figueroa-Cuilan W, Daniel JJ, Howell M, Sulaiman A, Brown PJ: Mini-Tn*7* insertion in an artificial *att*Tn*7* site enables depletion of the essential master regulator CtrA in the phytopathogen *Agrobacterium tumefaciens*. *Appl Environ Microbiol* 2016, 82:5015-5025.

38. Anderson-Furgeson JC, Zupan JR, Grangeon R, Zambryski PC: Loss of PodJ in *Agrobacterium tumefaciens* leads to ectopic polar growth, branching, and reduced cell division. *J Bacteriol* 2016, 198:1883-1891.

39. Meniche X, Otten R, Siegrist MS, Baer CE, Murphy KC, Bertozzi CR, Sassetti CM: Subpolar addition of new cell wall is directed by DivIVA in mycobacteria. *Proc Natl Acad Sci U S A* 2014, 111:E3243-3251.

40. Lavollay M, Arthur M, Fourgeaud M, Dubost L, Marie A, Riegel P, Gutmann L, Mainardi JL: The beta-lactam-sensitive D,D-carboxypeptidase activity of Pbp4 controls the L,D and D,D transpeptidation pathways in *Corynebacterium jeikeium*. *Mol Microbiol* 2009, 74:650-661.

41. Lavollay M, Arthur M, Fourgeaud M, Dubost L, Marie A, Veziris N, Blanot D, Gutmann L, Mainardi JL: The peptidoglycan of stationary-phase *Mycobacterium tuberculosis* predominantly contains cross-links generated by L,D-transpeptidation. *J Bacteriol* 2008, 190:4360-4366.

42. Lavollay M, Fourgeaud M, Herrmann JL, Dubost L, Marie A, Gutmann L, Arthur M, Mainardi JL: The peptidoglycan of *Mycobacterium abscessus* is predominantly cross-linked by L,D-transpeptidases. *J Bacteriol* 2011, 193:778-782.

43. Glauner B, Holtje JV, Schwarz U: The composition of the murein of *Escherichia coli*. *J Biol Chem* 1988, 263:10088-10095.

44. Gupta R, Lavollay M, Mainardi JL, Arthur M, Bishai WR, Lamichhane G: The *Mycobacterium tuberculosis* protein LdtMt2 is a nonclassical transpeptidase required for virulence and resistance to amoxicillin. *Nat Med* 2010, 16:466-469.

45. Schoonmaker MK, Bishai WR, Lamichhane G: Nonclassical transpeptidases of *Mycobacterium tuberculosis* alter cell size, morphology, the cytosolic matrix, protein localization, virulence, and resistance to beta-lactams. *J Bacteriol* 2014, 196:1394-1402.

46. Aldridge BB, Fernandez-Suarez M, Heller D, Ambravaneswaran V, Irimia D, Toner M, Fortune SM: Asymmetry and aging of mycobacterial cells lead to variable growth and antibiotic susceptibility. *Science* 2012, 335:100-104.

47. Singh B, Nitharwal RG, Ramesh M, Pettersson BM, Kirsebom LA, Dasgupta S: Asymmetric growth and division in *Mycobacterium spp*.: compensatory mechanisms for non-medial septa. *Mol Microbiol* 2013, 88:64-76.

CHAPTER 2

Live cell fluorescence microscopy to observe essential processes during microbial cell growth

Adapted from:

Howell, M., Daniel, J. J., & Brown, P. J. B.: Live cell fluorescence microscopy to observe essential processes during microbial cell growth. *J Vis Exp* 2017, 129.

ABSTRACT

Core cellular processes such as DNA replication and segregation, protein synthesis, cell wall biosynthesis, and cell division rely on the function of proteins that are essential for bacterial survival. A series of target-specific dyes can be used as probes to better understand these processes. Staining with lipophilic dyes enables the observation of membrane structure, visualization of lipid microdomains, and detection of membrane blebs. Use of fluorescent-D-amino acids (FDAAs) to probe the sites of peptidoglycan biosynthesis can indicate potential defects in cell wall biogenesis or cell growth patterning. Finally, nucleic acid stains can indicate possible defects in DNA replication or chromosome segregation. Cyanine DNA stains label living cells and are suitable for time-lapse microscopy enabling real-time observations of nucleoid morphology during cell growth. Protocols for cell labeling can be applied to protein depletion mutants to identify defects in membrane structure, cell wall biogenesis, or chromosome segregation. Furthermore, time-lapse microscopy can be used to monitor morphological changes as an essential protein is removed and can provide additional insights into protein function. For example, the depletion of essential cell division proteins results in filamentation or branching, whereas the depletion of cell growth proteins may cause cells to become shorter or rounder. Here, protocols for cell growth, target-specific labeling, and time-lapse microscopy are provided for the bacterial plant pathogen *Agrobacterium tumefaciens*. Together, target-specific dyes and time-lapse microscopy enable characterization of essential processes in *A. tumefaciens.* Finally, the protocols provided can be readily modified to probe essential processes in other bacteria.

INTRODUCTION:

Progression through the bacterial cell cycle requires the coordination of many processes, including membrane and cell wall biosynthesis, DNA replication and segregation, and cell division. To fully understand the complexity of bacterial cell biology, it is necessary to study these essential events; however, this is a non-trivial task since cell viability is compromised when key components of these pathways are mutagenized. Epifluorescence microscopy coupled with target-specific dyes is a powerful approach to probe these essential processes in wildtype and mutant bacterial strains.

Peptidoglycan-specific dyes include fluorescent antibiotics (vancomycin-FL, bocillin-FL) and fluorescent-D-amino acids (for example, 7-hydroxycoumarin-3-carboxylic acid-3-amino-D-alanine, HADA; 4-chloro-7-nitrobenzofurazan-3-amino- D-alanine, NADA; tetramethylrhodamine-3-amino-D-alanine; TADA). In Gram-positive bacteria, the use of sublethal concentrations of fluorescent antibiotic analogs to probe sites of peptidoglycan biosynthesis has been an effective strategy to reveal peptidoglycan insertion patterns [1-4]. While fluorescent vancomycin labeling has been used to gain insights into the peptidoglycan insertion patterns in fixed Gram-negative bacteria [5], the outer membrane generally provides a permeability barrier that prevents the use of fluorescent antibiotics as a probe for peptidoglycan biosynthesis in live cells. In contrast, short pulses of fluorescent-D-amino acids or D-amino acids with biorthogonal functional groups covalently label regions of recent peptidoglycan insertion in a wide range of living bacterial cells [6,7]. Patterns of peptidoglycan insertion that have been observed with

synthetic D-amino acids include punctate and septal (*Escherichia coli* and *Bacillus subtilis*), polar and septal (*Agrobacterium tumefaciens* and *Listeria monocytogenes*), septal only (*Staphylococcus aureus),* and apical (*Streptomyces venezuelae)* [6,7]. These observations indicate that bacteria exhibit diverse patterns of cell wall biogenesis and that the use of synthetic D-amino acids as probes for examining growth patterning is a valuable strategy in many bacteria.

Dyes that label bacterial chromosomes include the deoxyribonucleic acid (DNA) specific minor groove binder (4,6-diamidino-2-phenylindole; DAPI) and high affinity cyanine dyes (Green and Orange; see Table 2.1). DAPI staining of fixed cells assists in enumeration of bacteria from environmental samples [8], whereas DAPI staining of live cells is used to indicate bacterial viability [9]. In contrast, cyanine dyes such as Orange and Green are frequently described as membrane impermeant "dead" cell stains to enumerate non-viable cells[9]. Remarkably, when these reagents are used to probe the morphology of the bacterial nucleoid during cell growth, DAPI, Orange, and Green were all shown to be membrane permeant and capable of labeling live cells [10]. In live *E. coli* cells, DAPI staining of DNA appears diffuse due to auto-fluorescence from the cytoplasm and repeated exposures of DAPI-stained cells to ultraviolet (UV) light perturbs the nucleoid structure [10]. Staining *E. coli* or *B. subtilis* with Orange reveals that this dye is membrane permeant and provides long-lasting fluorescence upon binding to DNA in live cells without impacting cell growth, DNA replication, or chromosome segregation [10]. These observations suggest that cyanine DNA dyes can be used to monitor the morphology of nucleoids during cell growth in many bacteria.

Phospholipid-specific stryl dyes such as N-(3-triethylammoniumpropyl) -4-(6-(4-(diethylamino) phenyl)hexatrienyl)pyridinium dibromide (4-64; see Table 2.1) are cationic compounds and associate preferentially with negatively charged phospholipids such as cardiolipin and phosphatidylglycerol [11]. Distinct patterns are observed when 4-64 is used to label the membrane of different bacteria. In *Escherichia coli*, 4-64 is enriched in the poles, in bands along the lateral wall, and in the division sites of late pre-divisional cells [12]. In *Bacillus subtilis*, 4-64 labeling enables the visualization of lipid spirals [13]. In *Agrobacterium tumefaciens*, 4-64 labels the outer membrane and is observed in a characteristic "horseshoe" pattern in which the growth pole is devoid of labeling [14,15]. These observations indicate that these bacteria exhibit heterogeneous lipid distributions due to the presence of lipid domains which contribute to cellular asymmetry. Changes in 4-64 labeling patterns such as the presence of diffuse labeling, blebs or vesicles, invaginations, or membrane shrinkage can be informative in characterizing mutants that impact the distribution or biosynthesis of lipids.

Beyond staining cells, determining the function of proteins participating in essential processes is necessary. The characterization of essential proteins is technically challenging because it is not possible to delete essential genes and study the phenotypic consequences. Thus, alternative approaches that deplete the protein have emerged. For example, an essential gene can be put under the control of an inducible promoter rather than its native promoter. Inducible promoters are responsive to small molecules such as; zinc [16], isopropyl β-d-1-thiogalactopyranoside (IPTG) [17-21], arabinose [22],

vanillate [17,23], and xylose [23], thus the transcription of the target gene ceases and the protein of interest is depleted when the inducer is removed. Alternative approaches for depleting essential proteins of interest include synthetic riboswitches [24] which use small molecule-RNA interactions to hinder transcription of target genes, CRISPR interference [25,26] to block transcription of target genes, and inducible protein degradation [27,28] which uses peptide tags to target proteins for degradation by the ClpXP protease. Depletion strains provide only a short time for characterization before the cells lose viability, therefore, microscopic imaging of cells over time during protein depletion is a powerful approach for characterization. Indeed, microscopy of living bacterial cells has enabled researchers to gain insights into fundamental biological processes, including the mechanisms of cell shape maintenance, secretion, and compartmentalization [29].

A. tumefaciens is a bacterial plant pathogen [30] and natural genetic engineer [31,32]. Thus, mechanisms related to pathogenicity, including host-pathogen interactions [33-35], secretion [36], and host transformation [30,31,37] have been extensively investigated. To design strategies that prevent *A. tumefaciens* mediated disease or enhance plant transformation, the processes essential for *A. tumefaciens* survival need to be better understood. The use of target-specific dyes and the recent development of a protein depletion strategy for *A. tumefaciens* [18] provides a means to investigate essential processes.

Here, detailed protocols for microscopic analysis of wildtype, mutant, and protein depletion strains of *A. tumefaciens* are provided. The first two protocols describe how to prepare cells and label them with target-specific dyes. The third protocol provides step-by-step directions for preparing agarose pads (Figure 2.1) and imaging the bacterial cells (Figures 2.2, 2.3, 2.4). These protocols may also be suitable for other bacteria with additional adaptations to account for different media conditions, growth rates, oxygen requirements, and cell structures.

Table 2.1. List of materials

Name of Material/ Equipment	Company	Catalog Number	Comments/Description
Bacterial Strains			
Agrobacterium tumefaciens C58	ATCC	33970	Watson B, Currier TC, Gordon MP, Chilton MD, Nester EW. 1975. Plasmid required for virulence of *Agrobacterium tumefaciens*. J Bacteriol 123:255-264.
Agrobacterium tumefaciens C58Δ*tetRA*::mini-Tn7T-GM-Ptac-*ctrA* Δ*ctrA*			Figueroa-Cuilan W, Daniel JJ, Howell M, Sulaiman A, Brown PJB. 2016. Mini-Tn7 insertion in an artificial attTn7 site enables depeltion of the essentail master regulator CtrA in the phytopathogen *Agrobacterium tumefaciens*. Appl Environ Microbiol. 82:5015-5025.
Media Components			
ATGN Minimal Medium			To 1 L of sterilized water add 50 ml 20X Buffer, 50 ml 20X Salts, 12.5 ml 40% glucose. For plates, add 15 g Bacto Agar to 1 L of water and autoclave. Cool to 55 °C and add 50 ml 20X Buffer, 50 ml 20X Salts, 12.5 ml 40% glucose.
20X AT Buffer			Add 214 g/L KH_2PO_4 to water and adjust pH to 7.0 with sodium hydroxide. Autoclave.
NaOH	Fisher BioReagents	BP359	
KH_2PO_4	Fisher Chemical	P288	
20X AT Salts			Add 40 g/L $(NH_4)_2SO_4$, 3.2 g/L MgSO4•$7H_2O$, 0.2 g/L $CaCl_2$•$2H_2O$, and 0.024 g/L $MnSO_4$•H_2O to water. Autoclave.
$(NH_4)_2SO_4$	Fisher Chemical	A701	
$MgSO_4$•$7H_2O$	Fisher BioReagents	BP213	
$CaCl_2$•$2H_2O$	Fisher BioReagents	BP510	
$MnSO_4$•H_2O	Fisher Chemical	M114	
Glucose	Fisher Chemical	D16	Prepare 40% stock in water. Filter sterilize.
Bacto Agar	Fisher BioReagents	BP1423	Add 15 g to 1 L of water when preparing plates.
Optional Media Additives			
Kanamycin	GoldBio	K-120	Prepare as a 100 mg/ml stock solution in water and filter sterilize. Use at final concentration of 200 μg/ml.
IPTG	GoldBio	I2481C5	Prepare as a 1 M stock solution in water and filter sterilize. Use at final

			concentration of 1 mM as needed for induction.
Microscopy Materials			
Microscope Slides	Fisherbrand	12-550D	25 X 75 X 1.0 mm. Clean with Sparkle glass cleaner.
Microscope Cover Glass	Fisherbrand	12-541-B	22 X 22 mm. No. 1.5. Clean with Sparkle glass cleaner.
Sparkle Glass Cleaner	Home Depot	203261385	Ammonia and alcohol free.
Ultra Pure Agarose	Invitrogen	16500-100	Add to water, PBS, or media to a final concentration of 1 - 1.5%. Melt in microwave and place on 70 C
PBS	Fisher BioReagents	BP399500	10X solution to be diluted to 1X with sterile water.
Parafilm	Bemis	PM-999	Laboratory film used as gasket in agarose pad preparation.
VALAP			Add equal weights of lanolin, parafin wax, and petroleum jelly to a conical tube. Heat tube in 70 °C dry, bead or water bath to melt and mix. Apply VALAP while still molten.
Lanolin Butter	SAAQIN	SQ-LAB-R1	
Petroleum Jelly	Target Corp.	06-17644	
Paraffin Wax	Crafty Candles	263012	
Target-specific dyes			
DMSO	Fisher BioReagents	BP231-1	Use to dilute stock solutions of dyes as needed.
FDAAs (NADA, HADA,TADA)			FDAAs can be synthesized or acquired through agreement with Mike VanNieuwenhze (Indiana University). Prepare 100 mM stock solution in DMSO. Use at a final concentration of 5 mM.
DAPI	ThermoFisher Scientific	62247	Prepare 1 mg/ml stock solution in DMSO. Use at final concentration of 1 µg/ml.
SYTOX Orange Nucleic Acid Stain	Invitrogen	S11368	Stock concentration is 5 mM in DMSO. Use at final concentration of 5 µM.
FM4-64	Invitrogen	T3166	Prepare 8 mg/ml stock solution in DMSO. Use at final concentration of 8 µg/ml.
Equipment			
Dry bath	Sheldon Manufacturing, Inc.	52120-200	
Metallic thermal beads	Lab Armor	42370-002	
Epifluorescence microscope equipped with an EMCDD camera			Nikon Eclipse TiE equipped with a QImaging Rolera em-c2 1K electron-multiplying charge-coupled-device (EMCCD) camera is used in this work.

PROTOCOL:

1. Growth of *A. tumefaciens* strains

1.1. Culturing *A. tumefaciens* strains

1.1.1. Use a sterile wooden stick or pipet tip to inoculate 1 mL of ATGN growth medium (see Table 2.1 for the recipe) with a single colony of the desired strain.

Note: For *A. tumefaciens* depletion strains, the ATGN should contain 1 mM IPTG as an inducer to maintain biosynthesis of the essential protein.

1.1.2. Grow the *A. tumefaciens* strains overnight in ATGN at 28 °C with shaking at 225 rpm.

1.1.3. Measure the optical density of the cells at 600 nm (OD_{600}) using a spectrophotometer. Dilute the cell culture to an OD_{600} = ~0.2 and continue to grow until OD_{600} = ~0.6 is reached. For depletion strains, continue to grow with inducer until OD_{600} = ~0.6 is reached.

1.1.4. Use wildtype and mutant strains of *A. tumefaciens* at OD_{600} = ~0.6 for target-specific staining and/or time-lapse microscopy (see sections 2 and 3.1). For depletion strains, wash out the inducer (see section 1.2.)

1.2. Removal of inducer for characterization of *A. tumefaciens* protein depletion strains

1.2.1. Pellet 1 mL of exponential culture (OD_{600} = ~0.4-0.6) by centrifugation at 7,000 x *g* for 5 minutes in a desktop centrifuge at room temperature.

1.2.2. To wash, remove supernatant and resuspend the pellet in fresh medium without inducer and pellet the cells as described above (1.2.1). Wash the cells a total of 3 times in fresh media.

1.2.3. Resuspend the final pellet in fresh medium and concentrate the cells to an OD_{600} = ~0.8 for immediate staining with target specific dyes (section 2 and Figure 2.4B-D) or time-lapse microscopy (section 3.2 and Figure 2.4A). Alternatively, pre-deplete the cells for the desired amount of time by growing the cells in medium without inducer prior to staining and imaging of the cells.

2. Target-specific staining of *A. tumefaciens* cells

2.1. Fluorescent D-amino acid cell wall labeling

Note: FDAAs are non-toxic fluorescent D-amino acids which are readily incorporated into the *A. tumefaciens* peptidoglycan. This simple labeling procedure probes growth patterning in live cells [6]. Protocols for synthesis of four FDAAs are available [38].

2.1.1. Pellet 500 µL of exponential culture (OD_{600} = ~0.4-0.6) by centrifugation at 7,000 x *g* for 5 minutes in a desktop centrifuge. Resuspend the cell pellet in 100 µL of fresh medium.

2.1.2. Add 5 µL of 5 mM FDAA to washed and concentrated cells and incubate for 2 minutes in the dark.

Note: Limit FDAA exposure to light. The time of incubation will vary depending on the growth rate of the strain. Typically, incubation times should be 5-10% of the doubling time [6].

2.1.3. Pellet the cells by centrifugation and wash cell pellets with phosphate buffered saline (PBS) three times.

2.1.4. Resuspend pellet in ~50 µL PBS.

Note: The volume of PBS used for resuspension may vary based on pellet size.

2.1.5. Apply 0.8-1 µL of cells to an agarose pad and image using epifluorescence microscopy immediately (See sections 3.1 and 3.2).

2.1.5.1. Alternatively, stop further label incorporation by fixing the cells with ice-cold 70% ethanol. Resuspend the cell pellet in 1 mL of ice-cold 70% ethanol and incubate on ice for 15 minutes.

2.1.5.2. Collect cells by centrifugation and resuspend in a small volume of PBS for imaging at a later time. Store cell suspensions at 4 °C and image within 48 hours.

2.2. DNA staining with DAPI or Orange stain

Note: To observe DNA, cells are labeled with either DAPI or Orange (dead cell stain). Although classically described as a "dead-cell stain", Orange is permeant, photostable, and does not affect the growth of bacterial cells, enabling live-cell DNA imaging [10]. In *A. tumefaciens*, Orange labeling works well in living cells and is suitable for time-lapse microscopy (Figure 2.3). In contrast, the ultraviolet (UV) light exposure necessary for imaging DAPI-stained cells is phototoxic (Figure 2.3) and thus DAPI staining is best suited for staining live cells for immediate imaging or staining fixed cells.

2.2.1. DAPI staining of cells

2.2.1.1. Pellet 1 mL of exponential culture (OD_{600} = ~0.4-0.6) by centrifugation at 7,000 x *g* for 5 minutes in a desktop centrifuge.

2.2.1.2. **Optionally,** to fix cells prior to staining, resuspend the cell pellet in 1 mL of 70% ice-cold ethanol. Incubate on ice for 10-15 minutes. Collect the cells by centrifugation as described in 2.2.1.1.

2.2.1.3. Resuspend the cell pellet in 1 mL of PBS containing 1 µL of DAPI stock solution (1 mg/mL; see Table 2.1). Mix gently by pipetting and incubate for 5 minutes in the dark.

2.2.1.4. Pellet cells by centrifugation at 7,000 x *g* for 5 minutes and resuspend in 1 mL of PBS to remove excess DAPI. Wash the cells two more times and resuspend the pellet in 50 µL PBS or medium.

2.2.2.3. Apply 0.8-1 µL of cells to an agarose pad and image using epifluorescence microscopy immediately. See sections 3.1 and 3.2.

Note: This protocol is not optimal for time-lapse microscopy to observe chromosome dynamics (Figure 2.3). Consider using Orange staining as an alternative (see section 2.2.2).

2.2.2. Orange staining of live cells

2.2.2.1. Pellet 1 mL of exponential culture (OD_{600} = ~0.4-0.6) by centrifugation at 7,000 x *g* for 5 minutes in a desktop centrifuge. Resuspend cell pellet in 1 mL of PBS containing 1 µL of Orange stock solution (see Table 2.1). Mix gently by pipetting and incubate for 5 minutes in the dark.

2.2.2.2. Pellet cells by centrifugation and resuspend in 1 mL of PBS to remove excess Orange. Wash the cells two more times and resuspend the pellet in 50 µL PBS.

2.2.2.3. Apply 0.8-1 µL of cells to an agarose pad and image using epifluorescence microscopy immediately. See sections 3.1 and 3.2.

Note: This protocol works well with live cells and is suitable for time-lapse microscopy to observe chromosome dynamics (Figure 2.3). If it is not convenient to image immediately, cells may be fixed in ice-cold 70% ethanol (see section 2.2.1.2).

2.3. Membrane labeling

Note: The lipophilic styryl fluorescent dye 4-64 has been used extensively to observe the membrane of bacterial cells [12,39]. In contrast to many bacteria, 4-64 labeled *A. tumefaciens* cells do not label uniformly, but rather frequently exhibit a "horseshoe" pattern [14,15]. Remarkably, the growth pole is nearly devoid of stain whereas the old pole is intensely labeled. Thus, 4-64 enables visualization of both cell growth patterns and membrane structure in *A. tumefaciens*.

2.3.1. Add 4-64 to a final concentration of 8 µg/mL in 1 mL of exponential phase cell culture and incubate at room temperature for 5 minutes in the dark.

2.3.2. Pellet labeled cells by centrifugation at 7,000 x *g* for 5 minutes in a desktop centrifuge and resuspend cell pellet in 1 mL of PBS. Wash the cells a total of three times to remove excess dye.

2.3.3. Resuspend cells in a small volume of PBS and spot on an agarose pad to image immediately. (See sections 3.1 and 3.2)

Caution: Cells must be imaged immediately to observe characteristic labeling patterns.

3. Imaging of *A. tumefaciens* cells

3.1 Agarose pad preparation

Note: Figure 2.1 contains an image sequence (panel A) and schematic (panel B) of a typical agarose pad prepared for time-lapse microscopy. Agarose pads are typically prepared as needed.

3.1.1. Use a coverslip as a guide and cut a 22 mm x 22 mm square of laboratory film (see Table 2.1) by running a scalpel around the edges.

3.1.2. Cut a square out of the center of the laboratory film leaving a ~2-5 mm border to serve as a gasket for the agarose pad. Discard the center cutout.

3.1.3. Place the film gasket onto a glass slide (75 mm x 25 mm) cleaned with an ammonia and alcohol-free cleaner (see Table 2.1) and heat until the film is slightly melted onto glass (top image in Figure 2.1A). To melt laboratory film, use the edge of a heat block set to 70 °C or melt lightly over a flame.

3.1.4. Prepare agarose solution by mixing ~0.075 g agarose (see Table 2.1) in 5 mL of medium in a small flask. Heat the solution in a microwave with periodic swirling to mix until the agarose is dissolved and the solution is clear. Keep the agarose solution at 55–70 °C and use for construction of multiple agarose pads within 48 hours.

3.1.5. Pipette media containing 1.2–1.5% agarose into the center of the gasket.

Note: The volume of media is typically 50 – 60 µL but will vary based on gasket size. Adding media to a cold slide can cause the agarose to solidify too quickly, thus the slide should be kept on a warm surface. The edge of a heat block set to 70 °C works well. Water agarose or buffered agarose solutions such as PBS can be used instead of medium containing agarose for applications in which continued cell growth is not required. For imaging depletion strains, inducer can be present or absent in the media. Presence of inducer can be used as a control whereas the absence of inducer will reveal the depletion phenotype.

3.1.6. Place a coverslip over the gasket to evenly distribute the agarose.

3.1.7. Place slide on a cool, level surface to solidify for ~2 minutes. Avoid overdrying of the agarose pad as this will result in a wrinkled surface on the agarose pad and pooling of the cell suspension when applied to the surface.

3.1.8. Carefully slide the coverslip off the agarose pad.

Caution: Do not rush this step. The agarose pad can easily tear and an uneven agarose pad can make imaging difficult.

3.1.9. Allow the agarose pad to air dry for 1-2 minutes at room temperature until the surface of the pad appears dry. Using a scalpel, remove a small strip of agarose to create an air pocket (middle image, Figure 2.1A); the air pocket is typically ~2 mm x 7-10 mm and *A. tumefaciens* cells tend to grow best near the air pocket (Figure 2.1C).

Note: For imaging of fixed cells or under conditions where growth is not monitored, an air pocket is not necessary.

3.1.10. Spot 0.8-1 µL of cells on the agarose pad and cover with a new coverslip. Gently place the coverslip over the top of the agarose pad to distribute the cells across the surface of the agarose pad.

3.1.11. Seal the edges of the coverslip using melted VALAP (see materials for recipe; Figure 2.1A, bottom image). Failure to seal along all the edges and corners of the coverslip can cause drying of the agarose pad, which will lead to the drifting of cells during imaging. **Note:** Sealing of the coverslip is only needed for long-term time-lapse imaging.

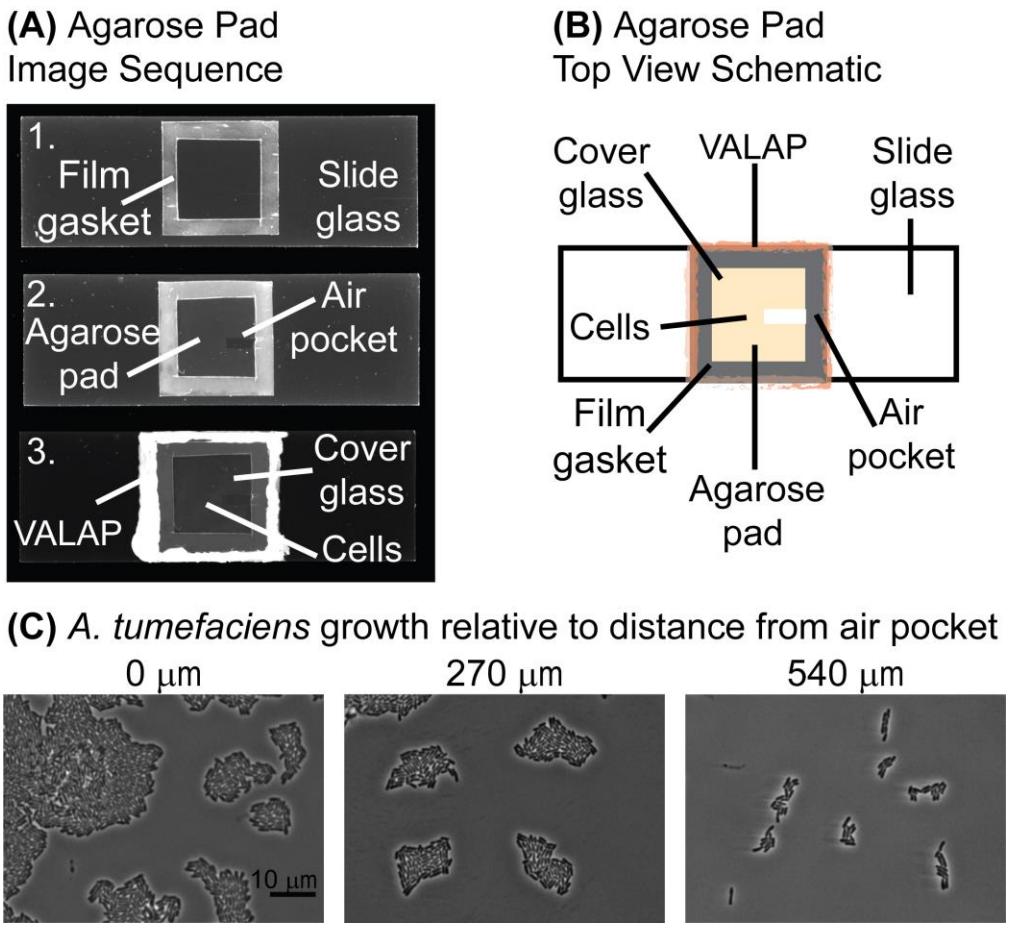

Figure 2.1. Agarose pad preparation. (A) Image sequence of the agarose pad preparation protocol. Image 1 is a slide with the laboratory film gasket. In image 2, the agarose pad and air pocket are visualized. Finally, image 3 shows the complete agarose pad with the cells under a coverglass and sealed with VALAP. (B) A schematic of an agarose pad for time-lapse microscopy is provided. Key features of the agarose pad are labeled on the schematic. (C) The air pocket promoted growth of *A. tumefaciens* on agarose pads. Images of wildtype *A. tumefaciens* cells grown on an agarose pad for 20 hours are shown. Images were taken at positions increasingly distant from the air pocket. The distance from the closest edge of the image to the air pocket is shown above each image. The scale bar is 10 μm in length.

3.2. Imaging

Note: Differential interference contrast, phase contrast, and epifluorescence imaging is performed with an inverted microscope equipped with hardware-based autofocusing, an automated stage, standard filters, an LED light source, 60x oil immersion objectives (1.4 NA) for phase contrast or differential interference contrast (DIC), and a 1K electron-multiplying charge-coupled-device (EMCCD) camera. The microscope should be placed in a temperature controlled room. Alternatively, a stage warmer or chamber can be used to maintain consistent temperatures during imaging.

3.2.1. Epifluorescence microscopy

Note: For fluorescence imaging of live cells, it is necessary to limit the number of image acquisitions and optimize the exposure time to minimize photobleaching and phototoxicity. For imaging of each dye, it is recommended to find an optimal exposure time which provides sufficient fluorescence detection but does not lead to photobleaching or phototoxicity. In Figures 2.2 – 2.4, exposure times of 200 ms were used for all fluorescence images. For the time-lapse sequences shown in Figure 2.3, images were acquired every 10 minutes for 3 hours.

3.2.1.1. Place immersion oil on the desired objective and place the inverted slide into the slide holder on the stage. Use the focusing knobs to bring the cells into focus.

3.2.1.2. Acquire images in phase (or DIC) and the desired fluorescence filter.

Note: The maximal excitation and emission wavelengths for the stains used in Figures 2.2-2.4 are as follows: HADA (405/460), NADA (450/555), TADA (555/570), 4-64 (515/640), DAPI (360/460), Orange (547/570).

3.2.2. Time-lapse microscopy

Notes: During time-lapse microscopy the following features are computer controlled: x, y, and z position, shutters, and fluorescence filters. A hardware-based auto-focus system is optimal to maintain focus during time-lapse imaging. Alternatively, a software-based auto-focusing loop can be used.

3.2.2.1. Place immersion oil on the desired objective and place the inverted slide into the slide holder on the stage. Use the focusing knobs to bring the cells into focus.

3.2.2.2. **Optionally,** acquire multiple (x,y) positions. Randomly select 10 fields of cells in close proximity to the air pocket of the agarose pads.

3.2.2.3. Set-up the time sequence acquisition to image in phase or DIC at the desired time interval.

Note: For the time-lapse sequence shown in Figure 2.4, DIC images were acquired with 30 ms exposure every 10 minutes for 14 h. When using fluorescence imaging during time-lapse microscopy, adjust the acquisition interval and exposure time to minimize photobleaching and phototoxicity.

REPRESENTATIVE RESULTS:

Target-specific labeling of wildtype *A. tumefaciens* cells: In order to illustrate that cell morphology is not impacted by the wash steps or treatment with 1% dimethyl sulfoxide (DMSO) (which is used to dilute the fluorescent dyes), cells were imaged directly from culture (Figure 2.2A, far left panel), after washing the cells by centrifugation as described in 1.2 (Figure 2.2A, left panel), or after incubating the cells with 1% DMSO for 10 minutes and washing the cells (Figure 2.2A, right panel). These images illustrate that morphology is not impacted by washing or the presence of DMSO. In addition, cell growth is not impacted by washing or DMSO treatment based on growth curve analysis (data not shown). In addition, fixing *A. tumefaciens* with ice-cold 100% ethanol does not cause gross changes in morphology (Figure 2.2A, far right panel).

Next, target specific dyes were used to observe cell wall biogenesis, membrane domains, and DNA within wildtype *A. tumefaciens* cells. The patterns of new peptidoglycan insertion were observed following labeling with three fluorescent-D-amino acids: HADA (Figure 2.2B, left panel), NADA (Figure 2.2B, center panel), and TADA (Figure 2.2C, right panel). In all three labeling experiments, new peptidoglycan labeling was enriched at the growth pole or septum of the cells. These growth patterns were consistently

observed with all three FDAAs, indicating that the FDAA selection can be modified to enable dual labeling with other stains or cells expressing fluorescently labeled proteins. The lipophilic dye 4-64 preferentially labels the old pole region of *A. tumefaciens* cells resulting in a characteristic horseshoe pattern (Figure 2.2C). Both Orange (Figure 2.2D, left panel) and DAPI (Figure 2.2D, right panel) label DNA within live *A. tumefaciens* cells. In late pre-divisional cells, two distinct nucleoids are observed with Orange staining, whereas DNA labeling appears more diffuse with DAPI staining (Figure 2.2D) consistent with experiments results observed in *E. coli* [10].

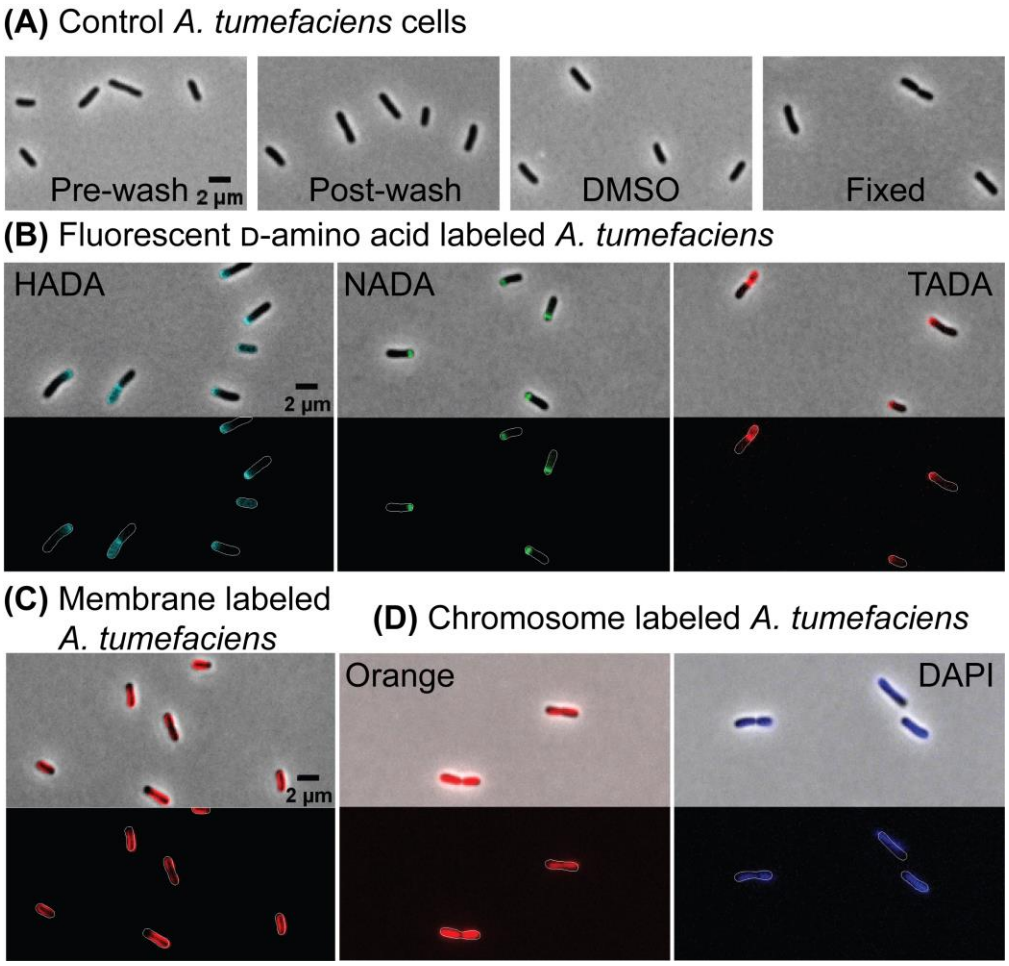

Figure 2.2. Representative images of wildtype *Agrobacterium tumefaciens* cells labeled with target specific dyes. (A) Phase contrast images of *A. tumefaciens* cells before and after the washing protocol, when treated with 1% DMSO, or after fixation with ice-cold ethanol. (B) Polar growth of *A. tumefaciens* cells is shown by labeling with the fluorescent D-amino acids HADA, NADA, and TADA. (C) Staining of *A. tumefaciens* with the lipophilic 4-64 stain. (D) Staining of *A. tumefaciens* cells with the DNA-specific dyes Orange and DAPI. For panels B-D, phase contrast (top) and epifluorescence (bottom) images are shown. Cell outlines are provided in fluorescence images for reference. The scale bar is 2 µm in length.

Suitability of DNA dyes for time-lapse microscopy: In order to determine if either DAPI or Orange are suitable for time-lapse imaging of nucleoid morphology during cell growth, an equal proportion of unlabeled, DAPI-labeled, and Orange-labeled wildtype *A. tumefaciens* cells were mixed and spotted on agarose pads. At time 0, initial images were taken using phase contrast, DAPI, and tetramethylrhodamine isothiocyanate (TRITC) filters to determine if each cell was labeled. The cell mixtures were then imaged under three different conditions: (1) phase contrast microscopy only, (2) phase contrast and epifluorescence microscopy using the TRITC filter and (3) phase contrast and epifluorescence microscopy using the DAPI filter. Images were acquired every 10 minutes for 3 hours. All cells grew well irrespective of the fluorescent stain used when imaged with phase contrast microscopy indicating that neither Orange or DAPI staining impair cell growth (Figure 2.3, top panel). All cells also grew well when imaged by phase microscopy and epifluorescence microscopy using the TRITC filter (Figure 2.3, center panel). The Orange label is subject to photobleaching but can be observed for at least 2 hours (13 total exposures of 200 ms), indicating the suitability of this dye for short-term microscopy of live cells. Irrespective of labeling, all cells stop growing within an hour when imaged by phase microscopy and epifluorescence microscopy using the DAPI filter (Figure 2.3, bottom panel). This observation demonstrates that *A. tumefaciens* is sensitive to UV exposure and indicates that dyes requiring a UV filter for imaging should be avoided for time-lapse microscopy experiments.

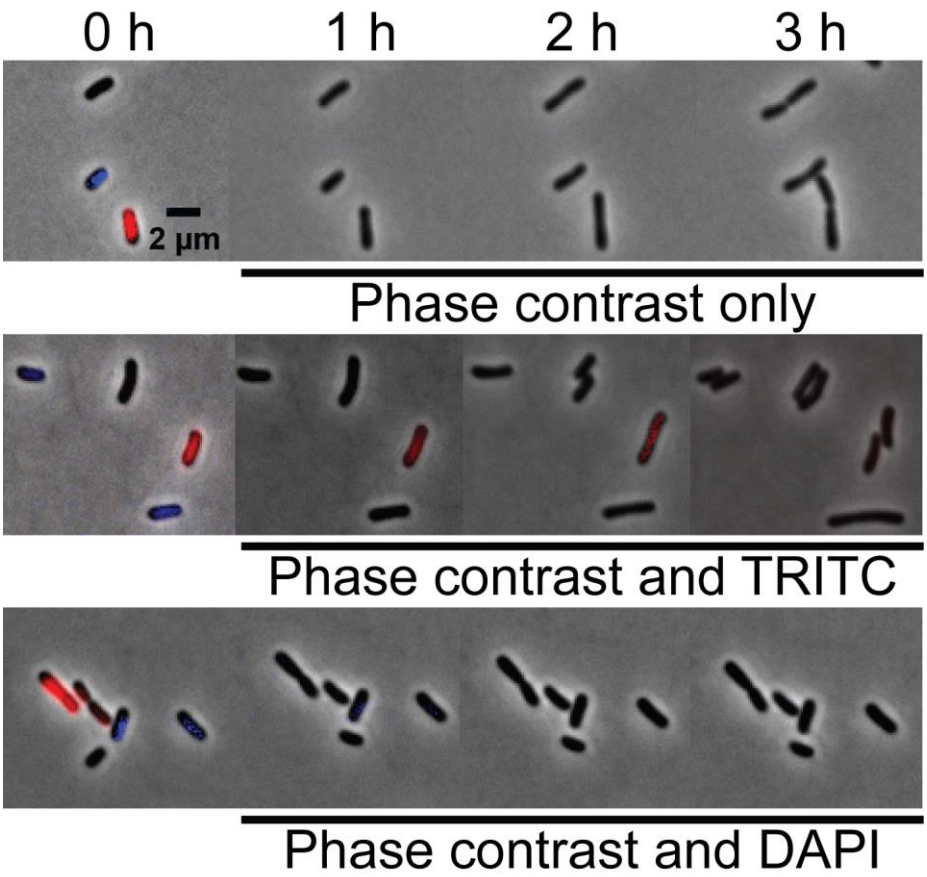

Figure 2.3. Comparison of DAPI and Orange labeling of DNA in live *A. tumefaciens* cells. Equal proportions of unlabeled, DAPI-labeled, and Orange-labeled wildtype *A. tumefaciens* cells were mixed and spotted on agarose pads. At time 0, initial images were taken using phase contrast, TRITC, and DAPI filters to determine if the cells were labeled. (A) Time-lapse of unlabeled, DAPI-labeled, and Orange-labeled cells imaged by phase contrast microscopy. (B) Time-lapse of unlabeled, DAPI-labeled, and Orange-labeled cells imaged by phase microscopy and epifluorescence microscopy using the TRITC filter. (C) Time-lapse of unlabeled, DAPI-labeled, and Orange-labeled cells imaged by phase microscopy and epifluorescence microscopy using the DAPI filter. The scale bar is 2 µm in length.

Time-lapse imaging and target-specific labeling of an *A. tumefaciens* depletion strain: Both saturating transposon mutagenesis [40] and failing to construct a deletion strain [18,41] indicate that the master regulator protein, CtrA, is essential in *A. tumefaciens*. To demonstrate the value of microscopic analysis of depletion strains, a previously described *ctrA* depletion strain [18] was subjected to characterization by microscopy. In Figure 2.4A, time-lapse microscopy was used to compare the growth of *ctrA* depletion cells in which *ctrA* expression was induced (top) and uninduced (bottom). In the presence of CtrA, a single cell gave rise to a microcolony within 14 hours. In contrast, when CtrA was depleted, cells either lysed or failed to divide. Cells that failed to divide exhibited gross morphological changes including rounding from mid-cell and at the cell poles. These observations suggest that CtrA has an important function in the regulation of cell division.

In Figures 2.4B-D, fluorescent dyes were used to characterize the *ctrA* depletion strain after induction or depletion of *ctrA* for 10 hours. Cells were pulse labeled with NADA for 2 minutes (Figure 2.4B). When CtrA was present (top panel), polar peptidoglycan biosynthesis was observed. In contrast, extensive NADA labelling occurred at the poles and large mid-cell swellings occurred when CtrA was depleted. This observation is consistent with continued peptidoglycan synthesis despite a failure of the cells to divide. The cyanine DNA dye Orange was used to characterize DNA distribution in the *ctrA* depletion strain (Figure 2.4C). When CtrA was present, growing cells had an even distribution of DNA and segregation of nucleoids was apparent in a late pre-divisional cell; in contrast, when CtrA was depleted, DNA was unevenly distributed throughout the cells. These observations suggest that CtrA contributes to proper DNA replication or

segregation. Finally, *ctrA* depletion cells were labeled with 4-64 (Figure 2.4D). In the presence of CtrA, the cell membrane was labeled with a characteristic horseshoe pattern in which the growth pole was devoid of stain. In cells depleted of CtrA, 4-64 appeared to label the entire membrane, although one pole was more intensely stained. This observation suggests that membranes remain intact although the lipid microdomain organization may be disrupted when CtrA is depleted.

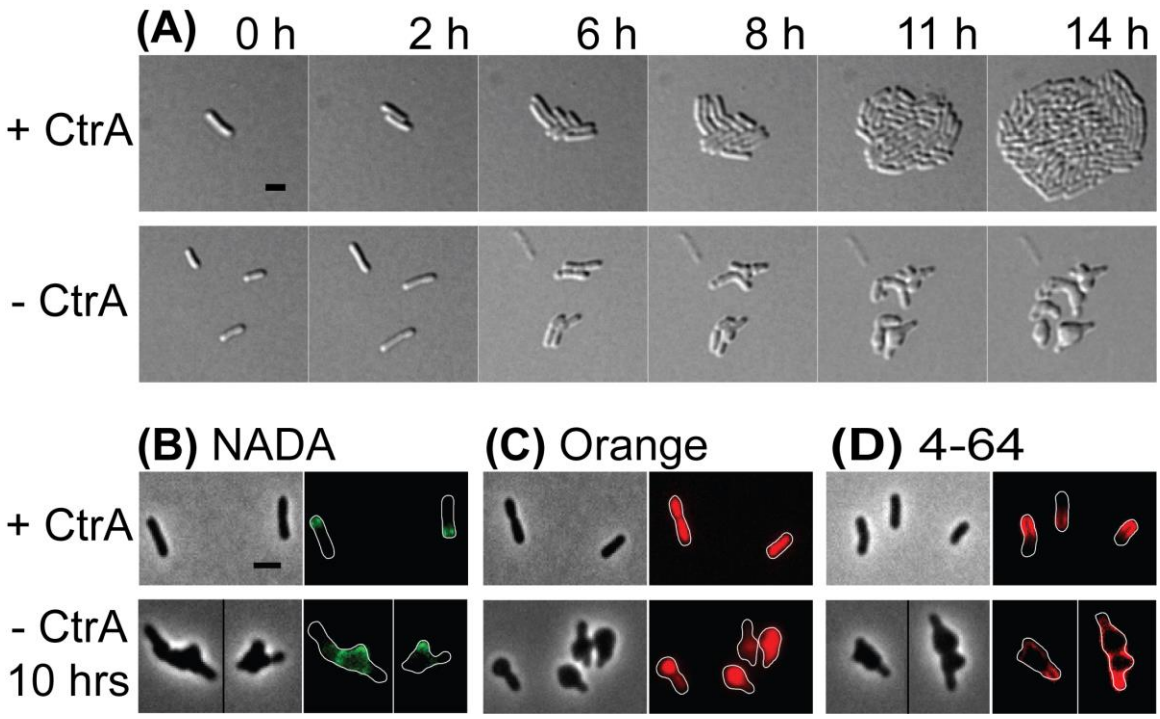

Figure 2.4. Representative images of the *ctrA* depletion strain in induced and uninduced conditions. (A) Time-lapse microscopy of the *ctrA* depletion strain under conditions where *ctrA* was induced (top) or depleted (bottom). The numbers above each panel indicate the time in hours. (B) Phase contrast (left) and epifluorescence (right) images of cells labeled with NADA. (C) Phase contrast (left) and fluorescence (right) images of cells labeled with Orange. (D) Phase contrast (left) and fluorescence (right) images of cells labeled with 4-64. Cell outlines were provided in fluorescence images for reference. The scale bar is 2 μm in length.

DISCUSSION:

This protocol contains a series of procedures for the investigation of *A. tumefaciens* wildtype, mutant, and depletion strains. It is worth noting that all of the procedures listed in the protocol section can be readily adapted for other bacterial strains with additional modifications to account for growth media, temperatures, and growth rates.

The use of target-specific dyes is a valuable tool for providing a detailed characterization of cell-cycle events in bacterial cells. Here, peptidoglycan insertion patterns were observed using fluorescent-D-amino acids, lipid domains were visualized with 4-64, and nucleoids were labeled with either DAPI or Orange. Each of the protocols can be adapted for use in other bacteria after optimizing the wash protocol and ensuring that the DMSO treatment does not impair growth or morphology. Key considerations include the selection of a buffer for wash steps, incubation times for label incorporation, and the selection of an appropriate fluorophore to avoid auto-fluorescence or to enable multiplex labeling studies. For example, an alternative to the lipophilic red-fluorescent membrane stain (4-64) is the green-fluorescent membrane stain (1-43). Similarly, blue-, green-, and red-fluorescent-D-amino acids are available [6,38] and D-amino acids with biorthogonal handles can be conjugated to common fluorophores through click chemistry [6,7]. Finally, in addition to the orange-fluorescent cyanine DNA dye, a green fluorescent cyanine DNA dye is available and performs well with live bacterial cells [10]. Visualization of key cell structures labeled with target-specific dyes can be combined with the observation of fluorescent proteins to gain mechanistic insights into essential processes in bacteria.

These protocols include the conditions necessary for microscopic observation of *A. tumefaciens* depletion strains, and it should be possible to extend these approaches to protein depletion strains in other bacteria. The characterization of depletion strains can be particularly challenging as there is a limited timeframe to complete investigations before the cells stop growing or lyse. It is crucial to adequately wash the cells to remove all traces of the excess dye during labeling; however, some cells depleted of essential proteins have defects in their cell surfaces which can cause them to be sensitive to wash steps. Increasing the starting volume of cell cultures can help compensate for loss of cells during the wash steps. Depletion strains that have compromised cell membranes or cell walls may be prone to cell lysis when grown in liquid culture without inducer. Inclusion of an osmoprotectant (5% w/v sucrose works well for *A. tumefaciens*) can help to maintain cell morphology and limit cell lysis during depletion. It is necessary to empirically determine the appropriate amount of time to pre-deplete the cells prior to staining with fluorescent dye. Cells with permeabilized membranes or cell walls may be prone to cell lysis or non-selective labeling with fluorescent reagents making imaging of late depletion time points particularly challenging.

A critical step for time-lapse microscopy of *A. tumefaciens* (or other bacterial cells) is the preparation of the agarose pad. To ensure good focus throughout time-lapse microscopy, the agarose must be level. In addition, the coverslip must be completely sealed to prevent the agarose pad from drying and changing the focal plane. For *A. tumefaciens*, oxygen is required for cell growth. Imaging near an air pocket is necessary to get robust growth of

A. tumefaciens during long time-lapse microscopy experiments (Figure 2.1C). If cells fail to grow or stop growing after just a few hours, it is advisable to prepare an agarose pad with a larger air pocket and image near the air pockets. Even a well-constructed agarose pad with a proper air pocket can only support *A. tumefaciens* growth for a maximum of ~24 hours. If longer time-lapse sequences are necessary, alternative approaches such as microfluidics or flow cells should be considered. If the cells drift out of focus during imaging, ensure that the agarose pad is level and properly sealed under the coverslip. Note that even with a near perfect agarose pad, it is possible that some cells will drift out of focus, thus imaging multiple fields and frequent refocusing are highly recommended. For other bacteria, alternative approaches of preparing agarose pads should be considered [42-44] to best meet the growth requirements for the bacterium. Agarose pads are also useful for immobilizing cells during imaging of labeled or fixed cells when time-lapse is not necessary. In this case, sealing the coverslip is not necessary and alternative approaches for constructing agarose pads which can be stored until later may be appropriate [44].

Overall, the use of target-specific dyes and time-lapse microscopy can provide insights about fundamental processes in bacteria. Here, we illustrate the usual horseshoe pattern of labeling with the lipophilic 4-64 dye and the characteristic polar and septal labeling with fluorescent-D-amino acids in *A. tumefaciens*. Observations of these patterns in *A. tumefaciens* are consistent with the polar growth of this bacterium [45] and it is likely that similar studies may reveal information about growth patterning in other bacteria. The finding that cyanine dyes such as Orange are suitable for time-lapse microscopy studies

[10] (Figure 2.3) will enable careful studies of nucleoid morphology during cell growth in wildtype and mutant strains. Imaging fluorescent target-specific dyes during the depletion of an essential protein can provide key observations to determine the function of the protein. Finally, since many of these dyes are available with different spectral properties, studies using multiple labels simultaneously should enable insights into the coordination of essential processes during cell cycle progression.

ACKNOWLEDGMENTS:

We thank Michael VanNieuwenhze (Indiana University) for the gift of the FDAAs used in Figures 2.2 and 2.4. We thank members of the Brown laboratory for feedback during the preparation of this manuscript. Research in the Brown laboratory on *A. tumefaciens* cell growth and division is supported by the National Science Foundation (IOS1557806).

REFERENCES

1. Daniel RA, Errington J: Control of cell morphogenesis in bacteria: two distinct ways to make a rod-shaped cell. *Cell* 2003, 113:767-776.

2. Tiyanont K, Doan T, Lazarus MB, Fang X, Rudner DZ, Walker S: Imaging peptidoglycan biosynthesis in *Bacillus subtilis* with fluorescent antibiotics. *Proc Natl Acad Sci U S A* 2006, 103:11033-11038.

3. Turner RD, Ratcliffe EC, Wheeler R, Golestanian R, Hobbs JK, Foster SJ: Peptidoglycan architecture can specify division planes in *Staphylococcus aureus*. *Nat Commun* 2010, 1:26.

4. Wheeler R, Mesnage S, Boneca IG, Hobbs JK, Foster SJ: Super-resolution microscopy reveals cell wall dynamics and peptidoglycan architecture in ovococcal bacteria. *Mol Microbiol* 2011, 82:1096-1109.

5. Turner RD, Hurd AF, Cadby A, Hobbs JK, Foster SJ: Cell wall elongation mode in Gram-negative bacteria is determined by peptidoglycan architecture. *Nat Commun* 2013, 4:1496.

6. Kuru E, Hughes HV, Brown PJ, Hall E, Tekkam S, Cava F, de Pedro MA, Brun YV, VanNieuwenhze MS: *In situ* probing of newly synthesized peptidoglycan in live bacteria with fluorescent D-amino acids. *Angew Chem Int Ed Engl* 2012, 51:12519-12523.

7. Siegrist MS, Whiteside S, Jewett JC, Aditham A, Cava F, Bertozzi CR: (D)-Amino acid chemical reporters reveal peptidoglycan dynamics of an intracellular pathogen. *ACS Chem Biol* 2013, 8:500-505.

8. Kepner RL, Jr., Pratt JR: Use of fluorochromes for direct enumeration of total bacteria in environmental samples: past and present. *Microbiol Rev* 1994, 58:603-615.

9. Johnson MB, Criss AK: Fluorescence microscopy methods for determining the viability of bacteria in association with mammalian cells. *J Vis Exp* 2013, 79.

10. Bakshi S, Choi H, Rangarajan N, Barns KJ, Bratton BP, Weisshaar JC: Nonperturbative imaging of nucleoid morphology in live bacterial cells during an antimicrobial peptide attack. *Appl Environ Microbiol* 2014, 80:4977-4986.

11. Barak I, Muchova K: The role of lipid domains in bacterial cell processes. *Int J Mol Sci* 2013, 14:4050-4065.

12. Fishov I, Woldringh CL: Visualization of membrane domains in *Escherichia coli*. *Mol Microbiol* 1999, 32:1166-1172.

13. Barak I, Muchova K, Wilkinson AJ, O'Toole PJ, Pavlendova N: Lipid spirals in *Bacillus subtilis* and their role in cell division. *Mol Microbiol* 2008, 68:1315-1327.

14. Cameron TA, Anderson-Furgeson J, Zupan JR, Zik JJ, Zambryski PC: Peptidoglycan synthesis machinery in *Agrobacterium tumefaciens* during unipolar growth and cell division. *MBio* 2014, 5:e01219-01214.

15. Zupan JR, Cameron TA, Anderson-Furgeson J, Zambryski PC: Dynamic FtsA and FtsZ localization and outer membrane alterations during polar growth and cell division in *Agrobacterium tumefaciens. Proc Natl Acad Sci U S A* 2013, 110:9060-9065.

16. Eberhardt A, Wu LJ, Errington J, Vollmer W, Veening JW: Cellular localization of choline-utilization proteins in *Streptococcus pneumoniae* using novel fluorescent reporter systems. *Mol Microbiol* 2009, 74:395-408.

17. Iniesta AA, Garcia-Heras F, Abellon-Ruiz J, Gallego-Garcia A, Elias-Arnanz M: Two systems for conditional gene expression in *Myxococcus xanthus* inducible by isopropyl-beta-D-thiogalactopyranoside or vanillate. *J Bacteriol* 2012, 194:5875-5885.

18. Figueroa-Cuilan W, Daniel JJ, Howell M, Sulaiman A, Brown PJ: Mini-Tn*7* insertion in an artificial *att*Tn*7* site enables depletion of the essential master regulator CtrA in the phytopathogen *Agrobacterium tumefaciens*. *Appl Environ Microbiol* 2016, 82:5015-5025.

19. Jacob F, Monod J: Genetic regulatory mechanisms in the synthesis of proteins. *J Mol Biol* 1961, 3:318-356.

20. Khan SR, Gaines J, Roop RM, 2nd, Farrand SK: Broad-host-range expression vectors with tightly regulated promoters and their use to examine the influence of TraR and TraM expression on Ti plasmid quorum sensing. *Appl Environ Microbiol* 2008, 74:5053-5062.

21. Yansura DG, Henner DJ: Use of the *Escherichia coli lac* repressor and operator to control gene expression in *Bacillus subtilis*. *Proc Natl Acad Sci U S A* 1984, 81:439-443.

22. Guzman LM, Belin D, Carson MJ, Beckwith J: Tight regulation, modulation, and high-level expression by vectors containing the arabinose P_{BAD} promoter. *J Bacteriol* 1995, 177:4121-4130.

23. Thanbichler M, Iniesta AA, Shapiro L: A comprehensive set of plasmids for vanillate- and xylose-inducible gene expression in *Caulobacter crescentus*. *Nucleic Acids Res* 2007, 35:e137.

24. Topp S, Reynoso CM, Seeliger JC, Goldlust IS, Desai SK, Murat D, Shen A, Puri AW, Komeili A, Bertozzi CR, et al.: Synthetic riboswitches that induce gene expression in diverse bacterial species. *Appl Environ Microbiol* 2010, 76:7881-7884.

25. Peters JM, Colavin A, Shi H, Czarny TL, Larson MH, Wong S, Hawkins JS, Lu CH, Koo BM, Marta E, et al.: A comprehensive, CRISPR-based functional analysis of essential genes in bacteria. *Cell* 2016, 165:1493-1506.

26. Qi LS, Larson MH, Gilbert LA, Doudna JA, Weissman JS, Arkin AP, Lim WA: Repurposing CRISPR as an RNA-guided platform for sequence-specific control of gene expression. *Cell* 2013, 152:1173-1183.

27. Griffith KL, Grossman AD: Inducible protein degradation in *Bacillus subtilis* using heterologous peptide tags and adaptor proteins to target substrates to the protease ClpXP. *Mol Microbiol* 2008, 70:1012-1025.

28. McGinness KE, Baker TA, Sauer RT: Engineering controllable protein degradation. *Mol Cell* 2006, 22:701-707.

29. Schneider JP, Basler M: Shedding light on biology of bacterial cells. *Philos Trans R Soc Lond B Biol Sci* 2016, 371.

30. Escobar MA, Dandekar AM: *Agrobacterium tumefaciens* as an agent of disease. *Trends Plant Sci* 2003, 8:380-386.

31. Gelvin SB: *Agrobacterium*-mediated plant transformation: the biology behind the "gene-jockeying" tool. *Microbiol Mol Biol Rev* 2003, 67:16-37.

32. Nester EW: *Agrobacterium*: nature's genetic engineer. *Front Plant Sci* 2014, 5:730.

33. Imam J, Singh PK, Shukla P: Plant microbe interactions in post genomic era: perspectives and applications. *Front Microbiol* 2016, 7:1488.

34. Subramoni S, Nathoo N, Klimov E, Yuan ZC: *Agrobacterium tumefaciens* responses to plant-derived signaling molecules. *Front Plant Sci* 2014, 5:322.

35. Yuan ZC, Williams M: A really useful pathogen, *Agrobacterium tumefaciens*. *Plant Cell* 2012, 24:tpc 112 tt1012.

36. Alvarez-Martinez CE, Christie PJ: Biological diversity of prokaryotic type IV secretion systems. *Microbiol Mol Biol Rev* 2009, 73:775-808.

37. Pitzschke A: *Agrobacterium* infection and plant defense-transformation success hangs by a thread. *Front Plant Sci* 2013, 4:519.

38. Kuru E, Tekkam S, Hall E, Brun YV, Van Nieuwenhze MS: Synthesis of fluorescent D-amino acids and their use for probing peptidoglycan synthesis and bacterial growth *in situ*. *Nat Protoc* 2015, 10:33-52.

39. Wang J, Han Y, Yang R, Zhao X: Optimization of labeling and localizing bacterial membrane and nucleus with FM4-64 and Hoechst dyes. *Wei Sheng Wu Xue Bao* 2015, 55:1068-1073.

40. Curtis PD, Brun YV: Identification of essential alphaproteobacterial genes reveals operational variability in conserved developmental and cell cycle systems. *Mol Microbiol* 2014, 93:713-735.

41. Kim J, Heindl JE, Fuqua C: Coordination of division and development influences complex multicellular behavior in *Agrobacterium tumefaciens*. *PLoS One* 2013, 8:e56682.

42. de Jong IG, Beilharz K, Kuipers OP, Veening JW: Live cell imaging of *Bacillus subtilis* and *Streptococcus pneumoniae* using automated time-lapse microscopy. *J Vis Exp* 2011, 53.

43. Turnbull L, Strauss MP, Liew AT, Monahan LG, Whitchurch CB, Harry EJ: Super-resolution imaging of the cytokinetic Z ring in live bacteria using fast 3D-structured illumination microscopy (f3D-SIM). *J Vis Exp* 2014:91.

44. Zeng L, Golding I: Following cell-fate in *E. coli* after infection by phage lambda. *J Vis Exp* 2011:56.

45. Brown PJ, de Pedro MA, Kysela DT, Van der Henst C, Kim J, De Bolle X, Fuqua C, Brun YV: Polar growth in the alphaproteobacterial order Rhizobiales. *Proc Natl Acad Sci U S A* 2012, 109:1697-1701.

Chapter 3

Absence of the polar organizing protein PopZ causes aberrant cell division in *Agrobacterium tumefaciens*

Adapted from:

Howell, M., Aliashkevich, A., Salisbury, A. K., Cava, F., Bowman, G. R., & Brown, P. J. B.: Absence of the polar organizing protein popz results in reduced and asymmetric cell division in *Agrobacterium tumefaciens*. *J Bacteriol* 2017, 199:e00101-17.

ABSTRACT

Agrobacterium tumefaciens is a rod-shaped bacterium that grows by polar insertion of new peptidoglycan during cell elongation. As the cell cycle progresses, peptidoglycan synthesis at the pole ceases prior to insertion of new peptidoglycan at mid-cell to enable cell division. The *A. tumefaciens* homolog of the *Caulobacter crescentus* polar organelle development protein PopZ has been identified as a growth pole marker and a candidate polar growth promoting factor. Here, we characterize the function of PopZ in cell growth and division of *A. tumefaciens*. Consistent with previous observations, we observe that PopZ localizes specifically to the growth pole in wildtype cells. Despite the striking localization pattern of PopZ, we find the absence of the protein does not impair polar elongation or cause major changes in the peptidoglycan composition. Instead, we observe an atypical cell length distribution including minicells, elongated cells, and cells with ectopic poles. Most minicells lack DNA, suggesting a defect in chromosome segregation. Furthermore, the canonical cell division proteins FtsZ and FtsA are misplaced, leading to asymmetric sites of cell constriction. Together these data suggest that PopZ plays an important role in the regulation of chromosome segregation and cell division.

IMPORTANCE

A. tumefaciens is a bacterial plant pathogen and a natural genetic engineer. Yet, very little is known about the spatial and temporal regulation of cell wall biogenesis that leads to polar growth in this bacterium. Understanding the molecular basis of *A. tumefaciens* growth may allow for the development of innovations to prevent disease or to promote

growth during biotechnology applications. Finally, since many closely related plant and animal pathogens exhibit polar growth, discoveries in *A. tumefaciens* may be broadly applicable for devising antimicrobial strategies.

INTRODUCTION

Agrobacterium tumefaciens, the causative agent of crown gall disease in flowering plants, has been studied extensively with regard to pathogenesis and its ability to transfer engineered DNA to plant cells using the type IV secretion system encoded by multiple *vir* genes. More recent observations of *A. tumefaciens* growth have revealed that this bacterium exhibits polar growth during elongation [1,2]. In *A. tumefaciens*, as well as other Rhizobiales, peptidoglycan is inserted at the new poles created by cell division until the cell doubles in length. The peptidoglycan synthesis is then directed to mid-cell to enable septum formation and cell division. The growth patterning of *A. tumefaciens* suggests that both spatial and temporal regulation are necessary to restrict cell wall biosynthesis to the pole during elongation and to mid-cell during cell division.

Many of the genes encoding canonical proteins known to function in cellular elongation, including MreB, MreC, MreD, RodA, PBP2 and RodZ, are absent from the *A. tumefaciens* genome; however, the genes encoding the cell division machinery are well conserved [1,3,4]. Remarkably, studies on the dynamics of FtsZ and FtsA suggest that both proteins have an expanded role contributing to the regulation of peptidoglycan biosynthesis not only at the mid-cell, but the growth pole as well [1,5,6]. FtsZ and FtsA persist at the growth pole and the delocalization of these proteins from the growth pole coincides with the transition of the growth pole to an inert, old pole [6]. Once delocalized from the pole, FtsZ and FtsA sequentially appear at mid-cell prior to the initiation of

peptidoglycan biosynthesis at mid-cell [5]. When the bacterium divides, FtsZ and FtsA are retained at the new cell poles formed from the division plane. These observations have led to the suggestion that a combination of cell division machinery and novel proteins are required for polar elongation [3].

What types of novel proteins may function in polar elongation? In many diverse bacteria, poles can act as a subcellular hub for proteins involved in cell development [7]. Among the alphaproteobacteria, polar organizing proteins are best described in *Caulobacter crescentus*. In *C. crescentus* PopZ ($PopZ_{Cc}$) localizes to the new pole, where it interacts with ParB and other chromosome partitioning machinery to segregate the chromosome [8-10]. $PopZ_{Cc}$ also localizes to the old pole, where it does not tether the chromosome, but rather functions in the localization of polar regulatory proteins, including histidine kinases which function in cell cycle control [8,10]. *A. tumefaciens* PopZ ($PopZ_{At}$) does not exhibit bipolar localization, but rather is found strictly at the new pole [5] and accumulates in ectopic poles formed in a mutant with cell division defects [11]. Based largely on its strict localization to growing poles, the polar organizing protein, PopZ, has been identified as a candidate protein for promoting polar growth in *A. tumefaciens* [5,11].

Here we characterize the role of PopZ in the regulation of growth patterning, polarity, and cell division of *A. tumefaciens*. Surprisingly, we find that polar elongation and biosynthesis of polar structures continues in the absence of PopZ; however, the loss of PopZ causes morphological defects indicative of a block in cell division. Furthermore, the cell division proteins FtsZ and FtsA are often misplaced, leading to the production of

asymmetric sites of constriction and a broad cell length distribution. A high proportion of cells lacking PopZ are devoid of DNA, suggesting a conserved function in chromosome segregation. Together, these results indicate that PopZ has a critical role in the regulation of cell division despite its strict growth pole localization pattern.

MATERIALS AND METHODS

Bacterial strains, plasmids, and growth conditions. A list of all bacterial strains and plasmids used in this study is provided in Table 3.S1. *Agrobacterium tumefaciens* C58C1 and derived strains were grown in ATGN minimal medium [12] without exogenous iron at 28°C with shaking. When appropriate, kanamycin was used at the working concentration of 300 μg/ml. When indicated, isopropyl β-D-1-thio-galactopyranoside (IPTG) was used as an inducer at a concentration of 1 mM.

Construction of strains and plasmids A list of all strains and plasmids used in this study is provided in Table 3.S1. To construct expression vectors for *popZ*-sf*gfp* and derived truncations, the respective coding sequence was amplified from genomic DNA, digested using restriction enzymes, and ligated into pSRKKm-Plac-sf*gfp* [13] using T4 ligase. Primers used for the construction of each *popZ* fragment are listed in Table 3.S2.

To construct an expression vector for *ftsA*-sf*gfp* under the control of the native promoter a gBlock (IDT; Table 3.S2) that contains the *qaz* promoter and a multiple cloning site was digested with *Eco*RI and *Hind*III and inserted into pSRKKm-Plac-sf*gfp* creating pSRKKM-P*qaz-sfgfp.* Next the *ftsA* coding sequence was amplified using the primers

indicated in Table 3.S2 and inserted into pSRKKM-P*qaz-sfgfp* to construct pSRKKM-P*qaz-ftsA-sfgfp*.

To construct an *ftsZ*-sf*gfp* expression vector, we amplified the *ftsZ* coding sequence (see Table 3.S2) and inserted *ftsZ* into pSRKKm-Plac-sf*gfp*. *ftsZ-sfgfp* was not expressed well from the *lac* promoter. Thus, *ftsZ-sfgfp* was amplified from pSRKKm-Plac-*ftsZ*-sf*gfp* and inserted into pRVGFPC-2 [14] digested with *Nde*I and *Eco*RI to remove GFP. *ftsZ-sfgfp* amplification was digested then ligated into the digested vector to create PRV-*ftsZ-sfgfp*. In *A. tumefaciens*, this vector provides a low level of constitutive expression of *ftsZ*.

The coding sequences for *fliM* and *yfp* were amplified from the *A. tumefaciens* genome or a source plasmid respectively using the primers indicated in Table 3.S2. The two fragments were cloned into plasmid pSRKKM [15] cut with *Nde*I and *Hind*III by isothermal cloning [16]. This plasmid (pGB1246) was transformed into *Agrobacterium* C58C1 strains with and without *popZ* [17].

All expression vectors were transformed into C58C1 and C58C1Δ*popZ* [17] , and C58C1 Δ*popZ::mchy-popZ* [17] as indicated using standard electroporation conditions [18].

Phase and Fluorescence microscopy. A small volume (~0.8 μl) of cells in exponential phase (OD_{600} = 0.4 - 0.6) was applied to a 1% agarose pad as described previously [1]. Phase contrast and epifluorescence microscopy were performed with an inverted Nikon Eclipse TiE and a QImaging Rolera em-c^2 1K EMCCD camera with Nikon Elements Imaging Software. To visualize DNA, cells were grown in ATGN medium to exponential phase and ethanol fixed. Cells were resuspended in phosphate buffered saline (PBS)

containing 1ug/ml of 4',6-diamidino-2-phenylindole dihydrochloride (DAPI) for 5 minutes. Excess dye was washed out with PBS and cells were imaged.

Quantification of cell length distributions. Cells were grown overnight in ATGN. Cells were diluted in ATGN to an OD_{600} = 0.10 and allowed to grow until reaching an OD_{600} = 0.4 - 0.6. Live cells were imaged using phase contrast microscopy and cell length distributions of at least 800 cells per strain were determined using the longest medial axis as measured by MicrobeJ software [19].

Localization of PopZ-GFP Truncations. Cells were grown overnight in ATGN in the presence of 1mM IPTG and kanamycin (300 μg/ml). Cells were diluted to an OD_{600} = 0.10 and allowed to grow until reaching an OD_{600} = 0.4 - 0.6. Live cells were then placed onto a 1.25% agarose ATGN pad and phase contrast and epifluorescence microscopy was performed.

Unipolar polysaccharide (UPP) labeling. Wheat germ agglutinin lectin conjugated to AlexaFluor488 (WGA-AF488) (Life Technologies) was used to detect polar polysaccharide in *A. tumefaciens.* In all experiments, a concentration of 0.5 μg/ml of WGA-AF488 was used and exponential phase cells were incubated for 30 minutes before excess lectin was removed by washing. 1 μl of washed culture was spotted on an agarose pad and cells were imaged.

Short-term binding assay. The short-term binding assay was conducted as described [20] with slight modifications. Briefly, bacteria were grown to exponential phase and 2 mL of culture at OD_{600} = 0.4 was placed in each well of a 6-well plate containing a glass coverslip and incubated for 1 hour. Planktonic cells were removed, and coverslips were

washed by pipetting media over the surface of the coverslip at least 4 times. Excess liquid was wicked off from the coverslip and the coverslip was inverted onto a microscope slide and immediately imaged.

Biofilm assay. Biofilm assays were conducted as described by [20]. Briefly, bacteria were grown to mid-log phase in ATGN media and diluted to OD_{600} = 0.03. 3 ml of diluted bacteria were placed in the wells of 12-well polystyrene plates containing polyvinyl chloride coverslips placed vertically in each well. Plates were incubated at room temperature for 48 hours. After incubation, OD_{600} of cultures from each well were measured to normalize for the density of cell culture. Coverslips were then removed and rinsed with distilled water (dH_2O) to remove planktonic cells. Coverslips were stained with 0.1% weight/volume crystal violet for 5-10 minutes and destained with 33% acetic acid. A_{600} of the solubilized crystal violet was measured. The biofilm score was calculated as the A_{600}/OD_{600} to allow for normalization based on cell density of each strain. Two biological replicates were completed in triplicate for each experiment.

FliM-YFP microscopy and image analysis. Cells were grown to exponential phase in ATGN and induced with 400 µM IPTG for 2-3 hours prior to time-lapse observation by fluorescence microscopy (as described in [21]) on ATGN-agarose pads. To determine the rate of cell growth and the movement of FliM-YFP foci from the nearest cell pole, the measuring tool in Zen software (Zeiss) was used to make length measurements at each time point. Measuring every available interval from 34 different cells from two independent experiments yielded a total number of 72 intervals.

Quantification of cell morphologies and FDAA labeling patterns. Cells were grown overnight in ATGN media, and diluted in the same conditions to an OD_{600} = 0.10 and

allowed to grow until reaching an OD_{600} = 0.4 - 0.6. At this point cells were labeled with the fluorescent-D-amino acid (FDAA) HCC-amino-D-alanine (HADA) as previously described [2]. Immediately following labeling, cells were ethanol fixed to prevent further growth. Phase contrast and epifluorescence microscopy was performed. 150 cells for each strain were used to quantify the three morphological categories: normal (>1.5 um without branches), small (<1.5 um), and branched (containing 3 or more poles) using ImageJ cell counter plugin. These cells were further subdivided based on differential FDAA labeling among the three morphologies.

Peptidoglycan compositonal analysis. Cell cultures were grown overnight in 3-ml culture tubes of ATGN minimal media at 28°C with shaking. The 3-ml cultures were then added to 50-ml flasks of fresh ATGN and allowed to grow under the same conditions until reaching an exponential phase OD_{600} of 0.5-0.6. Cultures were then pelleted by centrifugation at 4,000 x *g* for 15 minutes. Pellets were resuspended in a solution of 3 ml ATGN and 6 ml of 6% SDS. Cells were boiled while simultaneously stirred by magnetic bars for 4 hours. After 4 hours, boiling was halted, but aggitation was continued overnight. Peptidoglycan was pelleted by centrifuging for 13 minutes at 60,000 rpm (TLA100.3 Beckman rotor; Optima Max-TL ultracentrifuge Beckman), and the pellets were washed 3-4 times by repeated cycles of centrifugation and resuspension in water. The pellet from the final wash was resuspended in 50 µl of 50 mM sodium phosphate buffer pH 4.9, and subjected to overnight digestion with 100 µg/ml of muramidase (ThermoFisher) at 37ºC. Muramidase digestion was stopped by boiling for 4 min. Coagulated protein was removed by centrifugation for 15 min, 15,000 rpm in a desk-top microcentrifuge. The muropeptides were mixed with 15 µl 0.5 M sodium borate,

and subjected to reduction of muramic acid residues into muramitol by sodium borohydride (10 mg/ml final concentration, 20 minutes at room temperature) treatment. Samples were adjusted to pH 3-4 with orthophosphoric acid and filtered (0.2-μm filters).

Analysis of muropeptides was performed on an ACQUITY Ultra Performance Liquid Chromatography (UPLC) BEH C18 column, 130Å, 1.7 μm, 2.1 mm x 150 mm (Water, USA) and detected at Abs. 204 nm with an ACQUITY UPLC UV-visible detector. Muropeptides were separated using a linear gradient from buffer A (sodium phosphate buffer 50 mM pH 4.35) to buffer B (sodium phosphate buffer 50 mM pH 4.95 methanol 15% (v/v)) with a flow of 0.25 mL/minute in a 20 minute run. Individual muropeptides were quantified from their integrated areas using samples of known concentration as standards. Muropeptide abundance was statistically compared using unpaired t-test.

Distribution of constriction sites. Exponential phase cells were first labeled with lipophilic dye FM4-64, which preferentially labels the old pole [6]. 15 fields of cells were imaged with phase and epifluorescence microscopy. Cells were detected and the position of constrictions was determined using MicrobeJ [19]. Cells were orientated by defining the old pole as the pole with the most intense FM4-64 labeling. Potential constriction sites were identified using a local maxima algorithm to identify the lowest width value along the width profile excluding both ends of the medial axis [19]. For each potential constriction, the ratio of the median cell width/minimal cell width is calculated. Thus, larger ratio values represent deeper constrictions. A threshold of a 0.44 ratio value was used to indentify deep constrictions. The longitudinal position of the constriction site was plotted against the cell length. A value of 0 denotes mid-cell, negative numbers represent positions closer to the old pole, and positive numbers represent positions closer to the

new pole. Additionally, histograms plotting the relative logitudinal position of the septum were plotted on a cell outline.

RESULTS

Loss of PopZ causes cell division defects, ectopic pole formation, and minicell formation

To determine the role of PopZ in *A. tumefaciens*, a Δ*popZ* deletion strain was constructed in which the native gene of *popZ* was replaced with a genetic cassette bearing spectinomycin resistance [17]. The Δ*popZ* cells have a doubling time that is approximately 40% longer than wildtype cells (~167 minutes for Δ*popZ* compared to ~120 minute for wildtype cells [17]) and display a range of morphological defects including ectopic poles, bulged side walls, and abnormal cell lengths (Figure 3.1). In wildtype C58 C1 (WT) cells, less than 1% of the population display branches or bulges, while these phenotypes are observed in 40% of the Δ*popZ* population.

The morphological defects observed in Δ*popZ* result in a broader cell length distribution, including both increases in short and long cells (Figure 3.1B). In WT, 94% of the cells are between 1.5 and 3.5 μm in length, while only 70% of Δ*popZ* cells fall into this range. Remarkably, we observed a marked increase in the percentage of cells with lengths less than 1.5 μm in Δ*popZ* (29% Δ*popZ* cells compared to 6% in WT cells). To determine if the small cells contain DNA, we stained ethanol-fixed cells with DAPI to visualize the DNA (Figure 3.1D). Many of the small cells lack DNA and appear to arise from cell divisions near the pole prior to the completion of chromosome segregation. Furthermore,

we observed cells of typical cell lengths (between 1.5 – 3.5 μm) that lack DNA. These observations are consistent with a role for PopZ in chromosome segregation as described in *Caulobacer crescentus* [8,9]. Notably, replacement of the native *popZ* gene with a translational *mcherry-popZ* fusion mimics wildtype cell morphologies, length distributions, and DNA content, indicating that mChy-PopZ is functional (Figure 3.1).

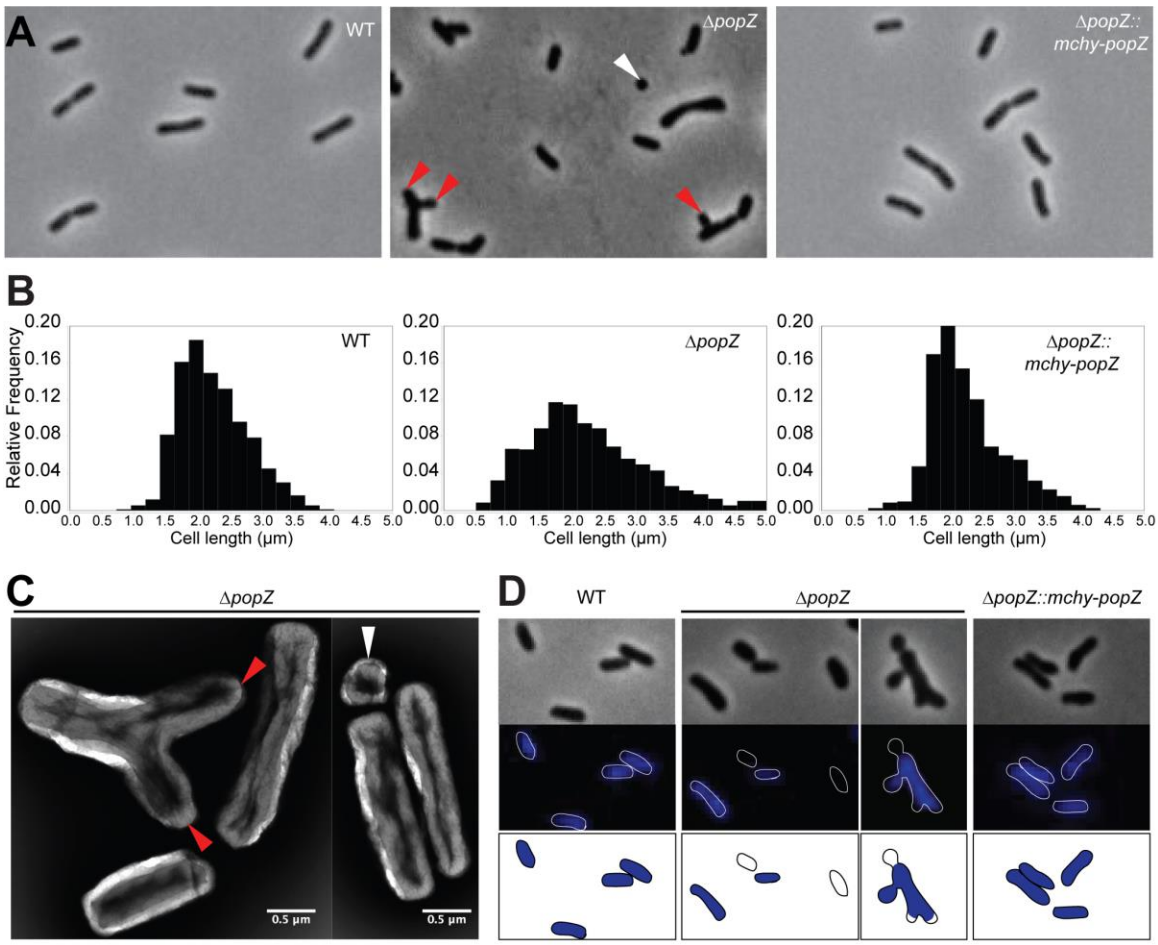

Figure 3.1. Analysis of morphology, cell length, and DNA content of the popZ deletion strain. A) Comparison of phase contrast images of wildtype, Δ*popZ*, and Δ*popZ::popZ-mcherry* strains grown to exponential phase in ATGN medium. The Δ*popZ* culture contains a high proportion of small cells (<1.5 μm in length; white arrowhead) and branched cells with ectopic poles (red arrowheads). B) Cell length distributions of WT cells (left; n=926), Δ*popZ* (center; n=1,664), and Δ*popZ::popZ-mchy* (n = 839) are shown. C) Transmission electron micrographs of nano-tungsten stained Δ*popZ* cells. The deletion of *popZ* results in an increased cell length distribution, including very small cells (white arrowhead) and cells with ectopic poles (red arrowheads). Scale bars = 0.5 μm. D) DAPI staining reveals the presence of anucleate cells in the Δ*popZ* population. Phase

(top) and fluorescent (middle) images of representative DAPI stained wildtype, Δ*popZ*, and Δ*popZ::popZ-mchy* cells are shown. Outlines are provided to indicate cell location in fluorescent images. Schematics of DAPI stained cells are provided in the bottom panel.

PopZ$_{R2-R3}$-sfGFP localizes to the new pole but does not rescue morphology defects

A previous report shows that in *A. tumefaciens*, PopZ localizes to the growing pole during cell elongation and arrives at the two newly formed poles just after cell division [5]. We observed the same localization pattern using a low copy plasmid with an IPTG-inducible *popZ-sfgfp* in a WT (Figure 3.2A top) and Δ*popZ* background (Figure 3.2A bottom). This construct was able to rescue the morphological defects of the *popZ* deletion, indicating that PopZ-sfGFP is functional (Figure 3.2B).

The PopZ protein is conserved among many alphaproteobacteria and typically contains three domains: R1 (aa 1-25) is an N-terminal domain containing an alpha helix, R2 (aa 26-258) is the central proline-rich domain, and R3 (aa 259-333) is the C-terminal domain containing multiple alpha helices [22,23]. Here, we sought to determine which of the PopZ domains are necessary for proper subcellular localization. Thus, we constructed truncations of PopZ fused to sfGFP at their C-termini which are present in both WT and Δ*popZ* backgrounds (Supplemental Figure 3.S1). In a WT background we noted that the R3 domain was necessary and sufficient for polar localization (Figure 3.2B, top). In the absence of native PopZ, however, the R3 domain was not sufficient for polar localization, and instead proper subcellular localization required both the R2 and R3 domains (Figure 3.2B, bottom). Although the PopZ R2-R3 domain is sufficient for polar localization of sfGFP, it does not rescue the morphological defects, suggesting a functional role for the R1 domain in *A. tumefaciens*. In *C. crescentus*, the conserved R1 domain of PopZ is required for interactions with chromosome portioning proteins ParA and ParB, and these interactions are required for proper cell division and chromosome segregation [24]. Indeed, none of the PopZ truncations could rescue the morphological defects in the

Δ*popZ* strain (Figure 3.2B), indicating that the three domains each have important contributions to PopZ function in *A. tumefaciens*.

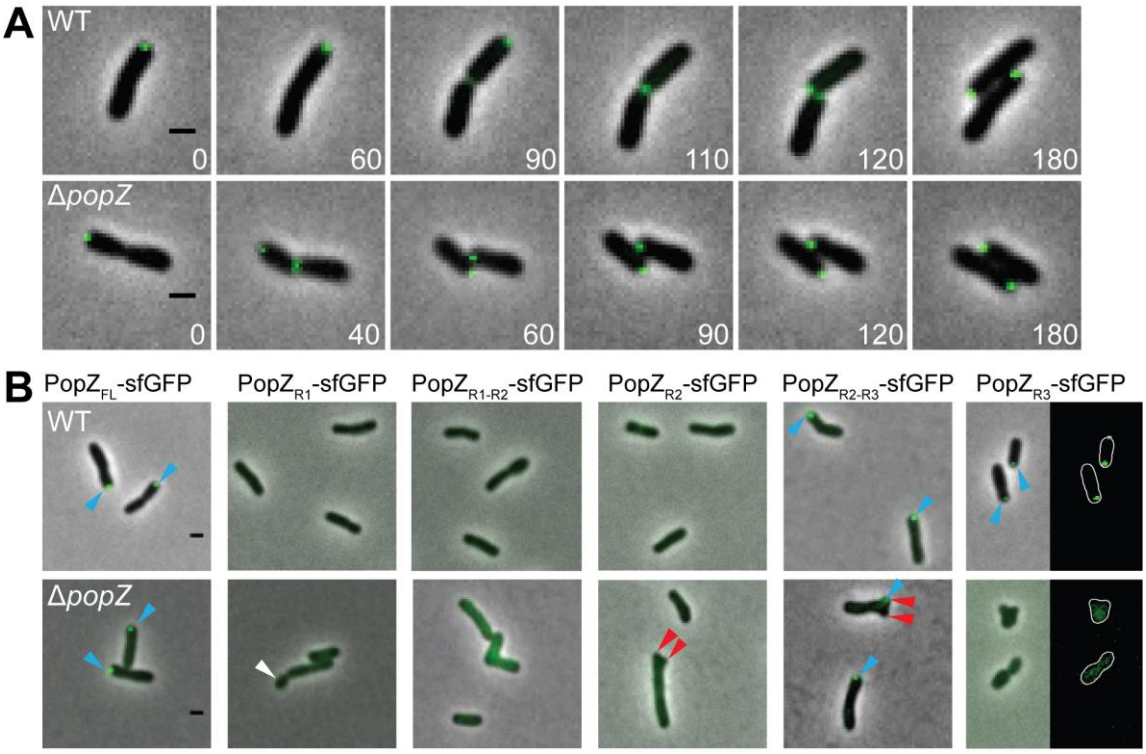

Figure 3.2. Polar localization of PopZ requires domains R2 and R3. A) Top panel: Timelapse microscopy of WT cells expressing full-length PopZ-sfGFP ($PopZ_{FL}$-sfGFP) reveals a new pole to mid-cell localization pattern. Bottom panel: $PopZ_{FL}$-sfGFP exhibits a similar localization pattern in Δ*popZ*. B) Representative images of the localization patterns of full-length and truncated versions of PopZ-sfGFP in WT and Δ*popZ* cells are shown. In WT cells, PopZ truncations containing domain R3 ($PopZ_{FL}$-sfGFP, $PopZ_{R2\text{-}R3}$-sfGFP and $PopZ_{R3}$-sfGFP) localize to growth poles (blue arrowheads). In the absence of PopZ, only the $PopZ_{FL}$-sfGFP and $PopZ_{R2\text{-}R3}$-sfGFP localize to growth poles (blue arrowheads). Truncated forms of PopZ do not complement the morphological defects of Δ*popZ* cells as indicated by the presence of small cells (white arrowheads) and ectopic poles (red arrowheads). All scale bars are 1 μm.

PopZ is not required for unipolar polysaccharide biosynthesis nor adhesion to abiotic surfaces

The subcellular localization pattern of PopZ in *A. tumefaciens* indicates that PopZ may function specifically at the new pole, which is the site of unipolar polysaccharide (UPP) biosynthesis, flagellum biosynthesis, and peptidoglycan biosynthesis during cellular elongation [25,26]. In order to determine if PopZ contributes to any of these processes, we examined the biosynthesis of each structure in WT and Δ*popZ* cells.

First, we determined the role of PopZ in the production and function of UPP. The UPP was detected using wheat germ agglutinin conjugated to Alexa Fluor 488 (WGA-488; Figure 3.3A). In WT, Δ*popZ*, and Δ*popZ::mchy-popZ* cell populations, UPP was detected at the pole in approximately 20% of the cells. In Δ*popZ,* the UPP is typically found at one pole; however, some cells with ectopic poles have UPP at multiple poles (Figure 3.3A). In order to assess if the UPP retained its function in surface attachment, we completed short-term binding assays (Figure 3.3B). Surprisingly, after 1 hour we observed a significant increase in the number of cells bound to a glass coverslip in the absence of *popZ*. Remarkably, the Δ*popZ* cells seem to form large aggregates that tightly bind to the glass coverslip. In addition, the loss of *popZ* results in a significant increase in biofilm formation after 48 hours (Figure 3.3C). While the biosynthesis and localization of the UPP do not seem to be disrupted in Δ*popZ* cells, these cells do exhibit increased surface attachment. It is possible that the quantity of UPP has increased due to a cell cycle perturbation, causing the cells to produce UPP for a longer duration, that adhesive and cohesive properties of the UPP have been modified, or that the production of another polysaccharide which contributes to surface attachment has been altered. Indeed, the *A. tumefaciens* genome indicates the presence of at least six biosynthetic pathways for

polysaccharides, including cellulose and succinoglycan, which may contribute to attachment and biofilm formation [25], and the observation of large aggregates formed by the Δ*popZ* cells is reminiscent of aggregates formed when cellulose is overexpressed [27].

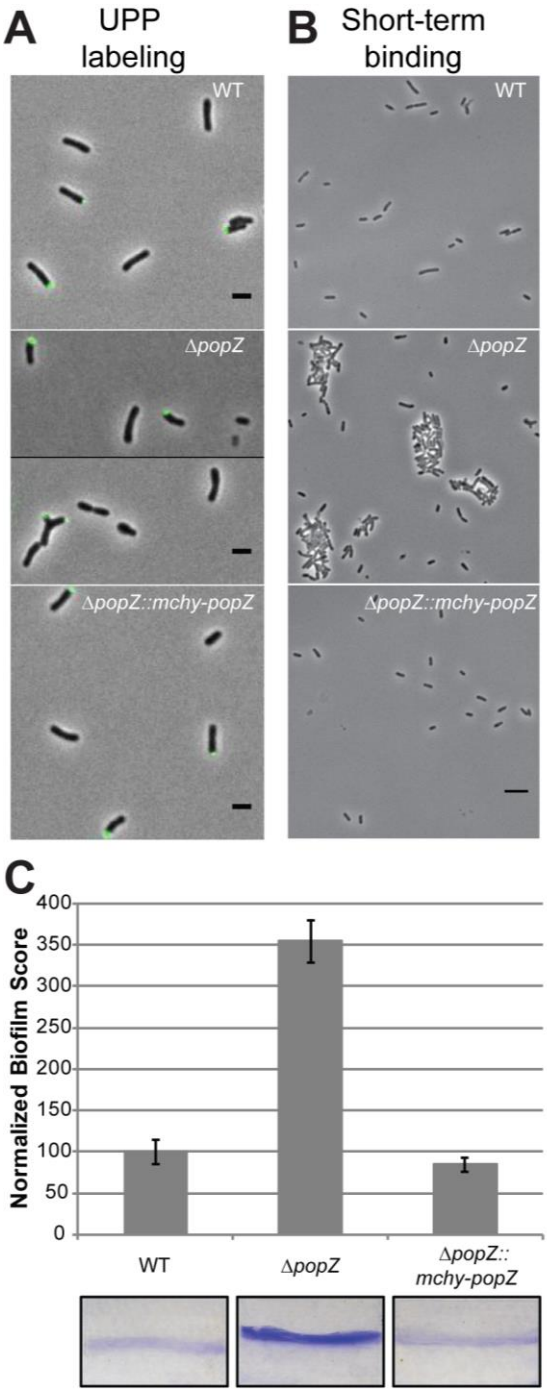

Figure 3.3. Analysis of biofilm formation in wildtype and Δ*popZ* mutants. A) UPP production and placement was identified by the binding of Alexa Fluor 488-labeled wheat germ agglutinin to cells on 1.5% agarose pads. In all three strains, approximately 20% of individual cells have a detectable UPP. Scale bars = 2 µm. B) Short-term binding was evaluated after 1 hour of attachment to glass coverslips. Scale bar = 5 µm. C) Strains were assayed for biofilm formation on vertical plastic coverslips immersed in ATGN media. Coverslips were removed after 48 hours of incubation at room temperature and rinsed to remove any loosely associated cells. Adherent biomass was determined as the absorbance of solubilized crystal violet (A_{600}) and the optical density of the planktonic culture (OD_{600}) was measured. Biofilm scores were calculated as the ratio of A_{600}/OD_{600} and data were normalized to WT. Data shown are the mean of two independent experiments completed in triplicate. Error bars are the standard error of the

mean. Representative coverslips prior to crystal violet solubilization are shown for each strain.

Flagellum placement is independent of PopZ

To determine the role of *A. tumefaciens* PopZ in the production of flagella, a fluorescently tagged basal body protein (FliM-YFP) was used to track the position of flagella relative to mChy-PopZ (Figure 3.4A). We observe that FliM-YFP foci are found near the pole containing mChy-PopZ, consistent with previous reports of subpolar flagella in *A. tumefaciens* [28]. Timelapse microscopy illustrates that as the cell elongates, the distance between the pole and FliM-YFP increases, indicating that the flagella remain fixed as new cell wall material is inserted at the growth pole. Indeed, the change in FliM-YFP distance from the pole is highly correlated with the increase in cell length (Figure 3.4B). When FliM-YFP is expressed in Δ*popZ* cells, FliM-YFP is observed in subpolar foci (Figure 3.4C). The distance of the FliM-YFP foci from the pole increases as the cells elongate, suggesting the basal bodies of the flagella are properly assembled in the Δ*popZ* cells, which is consistent with observations of motile cells in planktonic culture (data not shown) despite a slight defect in motility in swim plate assays (Supplmental Figure 3.S2) due to defects in cell morphology and division. Furthermore, the observation that the distance of basal bodies from the poles increases as the cells get longer suggests that Δ*popZ* cells are continuing to insert newly synthesized peptidoglycan at the growth pole, and this polar organizing protein may not be involved in organizing polar growth.

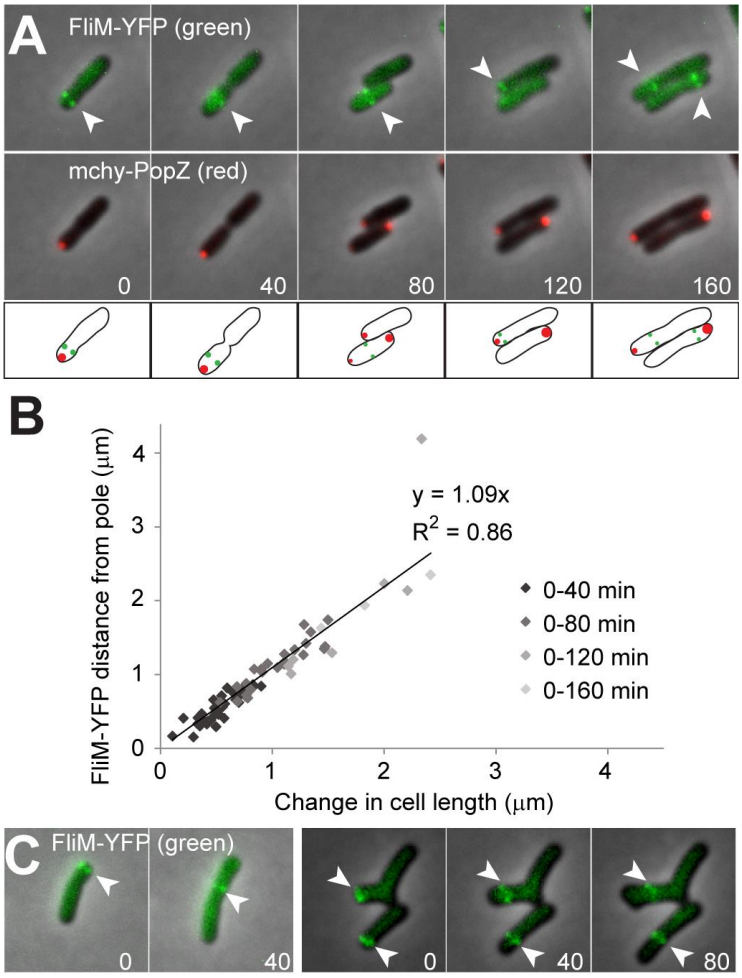

Figure 3.4. Analysis of flagellum localization in wildtype and Δ*popZ* mutants. A) Flagellar basal bodies were fluorescently labeled by expressing FliM-YFP, and their localization patterns (green) were observed by timelapse fluorescence microscopy in cells that also express Mchy-PopZ (red). FliM-YFP foci are indicated by arrowheads. Fluorescence images are overlayed on a phase contrast background, and time in minutes is shown in the lower corners of image panels. Schematics are provided below the images. B) For cells in A, a scatterplot compares the increase in cell length to the increase in the distance of the FliM-YFP foci from the cell poles. A total of 34 cells were measured in 2 independent experiments, and the slope of the linear regression and associated R-squared value is shown. There are fewer data points for later time points because most cells divided during the time course. C) Fluorescence localization of FliM-YFP (green) in Δ*popZ* cells.

Polar growth is retained in the absence of PopZ

Due to the predicted molecular scaffolding properties of PopZ, as well as its localization to the growth pole, PopZ has been hypothesized to function in unipolar growth of *A. tumefaciens* [5,11]. While our tracking of flagella basal bodies suggests that polar insertion of peptidoglycan continues in the Δ*popZ* cells, we used fluorescent-D-amino acids (FDAAs) to probe the growth pattern in the presence and absence of PopZ. In WT *A. tumefaciens*, FDAAs are preferentially incorporated into the muropeptide stem of peptidoglycan and reveal the subcellular regions exhibiting active peptidoglycan synthesis [2]. The typical FDAA labeling pattern of *A. tumefaciens* is consistent with three growth stages: (i) polar peptidoglycan synthesis during cellular elongation, (ii) a transition stage in which polar elongation is terminated and mid-cell peptidoglycan synthesis is initiated and (iii) strict mid-cell peptidoglycan synthesis enabling new growth active poles to form following cell division [2]. In the absence of PopZ polar growth is retained across three morphology types: (i) rod shaped, (ii) small, and (iii) branched/bulged (Figure 3.5). When Δ*popZ* cells retain their rod shape and typical cell length (1.5 – 3.5 μm), FDAA labeling indicates that peptidoglycan synthesis occurs at the pole and mid-cell (Figure 3.5A-D). 29% of *ΔpopZ* cells are shorter than 1.5 μm in length and the vast majority of these cells do not label with FDAAs (Figure 3.5G). Dual labeling with FDAAs and DAPI staining reveals that 95% (98/103) of small cells lacking active peptidoglycan biosynthesis also lack DNA (Supplemental Figure 3.3). Among the small cells with FDAA labeling, unipolar and bipolar localization was observed (Figure 3.5E-F). 41% of the Δ*popZ* cells have ectopic poles and many of these cells exhibit complex FDAA labeling patterns (Figure 3.5H-L); however, in almost all cells, FDAA labeling occurs exclusively at poles or mid-cell regions. Together, these data suggest that PopZ is

not required for polar growth, but the absence of PopZ allows growth to occur simultaneously from multiple poles.

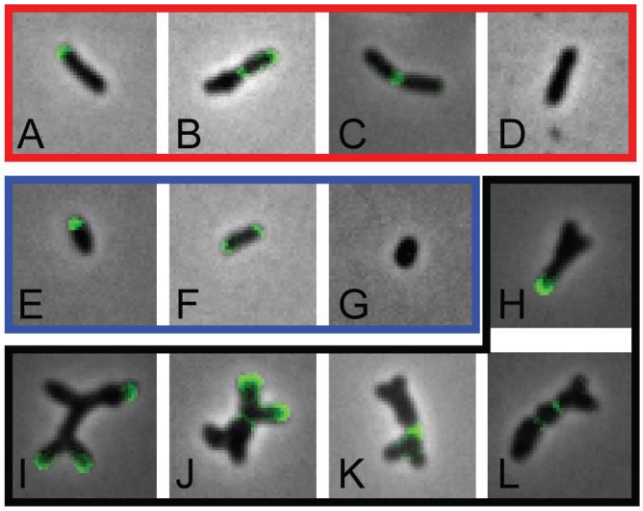

		WT	Δ*popZ*	Δ*popZ*:: *popZ-mchy*
Rod-shaped	A: Unipolar	78%	20%	73%
	B: Unipolar and Midcell	9%	1%	7%
	C: Midcell	1%	2%	2%
	D: None	6%	7%	8%
Small	E: Unipolar	2%	2%	1%
	F: Bipolar	4%	1%	2%
	G: None	0%	26%	7%
Branched	H: Unipolar	ND	17%	ND
	I: Multipolar	ND	15%	ND
	J: Polar and Midcell	ND	5%	ND
	K: Midcell	ND	3%	ND
	L: Other	ND	1%	ND

Figure 3.5. Deletion of *popZ* causes atypical growth patterning. Fluorescent-D-amino acid labeling was used as a proxy for sites of peptidoglycan synthesis in WT, Δ*popZ*, and Δ*popZ::popZ-mchy* strains. Representative images of cellular morphology and growth patterns from the Δ*popZ* mutant are shown (top panel). Patterns observed in typical rod-shaped bacteria (red), small cells (<1.5 μm; blue), and branched cells (black) are shown and quantitated in the table below. 150 cells were labeled and categorized as shown in the table for each strain. Branched cells were not detected (ND) in WT and Δ*popZ::popZ-mchy*.

Loss of PopZ causes minor changes in peptidoglycan composition

Although the FDAA labeling patterns were consistent with maintenance of proper cell wall biosynthesis at discrete subcellular localizations, we next determined if the absence of PopZ impacts peptidoglycan composition (Figure 3.6A). Overall proportions of monomers (~20% of the total muropeptides), dimers (~50%), and trimers (30%) were not statistically different whether PopZ was present or absent (Figure 6B). Further characterization of individual muropeptides does highlight a few subtle differences in the absence of PopZ, such as a decrease in muropeptides containing DD-crosslinks (D43 and D44) and an increase in muropeptides with LD-crosslinks (D33 and D34) (Figure 3.6C-D). These changes may indicate that PopZ regulates directly the activity of a subset of cellular transpeptidases (i.e. DD-transpeptidase penicillin-binding proteins (PBPs) or LD-transpeptidases). Alternatively, the altered cell morphology of the Δ*popZ* cells, in particular the accumulation of ectopic poles, may be responsible for the differences in peptidoglycan composition.

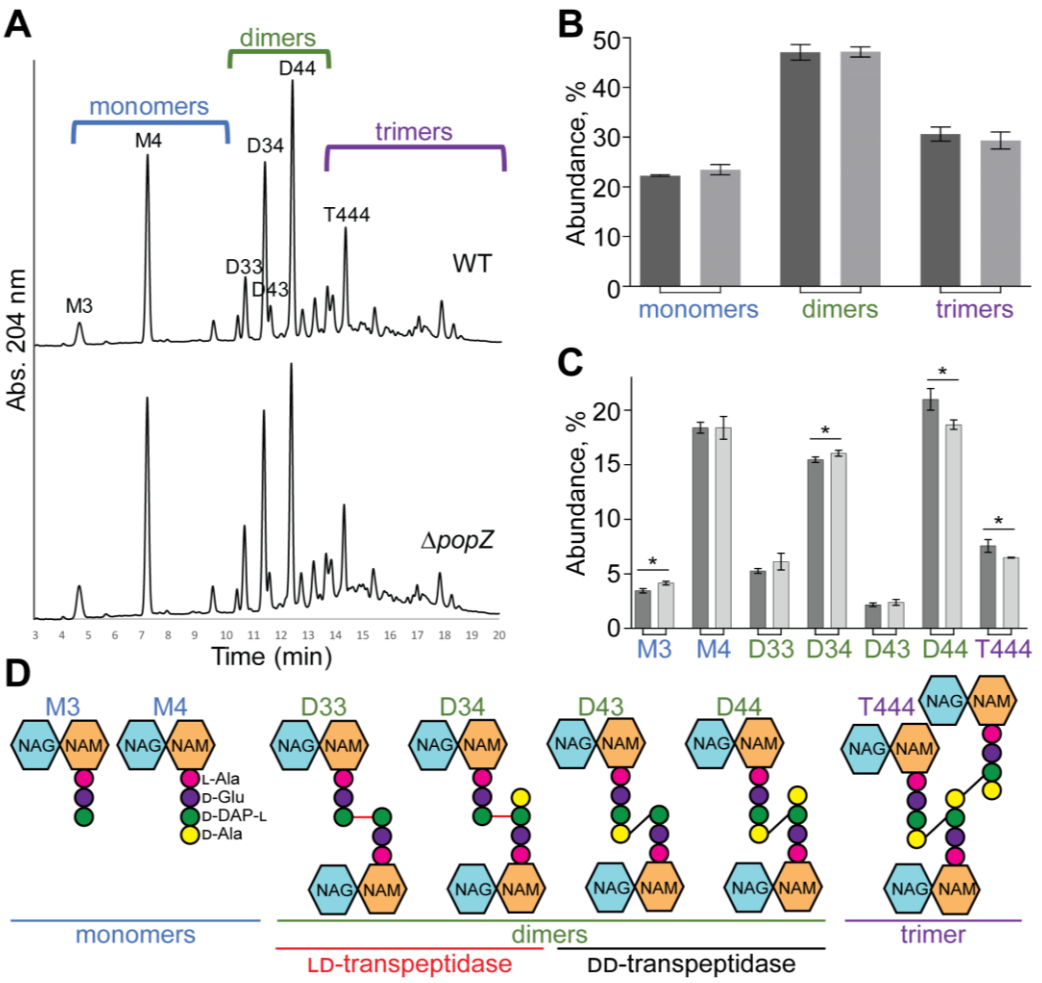

Figure 3.6. Peptidoglycan composition is slightly modified in Δ*popZ* cells. A) UPLC spectra of muropeptides derived from WT or Δ*popZ* cells. Major muropeptides are labeled. M= monomers, D= dimers, T= trimers. Numbers indicate the length of the muropeptide stems and the position of crosslink in dimers and trimers. B) Abundance of total monomers, dimers, and trimers in the muropeptide profile for WT (dark gray) and Δ*popZ* (light gray) cells. C) Quantitation of the major muropeptide peaks in WT (dark gray) and Δ*popZ* (light gray) cells. For C and D, data shown is the average abundance of each muropeptide and is taken from analysis of three independent biological samples. Statistical significance is indicated with an asterisk. D) Schematics of major

muropeptides are shown. The monomers (blue), dimers (green) and trimer (purple) are labeled. Note that the type of crosslink is shown for each dimer and trimer. DD-crosslinks are shown in black and LD-crosslinks are shown in red.

Loss of PopZ results in lower frequency of FtsA ring localization

The accumulation of ectopic poles through sidewall branching and tip splitting as well as the formation of small cells in the Δ*popZ* strain suggests that PopZ may function during the transition from polar peptidoglycan biosynthesis to mid-cell peptidoglycan synthesis to enable cell division. Next, we asked if the localization pattern of the essential cell division protein, FtsA is impaired in Δ*popZ* cells. In *A. tumefaciens*, FtsA localizes at the newly formed poles after cell division and remains at the growth poles during much of the elongation cycle before moving to mid-cell just prior to cell division [3,6]. We expressed *ftsA-sfgfp* under the control of its native promoter in both WT and Δ*popZ* cells (Figure 3.7). The FtsA localization pattern observed in WT cells was consistent with the previous results [3,6] (Figure 3.7A, top). In the absence of PopZ, FtsA-sfGFP is consistently found at the growing pole, dissociates from these poles once growth is terminated, and forms rings as cells divide (Figure 3.7A bottom). In contrast to WT cells, we observe that in Δ*popZ* cells, FtsA rings do not form precisely at the mid-cell and the cells do not always divide where a FtsA ring forms. When cell division failure leads to the formation of an ectopic pole, FtsA-sfGFP is present at the new growth pole. In order to better understand FtsA-sfGFP localization patterns in Δ*popZ* cells, we observed the subcellular localization of FtsA-sfGFP in hundreds of individual cells (Figure 3.7B-C). We find that the majority of WT and Δ*popZ* cells have FtsA-GFP at poles, indicating that PopZ is not required for FtsA localization at the growth pole. Next, we quantified cells with FtsA-sfGFP-rings rather than polar foci. In the WT population, 12% of cells undergo the transition from polar growth to mid-cell growth as indicated by the presence of both polar and mid-cell FtsA-sfGFP. In contrast, only 4% of the Δ*popZ* cells have both

polar and mid-cell FtsA-sfGFP localization. Only 7% of Δ*popZ* cells have FtsA-sfGFP present only as a ring, whereas FtsA-sfGFP-rings were present in 11% of the WT population. Together, these data show that nearly a quarter of the WT population have a FtsA-ring, while only ~10% of the Δ*popZ* population have a FtsA-ring. In the Δ*popZ* population, we observe an increase in transient localization of FtsA, often with multiple foci along the cell length (see other category in Figure 3.7B-C). Altogether, these data show that PopZ is not required for polar FtsA foci, nor the ability for FtsA to form a ring-like structure; however, the mislocalization of FtsA and inefficiency of FtsA-ring formation suggests that PopZ may play a role in establishing the proper cell division site.

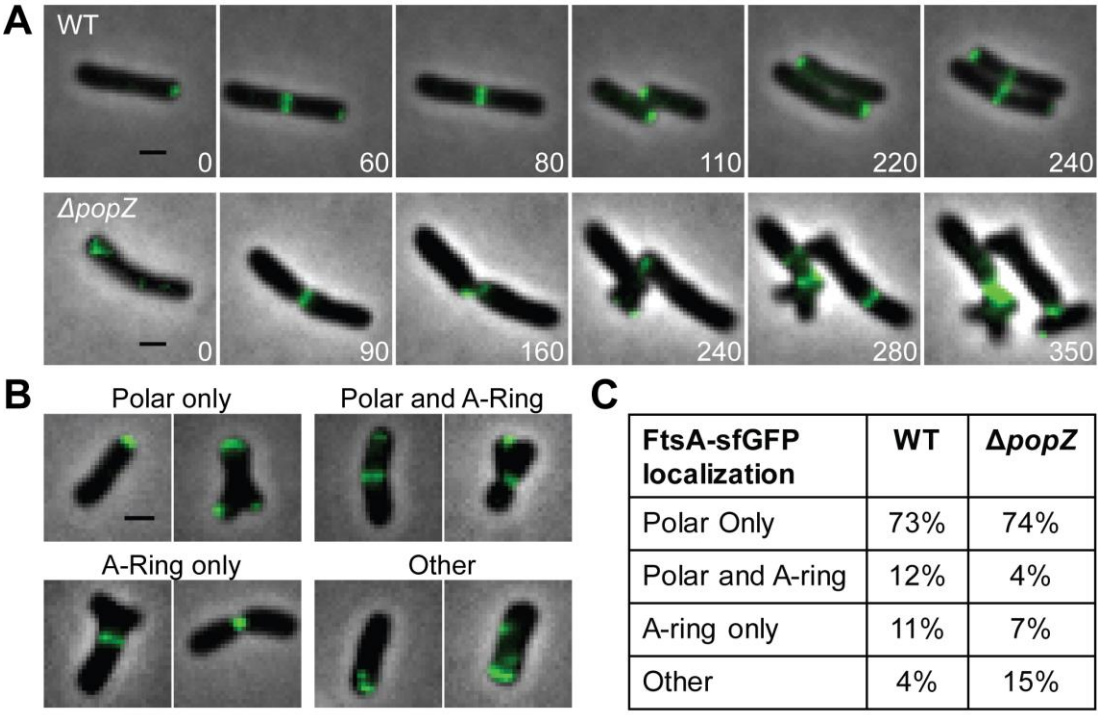

FtsA-sfGFP localization	WT	Δ*popZ*
Polar Only	73%	74%
Polar and A-ring	12%	4%
A-ring only	11%	7%
Other	4%	15%

Figure 3.7. FtsA forms polar foci and rings in Δ*popZ*. A) Timelapse microscopy of FtsA-sfGFP in WT cells (top panel) shows a polar to mid-cell localization pattern. Timelapse microscopy of FtsA-sfGFP in Δ*popZ* (bottom panel) shows cells with unipolar foci, multipolar foci, and both stable and unstable ring structures. B) Representative examples of FtsA-sfGFP localization patterns observed in Δ*popZ* cells. All scale bars are 1 μm. C) Percentage of cells with each category of FtsA-sfGFP localization pattern in WT (309 cells) and Δ*popZ* (328 cells).

Loss of PopZ results in asymmetric Z-rings and constriction sites

The reduction of FtsA-ring formation and production of minicells suggests that there is a cell division defect in the absence of PopZ. To better understand cell division in the Δ*popZ* mutant, the localization pattern of the essential division protein FtsZ when fused to sfGFP (FtsZ-sfGFP) was observed (Figure 3.8). Consistent with previous reports [3,6], in WT cells FtsZ-sfGFP forms a constricting ring at the mid-cell in late predivisional cells (Figure 3.8A, top). Following cell division, FtsZ-sfGFP foci are retained at the new pole for a portion of the cell cycle. As the cells elongate, FtsZ-sfGFP is released from the pole, exhibits transient localization, and then marks the new site of cell division. In Δ*popZ*, FtsZ-sfGFP maintains its ability to form functional FtsZ-rings (Figure 3.8A, bottom); however, the Z-rings formed are less consistent in size, placement, and stability. Timelapse microscopy of Δ*popZ* cells undergoing cell division reveals an unusually wide Z-ring (0 minutes) that marks the site of a cell division event. One of the resulting daughter cells is a short rod-shaped cell that eventually produces an FtsZ-ring at mid-cell (300 minutes); however, this cell does not elongate or divide, suggesting it lacks DNA, and the FtsZ-ring appears to disassemble (740 minutes). The other daughter cell is branched but forms a functional FtsZ-ring near mid-cell (440 minutes), producing two more daughter cells. These daughter cells form functional FtsZ-rings, although one is misplaced near the pole (740 minutes) and the other forms near mid-cell (940 minutes). To further characterize Z-ring placement, we analyzed the longitudinal position of FtsZ-ring in individual cells (Figure 3.8B-C). We considered FtsZ-rings to be positioned at mid-cell if they were located within 0.15 μm of the true mid-cell based on cell length measurements. Using this criterion, we observe that 90% of wildtype FtsZ-rings are

found at mid-cell, whereas only 60% of FtsZ-rings are found at mid-cell in Δ*popZ* cells (Figure 3.8C). Among the 40% of Δ*popZ* cells exhibiting asymmetric Z-rings, we observed that most of the Z-rings are found in close proximity to a pole (Figure 3.8C). To determine if constriction sites are established near a particular pole, we orientated the cells by treating with FM4-64, a fluorescent lipophilic dye that has been shown to preferentially label the old pole in *A. tumefaciens* [6]. We were then able to map the longitudinal position of constriction sites in individual cells (Figure 3.8D). In WT cells, constriction sites are identified in 41 of 330 cells analyzed and are located extremely close to the mid-cell (defined as a longitudinal position of 0). In contrast, constriction sites are observed in 41 of the 493 Δ*popZ* cells analyzed and are more variable in position. Remarkably, there is a clear bias for asymmetric constriction sites to form closer to the new pole. Together, these data suggest that PopZ is not required for functional Z-ring formation; however, PopZ is required to ensure proper subcellular localization of the Z-ring.

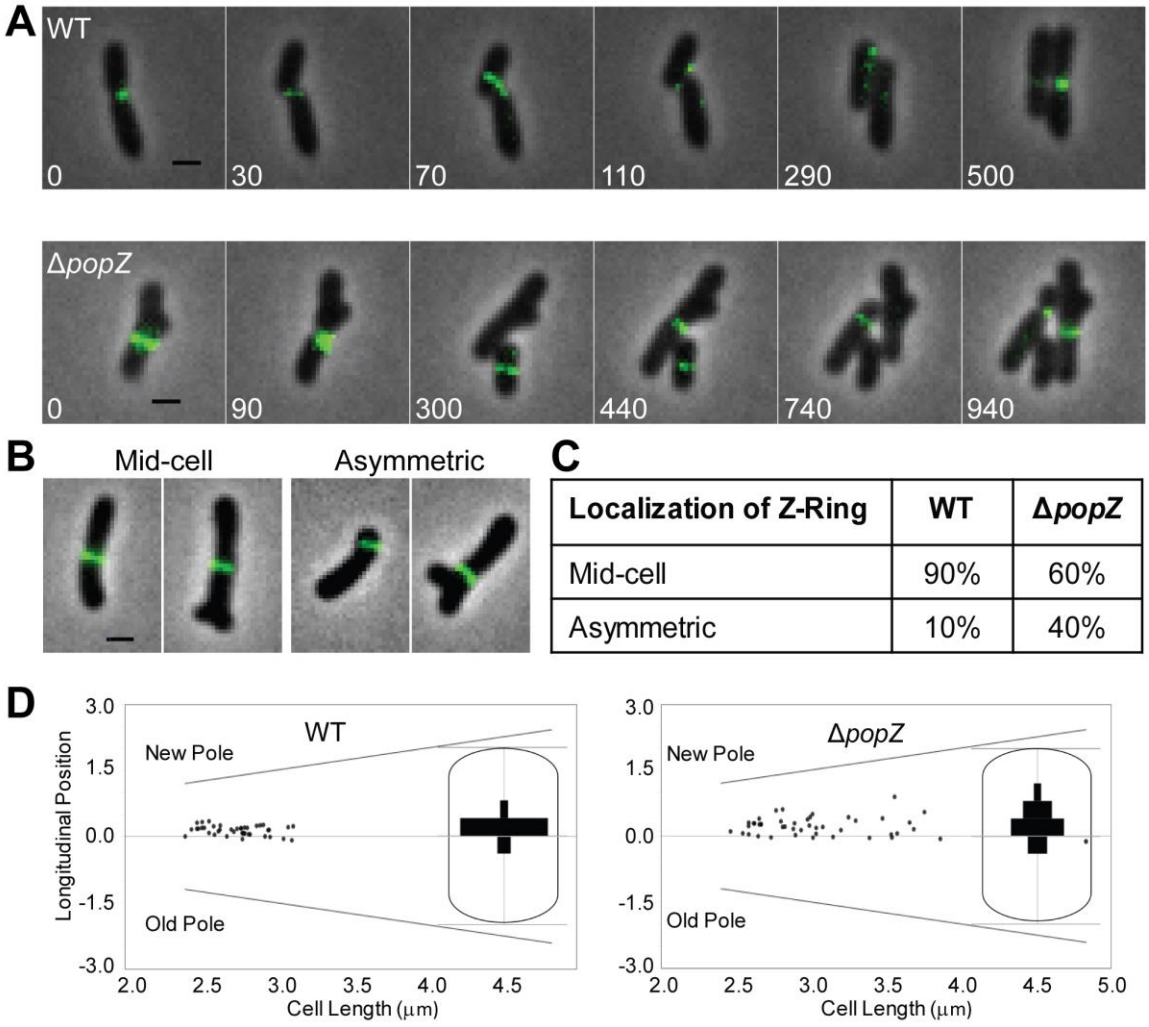

Localization of Z-Ring	WT	Δ*popZ*
Mid-cell	90%	60%
Asymmetric	10%	40%

Figure 3.8. Analysis of FtsZ localization and constriction sites in Δ*popZ*. A) Timelapse microscopy of FtsZ-sfGFP in WT cells (top panel) shows dynamic localization of FtsZ foci before Z-ring formation at mid-cell. Timelapse microscopy of FtsZ-sfGFP in Δ*popZ* (bottom panel) reveals atypical Z-ring size and positioning. B) Representative images showing mid-cell and asymmetric Z-rings Δ*popZ* cells. All scale bars are 1μm. C) Quantification of Z-ring position in WT and Δ*popZ* cells. Z-rings greater than 0.15 μm from mid-cell in either direction are defined as asymmetric. For this analysis, 77 Z-rings were analyzed in WT cells and 60 Z-rings were analyzed in Δ*popZ*. D) The longitudinal position of constriction sites is plotted against the cell length for 41

WT and 41 Δ*popZ* cells. The position of each pole is shown with a diagonal line. A longitudinal position of zero is mid-cell. Positive values are closer to the new pole whereas negative values are closer to the old pole. Insets show histograms illustrating the longitudinal position of constriction sites within a cell.

Discussion

PopZ has previously been reported in *C. crescentus* to play a crucial role in chromosome segregation and the establishment of polar identity by serving as a landmark protein [8-10,21-24]. The high degree of conservation between $PopZ_{Cc}$ and $PopZ_{At}$ in particular at the N-terminus and C-terminus [22] suggested that there may be some conservation of PopZ function. Indeed, here we show the C-terminus of $PopZ_{At}$ is important for proper subcellular localization, consistent with observations of $PopZ_{Cc}$ truncations, which demonstrate that C-terminus of PopZ is necessary and sufficient for polar localization [8,9]. Remarkably, Pop_{Cc} and $PopZ_{At}$ exhibit striking differences in subcellular localization pattern [5]. The localization of PopZ at the growing pole is reminiscent of other landmark proteins such as DivIVA that directs polar growth in *Streptomyces* [29,30]. Despite its strict localization to the growth pole we find that PopZ is not required to direct polar peptidoglycan biosynthesis in *A. tumefaciens*. In the absence of PopZ, polar growth continues and peptidoglycan composition is only slightly modified, suggesting that PopZ is not required to maintain polar growth. How peptidoglycan biosynthesis is directed specifically to the growth pole during elongation remains an important and unanswered question.

Our observations suggest that $PopZ_{At}$ functions during the transition from polar peptidoglycan synthesis to mid-cell peptidoglycan synthesis as the cells divide. The deletion of *popZ* results in the formation of ectopic poles that arise from branching at sites of failed cell division events and growth tip splitting. In addition, we find that the loss of PopZ leads to mislocalization of two essential cell division proteins, FtsA and FtsZ, suggesting that PopZ directly or indirectly impacts the site of Z-ring formation,

divisome assembly, and subsequent cell constriction. In the absence of PopZ, sites of constriction tend to form asymmetrically and are biased in positioning toward the new pole.

Why are FtsZ-rings positioned closer to the new pole in the absence of PopZ? Perhaps PopZ plays a direct role in regulating the localization of cell division proteins. Indeed, FtsZ and FtsA are retained at the growth pole following cell division and colocalize with PopZ during part of the cell cycle [5,6]; however, our data do not favor a direct role for PopZ in the localization of cell division protein. In the absence of PopZ, polar foci of FtsA and FtsZ are observed, suggesting that PopZ is not required for the retention of cell division proteins at the pole following cell division. Furthermore, in most cells neither FtsA nor FtsZ become trapped at the pole in the absence of PopZ, suggesting that PopZ is not required for the release of cell division proteins from the growth pole. Finally, localization studies with photoconvertible mEos3.2-PopZ demonstrate that PopZ is transferred to the opposite pole following cell division [17], suggesting that PopZ is unlikely to participate in divisome assembly at mid-cell.

We favor an indirect role for PopZ in the regulation of divisome assembly. DAPI staining of Δ*popZ* cells reveals that many cells lack DNA, consistent with a possible role for PopZ in chromosome segregation. Indeed, recent work from the Bowman laboratory has convincingly demonstrated that $PopZ_{At}$ is required for tethering the centromere of the circular chromosome at the new pole [17]. One possible explanation for our observations is that *A. tumefaciens* uses a negative regulator of FtsZ assembly to coordinate chromosome segregation and cell division. For example, nucleoid occlusion proteins prevent FtsZ-ring assembly over chromosomes in other bacterial systems [31,32]. A

simple explanation for our observations is that FtsZ-rings are assembling in the DNA-free zones formed due to the chromosome segregation defects in cells lacking PopZ; however, a nucleoid occlusion protein is not readily identifiable in the *A. tumefaciens* genome.

Alternatively, PopZ may function as a polar landmark protein and function to directly or indirectly recruit negative regulators of FtsZ assembly to the pole. For example, MinCD proteins function as negative regulators for FtsZ assembly near the cell poles [33,34] and *minCDE* genes are readily identifiable in the *A. tumefaciens* genome. Perhaps PopZ acts as a polar targeting protein to recruit or stabilize MinCD at the new cell pole to prevent FtsZ-ring assembly near the growth pole? Since the Min system of *A. tumefaciens* remains uncharacterized, it is unclear if polar targeting proteins are necessary to establish a gradient of FtsZ-ring inhibition near the cell poles. Notably, saturating transposon mutagenesis suggests that the *min* genes are dispensable for cell survival in *A. tumefaciens* [35], and absence of the entire Min system in the closely related bacterium *Sinorhizobium meliloti* does not impact cell growth or morphology [36], indicating that additional mechanisms to regulate the position of divisome assembly must exist.

We propose that PopZ may have a conserved role in the coordination of chromosome segregation and cell division in alphaproteobacteria. In *C. crescentus*, ParB anchors the chromosome to the pole through its interaction with PopZ [8,9] and regulates divisome assembly through its interactions with MipZ, a negative regulator of FtsZ-ring assembly [37,38]. Although *A. tumefaciens* does not have a MipZ homolog, our data suggest PopZ may function to directly or indirectly target regulators of FtsZ-ring assembly to the growth pole. Improved understanding of the mechanisms underlying FtsZ-ring

positioning in *A. tumefaciens* will be crucial to understanding the precise role of PopZ in these processes.

In *A. tumefaciens*, PopZ marks the growth pole while PodJ marks the old pole [5]. Remarkably, the phenotype described here for the Δ*popZ* mutant is strikingly similar to the phenotype of a Δ*podJ* mutant [11]. Loss of either PopZ or PodJ causes ectopic pole formation, mislocalization of cell division proteins, and asymmetric cell division suggesting that both proteins contribute to the regulation of divisome assembly. Furthermore, absence of either PopZ or PodJ results in the production of non-growing anucleate cells, suggesting that these proteins may function in chromosome segregation. Both PopZ and PodJ may have the capacity to act as polar landmark proteins and contribute to the new and old pole identity, respectively, by recruiting regulatory proteins to the poles. These findings highlight the need for further research to understand how PopZ and PodJ participate in the temporal and spatial coordination of cell cycle progression, peptidoglycan synthesis, and chromosome replication and segregation in *A. tumefaciens*.

ACKNOWLEDGEMENTS

We thank the Electron Microscopy Core at the University of Missouri for assistance collecting the transmission electron micrographs. We are grateful to Dr. George Smith, Chiqian Zhang, and members of the Brown lab for helpful discussions and critical reading of this manuscript.

REFERENCES

1. Brown PJB, de Pedro MA, Kysela DT, Van der Henst C, Kim J, De Bolle X, Fuqua C, Brun YV: Polar growth in the alphaproteobacterial order Rhizobiales. *Proc Natl Acad Sci U S A* 2012, 109:1697-1701.

2. Kuru E, Velocity Hughes H, Brown PJ, Hall E, Tekkam S, Cava F, de Pedro MA, Brun YV, VanNieuwenhze MS: *In situ* probing of newly synthesized peptidoglycan in live bacteria with fluorescent D-amino acids. *Angew Chem Int Ed* 2012, 51:12519-12523.

3. Cameron TA, Anderson-Furgeson J, Zupan JR, Zik JJ, Zambryski PC: Peptidoglycan synthesis machinery in *Agrobacterium tumefaciens* during unipolar growth and cell division. *mBio* 2014, 5:e01219-01214.

4. Margolin W: Sculpting the bacterial cell. *Current Biology* 2009, 19:R812-R822.

5. Grangeon R, Zupan JR, Anderson-Furgeson J, Zambryski PC: PopZ identifies the new pole, and PodJ identifies the old pole during polar growth in *Agrobacterium tumefaciens*. *Proc Natl Acad Sci U S A* 2015, 112:11666-11671.

6. Zupan JR, Cameron TA, Anderson-Furgeson J, Zambryski PC: Dynamic FtsA and FtsZ localization and outer membrane alterations during polar growth and cell division in *Agrobacterium tumefaciens*. *Proc Natl Acad Sci U S A* 2013, 110:9060-9065.

7. Treuner-Lange A, Sogaard-Andersen L: Regulation of cell polarity in bacteria. *J Cell Biol* 2014, 206:7-17.

8. Bowman GR, Comolli LR, Zhu J, Eckart M, Koenig M, Downing KH, Moerner WE, Earnest T, Shapiro L: A polymeric protein anchors the chromosomal origin/ParB complex at a bacterial cell pole. *Cell* 2008, 134:945-955.

9. Ebersbach G, Briegel A, Jensen GJ, Jacobs-Wagner C: A self-associating protein critical for chromosome attachment, division, and polar organization in *Caulobacter*. *Cell* 2008, 134:956-968.

10. Bowman GR, Comolli LR, Gaietta GM, Fero M, Hong SH, Jones Y, Lee JH, Downing KH, Ellisman MH, McAdams HH, et al.: *Caulobacter* PopZ forms a polar subdomain dictating sequential changes in pole composition and function. *Mol Microbiol* 2010, 76:173-189.

11. Anderson-Furgeson JC, Zupan JR, Grangeon R, Zambryski PC: Loss of PodJ in *Agrobacterium tumefaciens* leads to ectopic polar growth, branching, and reduced cell division. *J Bacteriol* 2016, 198:1883-1891.

12. Morton ER, Fuqua C: Laboratory maintenance of *Agrobacterium*. *Curr Protoc Microbiol* 2012, 24:3D.1-3d.1.16.

13. Figueroa-Cuilan W, Daniel JJ, Howell M, Sulaiman A, Brown PJ: Mini-Tn*7* insertion in an artificial *att*Tn*7* site enables depletion of the essential master regulator CtrA in the phytopathogen *Agrobacterium tumefaciens*. *Appl Environ Microbiol* 2016, 82:5015-5025.

14. Thanbichler M, Iniesta AA, Shapiro L: A comprehensive set of plasmids for vanillate- and xylose-inducible gene expression in *Caulobacter crescentus*. *Nucleic Acids Res* 2007, 35:e137.

15. Khan SR, Gaines J, Roop RM, 2nd, Farrand SK: Broad-host-range expression vectors with tightly regulated promoters and their use to examine the influence of TraR and TraM expression on Ti plasmid quorum sensing. *Appl Environ Microbiol* 2008, 74:5053-5062.

16. Gibson DG, Young L, Chuang RY, Venter JC, Hutchison CA, 3rd, Smith HO: Enzymatic assembly of DNA molecules up to several hundred kilobases. *Nat Methods* 2009, 6:343-345.

17. Ehrle H, Guidry J, Iacovetto R, Salisbury A, Sandidge D, Bowman GR: The polar organizing proterin PopZ is required for chromosome segregation in *Agrobacterium* 2017, 199:e111-117.

18. Morton ER, Fuqua C: Genetic manipulation of *Agrobacterium*. *Curr Protoc Microbiol* 2012, 25:3D.2.1-3D.2.15.

19. Ducret A, Quardokus EM, Brun YV: MicrobeJ, a tool for high throughput bacterial cell detection and quantitative analysis. *Nat Microbiol* 2016, 1:16077.

20. Morton ER, Fuqua C: Phenotypic analyses of *Agrobacterium*. *Curr Protoc Microbiol* 2012, 25:3D.3.1-3D.3.14.

21. Holmes JA, Follett SE, Wang H, Meadows CP, Varga K, Bowman GR: *Caulobacter* PopZ forms an intrinsically disordered hub in organizing bacterial cell poles. *Proc Natl Acad Sci U S A* 2016, 113:12490-12495.

22. Laloux G, Jacobs-Wagner C: Spatiotemporal control of PopZ localization through cell cycle-coupled multimerization. *J Cell Biol* 2013, 201:827-841.

23. Bowman GR, Perez AM, Ptacin JL, Ighodaro E, Folta-Stogniew E, Comolli LR, Shapiro L: Oligomerization and higher-order assembly contribute to sub-cellular localization of a bacterial scaffold. *Mol Microbiol* 2013, 90:776-795.

24. Ptacin JL, Gahlmann A, Bowman GR, Perez AM, von Diezmann AR, Eckart MR, Moerner WE, Shapiro L: Bacterial scaffold directs pole-specific centromere segregation. *Proc Natl Acad Sci U S A* 2014, 111:E2046-2055.

25. Heindl JE, Wang Y, Heckel BC, Mohari B, Feirer N, Fuqua C: Mechanisms and regulation of surface interactions and biofilm formation in *Agrobacterium*. *Front Plant Sci* 2014, 5.

26. Howell M, Brown PJB: Building the bacterial cell wall at the pole. *Curr Opin Microbiol* 2016, 34:53-59.

27. Xu J, Kim J, Koestler BJ, Choi JH, Waters CM, Fuqua C: Genetic analysis of *Agrobacterium tumefaciens* unipolar polysaccharide production reveals complex integrated control of the motile-to-sessile switch. *Mol Microbiol* 2013, 89:929-948.

28. Merritt PM, Danhorn T, Fuqua C: Motility and chemotaxis in *Agrobacterium tumefaciens* surface attachment and biofilm formation. *J Bacteriol* 2007, 189:8005-8014.

29. Flardh K, Richards DM, Hempel AM, Howard M, Buttner MJ: Regulation of apical growth and hyphal branching in *Streptomyces*. *Curr Opin Microbiol* 2012, 15:737-743.

30. Hempel AM, Wang SB, Letek M, Gil JA, Flardh K: Assemblies of DivIVA mark sites for hyphal branching and can establish new zones of cell wall growth in *Streptomyces coelicolor*. *J Bacteriol* 2008, 190:7579-7583.

31. Bernhardt TG, de Boer PA: SlmA, a nucleoid-associated, FtsZ binding protein required for blocking septal ring assembly over Ccromosomes in *E. coli*. *Mol Cell* 2005, 18:555-564.

32. Wu LJ, Errington J: Coordination of cell division and chromosome segregation by a nucleoid occlusion protein in *Bacillus subtilis*. *Cell* 2004, 117:915-925.

33. Rowlett VW, Margolin W: The bacterial Min system. *Current Biology* 2013, 23:R553-R556.

34. Rowlett VW, Margolin W: The Min system and other nucleoid-independent regulators of Z ring positioning. *Front Microbiol* 2015, 6:478.

35. Curtis PD, Brun YV: Identification of essential alphaproteobacterial genes reveals operational variability in conserved developmental and cell cycle systems. *Mol Microbiol* 2014, 93:713-735.

36. Cheng J, Sibley CD, Zaheer R, Finan TM: A *Sinorhizobium meliloti minE* mutant has an altered morphology and exhibits defects in legume symbiosis. *Microbiology* 2007, 153:375-387.

37. Kiekebusch D, Michie KA, Essen LO, Lowe J, Thanbichler M: Localized dimerization and nucleoid binding drive gradient formation by the bacterial cell division inhibitor MipZ. *Mol Cell* 2012, 46:245-259.

38. Thanbichler M, Shapiro L: MipZ, a spatial regulator coordinating chromosome segregation with cell division in *Caulobacter*. *Cell* 2006, 126:147-162.

CHAPTER 3: SUPLLEMENTARY MATERIALS

SUPPLEMENTARY METHODS

Western Blot Analysis of PopZ-GFP Fusions. To detect PopZ-GFP fusions 3-ml cultures were grown in the absence of inducer for 8 hours, followed by overnight growth in the presence of 1 mM isopropyl-β-D-1-thiogalactopyranoside (IPTG) as the inducer. The overnight cultures were diluted to an OD_{600} of 0.3 and grown for an additional 4 hours in the presence of inducer. 2 ml of culture was spun for 5 minutes at 7000 x *g* in a desktop centrifuge. Cell pellets were concentrated in GoldBio Bacterial Protein Extraction Lysis Buffer (GoldBio) containing a protease inhibitor (ProBlock Gold) to an OD_{600} of ~25 and lysed following the recommended protocol (GoldBio). Whole-cell lysates were cleared by centrifugation at 13,000 x g for 10 minutes. 1X Laemmli Sample Buffer was added to the cleared supernatents. The supernatents were boiled at 100°C prior to loading on an SDS 4-20% PAGE gel (GenScript) with recommended electrophoresis conditions. Proteins were electroblotted onto a PVDF membrane (Biorad) and blocked in 5% non-fat dry milk solubilized in TBST (1X TBS, 1% Tween-20) overnight. The blocked membranes were probed using anti-GFP monoclonal antibody (Pierce) (1:3000) in 2.5% nonfat milk solubilized in TBST for 2.5 hours. After washing, the membranes were incubated with anti-mouse HRP conjugated secondary antibody (Pierce) (1:3000) in 2.5% milk/TBST for 2.5 hours. The secondary antibody was detected using Clarity Western ECL Substrate (BioRad) for 10 minutes followed by SuperSignal West Pico Substrate (Thermo-Scientific) for an additional 10 min.

Swim Plate Assay. A fresh colony was picked with a pipette tip and stabbed into ATGN plates containing 0.3% agar followed by incubation in a sealed humid chamber for 7 days. Swim ring diameters were then measured. Each strain was tested using 8 independent colonies.

Dual Labeling with NADA and DAPI. Cells were grown in ATGN to exponential phase and labeled with a green FDAA (NBD-amino-D-alanine; NADA) for 5 minutes and then ethanol fixed. The cells were subsequently labeled with DAPI and imaged using phase contrast and epifluorescence microscopy with an inverted Nikon Eclipse TiE and a QImaging Rolera em-c^2 1K EMCCD camera.

SUPPLEMENTARY TABLES

Table 3.S1. Bacterial strains and plasmids used in this study.

Strain or plasmid	Relevant characteristics	Reference/Source
Plasmids		
pSRKKm-Plac	Km^r; broad host range vector containing $lacI^q$ and *lac* promoter	1
pKC129	Source of sfGFP	KC Huang Lab
pSRKKm-Plac-sf*gfp*	pSRKKm vector containing $lacI^q$ and *lac* promoter with sfGFP	2
pSRKKM-Plac-*popZR1*-sf*gfp*	Km^r; vector containing *popZR1-sfgfp* (bp 1-75).	This study
pSRKKM-Plac-*popZR2*-sf*gfp*	Km^r; vector containing *popZR2-sfgfp* (bp 76-774).	This study
pSRKKM-Plac-*popZR3*-sf*gfp*	Km^r; vector containing *popZR3-sfgfp* (bp 775-999).	This study
pSRKKM-Plac-*popZR1R2*-sf*gfp*	Km^r; vector containing *popZR1R2-sfgfp* (bp 1-774).	This study
pSRKKM-Plac-*popZR2R3*-sf*gfp*	Km^r; vector containing *popZR2R3-sfgfp* (bp 76-999).	This study
pSRKKM-Plac-*popZ*-sf*gfp*	Km^r; vector containing *popZ-sfgfp* (full length).	This study
pGB1246	Km^r; vector containing *fliM-eyfp*	This study

pSRKKM-P*qaz-sfgfp*	Km^r; vector containing *A. tumefaciens* native *QAZ* promoter.	This study
pSRKKM-P*qaz-ftsA*-sf*gfp*	Km^r; vector containing *A. tumefaciens* native *QAZ* promoter followed by *ftsA-sfGFP* coding sequence.	This study
pRVGFPC-2	Km^r; vector containing vanillate promoter which provides low constitutive expression in *A. tumefaciens*	3
pSRKKM-Plac-*ftsZ*-sf*gfp*	Km^r; Source of *ftsZ*-sf*gfp*.	This study
pRV-*ftsZ*-sf*gfp*	Km^r; Constitutive expression of *ftsZ*-sf*gfp*..	This study
E. coli strains		
DH5α	Cloning strain	Life Technologies
A. tumefaciens strains		
C58C1	C58 strain lacking pTiC58 plasmid	Bowman Lab
GB1163 C58C1 Δ*popZ*	C58C1 with *popZ* replaced with spec resistance cassette	4
GB1158 C58C1 Δ*popZ::mchy-popZ*	C58C1 Δ*popZ* with *mchy-popZ* integrated into the native locus	4
C58C1 pSRKKM *popZR1*-sf*gfp*	C58C1 with pSRKKM expressing *popZR1*-sf*gfp* under the *lac* promoter.	This study
C58C1 pSRKKM *popZR2*-sf*gfp*	C58C1 with pSRKKM expressing *popZR2*-sf*gfp* under the *lac* promoter.	This study
C58C1 pSRKKM *popZR3*-sf*gfp*	C58C1 with pSRKKM expressing *popZR3*-sf*gfp* under the *lac* promoter.	This study
C58C1 pSRKKM *popZR1R2*-sf*gfp*	C58C1 with pSRKKM expressing *popZR1R2*-sf*gfp* under the *lac* promoter.	This study
C58C1 pSRKKM *popZR2R3*-sf*gfp*	C58C1 with pSRKKM expressing *popZR2R3*-sf*gfp* under the *lac* promoter.	This study
C58C1 pSRKKM *popZ*-sf*gfp*	C58C1 with pSRKKM expressing *popZ*-sf*gfp* under the *lac* promoter.	This study
C58C1 Δ*popZ* pSRKKM *popZR1*-sf*gfp*	C58C1 Δ*popZ* with pSRKKM expressing *popZR1*-sf*gfp* under the *lac* promoter.	This study
C58C1 Δ*popZ* pSRKKM *popZR2*-sf*gfp*	C58C1 Δ*popZ* with pSRKKM expressing *popZR2*-sf*gfp* under the *lac* promoter.	This study
C58C1 Δ*popZ* pSRKKM *popZR3*-sf*gfp*	C58C1 Δ*popZ* with pSRKKM expressing *popZR3*-sf*gfp* under the *lac* promoter.	This study
C58C1 Δ*popZ* pSRKKM *popZR1R2*-sf*gfp*	C58C1 Δ*popZ* with pSRKKM expressing *popZR1R2*-sf*gfp* under the *lac* promoter.	This study
C58C1 Δ*popZ* pSRKKM *popZR2R3*-sf*gfp*	C58C1 Δ*popZ* with pSRKKM expressing *popZR2R3*-sf*gfp* under the *lac* promoter.	This study
C58C1 Δ*popZ* pSRKKM *popZ*-sf*gfp*	C58C1 Δ*popZ* with pSRKKM expressing *popZ*-sf*gfp* under the *lac* promoter.	This study
C58C1 pSRKKM-Pqaz-*ftsA*-sf*gfp*	C58C1 with pSRKKM expressing *ftsA*-sf*gfp* under the lac native *qaz* promoter.	This study
C58C1 Δ*popZ* pSRKKM-Pqaz-*ftsA*-sf*gfp*	C58C1 Δ*popZ* with pSRKKM expressing *ftsA*-sf*gfp* under the native *qaz* promoter.	This study
C58C1 pRV-*ftsZ*-sf*gfp*	C58C1 with pRV expressing *ftsZ*-sf*gfp* under the *van* promoter.	This study
C58C1 Δ*popZ*	C58C1 Δ*popZ* with pRV expressing *ftsZ*-sf*gfp* under the	This study

pRV-*ftsZ*-sf*gfp*	vanillate promoter.	
GB1250 C58C1 Δ*popZ::mchy-popZ* pGB1246	C58C1 Δ*popZ::mchy-popZ* with pSRKKM expressing YFP-FliM under the *lac* promoter	This study
GB1261 C58C1 Δ*popZ* pGB1246	C58C1 Δ*popZ* pSRKKM expressing YFP-FliM under the *lac* promoter	This study

Table 3.S2. Synthesized DNA primers and gene fragments used in this study.

Synthesized DNA	Sequence
Primers	
PopZ FL For NdeI	5'-CGC GAT CAT ATG GCT CAG CCA AGT GT -3'
PopZ R1 Rev BamHI	5'-GTC GCT GGA TCC GCT TTC GAT GAT CCG-3'
PopZ R2 For NdeI	5'-GTC GCT CAT ATG AAC GCG CCT GGA CCT-3'
PopZ R2 Rev BamHI	5'-GTC GCT GGA TCC ATC CGC AAT GTG CGC-3'
PopZ R3 For NdeI	5'-GTC GCT CAT ATG GGC CTG TCG CTC AAT-3'
PopZ FL Rev BamHI	5'-GTC GCT GGA TCC GCG GCG CGA GCC GCG-3'
FtsA For NdeI	5'-CGA CGC CAT ATG AGC TTT TTTGGT TC-3'
FtsA Rev BamHI	5'-CGG CAC GGA TCC TCA AAA ACT TTC TTT C-3'
FtsZ For NdeI	5'-CGA CGC CAT ATG ACG ATA CAG CTG C-3'
FtsZ Rev BamHI	5'-GCG TGA GGA TCC GTT GGA CTGGCG GCG C-3'
sfGFP Rev NheI	5'-GCT CAG GCT AGC CTA TTT GTA GAG TTC-3'
pSRK_FliM_FOR	5'-GAG CGG ATA ACA ATT TCA CAC AGG AAA CAG CAT ATG GCA AAA GCT GCA GCG C-3'
5'eYFP_ITCR_3'FliM	5'-GCC CTT GCT CAT GGA TCC AGA TCC ACC CAT CAA ATG TCG TAA GAT CTC-3'
3'FliM_ITC_5'eYFP	5'-TTG ATG GGT GGA TCT GGA TCC ATG AGC AAG GGC GAG GAG-3'
eYFP_pSRK_REV	5'-CCC TCG AGG TCG ACG GTA TCG ATA AGC TTT TAC TTG TAC AGC TCG TCC ATG C-3'
Gene Fragments	
QAZ promoter	5'- GGTAGAACGAAGCGGCGTCGAAGCCTGTAAAGCGGCGGTGCACA ATCTTCGAATTCGTAGCTGAGCTTGGACTCCTGTTGATAGATCCAG TAATGACCTCAGAACTCCATCTGGATTTGTTCAGAACGCTCGGTT GCCGCCGGGCGTTTTTTATTGGTGAGAATCCAAGCTAGACTGCGA TGAGTGGCAGGGGTAATGACTCTCTAGCTTGAGGCATCAAATAAA ACGAAAGGCTCAGTCGAAAGACTGGGCCTTTCGTTTTATCTGTTG TTTGTCGGTGAACGCCTCCTGAGTAGGACAAATCCGCCGCTAGGA GCTTGCGGCCACTAGTGTTTGGGTTCCATTTCAGATGATTGGAATG TCATGCCTTGGAAGGCAGGGACTGCGTTAACGCAATTTTTGTTCCT ATGGAATGCTAAAAAAGAAATAATGCAAATAATGTGATTGTTGA ACACCGCAGGCCTCGCAATGCACTGCCGGTCACGGTGCTGCGATT GAGAGACTGATTCAGGCCGCGGATTTAAAATGCTGAAACGCCAG ATAATTTTGTCTGGGGAATAAGCCCGTCTGTTAACGTTTCGACCTT

	GCCTTCATCGCGAAGTGGCGAACCCGCCAGGGCGGTTTTATTTCC GATCATTGAAAACCTGCATGTTGCAATCCGTACAACTCTCTGATTC CAAGGAGGTAATCGGGATTGATGCTGATTCTTTAACGGAACTCGG CATGTTGGACGCGGCGGTTAACGAAAGTAAACGATTCATTAACCT TAATGGCGTTTAACTGATCTCAAGGATCATGTGCCAGAATCACCG TCCGTTTCATTCGGTCGGTTTGGACATGGTTCGTAATGGAGAGTTG GTGTCAGAGGGTTCGCATATGCCTGCAGGCGCCTTAATTAATATG CATGGTACCTTAACATCTCGAGCTCCGGGATCCGCTGGCTCCGCT GCTGGTTCTGGCAAGCTTGGCGTGTCTAAAGGTG -3’

SUPPLEMENTAL FIGURES

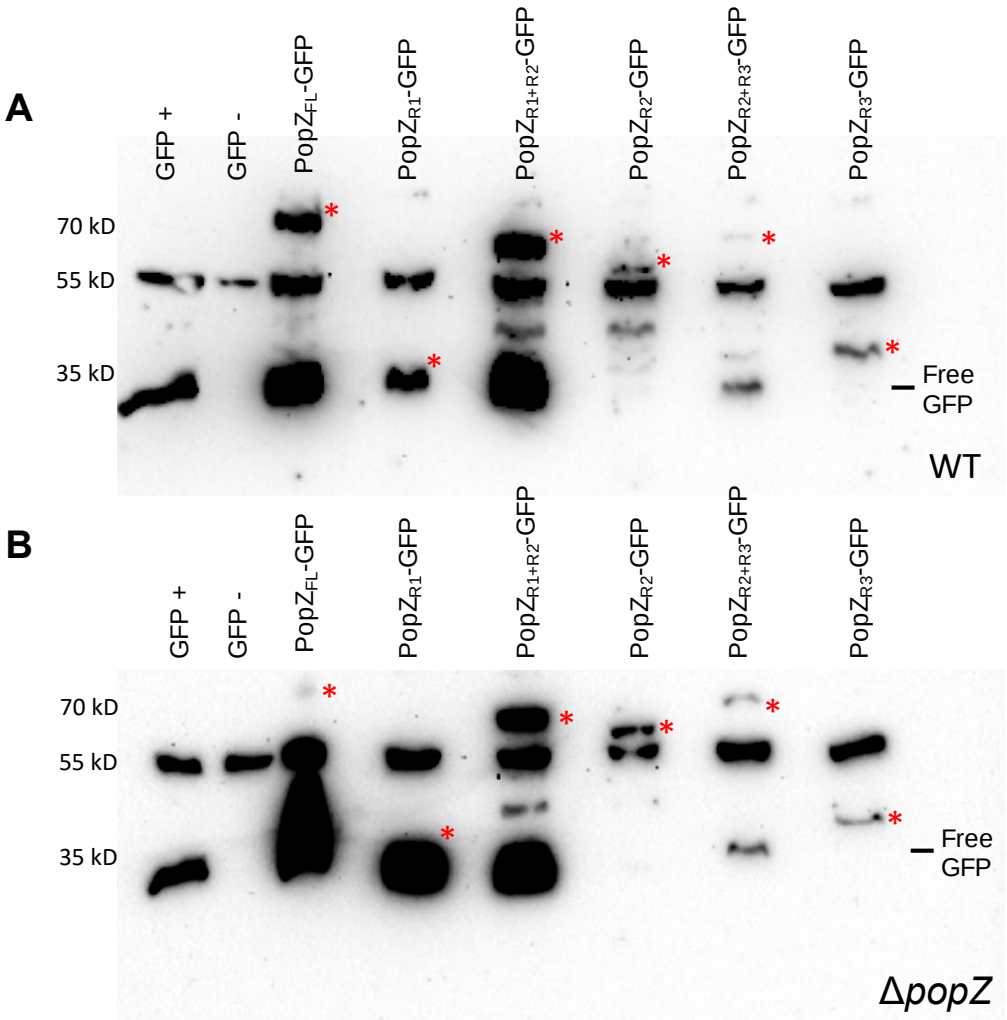

Supplemental Figure 3.S1. Western blot analysis of PopZ-GFP fusions. Western Blot analysis of PopZ-GFP fusion strains in wildtype (A) and Δ*popZ* (B) after overnight induction with IPTG using a monoclonal anti-GFP antibody. The position of each PopZ

fragment fused with GFP is shown with a red asterisk. The position of free GFP on each blot is indicated. A cross reacting band is present in all samples near 55 kD.

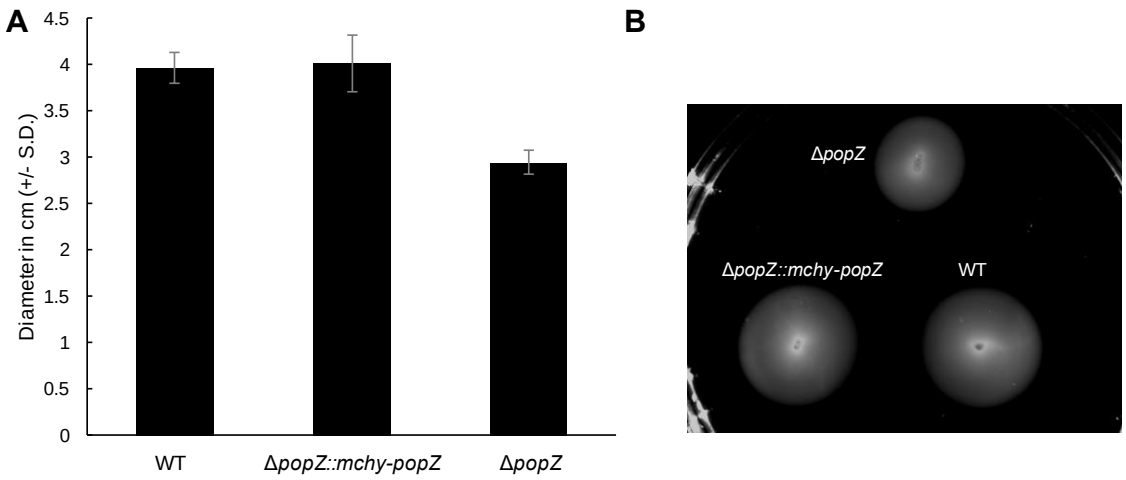

Supplemental Figure 3.S2. Δ*popZ* cells are motile. Indicated strains were assayed for motility on ATGN soft agar for 7 days. A. The average swim ring diameter and standard deviation was determined for each strain. Data were collected from 8 independent experiments. B) Representative image of swim rings formed by each strain after 7 days.

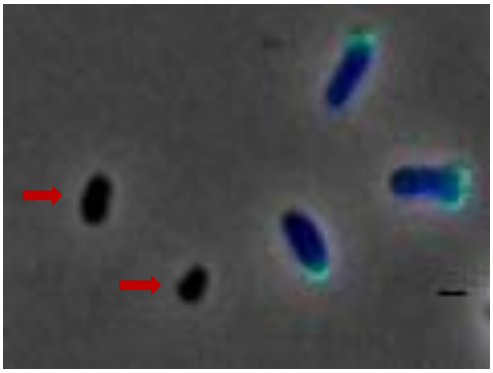

Supplemental Figure 3.S3. Small cells lack peptidoglycan synthesis and DNA. Representative image of Δ*popZ* cells dual labeled with NADA (green) and DAPI (blue).

Red arrows indicate two cells smaller than 1.5 μm. Scale bar is 1 μm. Quantitation of labeling patterns in small cells reveals that 95% of small cells that lack NADA labeling also do not label with DAPI (98/103).

Supplemental References

1. Khan SR, Gaines J, Roop RM, 2nd, Farrand SK: Broad-host-range expression vectors with tightly regulated promoters and their use to examine the influence of TraR and TraM expression on Ti plasmid quorum sensing. *Appl Environ Microbiol* 2008, 74:5053-5062.

2. Figueroa-Cuilan W, Daniel JJ, Howell M, Sulaiman A, Brown PJ: Mini-Tn*7* insertion in an artificial *att*Tn*7* site enables depletion of the essential master regulator CtrA in the phytopathogen *Agrobacterium tumefaciens*. *Appl Environ Microbiol* 2016, 82:5015-5025.

3. Thanbichler M, Iniesta AA, Shapiro L: A comprehensive set of plasmids for vanillate- and xylose-inducible gene expression in *Caulobacter crescentus*. *Nucleic Acids Res* 2007, 35:e137.

4.Ehrle HM, Guidry JT, Iacovetto R, Salisbury AK, Sandidge DJ, Bowman GR: Polar organizing protein PopZ is required for chromosome segregation in *Agrobacterium tumefaciens*. *J Bacteriol* 2017, 199:e00111-17.

CHAPTER 4

FtsZ is required for termination of polar growth and cell division in *Agrobacterium tumefaciens*

To be submitted as:

Howell, M., Aliashkevich, A., Cava, F., Goley, E., Daniel, J., Brown, P.J.B. FtsZ is required for termination of polar growth and cell division in *Agrobacterium tumefaciens*. 2018

Abstract

Bacteria within the Rhizobiales clade of alphaproteobacteria exhibit polar growth. Yet, the mechanisms that restrict peptidoglycan biosynthesis to the pole during elongation and re-direct peptidoglycan biosynthesis to mid-cell during cell division are largely unknown. Here, we demonstrate that only one of three candidate homologs of the cell division protein FtsZ has an obvious function in cell division. We find that $FtsZ_{AT}$ is required not only for constriction and cell separation, but also for the termination of polar growth and regulates peptidoglycan synthesis at mid-cell. Since *A. tumefaciens* is a polar-growing bacterium, depletion of FtsZ causes a striking phenotype: cells are extensively branched and accumulate growth active poles through tip splitting events. We find that the conserved C-terminal peptide of FtsZ is required for efficient termination of polar growth, whereas the C-terminal linker is required for proper peptidoglycan biosynthesis at mid-cell. When cell division is blocked at a later stage by depletion of FtsA or FtsW, we observe that polar growth is properly terminated, and peptidoglycan synthesis is initiated at mid-cell resulting in the emergence of ectopic growth poles when the cells fail to constrict or divide. These results indicate that the striking morphologies generated by blocks in cell division in *A. tumefaciens* are consequences of polar growth. Overall, this work suggests that *A. tumefaciens* cell division is comprised of at least two stages, including FtsZ-dependent termination of polar growth and initiation of mid-cell peptidoglycan biosynthesis followed by constriction and cell separation, which are likely dependent on the presence of a mature divisome.

Author Summary

Agrobacterium tumefaciens is best known as a bacterial plant pathogen with the ability to transfer DNA to plant cells, but these are not the only remarkable features of its biology. The cell growth cycle of *A. tumefaciens* consists of three steps: targeting of cell wall biosynthesis to the pole to allow the cell to get longer, redirecting of cell wall biosynthesis to mid-cell, and finally remodeling of the cell wall to enable cell separation. Thus, *A. tumefaciens* is an excellent model for the study of growth and division in a polar-growing alphaproteobacterium. In this work, we begin to unravel the regulatory mechanisms underlying cell wall biogenesis in *A. tumefaciens* and find that an essential cell division protein, $FtsZ_{AT}$, functions in stopping polar growth, beginning mid-cell growth, and enabling cells to separate. In contrast, characterization of two additional cell division proteins, FtsA and FtsW, implicates these proteins only function in later stages of cell division enabling cell separation. Overall, we expect that an improved understanding of *A. tumefaciens* growth processes may have implications for preventing the growth of this plant pathogen or promoting its growth for biotechnology applications.

Introduction

The spatial and temporal regulation of cell division is a vital process across bacterial species with implications for antibiotic targets [1]. The cell division process must coordinate membrane invagination(s), peptidoglycan (PG) biosynthesis and remodeling, and the physical separation of the two daughter cells, all while maintaining cellular integrity. Furthermore, cell division must be precisely regulated in order to ensure

coordination with other key cell cycle processes including cell elongation, DNA replication, and chromosome segregation to ensure that each daughter cell is of sufficient size and contains a complete genome [2,3].

To initiate bacterial cell division, the tubulin-like GTPase, FtsZ, polymerizes and forms a discontinuous ring-like structure at the future site of cell division [4-10]. The presence of FtsZ at mid-cell leads to the recruitment of many proteins that function in cell division, collectively called the divisome [11-14]. The divisome includes cell wall biosynthesis proteins, such as penicillin-binding protein, PBP3, and FtsW, which contribute to PG biosynthesis and remodeling necessary to form new poles in daughter cells [11]. Once the divisome is fully assembled, FtsZ filaments treadmill along the circumference of the mid-cell, driving the Z-ring constriction [9,10]. The movement of FtsZ filaments is correlated with the movement of enzymes that function in septal PG biogenesis. These finding are consistent with the notion that FtsZ not only recruits enzymes that function in PG biogenesis to mid-cell but also regulates their activities to promote proper cell wall biogenesis [15-17].

In most rod-shaped model organisms used to study cell division, a block in cell division leads to the production of long, smooth filamentous cells. This phenotype suggests that assembly or activation of some divisome components is necessary not only to enable the cells to divide but also to stop cellular elongation. Indeed, in *Escherichia coli*, FtsZ (along with the Z-ring stabilizing proteins FtsA, ZipA, and ZapA) has been proposed to

have an early function in the switch from lateral PG biogenesis to mid-cell PG biosynthesis [18]. Following maturation of the divisome by recruitment of additional PG remodeling enzymes and cell division proteins, PG biosynthesis is coordinated with membrane invagination, enabling cells to constrict and separate.

Remarkably, polar growing rods in the alphaproteobacterial clade Rhizobiales exhibit branched morphologies when cell division is blocked [19-26]. Examination of the cell morphologies resulting from the block in cell division suggests that different types of branched morphologies arise [27]. Drug treatments that block DNA replication cause an early block in cell division, resulting in a "Y" morphology in which the branches are formed from existing growth poles [24,25]. In contrast, antibiotics that target PBP3 cause mid-cell bulges and branches with some cells adopting a "T" or "+" morphologies [24,26]. These observations suggest that when cell division is blocked at a later stage, PG synthesis is redirected to mid-cell. The formation of two distinct phenotypes during early and late blocks in cell division suggests that divisome assembly and activation may contribute to termination of polar growth, onset of mid-cell PG biosynthesis, cell constriction, and ultimately cell separation.

In *Agrobacterium tumefaciens*, homologs of FtsZ and FtsA fused to fluorescent proteins localize at the growth pole during elongation and at mid-cell during division [26,28,29]. Timing of protein appearance at the mid-cell indicates that FtsZ appears at mid-cell considerably earlier than FtsA [29]. This indicates that FtsZ may be able to form initial

Z-rings prior to FtsA recruitment to the divisome. This observation is consistent with the described order of divisome assembly in *Caulobacter crescentus* [30] and suggests that *A. tumefaciens* FtsZ may have an early role in cell division, whereas FtsA may have a later function.

Here, we take advantage of the ability to deplete essential proteins in *A. tumefaciens* [31] to explore the function of cell division proteins FtsZ, FtsA, and FtsW in a polar growing alphaproteobacterium. Although the genome of *A. tumefaciens* contains three *ftsZ* homologs, we find that only one, henceforth referred to as ***ftsZ***$_{AT}$, is essential for cell survival. In the absence of FtsZ$_{AT}$, cells not only fail to divide but are also unable to stop polar growth. FtsZ$_{AT}$ is also required to recruit proteins to mid-cell and likely regulates the activity of PG biosynthesis enzymes at mid-cell. Remarkably, the absence of either FtsA or FtsW also causes a block in cell division; however, polar growth stops and PG synthesis is redirected to mid-cell. These observations suggest that only FtsZ is required for termination of polar growth and the onset of PG biosynthesis from mid-cell, whereas FtsZ, FtsA, and FtsW are all necessary for cell constriction, membrane invagination, and cell separation. Despite the striking morphologies produced during inhibition of cell division in a polar growing bacterium, these findings suggest that the sequential regulation of cell division is broadly conserved.

Materials and Methods

Bacterial strains and culture conditions. All bacterial strains and plasmids used are listed in Table S4.1. *A. tumefaciens* strains were grown in ATGN minimal medium with .5% glucose [32] at 28°C. *E. coli* strains were grown in Luria-Bertani medium at 37°C. When indicated, kanamycin (KM) was used at 300 μg/ml for *A. tumefaciens*, 50 μg/ml for *E. coli* DH5α, and 25 μg/ml for *E. coli* S17-1 λ *pir*. Gentamicin was used when indicated at 200 μg/ml for *A. tumefaciens* and 20 μg/ml for *E. coli* DH5α. IPTG was added at a concentration of 1 mM when indicated. Cumate was added at a concentration of 0.1 mM when indicated.

Construction of expression plasmids and strains. All strains and plasmids used are listed in Table S4.1, while primers used are listed in Table S4.2. For amplification of target genes, primer names indicate the primer orientation and added restriction sites. To construct expression vectors containing *ftsZ*$_{AT}$*-sfgfp, ftsZ*$_{1}$*-sfgfp, ftsZ*$_{3}$*-sfgfp*, and *ldtp*$_{0845}$*-sfgfp* the respective coding sequence was amplified from purified C58 genomic DNA using primers indicated in Table S4.2. The amplicons were digested overnight and ligated into cut pSRKKM-P$_{lac}$-*sfgfp* using NEB T4 DNA ligase at 4 degrees Celsius overnight. The newly formed *sfgfp* fusion of each gene was excised from the plasmid by overnight digestion with NdeI and NheI. Fragments containing *ftsZ*$_{AT}$*-sfgfp, ftsZ*$_{1}$*-sfgfp, ftsZ*$_{3}$*-sfgfp,* and *ldtp*$_{0845}$*-sfgfp* were then ligated into cut pRV-MCS2 to give constitutive expression vectors containing the fusions. To construct the *popZ-yfp* expression vector, *popZ* along with the upstream promoter sequence were amplified from purified C58 genomic DNA, digested and ligated into pMR10.

To construct pSRKKM-P_{cym}, a synthesized gBlock from IDT Integrated DNA Technologies was made containing the regulatory elements of the cumate system similar to previously described plasmid constructs [33,34]. The P_{cym} promoter region is annotated in Table S4.2. The sequence encoding the cumate repressor was codon optimized for *A. tumefaciens* and placed under the control of the constitutive kanamycin promoter from pSRKKm-P_{lac}-sf*gfp*. The synthesized gBlock was digested overnight with EcoRI and NdeI. The resulting fragment was then ligated into cut pSRKKm-P_{lac}-sf*gfp* thereby replacing the original *lac* promoter and repressor with the cumate repressor and cumate regulated promoter.

Next, *yfp-parB* was excised from pSRKKM-P_{lac}-*yfp-parB* [35]and ligated into pSRKKM-P_{cym} to create an expression vector compatible with the depletion strains. To create expression vectors for *ftsZ*$_{AT}$, *ftsZ*$_{AT}$Δ*CTP*, and *ftsZ*$_{AT}$Δ*CTL* the respective target gene was amplified utilizing indicated primers, digested overnight with NdeI and BamHI and ligated into pSRKKM-P_{cym}.

All expression vectors were verified by sequencing. All vectors were introduced into *A. tumefaciens* strains utilizing standard electroporation protocols [36] with the addition of IPTG in the media when introducing plasmids into in depletion backgrounds.

Construction of deletion/depletion plasmids and strains. Vectors for gene deletion by allelic exchange were constructed using recommended methods for *A. tumefaciens* [36]. Briefly, 500-bp fragments upstream and 500 bp downstream of the target gene were amplified using primer pairs P1/P2 and P3/4 respectively. Amplicons were spliced together by SOEing using primer pair P1/P4. The amplicon was digested and ligated into pNTPS139. The deletion plasmids were introduced into *A. tumefaciens* by mating using

an *E. coli* S17 conjugation strain to create KM resistant, sucrose sensitive primary integrants. Primary integrants were grown overnight in media with no selection. Secondary recombinants were screened by patching for sucrose resistance and KM sensitivity. Colony PCR with primers P5/P6 for the respective gene target was used to confirm deletion. PCR products from P5/P6 primer sets were sequenced to further confirm deletions.

For depletion strains, target genes (*ftsZ*$_{AT}$, *ftsA*, and *ftsW*) were amplified, digested and ligated into either pUC18-mini-Tn*7*T-GM-P$_{lac}$ or pUC18-mini-Tn*7*T-GM-P$_{lac}$. The mini-Tn*7* vectors, along with the pTNS3 helper plasmid, were introduced into C58Δ*tetRA*::a-*att*Tn*7* as described previously [31]. Transformants were selected for gentamicin resistance and insertion of the target gene into the a-*att* site was verified by colony PCR using the tet forward and Tn7R109 primer. PCR products were sequenced to confirm insertion of the correct gene. Next, the target gene was deleted from the native locus as described above in the presence of 1 mM IPTG to drive expression of the target gene from the engineered site.

DIC and phase contrast microscopy. Exponentially growing cells (OD_{600} = ~0.6) were spotted on 1% agarose ATGN pads as previously described [37]. Microscopy was performed with an inverted Nikon Eclipse TiE with a QImaging Rolera em-c^2 1K EMCCD camera and Nikon Elements Imaging Software. For timelapse microscopy, images were collected every ten minutes, unless otherwise stated.

Fluorescence microscopy. Plasmid encoded FtsZ$_{AT}$-sfGFP, FtsZ$_1$-sfGFP, FtsZ$_3$-sfGFP, and LDTP$_{0845}$-sfGFP fusions were expressed from the P$_{van}$ promoter, which provides constitutive low levels of expression (Figure S4.3C). Plasmid encoded FtsA-sfGFP and

PopZ-YFP fusions were expressed from the native promoters. Expression of plasmid encoded YFP-ParB was induced by the presence of 0.1 mM cumate for 2 hours (h). Cells containing plasmids with fluorescent protein fusions were grown to exponential phase before imaging on agarose pads.

To visualize DNA, 1 ml of exponentially growing cells was treated with 1 µl of Sytox Orange for 5 minutes. Cells were collected by centrifugation and washed with PBS 2 times followed by a final resuspension in PBS. Cells were then imaged on agarose pads.

To visualize sites of active peptidoglycan synthesis 1 ml of exponentially growing cells was labeled with the fluorescent D-amino acid (FDAA), HCC amino-D-alanine (HADA), as previously described [37,38].

Cell viability and growth curve assays. For cell viability spot assays, exponentially growing cultures were diluted to OD_{600} = 0.1 and serially diluted in ATGN. 3 µl of each dilution was spotted onto ATGN and incubated at 28°C for 3 days before imaging. When appropriate ATGN plates contained KM 300 µg/ml, IPTG 1mM, and cumate 0.1 mM as indicated in figure legends. For growth curve analysis, exponentially growing cultures were diluted to OD_{600} = .05 in 200 µl of ATGN in 96-well plates. Plates were shaken for 1 minute before OD_{600} readings, which were taken every 10 minutes.

Cell morphology and constriction rate analysis. Exponentially growing cells were imaged using phase contrast microscopy as described above. Cell length, area, and constrictions were detected using MicrobeJ software [39].

To calculate constriction rates, cells with detectable constrictions were tracked using time-lapse microscopy. The width of the cell constriction was measured at an initial

timepoint and the measurement was repeated after 10 minutes. The difference in constriction width was divided by the 10-minute time interval to give a constriction rate.

Western blot analysis. For western blot analysis of FtsZ depletion, the *ftsZ* depletion strain was grown in 40 ml ATGN with 1 mM IPTG to exponential phase. 2 ml of culture was collected prior to depletion (time 0) by centrifugation at 10,000 x *g* for 3 minutes. The remaining culture was collected by centrifugation at 3500 x *g* for 10 minutes, and supernatants were discarded. Cells were washed in sterile water and pelleted again. To deplete FtsZ, the pellet was resuspended in fresh ATGN without IPTG and grown under standard culturing conditions. 2-ml samples were collected by centrifugation after 30, 45, 60, 120, and 240 minutes of depletion. OD_{600} was taken for each sample prior to centrifugation so that samples could be normalized to an OD_{600} equivalent to 0.68. The cell pellets were incubated with 100 µl of a master mix containing 1 ml of BugBuster protein extraction reagent (Novagen) and supplemented with 1 EDTA-free protease inhibitor cocktail (Sigma), 10 µl of lysonase (Novagen), 2,500 U/ml DNase I (Thermo Scientific), and 1 mM dithiothreitol (DTT) (Thermo Scientific) for 25 minutes with shaking at room temperature to lyse the cell pellets. The whole-cell lysates were clarified by centrifugation at 10,000 rpm for 15 min. A final concentration of 1 X Laemmli buffer was added to the cleared cell lysates. Samples were boiled at 100°C for 5 min prior to loading on a 4-15% Mini-PROTEAN TGX Precast Gel (Bio-Rad). The separated proteins were electroblotted onto polyvinylidene difluoride (PVDF) membranes (Bio-Rad) and blocked overnight in 5% nonfat dry milk powder solubilized in 1% TBST (Tris-buffered saline [TBS], 1% Tween 20). The blocked PVDF membranes were probed with *Escherichia coli* anti-FtsZ (1:3000) monoclonal antibody (gift from Joe Lutkenhaus) for

1.5 h in 5% milk-TBST, followed by incubation with anti-rabbit (1:5000) HRP (Pierce 31460) secondary antibody for 1 h in 5% milk-TBST. The secondary antibody was detected using the ECL Plus HRP substrate (Thermo Scientific Pierce).

For comparison of expression from P_{van}, P_{lac}, and P_{cym} promoters, strains were grown in 2 ml ATGN with 200 ug/mL KM to exponential phase. P_{lac} and P_{cym} were induced with 1 mM IPTG and 50 μM cumate, respectively for 4 h. Cell pellets were lysed as described above and clarified whole-cell lysates were boiled with 1 X Laemmli buffer for 5 min prior to loading on 4-15% Mini-PROTEAN TGX Precast Gel (Bio-Rad). The separated proteins were electroblotted onto PVDF membranes (Bio-Rad), blocked as described above, and probed with anti-GFP (1:3,000) monoclonal antibody (Thermo Scientific Pierce) for 1 h in 5% milk-TBST, followed by incubation with a donkey anti-mouse (1:300) horseradish peroxidase-conjugated secondary antibody (Thermo Scientific Pierce) for 1 h in 5% milk-TBST. The secondary antibody was detected using the ECL Plus HRP substrate (Thermo Scientific Pierce).

Peptidoglycan composition analysis

Six cultures of WT and *ftsZ* depletion cells were grown in 10 ml of ATGN with IPTG to exponential phase. The 10-ml cell cultures were added to 40 ml of fresh media. The 50-ml cultures were grown to exponential phase and pelleted by centrifugation at 4000 x *g* for 10 minutes. Cell pellets were washed three times with ATGN by centrifugation and resuspension to remove IPTG. After the final wash 3 cell pellets were resuspended in 50 ml ATGN and the remaining 3 pellets were resuspended in 50 ml ATGN with 1 mM IPTG.

Each culture was grown for 14 h. The optical densities of the cells were monitored to ensure the optical density of the cultures never went above OD_{600} = 0.7 to avoid changes to peptidoglycan content due to stationary phase. If necessary, fresh medium was added to dilute the cultures to maintain exponential growth. After 14 h of growth, 50 ml of the exponential cultures were collected and pelleted by centrifugation at 4000 x *g* for 20 minutes. Cell pellets were resuspended in 1mL of ATGN and 2 mL of 6% SDS and stirred with magnets while boiling for 4 h. After 4 h, samples were removed from heat but continued to stir overnight. Samples were then shipped to Dr. Felipe Cava's laboratory for purification and analysis.

Upon arrival, cells were boiled and simultaneously stirred by magnets for 2 h. After 2 h, boiling was stopped and samples were stirred overnight. Peptidoglycan was pelleted by centrifugation for 13 min at 60,000 rpm (TLA100.3 Beckman rotor, Optima Max-TL ultracentrifuge; Beckman), and the pellets were washed 3 to 4 times by repeated cycles of centrifugation and resuspension in water. The pellet from the final wash was resuspended in 50 µl of 50 mM sodium phosphate buffer, pH 4.9, and digested overnight with 100 µg/ml of muramidase at 37°C. Muramidase digestion was stopped by boiling for 4 min. Coagulated protein was removed by centrifugation for 15 min at 15,000 rpm in a desktop microcentrifuge. The muropeptides were mixed with 15 µl 0.5 M sodium borate and subjected to reduction of muramic acid residues into muramitol by sodium borohydride (10 mg/ml final concentration, 20 min at room temperature) treatment. Samples were adjusted to pH 3 to 4 with orthophosphoric acid and filtered (0.2-µm filters).

Muropeptides were analyzed on a Waters UPLC system equipped with an ACQUITY UPLC BEH C18 Column, 130 Å, 1.7 μm, 2.1 mm × 150 mm (Waters) and a dual wavelength absorbance detector. Elution of muropeptides was detected at 204 nm. Muropeptides were separated at 45°C using a linear gradient from buffer A [formic acid 0.1% (v/v)] to buffer B [formic acid 0.1% (v/v), acetonitrile 20% (v/v)] in a 12 min run with a 0.250 ml/min flow. Peptidoglycan compositional analysis on triplicate samples was completed on two separate occasions.

Results and Discussion

FtsZ$_{AT}$ is required for cell division and termination of polar growth. *Agrobacterium tumefaciens* contains three homologs of FtsZ, Atu_2086, Atu_4673, and Atu_4215 (Figure 4.1A), based on sequence similarity to the well-characterized *Escherichia coli* FtsZ protein [26]. *E. coli* FtsZ is comprised of three regions: the conserved N-terminal tubulin domain with GTPase activity, a C-terminal linker (CTL), and a conserved C-terminal peptide (CTP), which anchors FtsZ to the membrane via interactions with FtsA [40]. Atu_2086 contains each of these domains and the tubulin domain and CTP share 52% and 67% identity to their respective domain in *E. coli* FtsZ, whereas the CTL is extended in length [26]. The gene encoding Atu_2086 is found in a putative operon with genes encoding DdlB, FtsQ, FtsA [41,42] and is predicted to be essential for cell survival based on saturating transposon mutagenesis [43]. Atu_2086 localizes to mid-cell in wildtype (WT) pre-divisional cells (Figure 4.1B) [26,28]; consistent with a role in cell division. Atu_4673 (called FtsZ$_1$; consistent with the genome annotation) contains a complete tubulin domain with 49% identity to tubulin domain of *E. coli* FtsZ but lacks

both the CTL and CTP [26]. Although Atu_4673 is not predicted to be required for cell survival based on saturating transposon mutagenesis [43], it localizes to mid-cell in pre-divisional cells, suggesting a possible role in cell division (Figure 4.1B). Atu_4215 (termed $FtsZ_3$ in this work) contains a partial tubulin domain with 48% identity to the N-terminal portion of the *E. coli* FtsZ tubulin domain and lacks both the CTL and CTP [26]. $FtsZ_3$ is not essential for survival of *A. tumefaciens* based on saturating transposon mutagenesis [43] and exhibits a diffuse localization pattern (Figure 4.1B). Together, these data suggest that Atu_2086 is the canonical FtsZ protein required for cell division, and this protein will be referred to as $FtsZ_{AT}$ throughout this work (although it is annotated as $FtsZ_2$ in the *A. tumefaciens* C58 genome [41,42]).

To characterize the function of each FtsZ homolog, we constructed deletions of $ftsZ_1$ and $ftsZ_3$ and a depletion strain of $ftsZ_{AT}$. Since we were unable to construct a deletion of $ftsZ_{AT}$, we used a depletion strategy in which $ftsZ_{AT}$ is present as a single copy under the control of an isopropyl β-D-1-thiogalactopyranoside (IPTG) inducible promoter at a neutral site in the chromosome [20,31]. Using western blot analysis, we have confirmed the depletion of $FtsZ_{AT}$ in the absence of IPTG (Figure S4.1A).

Deletion of $ftsZ_1$ or $ftsZ_3$ does not impact cell viability (Figure 4.1C), cell growth rates (Figure S4.1C), cell morphology (Figure 4.1D ; Table 4.1), microcolony formation (Figure 4.1D), constriction rate or position (Table 4.1) when compared to WT cells. Similarly, when $FtsZ_{AT}$ is expressed in the depletion strain (labeled in Figures as

+FtsZ$_{AT}$) the cells remain viable (Figure 4.1C), grow comparably to WT (Figure S4.1D), are similar in size to WT cells (Table 4.1; Figure 4.1E; top), properly position constrictions (Table 4.1), and complete cell divisions (Figure 4.1E; top). In contrast, depletion of FtsZ$_{AT}$ (labeled in Figures as –FtsZ$_{AT}$) causes a marked decrease in cell viability (Figure 4.1C), impairs cell growth (Figure S4.1D), triggers the formation of large cells with complex branched morphologies (Table 4.1; Figure 4.1D), and cells depleted of FtsZ$_{AT}$ do not divide (Figure 4.1E; bottom). To quantify changes in morphology during depletion of FtsZ$_{AT}$, the cell area of at least 100 cells was calculated based on phase contrast images of cells acquired immediately after removal of the inducer (-FtsZ$_{AT}$ 0 h), 8 h after removal of the inducer (-FtsZ$_{AT}$ 8 h), and 14 h after removal of the inducer (-FtsZ$_{AT}$ 14 h) (Table 4.1). Initially, the FtsZ$_{AT}$ depleted cells are similar to WT in cell size, but after 8 h of FtsZ$_{AT}$ depletion the cell area has nearly doubled (Table 4.1). Within 14 h of FtsZ$_{AT}$ depletion, the average cell area has dramatically increased (Table 4.1), consistent with time-lapse microscopy which indicates that the FtsZ$_{AT}$ depleted cells continue to grow without dividing, leading to rapid accumulation of cell biomass prior to cell lysis (Figure 4.1E; bottom). Observation of cells during FtsZ$_{AT}$ depletion by time-lapse microscope reveals remarkable changes in cell morphology (Figure 4.1E; bottom). As the cell elongates, an ectopic pole forms near mid-cell. Both the original growth pole and the ectopic pole are growth-active, resulting in the presence of multiple growth poles. These growth poles are unable to terminate cell elongation and ultimately most growth active poles are split, leading to the accumulation of many growth active poles and the rapid increase in cell area until the cell lyses.

Together, these results demonstrate that only the $FtsZ_{AT}$ homolog is required for proper cell growth and division.

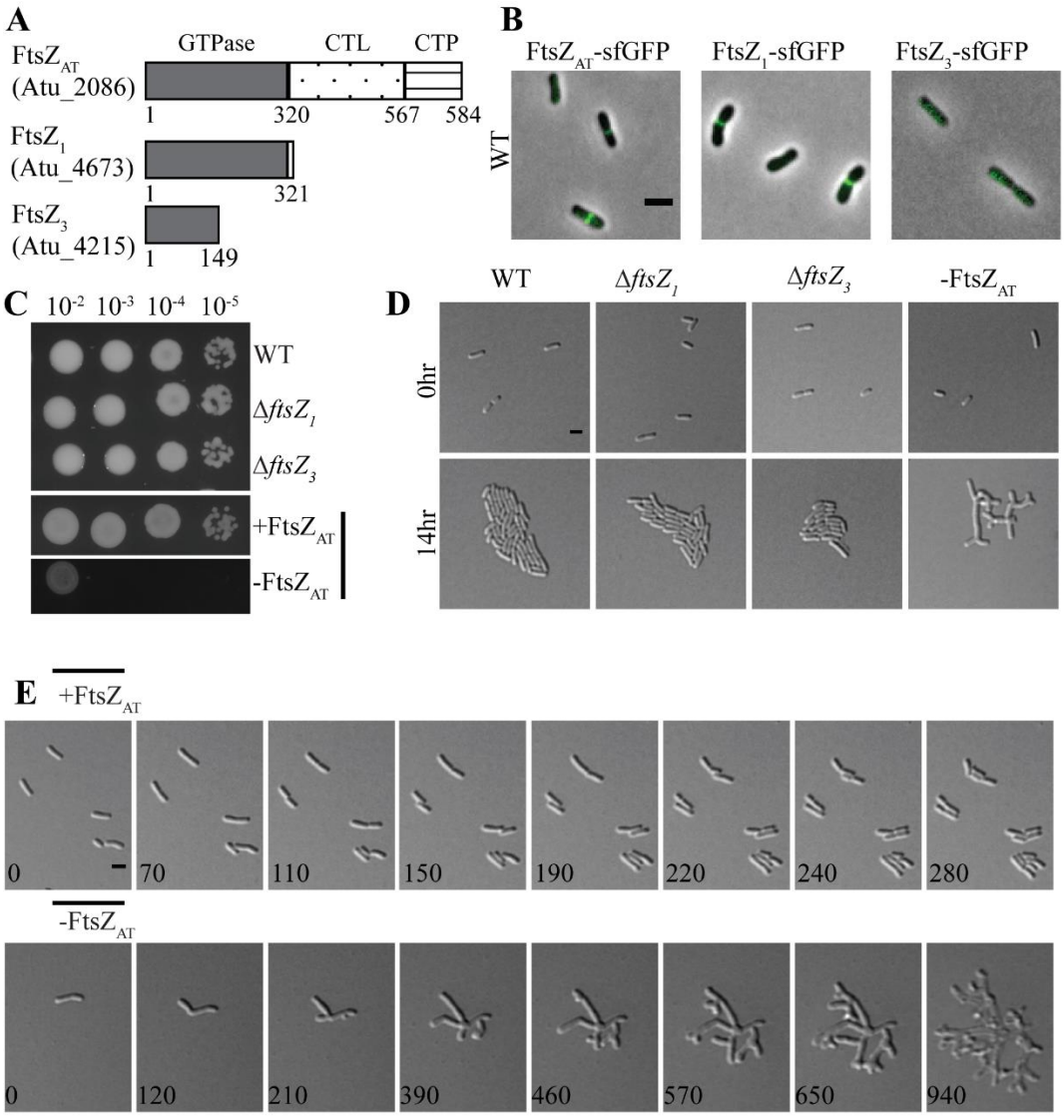

Figure 4.1. Characterization of FtsZ homologs in *A. tumefaciens*. A) Domain schematic of FtsZ homologs in *A. tumefaciens*. Note that domains are not drawn to scale. B) Representative image of localization patterns for each homolog. $FtsZ_{AT}$-sfGFP and $FtsZ_1$-sfGFP show mid-cell ring formation while $FtsZ_3$-sfGFP fails to localize. C) Cell viability is shown by spotting serial dilutions. Δ*ftsZ*$_1$, Δ*ftsZ*$_3$, and +*ftsZ*$_{AT}$ have similar

viability to WT, while -*ftsZ*$_{AT}$ displays a drastic decrease in viability. D) Cell morphology and microcolony formation of Δ*ftsZ*$_1$ and Δ*ftsZ*$_3$ are similar to WT, while -*ftsZ*$_{AT}$ results in long branched cells that fail to divide. E) Timelapse microscopy in minutes demonstrates proper cell division and microcolony formation in +*ftsZ*$_{AT}$ induced with IPTG (top panel). Timelapse during depletion of $FtsZ_{AT}$ demonstrates branches forming from tip splitting events (bottom panel). All scale bars are set to 2 μm.

		Average Cell Length[a] (μm +/- SD[b])	Average Cell Area[a] (μm^2 +/- SD)	Average Constriction Rate[c] (nm/min +/- SD)	Relative Constriction Position[d] +/- SD
WT		2.31 +/-.50	1.66 +/-.35	6.82 +/-3.19	.49 +/-.05
Δ*ftsZ$_1$*		2.25 +/-.49	1.52 +/-.33	6.99 +/-3.58	.46 +/-.05
Δ*ftsZ$_3$*		2.24 +/-.47	1.44 +/-.30	6.77 +/-2.77	.46 +/-.05
Δ*ftsZ$_1$* Δ*ftsZ$_3$*		2.25 +/-.51	1.47 +/-.34	6.61 +/-3.75	.46 +/-.04
ftsZ$_{AT}$ depletion	- FtsZ$_{AT}$ 0 h	2.71 +/-.70	1.56 +/-.39	6.38 +/-2.81	.49 +/-.07
	- FtsZ$_{AT}$ 8 h	ND[e]	2.95 +/-1.12	ND	ND
	- FtsZ$_{AT}$ 14 h	ND	11.37 +/-4.69	ND	ND

Table 4.1. Quantitation of cell size and constriction of *ftsZ* mutants

[a]At least 100 cells were used to quantify the cell length and area for each strain

[b]SD – standard deviation.

[c]At least 30 cells were used to quantify the constriction rates for each strain

[d]Relative constriction position for at least 40 cells is shown. A value of 0 corresponds to the new pole, 0.5 corresponds to mid-cell, and a value of 1 corresponds to the old pole.

[e]ND – not determined.

The branched morphology observed during $FtsZ_{AT}$ depletion is in stark contrast to FtsZ depletion observed in other organisms. In species like *E. coli* and *B. subtilis*, which utilize lateral peptidoglycan biosynthesis during elongation, depletion of FtsZ results in long unbranched filaments. We hypothesize that the branching morphology observed in *A. tumefaciens* can be attributed to polar elongation. During the block in cell division, the growth pole continues to grow and presumably recruits newly synthesized peptidoglycan biosynthesis proteins. This could lead to an over-accumulation of elongasome proteins, causing the pole to split into two poles. A similar type of branching has been characterized in the polar growing *Streptomyces coelicolor* [44]. In this organism, the DivIVA led elongasome has been demonstrated to split, leaving a small elongasome foci behind as growth continues. With time, the subpolar elongasome accumulates in size and eventually forms a new growth pole. Although the polar growth molecular mechanisms are not conserved between *A. tumefaciens* and *S. coelicolor*, the fundamentals of tip splitting as a consequence of polar growth appear to be shared.

Deletion of *ftsZ₁* and *ftsZ₃* does not change the $FtsZ_{AT}$ depletion phenotype. Since the *ftsZ₁* and *ftsZ₃* single deletions do not have an obvious impact on cell morphology, growth, or division, we constructed double and triple mutants to determine if there is an additive effect of removing multiple *ftsZ* homologs. Double deletion of *ftsZ₁* and *ftsZ₃* does not cause a decrease in cell viability (Figure 4.2A, top panel), growth rate (Figure S4.1B), cell morphology (Table 4.1), or microcolony formation (Figure 4.2A, bottom panel). Furthermore, *ΔftsZ₁ ΔftsZ₃* cells properly place constrictions and have an average constriction rate similar to WT (Table 4.1). Next, we introduced the *ΔftsZ₁*, *ΔftsZ₃*, and

ΔftsZ$_1$ *ΔftsZ*$_3$ mutations into the *ftsZ*$_{AT}$ depletion strain to determine if loss of multiple *ftsZ* homologs causes an additive effect. Consistent with previous results, the combination of the *ftsZ*$_{AT}$ depletion strain with *ΔftsZ*$_1$, *ΔftsZ*$_3$, or *ΔftsZ*$_1$ *ΔftsZ*$_3$ mutations did not result in a further decrease in cell viability (Figure 4.2B, top panel) or a worsening of cell morphology (Figure 4.2B, bottom panel) when compared to FtsZ$_{AT}$ depletion alone. Together, these results suggest that the FtsZ$_1$ and FtsZ$_3$ homologs do not have a major impact on cell division under the conditions tested. It is possible that FtsZ$_1$ or FtsZ$_3$ may have important contributions to cell growth or division in different environments (for example, *in planta*).

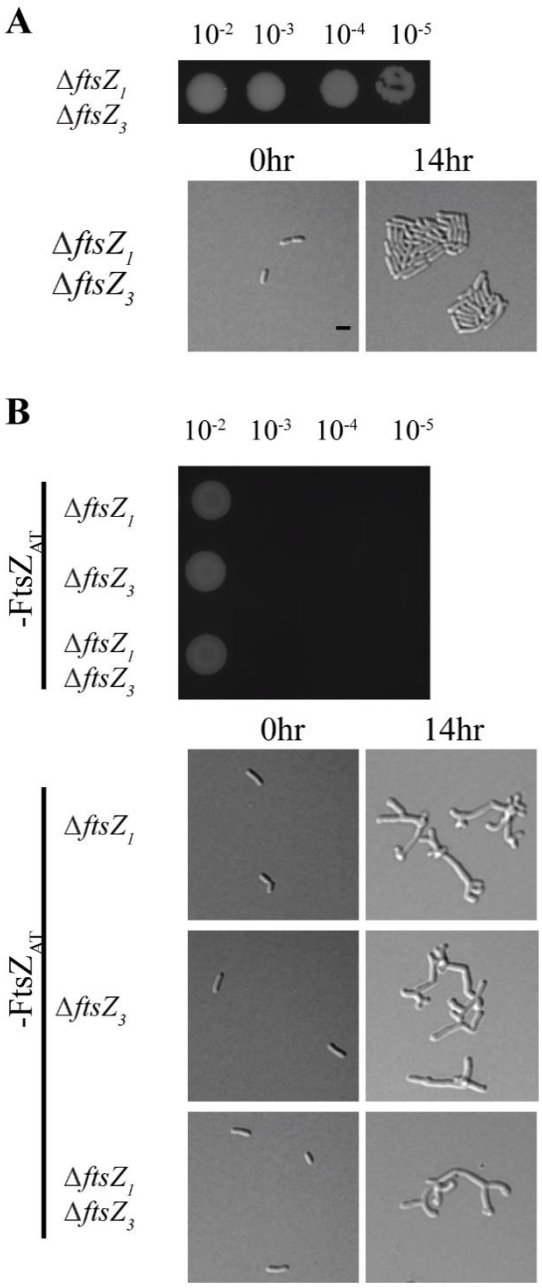

Figure 4.2. Deletion of multiple *ftsZ* homologs does not yield an additive effect. A) Cell viability (top) and morphology (bottom) of the double mutant Δ*ftsZ*$_1$Δ*ftsZ*$_3$ is indistinguishable from WT. B) Cell viability (top) and morphology (bottom) of Δ*ftsZ*$_1$, Δ*ftsZ*$_3$, or Δ*ftsZ*$_1$Δ*ftsZ*$_3$ during FtsZ$_{AT}$ depletion are indistinguishable from FtsZ$_{AT}$ depletion alone. All scale bars are set to 2 μm. Black bar denotes *ftsZ*$_{AT}$ depletion strain background

FtsZ$_{At}$ is required for the mid-cell localization of divisome components. In the absence of FtsZ$_{AT}$, cells fail to form constrictions and presumably fail to recruit divisome components to mid-cell. To test this, we examined the localization of FtsZ$_1$-sfGFP and FtsA-sfGFP in both WT and the *ftsZ$_{AT}$* depletion strain (Figure 4.3). In WT cells, FtsZ$_1$-sfGFP does not localize in newborn cells but forms FtsZ-like rings at the future site of division in pre-divisional cells (Figure 4.3A, top panel). This Z-like ring constricts to form a single focus in dividing cells. These observations suggest that FtsZ$_1$ may be a divisome component despite the absence of a cell division phenotype in the Δ*ftsZ$_1$* strain. To explore this possibility, we next visualized FtsZ$_1$-sfGFP localization during the depletion of FtsZ$_{AT}$ (Figure 4.3A, bottom panel). We pre-depleted FtsZ$_{AT}$ for 4 h in liquid to avoid cell crowding caused by division events prior to sufficient FtsZ$_{AT}$ depletion. Early during the depletion of FtsZ$_{AT}$, FtsZ$_1$-sfGFP localizes in an FtsZ-like ring near mid-cell; however, the Z-like ring disperses over time. As the FtsZ$_{AT}$ depletion continues, FtsZ$_1$-sfGFP rings and foci are no longer observed, suggesting that localization of FtsZ$_1$-sfGFP to mid-cell requires the presence of FtsZ$_{AT}$. This observation supports the possibility that FtsZ$_1$ may be a divisome component.

FtsA is an actin-like protein that associates with the membrane through an amphipathic helix and binds the FtsZ CTP to anchor FtsZ polymers to the membrane [45,46]. In *C. crescentus*, recruitment of FtsA to mid-cell occurs well after the establishment of the FtsZ-ring and is dependent on the presence of FtsZ [13,47]. In *A. tumefaciens*, FtsA-sfGFP is retained at the growth pole prior to appearing at mid-cell just before cell division [26,29]. Here, we confirm that FtsA-sfGFP is observed as a focus at the growth

pole until transitioning to a ring-like structure at mid-cell (Figure 4.3B, top panel). In fact, at some timepoints, both a polar focus and a mid-cell ring of FtsA are observed. Eventually, the polar focus disappears as the FtsA-sfGFP ring becomes more intense just prior to cell division. During the depletion of $FtsZ_{AT}$, a focus of FtsA-sfGFP can be found at the growing pole, and at a newly formed ectopic pole near mid-cell (Figure 4.3B, bottom panel). FtsA-sfGFP remains associated with each growth pole, and as the poles undergo a tip splitting event, each focus of FtsA-sfGFP is also split, resulting in the presence of FtsA-sfGFP in each of the 4 growth-active poles. These observations suggest that $FtsZ_{AT}$ is required not only for proper mid-cell localization of FtsA to mid-cell prior to cell division but also contributes to release of FtsA-sfGFP from the growth pole.

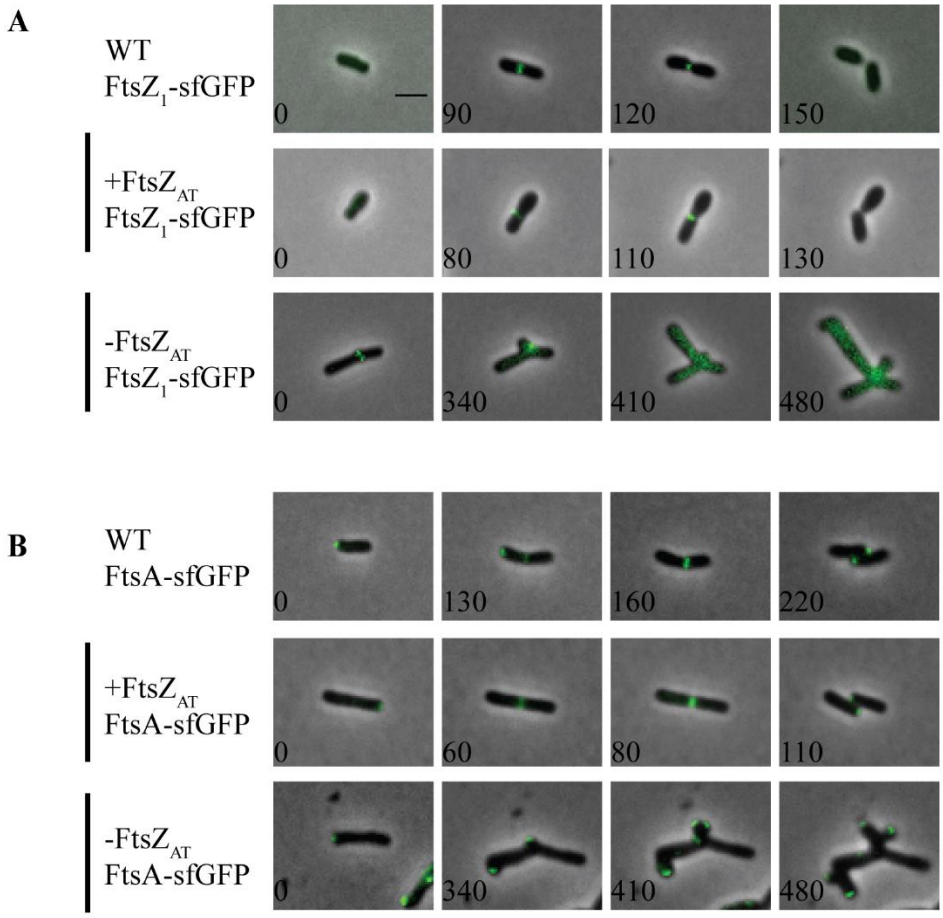

Figure 4.3. Localization of divisome components in WT and *ftsZ* depletion strain. A) $FtsZ_1$-sfGFP forms a mid-cell ring which constricts in WT and when *ftsZ*$_{AT}$ is induced. $FtsZ_1$-sfGFP fails to constrict early rings and disassembles during $FtsZ_{AT}$ depletion. B) FtsA-sfGFP persists at growth poles and forms mid-cell ring which constrict in WT and when *ftsZ*$_{AT}$ is induced. FtsA-sfGFP becomes trapped at the growth poles and foci split as the growth poles split during $FtsZ_{AT}$ depletion. Scale bar is set to 2 μm. Black bar denotes *ftsZ*$_{AT}$ depletion strain background

PopZ-YFP is trapped at growing poles in the absence of FtsZ$_{AT}$. After observing that release of FtsA-sfGFP from the growth pole is dependent on FtsZ$_{AT}$, we hypothesized that other proteins with a similar localization pattern could become trapped at the pole during depletion of FtsZ. To test this hypothesis, we localized the polar organizing protein, PopZ-YFP. In WT, PopZ-YFP localizes to the growing pole during elongation and is recruited to mid-cell just prior to cell separation (Figure 4.4A, top panel) [35,48,49]. Deletion of *popZ* has been shown to cause ectopic poles and cells devoid of DNA, demonstrating a role in coordinating cell division with chromosome segregation [35,48]. We hypothesize that PopZ dependent coordination of cell division likely involves FtsZ. When FtsZ$_{AT}$ is expressed in the *ftsZ$_{AT}$* depletion strain, PopZ-YFP has a similar localization pattern as in WT cells (Figure 4.4A, middle panel). When FtsZ$_{AT}$ is depleted, PopZ-YFP becomes trapped at the growth poles and as tip splitting events lead to the production of new growth poles, PopZ-YFP appears to be split and retained at all growth active poles (Figure 4.4A, bottom panel). These observations indicate that FtsZ is required for the release of PopZ from the growth poles. Remarkably, both FtsZ and FtsA are mislocalized in the absence of PopZ, leading to the establishment of asymmetric constrictions sites and a broad range of cell lengths [48]. Together, these data suggest that the presence of both PopZ and FtsZ are important for proper positioning and functioning of the divisome.

In addition to its function in maintaining proper cell division, *A. tumefaciens* PopZ is also required for correct chromosome segregation and tethers the centromere of at least one chromosome to the growth pole [35]. Thus, we examined the DNA content of cells

depleted of $FtsZ_{AT}$. In both WT cells and in conditions where *ftsZ* is induced in the *ftsZ*$_{AT}$ depletion strain, DNA labeled with Sytox orange is diffuse throughout most cells (Figure 4.4B, top two panels). In late divisional cells, true separation of nucleoids is observed indicating successful completion of chromosome segregation (Figure 4.4B, marked with an asterisk in the top two panels). In cells depleted of $FtsZ_{AT}$ for both 8 and 14 h, DNA is diffuse throughout the elongated branches (Figure 4.4B, bottom two panels). The absence of distinct nucleoids may suggest that final stages of chromosome segregation are coordinated with cell separation as has been described for other bacteria including *E. coli* and *C. crescentus* [50].

To look more carefully at genomic content, we visualized YFP-ParB1, which serves as a proxy to track centromere partitioning in *A. tumefaciens* [35], in WT and *ftsZ*$_{AT}$ depletion cells. In both WT cells and cells expressing $FtsZ_{AT}$ in the *ftsZ*$_{AT}$ depletion strain, a single YFP-ParB1 focus is present at the old pole in new cells generated by a recent cell division event (Figure 4.4C, top and middle panels). As the cells elongate, a second focus appears and translocates across the longitudinal axis to the growing pole (Figure 4.4C, top and middle panels). After 4 h of $FtsZ_{AT}$ pre-depletion, YFP-ParB1 foci can be seen at both poles, but when the cell fails to divide, a third focus of YFP-ParB1 appears and translocates along the longitudinal axis of the cell before taking a rapid turn toward a new ectopic pole formed from near mid-cell (Figure 4.4C, bottom panel). Next, we quantified the number of YFP-ParB1 foci relative to cell area (Figure 4.4D). In WT and $FtsZ_{AT}$ expressing cells in the *ftsZ*$_{AT}$ depletion strain, small cells have only a single focus of YFP-ParB1. This is followed by a transition period in which elongating cells

accumulate a second focus of YFP-ParB1. Finally, the largest, pre-divisional cells have two YFP-ParB1 foci (Figure 4.4D). Cells depleted of $FtsZ_{AT}$ for 8 h accumulate YFP-ParB1foci as they increase in area (Figure 4.4D). Cells with an area larger than 3 μm^2 all have at least 2 YFP-ParB1 foci, suggesting that chromosome replication is not blocked during FtsZ depletion. Furthermore, in larger cells additional YPF-ParB1 foci accumulate. These data suggest that cell division is not strictly required for the initiation of DNA replication in *A. tumefaciens*, although completion of chromosome segregation may be coordinated with cell division.

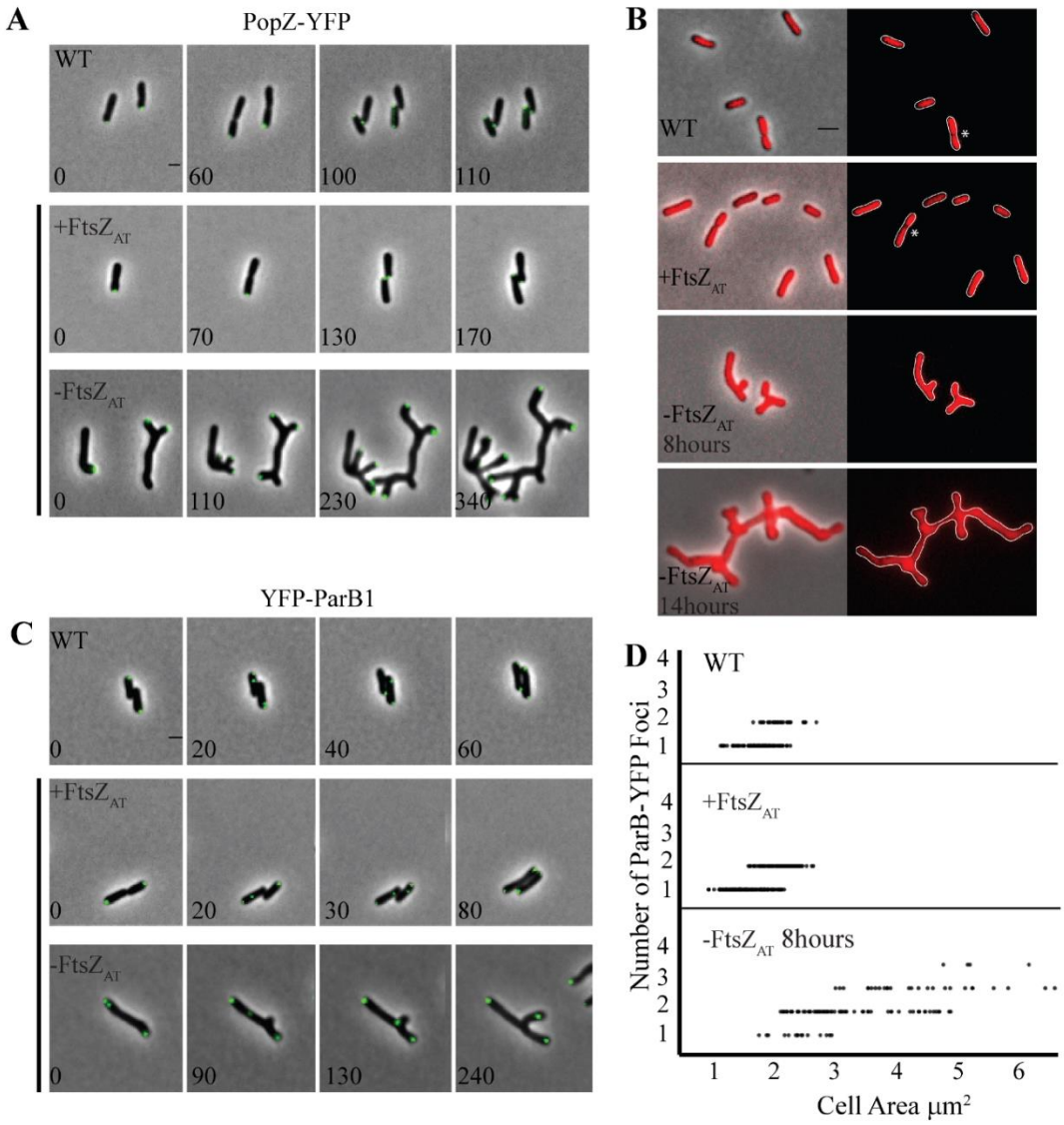

Figure 4.4. Characterization of genomic content during $FtsZ_{AT}$ depletion. A) Timelapse microscopy shows that PopZ-YFP maintains polar localization during elongation and dissociates moving to the mid-cell at division in WT and when *$ftsZ_{AT}$* is induced. PopZ-YFP becomes trapped at the growth poles during $FtsZ_{AT}$ depletion. B) Sytox Orange labeled DNA is diffuse throughout young cells and separated nucleoids are seen in late divisional cells in WT and when $FtsZ_{AT}$ is induced. These DNA free regions are marked with an asterisk. Nucleoids fail to form, as diffuse DNA labeling is observed during $FtsZ_{AT}$ depletion at both 8 h and 14 h depletion timepoints. C) Timelapse

microscopy demonstrates YFP-ParB1 form a single focus at the old pole in WT and when *ftsZ$_{AT}$* is induced. A second focus then translocates the cell length to the growth pole. Timelape microscopy during FtsZ$_{AT}$ depletion reveals a third focus which translocates the cell towards an ectopic pole. D) Quantitation of YFP-ParB1 foci plotted against cell area. Number of foci increase as cell area increases. All scale bars are set to 2 μm.

Loss of septal PG synthesis results in altered total PG composition. Since polar growth appears to continue in the absence of FtsZ (Figure 4.1E, bottom panel), we used fluorescent-D-amino acids (FDAAs), to probe sites enriched in peptidoglycan synthesis [38] during depletion of $FtsZ_{AT}$. In WT cells, FDAAs localize at a single pole in elongating cells and at mid-cell in pre-divisional cells (Figure 4.5A) [38]. As $FtsZ_{AT}$ is depleted, FDAAs are targeted strictly to the poles, confirming that polar peptidoglycan synthesis is responsible for the observed increase in cell biomass after 8 h and 14 h of depletion (Figure 4.5A).

Since cells depleted of $FtsZ_{AT}$ fail to terminate polar growth and do not produce septal peptidoglycan, we hypothesized that the peptidoglycan composition may reveal chemical signatures of peptidoglycan derived from polar growth. Thus, we characterized the peptidoglycan composition of both WT cells and the *ftsZ*$_{AT}$ depletion strain in both the presence and absence of IPTG using ultrapure liquid chromatography (UPLC) [51]. The major muropeptides found in WT *A. tumefaciens* PG and quantified in these studies are shown in Figure S4.2A and include monomeric (M), dimeric (D), and trimeric (T) muropeptides. The muropeptide composition and abundance in WT cells, WT cells grown in the presence of IPTG, and the *ftsZ*$_{AT}$ depletion strain grown in the presence of IPTG such that $FtsZ_{AT}$ is expressed are quite similar (Figure S4.2B), suggesting that there are no major changes in PG composition due to IPTG and that the presence of IPTG leads to complementation in the *ftsZ*$_{AT}$ depletion strain. In contrast, when the *ftsZ*$_{AT}$ depletion strain is grown in the absence of IPTG for 14 h, marked changes in muropeptide composition are observed (Figure 4.5B-D). While the overall abundance of monomeric,

dimeric, and trimeric muropeptides are not dramatically impacted (Figure 4.5C), the abundance of specific muropeptides is modified. When $FtsZ_{AT}$ is depleted, there is a significant increase in the abundance of monomeric muropeptide M3 and a decrease in the abundance of M4 (Figure 4.5B). This observation is consistent with the possibility that the absence of $FtsZ_{AT}$ leads to an increase in LD-carboxypeptidase activity, which would remove the terminal peptide from M4, leading to both a reduction in the levels of M4 and an increase in the abundance in M3. Following $FtsZ_{AT}$ depletion, the overall degree of muropeptide crosslinking decreases (Figure 4.5D). In particular, there is a marked decrease in DD-crosslinkages, which are formed by the DD-transpeptidase activity associated with penicillin-binding proteins (PBPs). The dominant dimeric muropeptide formed in the presence of $FtsZ_{AT}$ is D44, which contains a DD-crosslink; in contrast, the dominant dimer formed in the absence of $FtsZ_{AT}$ is D33, which contains an LD-crosslink (Figure 4.5B). These data indicate that the activity of LD-transpeptidases is increased and the activity of PBP-mediated DD-transpeptidases is decreased during $FtsZ_{AT}$ depletion. The increased pool of M3 may provide additional substrate needed to increase the production of D33 (requires a monomeric M3 acceptor and an M4 donor) relative to D44 (requires a monomeric M4 acceptor and an M5 donor). In addition, increased LD-carboxypeptidase activity could contribute to the increased of levels of D33 if D34 is used as a substrate.

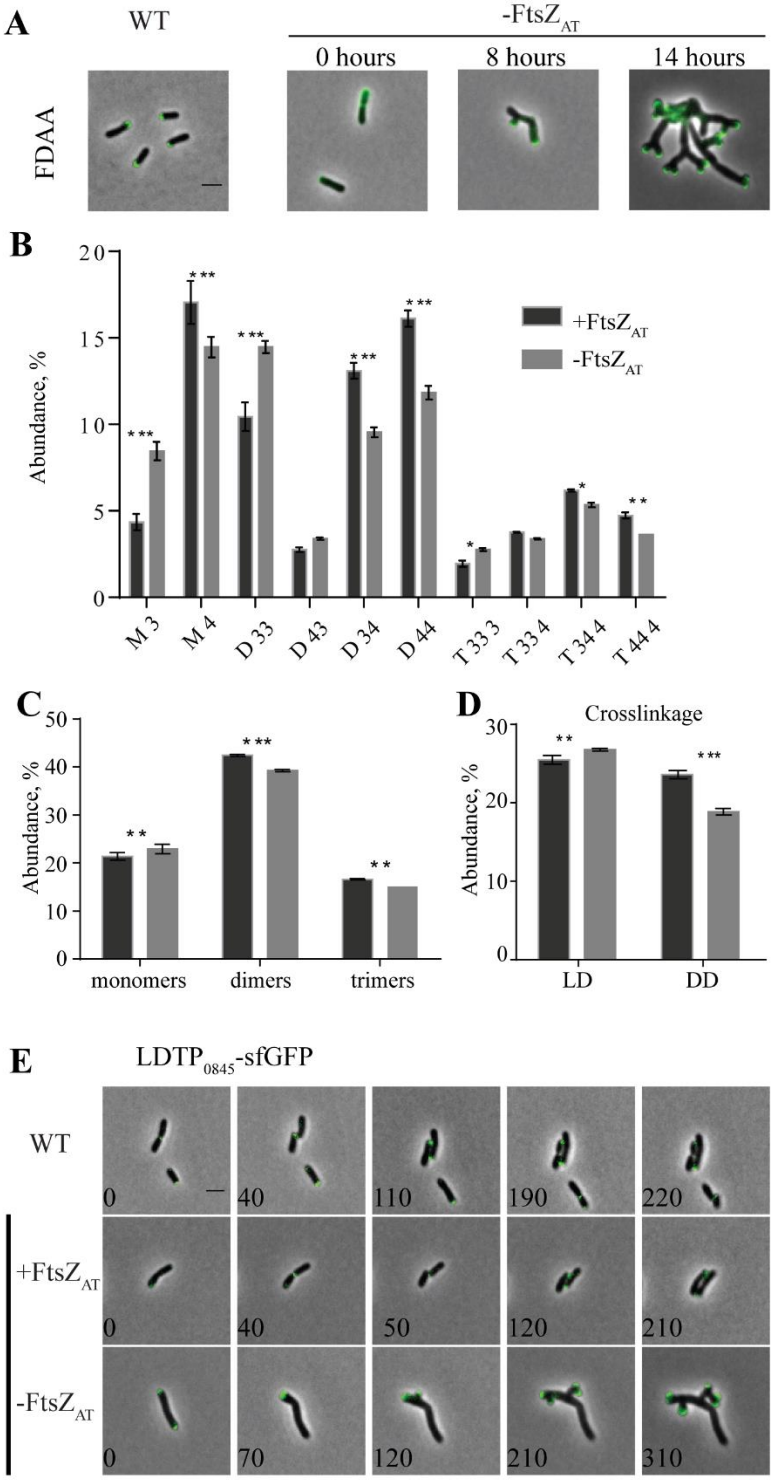

Figure 4.5. Characterization of polar peptidoglycan synthesis during FtsZ$_{AT}$ depletion. A) FDAA labels active peptidoglycan synthesis at a single growing pole and

septum in WT and cells depleted of $FtsZ_{AT}$ for 0 h. As $FtsZ_{AT}$ is depleted for 8 and 14 h, multiple growth poles are labeled, and septum labeling is lost. B) Quantitation of the major muropeptide peaks in *ftsZ$_{AT}$* depletion strain induced. C) Abundance of total monomers, dimers, and trimers in the muropeptide profile in *ftsZ$_{AT}$* depletion strain. D) Abundance of total LD and DD crosslinkage in *ftsZ$_{AT}$* depletion strain. For B, C,and D, data shown are the average abundance of each muropeptide and are taken from analysis of three independent biological samples of *ftsZ$_{AT}$* depletion strain induced (black bars) and depleted for 14 h (gray bars). Statistical significance is indicated with an asterisk. E) Timelapse microscopy of $LDTP_{0845}$-sfGFP in WT and when *ftsZ$_{AT}$* is induced yields growth pole localization during elongation and mid-cell localization during septum formation. In cells depleted of $FtsZ_{AT}$, localization is trapped at the growing poles. All scale bars are set to 2 μm.

The *A. tumefaciens* genome contains 14 LD-transpeptidases, with 7 of those specific to Rhizobiales. The Rhizobiales-specific LD-transpeptidase encoded by *Atu_0845* has been shown to localize to the growing pole in WT cells and has been hypothesized to contribute to polar growth [29]. We find that this LD-transpeptidase becomes trapped at growth poles during depletion of $FtsZ_{AT}$ (Figure 4.5E). This observation suggests that this LD-transpeptidase may contribute to changes in PG composition during $FtsZ_{AT}$ depletion and supports a potential role for LD-transpeptidases in polar growth during elongation. The localization and function of the LD-carboxypeptidases in *A. tumefaciens* remain to be explored. Overall, these findings suggest that LD-carboxypeptidase and LD-transpeptidase activity is increased during $FtsZ_{AT}$ depletion, indicating that these enzymes may contribute to polar growth of *A. tumefaciens*.

The C-terminal Conserved Peptide (CTP) of $FtsZ_{AT}$ is required for termination of polar growth. To better understand the mechanism by which $FtsZ_{AT}$ terminates polar growth, we constructed truncated proteins to analyze the function of the C-terminal conserved peptide (CTP) and the C-terminal linker (CTL) (Figure 4.1A). The CTP is a highly conserved domain which binds proteins such as FtsA to tether FtsZ to the membrane [46,52,53]. The CTL is an intrinsically disordered region of variable length found in FtsZ proteins, which functions in the regulation of PG biosynthesis and protofilament assembly [17,54-56]. To probe the function of the $FtsZ_{AT}$ CTP and CTL domains, we expressed $FtsZ_{AT}\Delta$CTP and $FtsZ_{AT}\Delta$CTL in both WT and an $FtsZ_{AT}$ depletion background.

In order to execute these experiments, we constructed a vector with an alternative "inducible" promoter system, which is compatible with the chromosomal IPTG depletion system. We modified pSRKKm [57] by replacing *lacI*^{q} with the gene encoding the cumate responsive repressor CymR [58,59] and replacing the *lacO* operator sites with *cuO* operator sites (Figure S4.3A). This approach allows the same promoter to drive expression of both chromosomal full-length *ftsZ*$_{AT}$ using IPTG and plasmid-encoded *ftsZ* variants using cumate. For simplicity, henceforth we referred to IPTG induction as mediated by P_{lac} and cumate induction as mediated by P_{cym}. Expression of sfGFP from P_{cym} requires the presence of cumate (FigureS3B) and is comparable to expression of sfGFP from P_{lac} (Figure S4.3C). Although higher concentrations of cumate inhibit growth of WT *A. tumefaciens*, 0.01 mM cumate does not impair growth of WT cells (Figure S4.3D; left) and is sufficient to complement growth of the *ftsZ*$_{AT}$ depletion strain in the absence of IPTG (Figure S4.3D; right).

In the *ftsZ*$_{AT}$ depletion strain, we introduced 4 vectors: an empty vector with P_{cym} (pEmpty), P_{cym}-*ftsZ*$_{AT}$ (pFtsZ$_{AT}$), P_{cym}-*ftsZ*$_{AT}$Δ*CTP* (pFtsZ$_{\Delta CTP}$) or P_{cym}-*ftsZ*$_{AT}$Δ*CTL* (pFtsZ$_{\Delta CTL}$). When full-length *ftsZ*$_{AT}$ is expressed from the chromosome, the viability of cells is not impacted by the presence of the P_{cym} vectors (Figure 4.6A, top left panel). In the absence of induction of *ftsZ* from the chromosome, the presence of the uninduced P_{cym} vectors, including pFtsZ$_{AT}$, is not sufficient to rescue viability of the FtsZ-depleted cells (Figure 4.6A, top right panel); however, viability is significantly restored by expression of plasmid-encoded FtsZ$_{AT}$ in the presence of cumate (Figure 4.6A, bottom left panel). Expression of plasmid-encoded FtsZ$_{AT}$ΔCTP partially rescues the depletion of

$FtsZ_{AT}$ (Figure 4.6A, bottom left panel). In contrast, expression of plasmid-encoded $FtsZ_{AT}\Delta$CTL does not rescue the depletion of $FtsZ_{AT}$ (Figure 4.6A, bottom left panel) and when both chromosomal full-length $FtsZ_{AT}$ and $FtsZ_{AT}\Delta$CTL are expressed, viability is impaired, suggesting that $FtsZ_{AT}\Delta$CTL may have a dominant negative phenotype (Figure 4.6A, bottom right panel).

Next, we observed cell morphology of the *ftsZ$_{AT}$* depletion strain carrying each of the four vectors under conditions where the chromosomal $FtsZ_{AT}$ is depleted and the plasmid-encoded FtsZ variants are expressed for 6 or 14 h (Figure 4.6B). The presence of pEmpty does not impact the $FtsZ_{AT}$ depletion phenotype: branched cells with multiple growth active poles are observed (Figure 4.6B). Plasmid-encoded $FtsZ_{AT}$ rescues the chromosomal $FtsZ_{AT}$ depletion, resulting in the production of typical rod-shaped cells with PG biosynthesis occurring at a single pole or mid-cell (Figure 4.6B, middle left). The partial rescue of $FtsZ_{AT}$ depletion in viability by expression of $FtsZ_{AT}\Delta$CTP was matched by a less severe defect in cell morphology (Figure 4.6B, middle right). Although cells are branched, they are much shorter and have fewer branches than $FtsZ_{AT}$ depletion. FDAA labeling reveals that the expression of $FtsZ_{AT}\Delta$CTP enables mid-cell labeling, suggesting that PG is synthesized at mid-cell and that some cells may undergo division. Indeed, timelapse microscopy of the $FtsZ_{AT}$ depletion strain expressing only FtsZΔCTP reveals that the cells are capable of cell division events (Figure 4.6C, top panel). Remarkably, the site of cell constriction and cell division are atypical, giving rise to cells with a broad length distribution. Furthermore, polar growth is not terminated efficiently and both polar elongation and tip splitting events are evident. Together, these

observations suggest that the FtsZ CTP contributes to proper termination of polar growth and divisome assembly. Expression of plasmid-encoded $FtsZ_{AT}\Delta CTL$ in the absence of chromosome-encoded $FtsZ_{AT}$ gives rise to a distinct cell morphology (Figure 4.6B, far right panel). After 6 h of $FtsZ_{AT}\Delta CTL$ expression, some cells contain mid-cell bulges. Remarkably, in these cells, FDAA labeling reveals that PG biosynthesis is occurring in the bulges and not at either pole. After 14 h, most cells have mid-cell swelling and multiple ectopic poles. Timelapse microscopy reveals that polar growth is terminated and growth appears to be directed to mid-cell (Figure 4.6C, bottom panel, 320 min). When cell division fails, ectopic growth poles emerge from the mid-cell bulges (Figure 4.6C, bottom panel 520 min). The ectopic poles elongate, polar growth is terminated, and new ectopic growth poles are formed near the initial bulge site (Figure 4.6C, bottom panel). These observations suggest that the CTL of $FtsZ_{AT}$ is required for cell division but not required for the termination of polar growth.

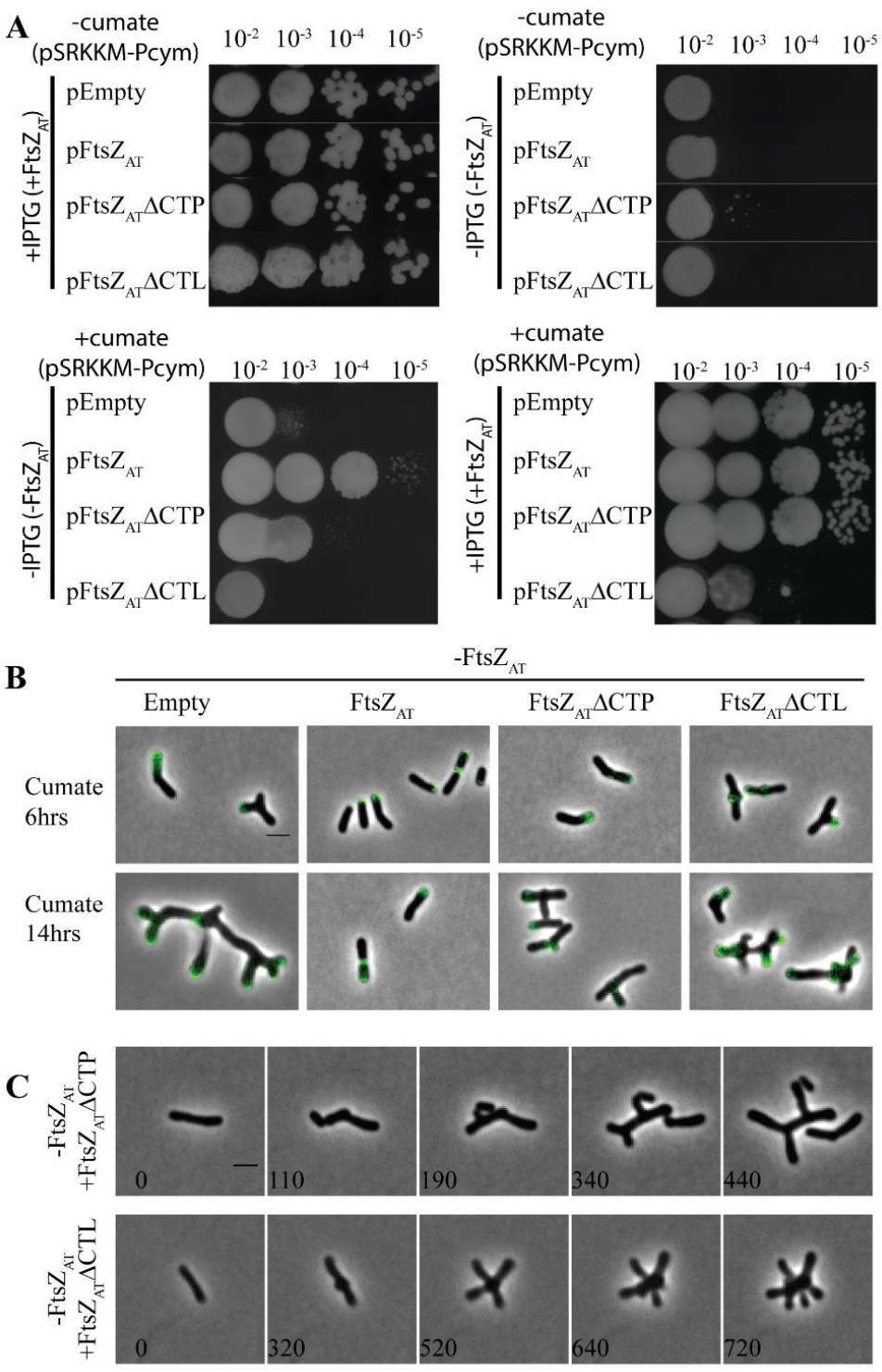

Figure 4.6. Functional analysis of FtsZ$_{AT}$ΔCTL and FtsZ$_{AT}$ΔCTP. A) Cell viability is measured by spotting serial dilutions of *ftsZ$_{AT}$* variants in the *ftsZ$_{AT}$* depletion background. When chromosomal *ftsZ$_{AT}$* is induced by IPTG and plasmid driven *ftsZ$_{AT}$* variants are

uninduced, all strains have similar viability (top left). When both chromosomal *ftsZ$_{AT}$* is uninduced and plasmid driven *ftsZ$_{AT}$* variants are uninduced, all strains exhibit an equal decrease in viability (top right). When chromosomal *ftsZ$_{AT}$* is uninduced and plasmid driven *ftsZ$_{AT}$* variants are induced by cumate, FtsZ$_{AT}$ expression rescues viability, FtsZ$_{AT}$ΔCTP partially rescues, and FtsZ$_{AT}$ΔCTL fails to rescue viability (bottom left). When both chromosomal *ftsZ$_{AT}$* is induced with IPTG and plasmid driven *ftsZ$_{AT}$* variants are induced by cumate, FtsZ$_{AT}$ΔCTL expression reduces viability while other variants have no impact (bottom right). B) Representative images displaying morphology and FDAA labeling while chromosomal *ftsZ$_{AT}$* is uninduced and plasmid driven *ftsZ$_{AT}$* variants are induced for 6 and 14 h. C) Timelapse microscopy while chromosomal *ftsZAT* is uninduced and plasmid driven FtsZ$_{AT}$ΔCTP is expressed reveal that polar growth fails to terminate and undergoes tip splitting, although septum formation and cell division also take place (top panel). Timelapse microscopy while chromosomal *ftsZ$_{AT}$* is uninduced and plasmid driven FtsZ$_{AT}$ΔCTL is expressed shows termination of polar growth and new pole formation near mid-cell (bottom panel).

FtsA is required for cell division but not termination of polar growth. Since FtsA tethers FtsZ to the membrane and enables divisome assembly [46,52,53], we expected that the depletion of FtsA would phenocopy the depletion of FtsZ. Although a saturating transposon mutagenesis screen indicated that *ftsA* is not essential for *A. tumefaciens* cell survival [43], we were unable to construct a Δ*ftsA* mutant. Thus, we constructed a depletion strain in which expression of *ftsA* is controlled by P_{lac}. Under conditions where FtsA is present in the *ftsA* depletion strain, cells maintain proper rod-shaped morphology, polar growth, and cell division occurs from constrictions formed near mid-cell (Figure 4.7A-B, top panels). In contrast, when FtsA is depleted, the cells exhibit a marked change in morphology (Figure 4.7A, bottom panel). During the depletion of FtsA, rod-shaped cells initially elongate from a growth pole (Figure 4.7A, bottom panel, 0 min). Polar growth is terminated and growth is re-initiated from near mid-cell, typically resulting in the formation of two ectopic poles perpendicular to the original longitudinal axis of the cell (Figure 4.7A, bottom panel, 170 min). Cells depleted of FtsA continue multipolar growth (Figure 4.7A, bottom panel, 360 min), terminate growth from both poles and reinitiate growth from near mid-cell resulting in the formation of a new pair of ectopic growth poles (Figure 4.7A, bottom panel, 510 min). This pattern of multipolar growth, polar growth termination, and new branch formation is continued until cells eventually bulge at the mid-cell and lyse. Overall these observations indicate that the phenotypes caused by FtsZ and FtsA depletion are distinct and suggest that only FtsZ is required for proper termination of polar growth.

To confirm that polar growth occurs and is terminated during FtsA depletion, cells were labeled with FDAAs (Figure 4.7B, bottom panel). Indeed, FDAAs label the tips of two poles, which are emerging from near mid-cell consistent with the re-initiation of polar growth. To further confirm that polar growth is terminated during FtsA depletion, we observed the localization of PopZ-YFP (Figure 4.7C, top panel). PopZ marks the growth poles [49] and becomes trapped at growth poles during depletion of FtsZ (Figure 4.4A). During FtsA depletion, PopZ-YFP is initially present at the growth pole (Figure 4.7C, top panel, 0 min). Next, PopZ-YFP disappears from the growth poles and reappears near mid-cell (Figure 4.7C, top panel, 80 min) indicating that polar growth is terminated. Throughout the FtsA depletion, PopZ-YFP continues to disappear from growth poles and reappears at the tips of newly emerging growth poles. Overall, these observations clearly indicate that FtsA is not necessary for termination of polar growth; however, FtsA has an essential function at a later stage of cell division since the cells fail to divide and are prone to lysis.

The ability of cells to target growth to near mid-cell during FtsA depletion suggests that FtsZ-rings may form, enabling the termination of polar growth. Indeed, $FtsZ_{AT}$-sfGFP-rings form near mid-cell early during FtsA depletion (Figure 4.7C, bottom panel). $FtsZ_{AT}$-sfGFP is briefly retained at new growth poles before reappearing to mark the site where a new growth pole will emerge. These observations are consistent with the finding the FtsA is retained at the growth pole longer than FtsZ [26,60], and suggest that FtsA arrives at mid-cell after Z-ring assembly and the initiation of FtsZ-dependent cell wall biogenesis. The results observed here in *A. tumefaciens* are consistent with the

observation that FtsA arrives to mid-cell after FtsZ and the onset of mid-cell cell wall biogenesis in *C. crescentus* [13,47]. In both *A. tumefaciens* and *C. crescentus*, the late arrival of FtsA to the divisome suggests that other proteins contribute to proper tethering of FtsZ to the membrane. In *C. crescentus*, the FtsZ-binding protein, FzlC, functions as a membrane anchor early during the establishment of the divisome [30,61]. A homolog of FzlC is readily found in the *A. tumefaciens* genome (Atu2824) and may contribute to the ability of FtsZ-rings to form in the absence of FtsA.

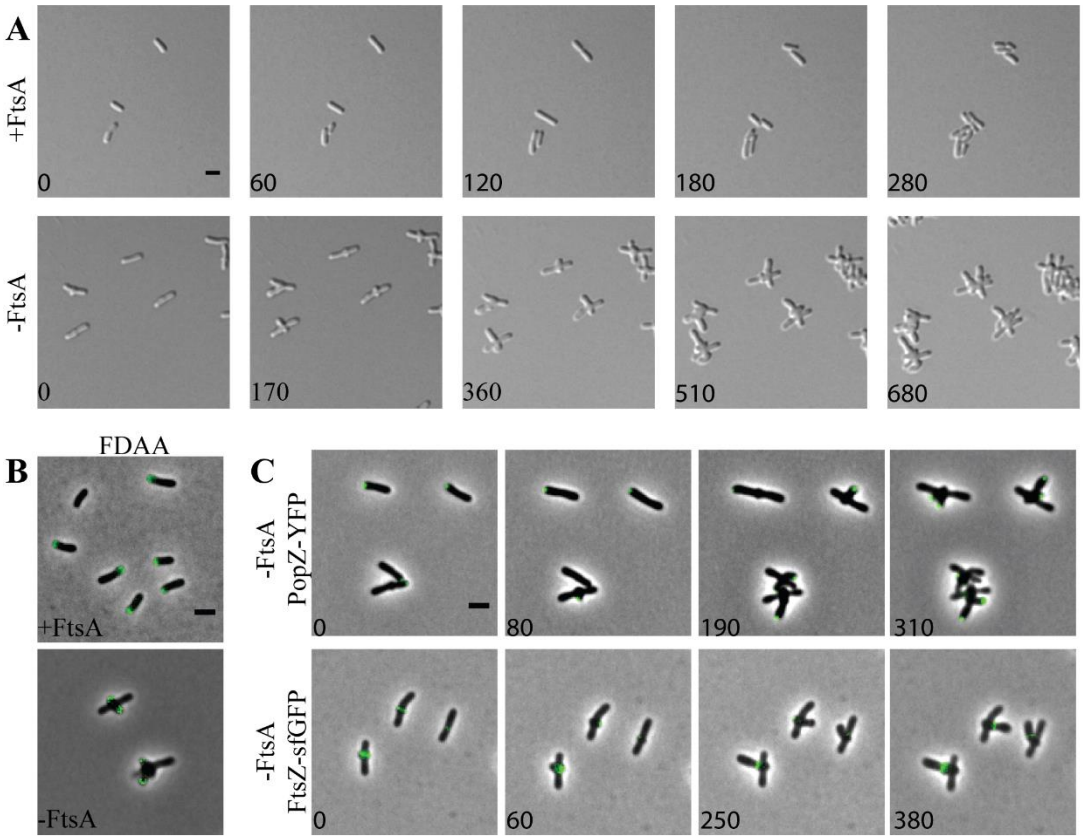

Figure 4.7. FtsA is not required for termination of polar growth. A) Timelapse microscopy shows cells expressing FtsA grow and divide normally forming microcolonies (top panel). Cells depleted of FtsA terminate polar growth and form new growth poles near the mid-cell (bottom panel). B) FDAAs label a single growth pole when FtsA is present (top) and label multiple poles emerging from the mid-cell when FtsA is absent (bottom). C) Timelapse microscopy during FtsA depletion shows PopZ-YFP localizes to the growth poles and dissociates as growth is terminated. It then reappears at the new pole sites (top). During FtsA depletion, FtsZ-sfGFP forms rings marking the future sites of pole formation (bottom).

Depletion of the downstream divisome component FtsW phenocopies depletion of FtsA. We hypothesized that the phenotype observed during FtsA depletion will be shared when cell division is blocked after FtsZ-ring assembly. To test this hypothesis, we constructed a depletion strain of FtsW, which is recruited to mid-cell after FtsA in both *E. coli* and *C. crescentus* divisome assembly models [13,62]. Depletion of FtsW results in a phenotype which is strikingly similar to the depletion of FtsA (Figure 4.8). During FtsW depletion, polar growth is terminated, resulting in the establishment of growth-active poles from near mid-cell (Figure 4.8A, bottom panel). Multiple rounds of termination of polar growth following by reinitiation of growth from near mid-cell occur until the mid-cell bulges and the cells ultimately lyse (Figure 4.8A, bottom panel). Labeling of growth active poles with FDAAs (Figure 4.8B) or by tracking PopZ-YFP localization (Figure 4.8C, top panel) confirmed that new branches which emerge from mid-cell are formed by polar growth. Finally, we confirmed that FtsZ-rings form during the depletion of FtsW and the presence of an $FtsZ_{AT}$-sfGFP-ring typically marks the site where an ectopic growth pole will form (Figure 4.8C, bottom panel). Together, these observations suggest that FtsZ-rings are formed in the absence of FtsW, enabling the initiation of cell wall biogenesis. Given that FtsW drives septal PG biosynthesis, [63] these findings indicate that the cell wall biogenesis that occurs during depletion of FtsA or FtsW may require the elongation machinery, which typically functions in polar growth. Since the elongation machinery for *A. tumefaciens* remains to be identified, it is possible that there is considerable overlap between the machineries that contribute to polar and septal PG biosynthesis.

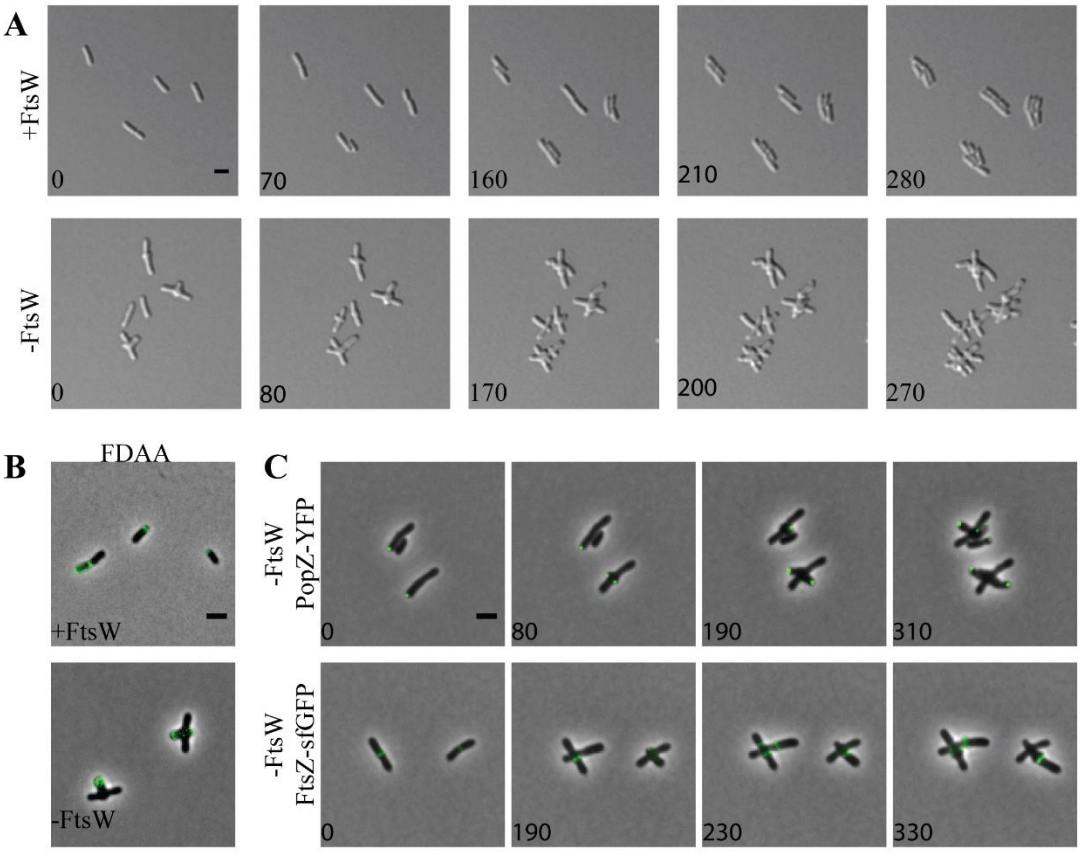

Figure 4.8. FtsW is not required for termination of polar growth A) Timelapse microscopy shows cells expressing FtsW grow and divide normally forming microcolonies (top panel). Cells depleted of FtsW terminate polar growth and form new growth poles near the mid-cell (bottom panel). B) FDAA labels a single growth pole when FtsW is present (top) and labels multiple poles emerging from the mid-cell when FtsW is absent (bottom). C) Timelapse microscopy during FtsW depletion shows PopZ-YFP localizes to the growth poles and dissociates as growth is terminated. It then reappears at the new pole sites (top). During FtsW depletion, FtsZ-sfGFP forms rings marking the future sites of pole formation (bottom).

Concluding Remarks

While many questions remain unanswered about the regulation of cell wall biogenesis in *A. tumefaciens*, our work sheds light on the transition from polar growth to mid-cell growth. We find that $FtsZ_{AT}$, FtsA, and FtsW are required for constriction and cell separation, but $FtsZ_{AT}$ is also required to terminate polar growth and initiate mid-cell peptidoglycan synthesis (Figure 4.1, 4.7-4.8). How might the formation of an $FtsZ_{AT}$-ring at mid-cell cause the termination of polar growth? We find that PopZ, and $LDTP_{0845}$ become trapped at the growth poles during FtsZ depletion (Figure 4.5). It is possible that one or more of these proteins contributes to both polar peptidoglycan biosynthesis and mid-cell peptidoglycan synthesis and that the FtsZ-dependent targeting of these proteins (and likely others) to mid-cell triggers the termination of polar growth. While the mid-cell localization of PopZ is dependent on the presence of $FtsZ_{AT}$ (Figure 4.4), $FtsZ_{AT}$-ring stability and placement are impacted by the absence of PopZ [48]. Furthermore, deletion of *popZ* impairs termination of polar growth and results in cell division defects [35,48,64]. The apparent co-dependence of FtsZ and PopZ for localization may suggest that these proteins function together during the early stages of cell division, particularly the termination of polar growth and onset of mid-cell PG biosynthesis.

Overall, our results are consistent with a general model, which is highly conserved in bacteria, in which the establishment of an FtsZ-ring leads to the recruitment of many other cell division proteins to mid-cell [11], but many mechanistic questions remain. How is $FtsZ_{AT}$ targeted to mid-cell? A variety of mechanisms that contribute to the proper placement of FtsZ at mid-cell have been described (for review see[65,66]). The most well

studied mechanisms of FtsZ positioning include negative regulation by the Min system and nucleoid occlusion. While genes encoding components of the Min system are readily identifiable in the *A. tumefaciens* genome, the deletion of *minCDE* has a minimal impact on placement of constriction sites and cell division efficiency [67]. Furthermore, $FtsZ_{AT}$-GFP rings form over DNA prior to nucleoid separation in *A. tumefaciens*. These observations indicate that additional regulatory mechanisms must contribute to proper division site selection in *A. tumefaciens*. Following the appearance of FtsZ at mid-cell, how is the $FtsZ_{AT}$-ring stabilized? In *E. coli*, the FtsZ-ring is stabilized by interactions with FtsA and ZipA, which tether FtsZ filaments to the membrane [46,53,68,69]. In *A. tumefaciens*, $FtsZ_{AT}$ appears at mid-cell well before FtsA [29] and we observe that $FtsZ_{AT}$ rings form even when FtsA is depleted (Figure 4.7C, bottom panel). Furthermore, the position of $FtsZ_{AT}$-GFP rings marks the site of ectopic pole formation. These observations suggest the $FtsZ_{AT}$ is stabilized, at least early during cell division by other proteins. While there are no obvious ZipA homologs encoded in the *A. tumefaciens* genome, a homolog of FzlC, which functions to stabilize FtsZ in *C. crescentus* [30,61], is encoded in the genome.

The observation that FtsZ is necessary for the initiation of mid-cell PG biosynthesis suggests that FtsZ is necessary for recruitment of PG biosynthesis enzymes to mid-cell. Septal PG biosynthesis is likely mediated by FtsW, a putative PG glycosyltransferase [70-72], and PBP3 (FtsI), a PG DD-transpeptidase [73]. In *A. tumefaciens*, depletion of FtsW does not cause a complete block of PG synthesis at mid-cell (Figure 4.8). This observation may suggest that mid-cell PG biosynthesis is mediated by other cell wall

biogenesis enzymes while the activity of FtsW contributes to later stages of cell division, consistent with the inability of cells to form constrictions and separate in the absence of FtsW. These observations may indicate that the initial PG biosynthesis at mid-cell may comprise the final stage of cell elongation, consistent with descriptions of FtsZ-dependent mid-cell elongation in *C. crescentus* [16]. The observation that growth-active, ectopic poles emerge from near mid-cell during FtsW depletion (Figure 4.8B) provides evidence in support of this possibility. Thus, FtsZ-dependent PG biosynthesis may contribute to both elongation and cell division in *A. tumefaciens*. For a polar growing bacterium, it is tempting to speculate that the retention of PG biosynthesis machinery dedicated to elongation at the site of cell division may prime the newly formed poles to become growth active following cell separation.

References

1. den Blaauwen T, Andreu JM, Monasterio O: Bacterial cell division proteins as antibiotic targets. *Bioorg Chem* 2014, 55:27-38.

2. Haeusser DP, Levin PA: The great divide: coordinating cell cycle events during bacterial growth and division. *Curr Opin Microbiol* 2008, 11:94-99.

3. Wu LJ, Errington J: Coordination of cell division and chromosome segregation by a nucleoid occlusion protein in *Bacillus subtilis*. *Cell* 2004, 117:915-925.

4. Bi EF, Lutkenhaus J: FtsZ ring structure associated with division in *Escherichia coli*. *Nature* 1991, 354:161-164.

5. de Boer P, Crossley R, Rothfield L: The essential bacterial cell-division protein FtsZ is a GTPase. *Nature* 1992, 359:254-256.

6. Li Z, Trimble MJ, Brun YV, Jensen GJ: The structure of FtsZ filaments *in vivo* suggests a force-generating role in cell division. *Embo J* 2007, 26:4694-4708.

7. Fu G, Huang T, Buss J, Coltharp C, Hensel Z, Xiao J: *In vivo* structure of the *E. coli* FtsZ-ring revealed by photoactivated localization microscopy (PALM). *PLoS One* 2010, 5:e12682.

8. Holden SJ, Pengo T, Meibom KL, Fernandez Fernandez C, Collier J, Manley S: High throughput 3D super-resolution microscopy reveals *Caulobacter crescentus* in vivo Z-ring organization. *Proc Natl Acad Sci U S A* 2014, 111:4566-4571.

9. Bisson-Filho AW, Hsu YP, Squyres GR, Kuru E, Wu F, Jukes C, Sun Y, Dekker C, Holden S, VanNieuwenhze MS, et al.: Treadmilling by FtsZ filaments drives peptidoglycan synthesis and bacterial cell division. *Science* 2017, 355:739-743.

10. Yang X, Lyu Z, Miguel A, McQuillen R, Huang KC, Xiao J: GTPase activity-coupled treadmilling of the bacterial tubulin FtsZ organizes septal cell wall synthesis. *Science* 2017, 355:744-747.

11. Du S, Lutkenhaus J: Assembly and activation of the *Escherichia coli* divisome. *Mol Microbiol* 2017, 105:177-187.

12. Meier EL, Goley ED: Form and function of the bacterial cytokinetic ring. *Curr Opin Cell Biol* 2014, 26:19-27.

13. Goley ED, Yeh YC, Hong SH, Fero MJ, Abeliuk E, McAdams HH, Shapiro L: Assembly of the *Caulobacter* cell division machine. *Mol Microbiol* 2011, 80:1680-1698.

14. Erickson HP, Anderson DE, Osawa M: FtsZ in bacterial cytokinesis: cytoskeleton and force generator all in one. *Microbiol Mol Biol Rev* 2010, 74:504-528.

15. Varma A, Young KD: FtsZ collaborates with penicillin binding proteins to generate bacterial cell shape in *Escherichia coli*. *J Bacteriol* 2004, 186:6768-6774.

16. Aaron M, Charbon G, Lam H, Schwarz H, Vollmer W, Jacobs-Wagner C: The tubulin homologue FtsZ contributes to cell elongation by guiding cell wall precursor synthesis in *Caulobacter crescentus*. *Mol Microbiol* 2007, 64:938-952.

17. Sundararajan K, Miguel A, Desmarais SM, Meier EL, Huang KC, Goley ED: The bacterial tubulin FtsZ requires its intrinsically disordered linker to direct robust cell wall construction. *Nat Commun* 2015, 6:7281.

18. Aarsman ME, Piette A, Fraipont C, Vinkenvleugel TM, Nguyen-Disteche M, den Blaauwen T: Maturation of the *Escherichia coli* divisome occurs in two steps. *Mol Microbiol* 2005, 55:1631-1645.

19. Pini F, De Nisco NJ, Ferri L, Penterman J, Fioravanti A, Brilli M, Mengoni A, Bazzicalupo M, Viollier PH, Walker GC, et al.: Cell cycle control by the master regulator CtrA in *Sinorhizobium meliloti*. *PLoS Genetics* 2015, 11:e1005232.

20. Howell M, Brown PJB: Building the bacterial cell wall at the pole. *Curr Opin Microbiol* 2016, 34:53-59.

21. Pini F, Frage B, Ferri L, De Nisco NJ, Mohapatra SS, Taddei L, Fioravanti A, Dewitte F, Galardini M, Brilli M, et al.: The DivJ, CbrA and PleC system controls DivK phosphorylation and symbiosis in *Sinorhizobium melilot*i. *Mol Microbiol* 2013, 90:54-71.

22. Bellefontaine AF, Pierreux CE, Mertens P, Vandenhaute J, Letesson JJ, De Bolle X: Plasticity of a transcriptional regulation network among alpha-proteobacteria is supported by the identification of CtrA targets in *Brucella abortus*. *Mol Microbiol* 2002, 43:945-960.

23. Cheng J, Sibley CD, Zaheer R, Finan TM: A *Sinorhizobium meliloti minE* mutant has an altered morphology and exhibits defects in legume symbiosis. *Microbiology* 2007, 153:375-387.

24. Latch JN, Margolin W: Generation of buds, swellings, and branches instead of filaments after blocking the cell cycle of *Rhizobium meliloti*. *J Bacteriol* 1997, 179:2373-2381.

25. Fujiwara T, Fukui S: Effect of D-alanine and mitomycin-C on cell morphology of *Agrobacterium tumefaciens*. *Gen App Microbiol* 1974, 20:345-349.

26. Zupan JR, Cameron TA, Anderson-Furgeson J, Zambryski PC: Dynamic FtsA and FtsZ localization and outer membrane alterations during polar growth and cell

division in *Agrobacterium tumefaciens*. *Proc Natl Acad Sci U S A* 2013, 110:9060-9065.

27. Figueroa-Cuilan WM, Brown PJB: Cell wall biogenesis during elongation and division in the plant pathogen *Agrobacterium tumefaciens*. *Curr Top Microbiol Immunol* 2018 (epub before print).

28. Brown PJB, de Pedro MA, Kysela DT, Van der Henst C, Kim J, De Bolle X, Fuqua C, Brun YV: Polar growth in the alphaproteobacterial order Rhizobiales. *Proc Natl Acad Sci U S A* 2012, 109:1697-1701.

29. Cameron TA, Anderson-Furgeson J, Zupan JR, Zik JJ, Zambryski PC: Peptidoglycan synthesis machinery in *Agrobacterium tumefaciens* during unipolar growth and cell division. *mBio* 2014, 5.

30. Goley ED, Dye NA, Werner JN, Gitai Z, Shapiro L: Imaging-based identification of a critical regulator of FtsZ protofilament curvature in *Caulobacte*r. *Mol Cell* 2010, 39:975-987.

31. Figueroa-Cuilan W, Daniel JJ, Howell M, Sulaiman A, Brown PJ: Mini-Tn*7* insertion in an artificial *att*Tn*7* site enables depletion of the essential master regulator CtrA in the phytopathogen *Agrobacterium tumefaciens*. *Appl Environ Microbiol* 2016, 82:5015-5025.

32. Morton ER, Fuqua C: Laboratory maintenance of *Agrobacterium*. *Curr Protoc Microbiol* 2012, Chapter 1:Unit3 D.1.

33. Choi YJ, Morel L, Le Francois T, Bourque D, Bourget L, Groleau D, Massie B, Miguez CB: Novel, versatile, and tightly regulated expression system for *Escherichia coli* strains. *Appl Environ Microbiol* 2010, 76:5058-5066.

34. Denkovskiene E, Paskevicius S, Werner S, Gleba Y, Razanskiene A: Inducible expression of *Agrobacterium* virulence gene VirE2 for stringent regulation of T-DNA transfer in plant transient expression systems. *Mol Plant Microbe Interact* 2015, 28:1247-1255.

35. Ehrle HM, Guidry JT, Iacovetto R, Salisbury AK, Sandidge DJ, Bowman GR: Polar organizing protein PopZ is required for chromosome segregation in *Agrobacterium tumefaciens*. *J Bacteriol* 2017, 199:e00111-17.

36. Morton ER, Fuqua C: Unit 3D.2 Genetic manipulation of *Agrobacterium*. *Curr Protoc Microbiol* 2012, Chapter1:Unit 3 D.2.

37. Howell M, J. Daniel J, J.B. Brown P: Live cell fluorescence microscopy to observe essential processes during microbial cell growth. *J Vis Exp* 2017, 129: e56497.

38. Kuru E, Velocity Hughes H, Brown PJ, Hall E, Tekkam S, Cava F, de Pedro MA, Brun YV, VanNieuwenhze MS: *In situ* probing of newly synthesized peptidoglycan in live bacteria with fluorescent D-amino acids. *Angew Chem Int Ed Engl* 2012, 51:12519-12523.

39. Ducret A, Quardokus EM, Brun YV: MicrobeJ, a tool for high throughput bacterial cell detection and quantitative analysis. *Nat Microbiol* 2016, 1:16077.

40. Ortiz C, Natale P, Cueto L, Vicente M: The keepers of the ring: regulators of FtsZ assembly. *FEMS Microbiol Rev* 2016, 40:57-67.

41. Wood DW, Setubal JC, Kaul R, Monks DE, Kitajima JP, Okura VK, Zhou Y, Chen L, Wood GE, Almeida NF, Jr., et al.: The genome of the natural genetic engineer *Agrobacterium tumefaciens* C58. *Science* 2001, 294:2317-2323.

42. Goodner B, Hinkle G, Gattung S, Miller N, Blanchard M, Qurollo B, Goldman BS, Cao Y, Askenazi M, Halling C, et al.: Genome sequence of the plant pathogen and biotechnology agent *Agrobacterium tumefaciens* C58. *Science* 2001, 294:2323-2328.

43. Curtis PD, Brun YV: Identification of essential alphaproteobacterial genes reveals operational variability in conserved developmental and cell cycle systems. *Mol Microbiol* 2014, 93:713-735.

44. Richards DM, Hempel AM, Flardh K, Buttner MJ, Howard M: Mechanistic basis of branch-site selection in filamentous bacteria. *PLoS Comput Biol* 2012, 8:e1002423.

45. Pichoff S, Lutkenhaus J: Identification of a region of FtsA required for interaction with FtsZ. *Mol Microbiol* 2007, 64:1129-1138.

46. Szwedziak P, Wang Q, Freund SM, Lowe J: FtsA forms actin-like protofilaments. *Embo J* 2012, 31:2249-2260.

47. Moll A, Thanbichler M: FtsN-like proteins are conserved components of the cell division machinery in proteobacteria. *Mol Microbiol* 2009, 72:1037-1053.

48. Howell M, Aliashkevich A, Salisbury AK, Cava F, Bowman GR, Brown PJB: Absence of the polar organizing protein popz results in reduced and asymmetric cell division in *Agrobacterium tumefaciens*. *J Bacteriol* 2017, 199: e00101-17.

49. Grangeon R, Zupan JR, Anderson-Furgeson J, Zambryski PC: PopZ identifies the new pole, and PodJ identifies the old pole during polar growth in *Agrobacterium tumefaciens. Proc Natl Acad Sci U S A* 2015, 112:11666-11671.

50. Thanbichler M: Synchronization of chromosome dynamics and cell division in bacteria. *Cold Spring Harb Perspect Biol* 2010, 2:a000331.

51. Alvarez L, Hernandez SB, de Pedro MA, Cava F: Ultra-sensitive, high-resolution liquid chromatography methods for the high-throughput quantitative analysis of bacterial cell wall chemistry and structure. *Methods Mol Biol* 2016, 1440:11-27.

52. Vaughan S, Wickstead B, Gull K, Addinall SG: Molecular evolution of FtsZ protein sequences encoded within the genomes of archaea, bacteria, and eukaryota. *J Mol Evol* 2004, 58:19-29.

53. Ma X, Margolin W: Genetic and functional analyses of the conserved C-terminal core domain of *Escherichia coli* FtsZ. *J Bacteriol* 1999, 181:7531-7544.

54. Sundararajan K, Goley ED: The intrinsically disordered C-terminal linker of FtsZ regulates protofilament dynamics and superstructure *in vitro*. *J Biol Chem* 2017, 292:20509-20527.

55. Buske PJ, Levin PA: A flexible C-terminal linker is required for proper FtsZ assembly *in vitro* and cytokinetic ring formation *in vivo*. *Mol Microbiol* 2013, 89:249-263.

56. Gardner KA, Moore DA, Erickson HP: The C-terminal linker of *Escherichia coli* FtsZ functions as an intrinsically disordered peptide. *Mol Microbiol* 2013, 89:264-275.

57. Khan SR, Gaines J, Roop RM, 2nd, Farrand SK: Broad-host-range expression vectors with tightly regulated promoters and their use to examine the influence of TraR and TraM expression on Ti plasmid quorum sensing. *Appl Environ Microbiol* 2008, 74:5053-5062.

58. Kaczmarczyk A, Vorholt JA, Francez-Charlot A: Cumate-inducible gene expression system for sphingomonads and other alphaproteobacteria. *Appl Environ Microbiol* 2013, 79:6795-6802.

59. Eaton RW: p-Cumate catabolic pathway in *Pseudomonas putida* Fl: cloning and characterization of DNA carrying the *cmt* operon. *J Bacteriol* 1996, 178:1351-1362.

60. Cameron TA, Zupan JR, Zambryski PC: The essential features and modes of bacterial polar growth. *Trends Microbiol* 2015, 23:347-353.

61. Meier EL, Razavi S, Inoue T, Goley ED: A novel membrane anchor for FtsZ is linked to cell wall hydrolysis in *Caulobacter crescentus*. *Mol Microbiol* 2016, 101:265-280.

62. Du S, Lutkenhaus J: Assembly and activation of the *Escherichia coli* divisome. *Mol Microbiol* 2017, 105:177-187.

63. Fraipont C, Alexeeva S, Wolf B, van der Ploeg R, Schloesser M, den Blaauwen T, Nguyen-Disteche M: The integral membrane FtsW protein and peptidoglycan synthase PBP3 form a subcomplex in *Escherichia coli*. *Microbiology* 2011, 157:251-259.

64. Grangeon R, Zupan J, Jeon Y, Zambryski PC: Loss of PopZ At activity in *Agrobacterium tumefaciens* by deletion or depletion leads to multiple growth poles, minicells, and growth defects. *mBio* 2017, 8.

65. Rowlett VW, Margolin W: The Min system and other nucleoid-independent regulators of Z ring positioning. *Front Microbiol* 2015, 6:478.

66. Monahan LG, Hajduk IV, Blaber SP, Charles IG, Harry EJ: Coordinating bacterial cell division with nutrient availability: a role for glycolysis. *mBio* 2014, 5:e00935-00914.

67. Flores SA, Howell M, Daniel JJ, Piccolo R, Brown PJB: Absence of the Min system does not cause major cell division defects in *Agrobacterium tumefaciens*. *Front Microbiol* 2018, 9:681.

68. Mosyak L, Zhang Y, Glasfeld E, Haney S, Stahl M, Seehra J, Somers WS: The bacterial cell-division protein ZipA and its interaction with an FtsZ fragment revealed by X-ray crystallography. *Embo J* 2000, 19:3179-3191.

69. Haney SA, Glasfeld E, Hale C, Keeney D, He Z, de Boer P: Genetic analysis of the *Escherichia coli* FtsZ ZipA interaction in the yeast two-hybrid system. Characterization of FtsZ residues essential for the interactions with ZipA and with FtsA. *J Biol Chem* 2001, 276:11980-11987.

70. Cho H, Wivagg CN, Kapoor M, Barry Z, Rohs PD, Suh H, Marto JA, Garner EC, Bernhardt TG: Bacterial cell wall biogenesis is mediated by SEDS and PBP polymerase families functioning semi-autonomously. *Nat Microbiol* 2016:16172.

71. Meeske AJ, Riley EP, Robins WP, Uehara T, Mekalanos JJ, Kahne D, Walker S, Kruse AC, Bernhardt TG, Rudner DZ: SEDS proteins are a widespread family of bacterial cell wall polymerases. *Nature* 2016, 537:634-638.

72. Emami K, Guyet A, Kawai Y, Devi J, Wu LJ, Allenby N, Daniel RA, Errington J: RodA as the missing glycosyltransferase in *Bacillus subtilis* and antibiotic discovery for the peptidoglycan polymerase pathway. *Nat Microbiol* 2017, 2:16253.

73. Botta GA, Park JT: Evidence for involvement of penicillin-binding protein 3 in murein synthesis during septation but not during cell elongation. *J Bacteriol* 1981, 145:333-340.

Supplementary Materials

Supplemental Tables

Table S4.1. Bacterial strains and plasmids used in this study.

Strain or plasmid	Relevant characteristics	Reference/ Source
Source plasmids		
pSRKKm-Plac	Km^r; broad host range vector containing *lacI*^{q} and lac promoter	[1]
pSRKKm-Plac-sf*gfp*	pSRKKm vector containing *lacI*^{q} and lac promoter with sfGFP	[2]
pRVMCS-2	Km^r; vector containing vanillate promoter which provides low constitutive expression in *A. tumefaciens*	[3]
pMR10	Km^r; mini-RK2 vector; constitutive expression	Brun Lab
pNTPS139	Km^r; Suicide vector containing *oriT* and *sacB*	D. Alley
pUC18-mini-Tn7T-GM-LAC	Ap^r Gm^r; mini-Tn7 vector containing *lacI*^{q} and tac promoter	[4]
pUC18-mini-Tn7T-GM-Plac	Ap^r Gm^r; mini-Tn7 vector containing *lacI*^{q} and lac promoter	[2]
pTNS3	Ap^r; helper plasmid encoding the site-specific TnsABCD Tn*7* transposition pathway	[1]
Replicating plasmids		
pRV-*ftsZ*$_{AT}$-sf*gfp*	Km^r; Constitutive expression of *ftsZ*$_{AT}$-sf*gfp*	[5]
pRV-*ftsZ*$_1$-sf*gfp*	Km^r; Constitutive expression of *ftsZ*$_1$-sf*gfp*	This Study
pRV-*ftsZ*$_3$-sf*gfp*	Km^r; Constitutive expression of *ftsZ*$_3$-sf*gfp*	This Study
pSRKKM-Pqaz-*ftsA*-sf*gfp*	Km^r; vector containing *A. tumefaciens* native *ftsQAZ* promoter followed by *ftsA-sfGFP* coding sequence.	[5]
pSRKKm-Plac-*yfp-parB*	pSRKKm vector containing *yfp-parB* under control of the lac promoter	[6]
pSRKKm-Pcym	pSRKKm vector containing lac promoter flanked by *cuO* operator site along with the *cymR* repressor gene	This Study
pSRKKm-Pcym-*yfp-parB*	pSRKKm vector containing *yfp-parB* under control of the cym promoter	This Study
pMR10-PpopZ-*popZ-yfp*	pMR10 vector containing *popZ-yfp* under control of the native promoter	Brun Lab
pRV-*ldtp*$_{0845}$-sf*gfp*	Km^r; Constitutive expression of *ldtp*$_{0845}$-sf*gfp*	This Study
pSRKKm-Pcym-*ftsZ*$_{AT}$	pSRKKm vector containing *ftsZ*$_{AT}$ under control of the cym promoter	This Study
pSRKKm-Pcym-*ftsZ*$_{\Delta CTC}$	pSRKKm vector containing *ftsZ*$_{\Delta CTC}$ under control of the cym promoter	This Study
pSRKKm-Pcym-*ftsZ*$_{\Delta CTL}$	pSRKKm vector containing *ftsZ*$_{\Delta CTL}$ under control of the cym promoter	This Study
Deletion plasmids		
pNTPS139Δ*ftsZ*$_{AT}$	Km^r Suc^s; deletion plasmid for *ftsZ*$_{AT}$	This Study
pNTPS139Δ*ftsZ*$_1$	Km^r Suc^s; deletion plasmid for *ftsZ*$_1$	This Study
pNTPS139Δ*ftsZ*$_3$	Km^r Suc^s; deletion plasmid for *ftsZ*$_3$	This Study
pNTPS139Δ*ftsA*	Km^r Suc^s; deletion plasmid for *ftsA*	This Study
pNTPS139Δ*ftsW*	Km^r Suc^s; deletion plasmid for *ftsW*	This Study

Depletion plasmids		
pUC18-mini-Tn*7*T-GM-LAC *ftsZ$_{AT}$*	Ap^r Gm^r; mini-Tn*7* vector containing *ftsZ$_{AT}$* under control of the tac promoter	This Study
pUC18-mini-Tn*7*T-GM-Plac *ftsA*	Ap^r Gm^r; mini-Tn*7* vector containing *ftsA* under control of the lac promoter	This Study
pUC18-mini-Tn*7*T-GM-Plac *ftsW*	Ap^r Gm^r; mini-Tn*7* vector containing *ftsW* under control of the lac promoter	This Study
E. coli strains		
DH5α	Cloning strain	Life Technologies
S17-1	Smr;RP4-2 TC::MU Km-Tn*7*; for plasmid mobilization	[7]
A. tumefaciens strains		
C58	Nopaline type strain; pTiC58; pAtC58	
C58ΔtetRA::a-*att*Tn*7*	Replacement of the *tetRA* locus with an artificial *att*Tn*7* site	[2]
C58ΔtetRA::a-*att*Tn*7* pRV-*ftsZ$_{AT}$-sfgfp*	C58ΔtetRA::a-*att*Tn*7* with pRV expression FtsZ$_{AT}$-sfGFP constitutively	This Study
C58ΔtetRA::a-*att*Tn*7* pRV-*ftsZ$_1$-sfgfp*	C58ΔtetRA::a-*att*Tn*7* with pRV expression FtsZ$_1$-sfGFP constitutively	This Study
C58ΔtetRA::a-*att*Tn*7* pRV-*ftsZ$_3$-sfgfp*	C58ΔtetRA::a-*att*Tn*7* with pRV expression FtsZ$_3$-sfGFP constitutively	This Study
C58ΔtetRA::a-*att*Tn*7* Δ*ftsZ$_1$*	Δ*ftsZ$_1$*	This Study
C58ΔtetRA::a-*att*Tn*7* Δ*ftsZ$_3$*	Δ*ftsZ$_3$*	This Study
C58ΔtetRA::a-*att*Tn*7* Δ*ftsZ$_1$* Δ*ftsZ$_3$*	Δ*ftsZ$_1$* Δ*ftsZ$_3$*	This Study
C58ΔtetRA::mini-Tn*7*-GM-Ptac-*ftsZ$_{AT}$*	Mini-Tn*7*T-GM-Ptac-*ftsZ$_{AT}$* inserted into a-*att*Tn*7* site	This Study
C58ΔtetRA::mini-Tn*7*-GM-Ptac-*ftsZ$_{AT}$*, Δ*ftsZ$_{AT}$*	Chromosome-based complementation of Δ*ftsZ$_{AT}$* with C58ΔtetRA::mini-Tn*7*-GM-Ptac-*ftsZ$_{AT}$* allowing depletion of FtsZ$_{AT}$ under control of the tac promoter	This Study
C58ΔtetRA::mini-Tn*7*-GM-Ptac-*ftsZ$_{AT}$*, Δ*ftsZ$_{AT}$* Δ*ftsZ$_1$*	FtsZ$_{AT}$ depletion background; Δ*ftsZ$_1$*	This Study
C58ΔtetRA::mini-Tn*7*-GM-Ptac-*ftsZ$_{AT}$*, Δ*ftsZ$_{AT}$* Δ*ftsZ$_3$*	FtsZ$_{AT}$ depletion background; Δ*ftsZ$_3$*	This Study
C58ΔtetRA::mini-Tn*7*-GM-Ptac-*ftsZ$_{AT}$*, Δ*ftsZ$_{AT}$* Δ*ftsZ$_1$* Δ*ftsZ$_3$*	FtsZ$_{AT}$ depletion background; Δ*ftsZ$_1$* Δ*ftsZ$_3$*	This Study
C58ΔtetRA::mini-Tn*7*-GM-Ptac-*ftsZ$_{AT}$*; pRV-*ftsZ$_1$-sfgfp*	FtsZ$_{AT}$ depletion background with pRV constitutive expression of FtsZ$_1$-sfGFP	This Study
C58ΔtetRA::a-*att*Tn*7*; pSRKKm Pqaz-*ftsA-sfgfp*	constitutive expression of FtsA-sfGFP from Pqaz	This study
C58ΔtetRA::mini-Tn*7*-GM-Ptac-*ftsZ$_{AT}$* ; pSRKKm Pqaz-*ftsA-sfgfp*	FtsZ$_{AT}$ depletion background with constitutive expression of FtsA-sfGFP from Pqaz	This Study
C58ΔtetRA::a-*att*Tn*7*; pSRKKm PpopZ-*popZ-yfp*	constitutive expression of PopZ-YFP from native promoter	This study

C58ΔtetRA::mini-Tn*7*-GM-Ptac-*ftsZ*$_{AT}$; pSRKKm PpopZ-*popZ-yfp*	FtsZ$_{AT}$ depletion background with constitutive expression of PopZ-YFP from native promoter	This Study
C58ΔtetRA::a-*att*Tn*7* pRV-*yfp-ParB*	C58ΔtetRA::a-*att*Tn*7* with pRV constitutive expression of YFP-ParB	This Study
C58ΔtetRA::mini-Tn*7*-GM-Ptac-*ftsZ*$_{AT}$; pRV-*yfp-ParB*	FtsZ$_{AT}$ depletion background with pRV constitutive expression of YFP-ParB	This Study
C58ΔtetRA::a-*att*Tn*7* pRV-*ldtp*$_{0845}$-*sfgfp*	C58ΔtetRA::a-*att*Tn*7* with pRV constitutive expression of LDTP$_{0845}$-sfGFP	This Study
C58ΔtetRA::mini-Tn*7*-GM-Ptac-*ftsZ*$_{AT}$; pRV-*ldtp*$_{0845}$-*sfgfp*	FtsZ$_{AT}$ depletion background with pRV constitutive expression of LDTP$_{0845}$-sfGFP	This Study
C58ΔtetRA::a-*att*Tn*7*; pSRKKm Pcym	Empty pSRKKm with Pcym	This Study
C58ΔtetRA::a-*att*Tn*7*; pSRKKm Pcym-*ftsZ*$_{AT}$	Cumate induced expression of FtsZ$_{AT}$	This Study
C58ΔtetRA::a-*att*Tn*7*; pSRKKm Pcym-*ftsZ*$_{\Delta CTC}$	Cumate induced expression of FtsZ$_{\Delta CTC}$	This Study
C58ΔtetRA::a-*att*Tn*7*; pSRKKm Pcym-*ftsZ*$_{\Delta CTL}$	Cumate induced expression of FtsZ$_{\Delta CTL}$	This Study
C58ΔtetRA::mini-Tn*7*-GM-Ptac-*ftsZ*$_{AT}$ pSRKKm Pcym-*ftsZ*$_{\Delta AT}$	FtsZ$_{AT}$ depletion background with cumate induced expression of FtsZ$_{AT}$	This Study
C58ΔtetRA::mini-Tn*7*-GM-Ptac-*ftsZ*$_{AT}$ pSRKKm Pcym-*ftsZ*$_{\Delta CTC}$	FtsZ$_{AT}$ depletion background with cumate induced expression of FtsZ$_{CTC}$	This Study
C58ΔtetRA::mini-Tn*7*-GM-Ptac-*ftsZ*$_{AT}$ pSRKKm Pcym-*ftsZ*$_{\Delta CTL}$	FtsZ$_{AT}$ depletion background with cumate induced expression of FtsZ$_{CTL}$	This Study
C58ΔtetRA::mini-Tn*7*-GM-Plac-*ftsA*	Mini-Tn*7*T-GM-Plac-*ftsA*inserted into a-*att*Tn*7* site	This Study
C58ΔtetRA::mini-Tn*7*-GM-Plac-*ftsA*, Δ*ftsA*	Chromosome-based complementation of Δ*ftsA* with C58ΔtetRA::mini-Tn*7*-GM-Plac-*ftsA* allowing depletion of FtsA under control of the lac promoter	This Study
C58ΔtetRA::mini-Tn*7*-GM-Plac-*ftsA*, Δ*ftsA;* pSRKKM PpopZ-*popZ-sfgfp*	FtsA depletion background with constitutive expression of PopZ-sfGFP	This Study
C58ΔtetRA::mini-Tn*7*-GM-Plac-*ftsA*, Δ*ftsA;* pRV-*ftsZ*$_{AT}$-*sfGFP*	FtsA depletion background with constitutive expression of FtsZAT-sfGFP	This Study
C58ΔtetRA::mini-Tn*7*-GM-Plac-*ftsW*	Mini-Tn*7*T-GM-Plac-*ftsW* inserted into a-*att*Tn*7* site	This Study
C58ΔtetRA::mini-Tn*7*-GM-Plac-*ftsW*, Δ*ftsW*	Chromosome-based complementation of Δ*ftsW* with C58ΔtetRA::mini-Tn*7*-GM-Plac-*ftsW* allowing depletion of FtsW under control of the lac promoter	This Study
C58ΔtetRA::mini-Tn*7*-GM-Plac-*ftsW*, Δ*ftsW;*	FtsW depletion background with constitutive expression of PopZ-sfGFP	This Study

pSRKKM PpopZ-*popZ-sfgfp*		
C58ΔtetRA::mini-Tn*7*-GM-Plac-*ftsW*, Δ*ftsW;* pRV-*ftsZ$_{AT}$-sfGFP*	FtsW depletion background with constitutive expression of FtsZAT-sfGFP	This Study

Table S4.2. Synthesized DNA primers and gene fragments used in this study.

Synthesized DNA	Sequence (5' – 3')
Primers for gene amplification	
FtsZ$_{AT}$ For NdeI	CGA CGC CAT ATG ACG ATA CAG CTG C
FtsZ$_{AT}$ Rev BamHI for *gfp* fusion	GCG TGA GGA TCC GTT GGA CTGGCG GCG C
FtsZ$_{AT}$ Rev BamHI stop codon	CGG CAC GGA TCC TTA GTT GGA CTG GC
FtsZΔCTP Rev NheI	GCT AGC TTA GTG ATG GCT GGA CGA GGA AAG
FtsZ$_1$ For NdeI	GCA CGT CAT ATG ACC CAG TCT CCG CGC GCC
FtsZ$_1$ Rev BamHI for *gfp* fusion	GCA CGT GGA TCC GTT ACG CAA GCC GGT GGC CAC
FtsZ$_1$ Rev BamHI stop codon	GCA CGT GGA TCC TCA GTT ACG CAA GCC GGT GGC CAC
FtsZ$_3$ For AseI	GCA CGT ATT AAT ATG AAA CCA ACA ATG GCC ACA
FtsZ$_3$ Rev BamHI for *gfp* fusion	GCA CGT GGA TCC TGT CGG CTC CGC GTT CTC AA
FtsZ$_3$ Rev BamHI stop codon	GCA CGT GGA TCC TCA TGT CGG CTC CGC GTT CTC AA
FtsA For NdeI	CGA CGC CAT ATG AGC TTT TTT GGT TC
FtsA Rev BamHI	CGG CAC GGA TCC AAA ACT TTC TTT CAG CC
PopZ XmaI For	GCA TTA CCC GGG ATG GCT CAG CCA AGT
PopZ BamHI Rev	GTC GCT GGA TCC GCG GCG CGA GCC GCG CGC CAC A
Ldtp0845 NdeI for	GCC TAC ATA TGT ACA GCG GCG ATA TAG CCG
Ldtp0845 BamHI rev	CGC TCG GAT CCT TAC TGC CAC ACC ACC ACA CG
FtsZΔCTC Rev NheI	GCT AGC TTA GTG ATG GCT GGA CGA GGA AAG
FtsW For AseI for	GCA CGT ATT AAT ATG GTA AGC CGA GTT GAT CGC G
FtsW Rev BamHI	GCA CGT GGA TCC CTC CGC AGG AAC GCC GGA ACC G
Primers for deletion vectors and deletion confirmation	
FtsZ$_1$ P1	GGA TCC CCT CTT CTT CCG CCT G
FtsZ$_1$ P2	AAG CGC CCC GTC TTA TTC TCT TTC
FtsZ$_1$ P3	TAA GAC GGG GCG CTT TCG CAG C
FtsZ$_1$ P4	ACT AGT CCA TGG TCG AAC GGT TCG
FtsZ$_1$ P5	CTA CGG CCT GAT CCA GCC
FtsZ$_1$P6	GTA CAT CAG CAC CAG CGC ATC
FtsZ$_3$ P1	GCT GCA ACT AGT AAG TGG GGC ACG CAG GGC CAT

$FtsZ_3$ P2	AAG CAT GGT ACC GAA TTC GGA AGC CGA TCT CCT GGC AA
$FtsZ_3$ P3	GAA TTC GGT ACC ATG CTT TGA GTG AGA CAA CGT TCT A
$FtsZ_3$ P4	GCA CGT AAG CTT CCG GTC TTG CGG TCT TGT CC
$FtsZ_3$ P5	GAG CCA CCC CGA TTG CCG AAC
$FtsZ_3$ P6	CTC ACG CGC TAT CGT GCG TTG
$FtsZ_{AT}$ P1	GCA ACT AGT GAT CGC GAT CAA CCA TCG
$FtsZ_{AT}$ P2	AAG CTT GGT ACC GAA TTC TTT ACC ATT CCT TCT TTC
$FtsZ_{AT}$ P3	GAA TTC GGT ACC AAG CTT AGG CGA TTC CAT ACG CTC
$FtsZ_{AT}$ P4	GCA GGA TCC GAT AGC GAA CGG CCG AGC
$FtsZ_{AT}$ P5	AAT CGA AGA TGC GGA GAG
$FtsZ_{AT}$ P6	AGG TTG TCG AGG CCC ATC
FtsA P1	GCA TAG ACT AGT GAA CTG TCG CTG ATC GAA
FtsA P2	AAG CTT GGT ACC GAA TTC GAC GAT GTG GCT GCG CTT
FtsA P3	GAA TTC GGT ACC AAG CTT GGA ATG TTT TCG CCG TTT GG
FtsA P4	GCA TAG GGA TCC GCC GCC GCC CAT GCC GGC
FtsA P5	CGA AGA CGG TGG AAG TTC GCC TG
FtsA P6	CGA TGC CCT GTT CGG CCA GAC
FtsW P1	GCT GCA ACT AGT GGA AAT TCG TGC CGG TCT CAA GTC
FtsW P2	AAG CAT GGT ACC GAA TTC GGC CTC AGC CCC CTT TTC CAG
FtsW P3	GAA TTC GGT ACC ATG CTT TAA ACG ATC ATG AAC AAG GGT A
FtsW P4	GCA CGT GGA TCC ACC GGA TTG CCG GTC GCA ACC GT
FtsW P5	GAC GGT ATC CAG ACG CTT CGC GGC AGC CA
FtsW P6	GGT CTC GCC CGT CTG TGA AGG CGT ATA G
Primers for confirmation of Mini-Tn7 vector insertion	
Tet forward	ACA TGT TGT ATA CCG GAA ACT GAT TGC AC
Tn7R109	CAG CAT AAC TGG ACT GAT TTC AG
Gene fragment	
Cumate promoter region Orange text = *cymR* encodes cumate repressor Yellow highlight = Kan Promoter Blue text = cuO cumate operator sites	5'GCCGTGAGCAATCTAGGAATTCTTACTAGCGCTTGAATT TCGCGTAACGCTCGCGCGCAATTTCGAGGGTCGAGTTACG GACACGCTCAAAGCGTTCTTTGTCCTTCTGCCACAGGCTG CGAACAGCAAGCCCACGCACCGAATTGAAGATCAACCAA AGGATATCTTCTGCATCATCACGCGAAAGACCACGGCTCA CCAGAACACCAAGCCACATATCCTCGACGACAAAGCGAT TACGCTCTACCGTGCGCTGAATACCCTCGCGTAACGCTGG ATCGCGGTCGGCAGCCACAATCAAATCAAGGCTGATAGA GAAGTCATCGTCGAGGAAAAATTCGGCGGCGTCGTCCAG CATTTGCTGGATGACGTCATCCTCTGGCTTCAATTTCGCTA

Green text = lac promoter Cyan highlight = Multiple Cloning Site	AGCGAGCACGGCTGCGTTCGGTGATCTGTTCGTAAAGCCA TTCAAAAGTGGCAAGCAGAAGCTCAAGTTTGGTCGGGAA ATGATGGCTCTGCGCGCCGCGCGAGACACCTGCAGCACC CGGCACATCTGCGATGCGGAAGCCCGCGTAACCTTTTTCG CGTAAAACCCCCAGGGCCGCTGCAATCAACTTGCCCTGGG TCTCCATTGCGCGCTCTGCCTGGGTACGGCGCTTTGGACT CATGCGAAACGATCCTCATCCTGTCTCTTGATCAGATCTT GATCCCCTGCGCCATCAGATCCTTGGCGGCAAGAAAGCC ATCCAGTTTACTTTGCAGGGCTTCCCAACCTTACCAGAGG GCGCCCCAGCTGGCAATTCCGGTTCGCTTGCTGTCCATAA AGACCGGTAGCTAGACTGCGATGAGTGGCAGGGCGACAG CTCACTCATTAAACAAACAGACAATCTGGTCTGTTTGTAT TATGATCGATGCACCCAGGCTTTACACTTTATGCTTCCGG CTCGTATGTTGTGGTTAACAAACAGACAATCTGGTCTGTT TGTATTATCGAGTCAAGGAAGACAGCATATGCCTGCAGG CGCCGG -3’

Supplemental Figures

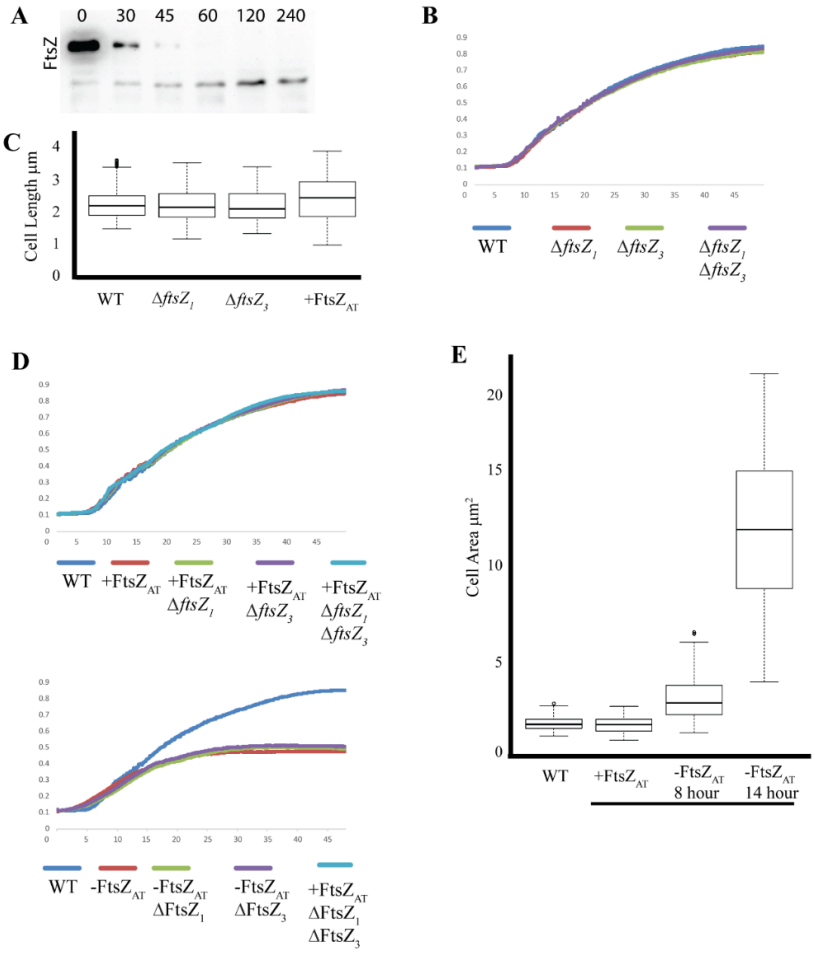

Supplemental Figure 4.1. Cell growth and morphology of *ftsZ* mutants. A.) Western blot analysis showing the depletion of FtZ_{AT} after the removal of inducer. B) Growth Curve analysis demonstrating indistinguishable growth between WT, Δ*ftsZ1*, Δ*ftsZ3*, and Δ*ftsZ1*Δ*ftsZ3*. C) Cell lengths of WT, Δ*ftsZ1*, Δ*ftsZ3*, and induced $ftsZ_{AT}$. are indistinguishable. D) Growth curve analysis showing no impact from Δ*ftsZ1*, Δ*ftsZ3*, or Δ*ftsZ1*Δ*ftsZ3* in the $ftsZ_{AT}$ depletion strain when $FtsZ_{AT}$ is expressed (Top), and no additive effect on growth when $FtsZ_{AT}$ is depleted (bottom). E) Cell area in WT and induced $ftsZ_{AT}$ are the same while cells depleted of $FtsZ_{AT}$ for 8 and 14 hours accumulate cell area.

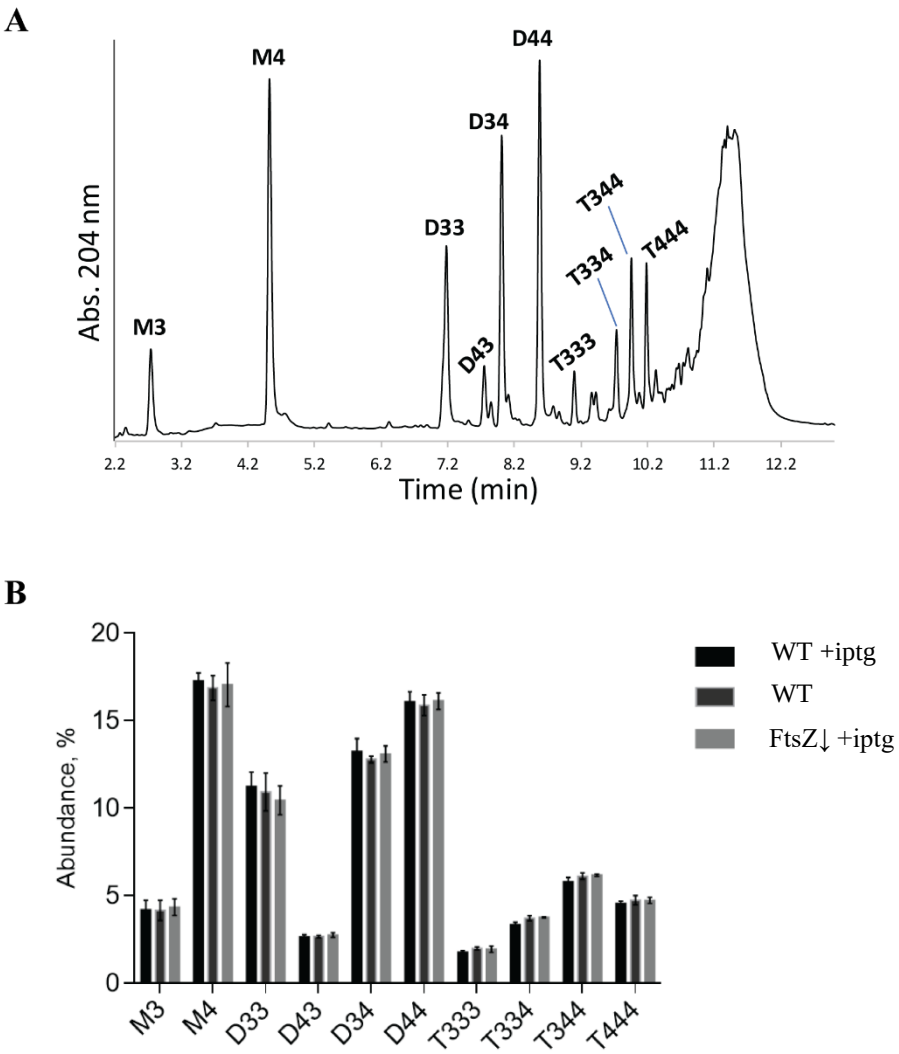

Supplemental Figure 4.2. Peptidoglycan analysis of control strains A) UPLC spectra of muropeptides derived from WT cells. Major muropeptides are labeled. M= monomers, D= dimers, T= trimers. Numbers indicate the length of the muropeptide stems and the position of crosslink in dimers and trimers. B) Quantitation of the major muropeptide peaks in WT with IPTG (black), WT without IPTG (black with gray outline), and *ftsZ*$_{AT}$ depletion strain induced with IPTG (Gray). Data shown are the average abundance of each muropeptide and is taken from analysis of three independent biological samples. Statistical significance is indicated with an asterisk.

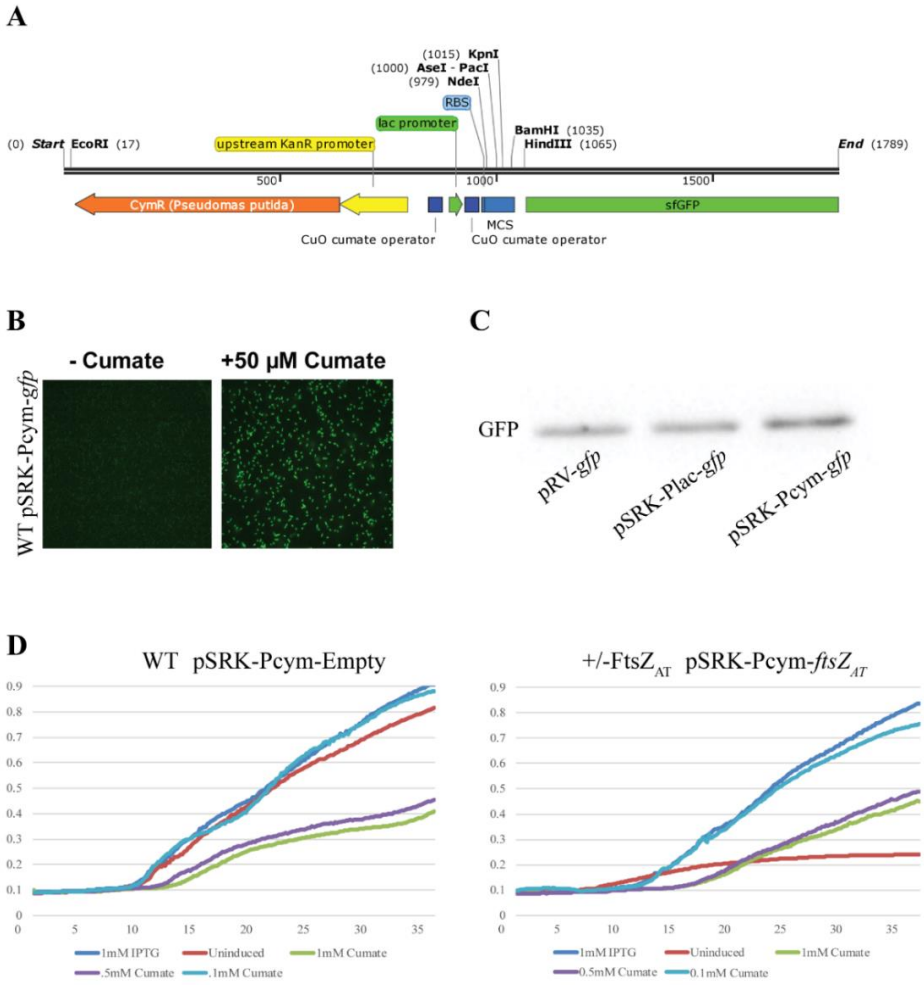

Supplemental Figure 4.3. Validation of a cumate inducible vector in *A. tumefaciens.* A) Sequence schematic of the cumate operon modified for use in a pSRKKm-*sfgfp* backbone. Regions are color coded to match sequence found in Table S2. B) Representative image of WT cells harboring pSRKKm-Pcym-*sfgfp* uninduced (left) and induced (right). C) Western blot analysis comparing expression levels of sfGFP expressed from pRV, pSRKKm-Plac, and pSRKKm-Pcym. D) Growth curve analysis of WT cells harboring psRKKm-Pcym-empty induced with different levels of cumate (left). pSRKKm-Pcym-$ftsZ_{AT}$ rescues chromosomal $FtsZ_{AT}$ depletion with 0.01 mM cumate (right).

Supplemental References

1. Choi YJ, Morel L, Le Francois T, Bourque D, Bourget L, Groleau D, Massie B, Miguez CB: Novel, versatile, and tightly regulated expression system for *Escherichia coli* strains. *Appl Environ Microbiol* 2010, 76:5058-5066.

2. Figueroa-Cuilan W, Daniel JJ, Howell M, Sulaiman A, Brown PJ: Mini-Tn*7* insertion in an artificial *att*Tn*7* site enables depletion of the essential master regulator Ctra in the phytopathogen *Agrobacterium tumefaciens*. *Appl Environ Microbiol* 2016, 82:5015-5025.

3. Thanbichler M, Iniesta AA, Shapiro L: A comprehensive set of plasmids for vanillate- and xylose-inducible gene expression in *Caulobacter crescentus*. *Nucleic Acids Res* 2007, 35:e137.

4. Choi K-H, Schweizer HP: mini-Tn*7* insertion in bacteria with single *att*Tn*7* sites: example *Pseudomonas aeruginosa*. *Nat. Protocols* 2006, 1:153-161.

5. Howell M, Aliashkevich A, Salisbury AK, Cava F, Bowman GR, Brown PJB: Absence of the polar organizing protein PopZ results in reduced and asymmetric cell division in *Agrobacterium tumefacien*s. *J Bacteriol* 2017, 199: e00101-17.

6. Ehrle HM, Guidry JT, Iacovetto R, Salisbury AK, Sandidge DJ, Bowman GR: Polar organizing protein PopzZ is required for chromosome segregation in *Agrobacterium tumefaciens*. *J Bacteriol* 2017, 199: e00111-17.

7. Simon R, Priefer U, Pühler A: A broad host range mobilization system for *in vivo* genetic engineering: transposon mutagenesis in gram negative bacteria. *Nat Biotechnol* 1983, 1:784-791

CHAPTER 5

Concluding Remarks

Understanding the mechanisms underlying cell growth and division is a fundamental goal in bacterial cell biology with potential implications for antibiotic development. Given the emergence of antibiotic resistant infections, it is more important than ever to improve our understanding of bacterial cell growth. Indeed, impressive progress has been made in the past few years in understanding the mechanisms underpinning bacterial cell growth and division in a few model bacterial systems [1,2]. Bacterial cells elongate by expansion of peptidoglycan (PG), a polymer of polysaccharides and amino acids that surrounds the cell, forming the cell wall. In a majority of rod-shaped bacteria in which growth has been observed, cells elongate by the lateral insertion of newly synthesized PG along the sidewalls. Following completion of elongation, PG synthesis is redirected to mid-cell, existing PG is remodeled and hydrolyzed to enable cell constriction and cell separation. Remarkably, not all rod-shaped bacteria share this well-characterized growth cycle.

Polar growth is responsible for elongation in the Rhizobiales, a large clade of bacteria that includes symbionts and pathogens of plants, animals, and humans. The growth pattern of *A. tumefaciens* has been established through careful observations of PG biosynthesis [3-5]. PG synthesis occurs at the cell pole during elongation and is redirected to mid-cell prior to cell division. As the cell prepares for cell division, PG biosynthesis occurs exclusively at mid-cell. The new poles generated by cell division become the growth-active poles as the cells begin to elongate. While the phenomenology of the *A. tumefaciens* growth cycle had been well established, the molecular mechanisms responsible for driving this growth pattern are relatively undescribed.

Optimization of protocols for timelapse microscopy and labeling of cells with fluorescent reagents to observe DNA and sites of cell wall biogenesis has improved our ability to characterize the cell growth pattern of *A. tumefaciens* (Chapter 2) [6]. Utilizing these techniques, we are able to demonstrate that both PopZ and $FtsZ_{AT}$ play a role in transition from polar growth to cell division (Chapter 3 and Chapter 4) [7]. The early mid-cell recruitment of FtsZ is required to terminate polar growth, while PopZ marks the new poles and coordinates cell division with chromosome segregation (Figure 5.1).

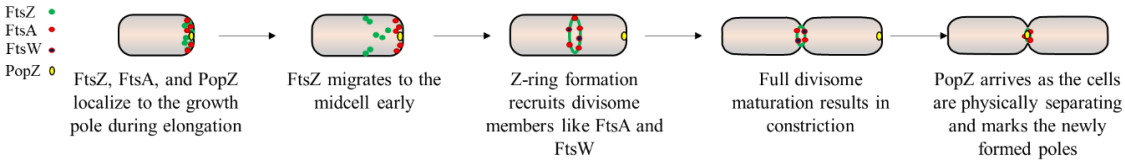

Figure 5.1 A model of the transition from polar elongation to cell division. The localization of patterns of proteins involved in transitioning from polar elongation to cell division are shown.

This dissertation work has provided answers to many questions; however, many new questions have emerged. How is the cell elongation machinery recruited and retained at the new pole? When cell division is completed, the previous site of divisome activity gives rise to the newly formed poles, which become the sites of elongasome activity (Figure 5.1). Thus, it is tempting to speculate that there may be overlap between components of the divisome and elongasome. Our observation that depletion of FtsW, a key protein in septal peptidoglycan synthesis, does not block PG biosynthesis near the

mid-cell may suggest that *A. tumefaciens* uses a previously undescribed $FtsZ_{AT}$-dependent pathway for cell elongation from mid-cell. How does the formation of a $FtsZ_{AT}$ ring at mid-cell lead to the termination of polar growth? Perhaps the recruitment of PopZ to mid-cell contributes to termination of polar growth and enables elongation from mid-cell. Alternatively, PopZ-dependent activities could contribute to priming the new poles formed during cell division to become growth-active poles? Overall, our result indicate that further research is necessary to tease out the activities and functions of proteins recruited to mid-cell as the cell approaches cell division. Further characterization of divisome members could reveal mechanistic insights into the termination of polar growth as well as the activation of division.

Additional remaining question are: how does $FtsZ_{AT}$ find the middle of the cell and how are $FtsZ_{AT}$ rings stabilized? We have established that $FtsZ_{AT}$ is an early recruit to the mid-cell and is required for the recruitment of downstream divisome components, including $FtsZ_1$ and FtsA. Remarkably, we observe that $FtsZ_{AT}$ is able to form stable rings without FtsA. This observation indicates that other factors must contribute to the stabilization of $FtsZ_{AT}$ by tethering it to the membrane. Furthermore, we know very little about how $FtsZ_{AT}$ finds the mid-cell and marks the future site of cell division. Thus, we are seeking to identify regulatory elements that direct FtsZ to mid-cell. We have conducted a systematic characterization of the Min system, which is a known negative regulator of FtsZ assembly in many bacteria. In *A. tumefaciens*, although the Min system is not required for cell survival or cell division, it contributes to the precise placement of FtsZ-rings near mid-cell [8](See appendix A). Furthermore, $FtsZ_{AT}$-rings form over DNA

since $FtsZ_{AT}$ rings appear early in the cell cycle before the chromosomes are fully segregated. This suggests that a nucleoid occlusion system is not primarily responsible for directing $FtsZ_{AT}$ to the mid-cell. Based on these observations, we hypothesize that additional regulatory mechanisms must contribute to proper division site selection in *A. tumefaciens*.

As described in Chapter 1, the machinery utilized for polar growth appears to be different between Rhizobiales and Actinobacteria, yet some features of polar appear to be conserved since blocking cell division tends to result in branched cells [2]. Interestingly, we observed an increase in LD-crosslinkage when polar growth was enriched by blocking cell division. Distantly related polar-growing species, including the Mycobacteria, have been shown to have highly abundant LD-crosslinking in the peptidoglycan when compared to species which undergo lateral dispersed elongation [9,10]. This finding further suggests conserved principles in polar growth. Yet, it remains to be seen if principles governing the termination of polar growth and initiation of cell division are conserved across evolutionary distant polar growing species.

As additional research reveals the mechanisms of polar growth, we can begin to ask what are the advantages of polar growth? Many interesting hypotheses have been proposed [3,11,12]. For example, polar growth results in a daughter cell of entirely new peptidoglycan, which could allow bacteria to rapidly respond to their environment by altering PG or outer membrane protein composition. When a bacterium associates with a host, the ability to rapidly change the surface proteome may allow the bacterium to evade

the host immune response. Another hypothesis is a reduced energy expenditure by concentrating growth to one area rather than throughout the cell. Overall, the work presented in this dissertation provides a few pieces of the polar growth puzzle, however more research is needed to uncover all of the mechanisms governing the coordination of polar growth and cell division in *A. tumefaciens*.

References

1. Du S, Lutkenhaus J: Assembly and activation of the *Escherichia coli* divisome. *Mol Microbiol* 2017, 105:177-187.

2. Howell M, Brown PJB: Building the bacterial cell wall at the pole. *Curr Opin Microbiol* 2016, 34:53-59.

3. Brown PJB, de Pedro MA, Kysela DT, Van der Henst C, Kim J, De Bolle X, Fuqua C, Brun YV: Polar growth in the alphaproteobacterial order Rhizobiales. *Proc of the Nat Acad of Sci U S A* 2012, 109:1697-1701.

4. Kuru E, Velocity Hughes H, Brown PJ, Hall E, Tekkam S, Cava F, de Pedro MA, Brun YV, VanNieuwenhze MS: *In situ* probing of newly synthesized peptidoglycan in live bacteria with fluorescent D-amino acids. *Angew Chem Int Ed Engl* 2012, 51:12519-12523.

5. Zupan JR, Cameron TA, Anderson-Furgeson J, Zambryski PC: Dynamic FtsA and FtsZ localization and outer membrane alterations during polar growth and cell division in *Agrobacterium tumefaciens*. *Proc Natl Acad Sci U S A* 2013, 110:9060-9065.

6. Howell M, J. Daniel J, J.B. Brown P: Live cell fluorescence microscopy to observe essential processes during microbial cell growth. *J Vis Exp* 2017, 129

7. Howell M, Aliashkevich A, Salisbury AK, Cava F, Bowman GR, Brown PJB: Absence of the polar organizing protein PopZ results in reduced and asymmetric cell division in *Agrobacterium tumefaciens*. *J Bacteriol* 2017, 199: e00101-17.

8. Flores SA, Howell M, Daniel JJ, Piccolo R, Brown PJB: Absence of the Min system does not cause major cell division defects in *Agrobacterium tumefaciens*. *Front Microbiol* 2018, 9:681.

9. Lavollay M, Fourgeaud M, Herrmann JL, Dubost L, Marie A, Gutmann L, Arthur M, Mainardi JL: The peptidoglycan of *Mycobacterium abscessus* is predominantly cross-linked by L,D-transpeptidases. *J Bacteriol* 2011, 193:778-782.

10. Cordillot M, Dubee V, Triboulet S, Dubost L, Marie A, Hugonnet JE, Arthur M, Mainardi JL: In vitro cross-linking of *Mycobacterium tuberculosis* peptidoglycan by L,D-transpeptidases and inactivation of these enzymes by carbapenems. *Antimicrob Agents Chemother* 2013, 57:5940-5945.

11. Lindner AB, Madden R, Demarez A, Stewart EJ, Taddei F: Asymmetric segregation of protein aggregates is associated with cellular aging and rejuvenation. *Proc Natl Acad Sci U S A* 2008, 105:3076-3081.

12. Cameron TA, Zupan JR, Zambryski PC: The essential features and modes of bacterial polar growth. *Trends Microbiol* 2015, 23:347-353.

Appendix A

Absence of the Min system does not cause major cell division defects in *Agrobacterium tumefaciens*

Adapted from:

Flores SA, Howell M, Daniel JJ, Piccolo R, Brown PJB: Absence of the Min system does not cause major cell division defects in *Agrobacterium tumefaciens*. *Front Microbiol* 2018, 9:681.

ABSTRACT

In *A. tumefaciens*, the essential FtsZ protein is located at the growth pole before shifting to the mid-cell right before division. Loss of FtsZ causes a halt in cell separation and lysis of cells. To understand how FtsZ polymerization is regulated to properly localize the FtsZ-ring at the mid-cell, we have conducted a systematic characterization of the Min system in *A. tumefaciens*. Our findings indicate that the Min system is not required for cell survival. Yet, we find that the deletion of either *minE* or *minCDE* results in a broad cell size distribution, including an increase in the proportion of short and long cells. We observe that the site of constriction is misplaced in the *minE* or *minCDE* deletion strains allowing for short cells to arise from sites of constriction near the cell poles. Remarkably, the short cells are viable and contain DNA. In order to observe chromosome replication and segregation in these strains, YFP-ParB is used as a proxy to track the origin of replication as cells elongate and divide. In the absence of the Min proteins, duplication and segregation of the origin of replication is frequently delayed. Taken together, our data suggest that the Min system contributes to the proper regulation of FtsZ placement and subsequent cell division. Furthermore, the failure to precisely place FtsZ-rings at mid-cell in the *min* mutants impacts other cell cycle features including chromosome segregation.

Keywords: *Agrobacterium*, cell division, Min system, FtsZ, chromosome segregation

Introduction

Most bacteria precisely place the site of cell division at or near mid-cell through proper positioning of FtsZ to initiate divisome assembly. FtsZ forms a ring-like structure at or near the mid-cell along the cytoplasmic surface of the inner membrane [1]. FtsZ is stabilized along the membrane by interactions with FtsA leading to the formation of FtsZ filaments [2]. The FtsZ filaments form a ring-like structure at the future site of cell division and guide other divisome proteins, including peptidoglycan synthases, to the mid-cell [3-7]. The order of recruitment and essentiality of individual cell division proteins varies across species, but the general mechanism of cell division appears to be broadly conserved [8]. After assembly of the cell division machinery is complete, peptidoglycan biosynthesis is activated at mid-cell [9-11]. As the ring constricts, septal peptidoglycan is synthesized inwards to build the new poles of the daughter cells. Septal peptidoglycan synthesis requires the monofunctional PBP3, the SEDS protein FtsW, and the bifunctional PBP1b [12-14]. The GTPase-dependent treadmilling motion of the FtsZ filaments drives the movement of the peptidoglycan biosynthesis machinery around the circumference of the cell division site, enabling the synthesis of concentric rings of peptidoglycan to form the septum [15,16].

How is FtsZ properly positioned at mid-cell? There are several well characterized mechanisms to ensure proper positioning of the FtsZ-rings (for review see [17,18]). In rod-shaped bacteria such as *Escherichia coli* and *Bacillus subtilis*, the Min system and nucleoid occlusion (NO) prevent FtsZ-rings from forming near cell poles or over nuceloids, respectively. In *E. coli*, the MinCDE proteins rapidly oscillate from pole to

pole guiding FtsZ to the mid-cell [19-23]. Since MinC is an inhibitor of FtsZ-ring assembly [24-26], FtsZ-rings only form in mid-cell regions where the concentration of MinC is low. MinC forms a complex with MinD, an ATPase which dimerizes and binds to the cell membrane when bound to adenosine triphosphate (ATP) [27-29]. MinE binds to MinD-ATP causing ATP hydrolysis and release of the MinCD complex from the membrane [30]. Remarkably, MinE can remain bound to the membrane at the pole to dislodge additional MinCD complexes [31-33]. Meanwhile, MinD-ATP is regenerated and cooperatively binds the membrane at the opposite pole. After removing the MinCD complexes from one cell pole, MinE will travel to the opposite pole. Thus, MinE chases MinCD from pole to pole giving rise to regular oscillations. The oscillation of the Min proteins results in a minimum of FtsZ inhibitory activity at mid-cell [20,34].

When the genes encoding the Min proteins in *E. coli* are removed simultaneously or individually, cell division and survival are adversely impacted. In the absence of MinE, the cells usually cannot divide and the cells form long, smooth filaments. The block in cell division occurs because inhibition of FtsZ polymerization by MinC occurs throughout the cell [25,35]. In the absence of MinC, or its activator MinD, a broad distribution of cell lengths is observed [35]. Both minicells and long filaments are observed since FtsZ polymerization can occur at the cell poles or near mid-cell leading to asymmetric cell division events. FtsZ polymerization is restricted to poles and mid-cell in the absence of the Min system due to the presence of the nucleoid occlusion protein, SlmA [36]. The FtsZ inhibitory activity of SlmA is activated by binding specific sites on the DNA near the origin of replication [37,38]. Thus, as DNA replication is completed

and the origins segregate to the cell poles, a minimal inhibitory zone is formed at mid-cell. SlmA binding to DNA activates its ability to bind the C-terminal tail of FtsZ causing depolymerization of FtsZ filaments [39]. Under nutrient rich conditions, loss of the Min system and nucleoid occlusion is synthetically lethal; however under nutrient limited conditions the cells continue to grow and divide relatively well [36]. When both the Min proteins and SlmA are absent, FtsZ-ring placement is more accurate than in cells with only SlmA suggesting that other mechanisms contribute to the proper placement of FtsZ-ring in the absence of both Min proteins and SlmA [40,41].

Indeed, the Min system is not universally distributed among bacteria suggesting the existence of alternative mechanisms of FtsZ positioning. MinCD is present in diverse bacteria, MinE is found in a more restricted range of bacteria, and other bacteria do not contain a Min system [42]. For example, the Caulobacterales clade of alphaproteobacteria do not contain obvious homologs of the Min proteins. Furthermore, in *Caulobacter crescentus*, a bacterial model system within the Caulobacterales, only the final step of cell division takes place after completion of chromosome segregation suggesting that nucleoid occlusion does not occur [43]. Instead, *C. cresentus* uses at least two distinct mechanisms for regulation of cell division [44-46]. MipZ is a distinct member of the MinD/ParA family of ATPases that contribute to spatial organization with bacterial cells [47]. MipZ forms a bipolar gradient on the nucleoid by binding to DNA sites near the origin of replication and directly interacts with FtsZ, inhibiting filament formation near the cell poles [45,46]. KidO is an NAD(H)-binding oxidoreductase that provides temporal regulation of FtsZ-ring assembly [44]. KidO binds FtsZ and prevents premature

filament assembly at mid-cell. KidO is proteolytically cleared from the cell during elongation and the initiation of cell division, enabling efficient FtsZ-ring formation at mid-cell. KidO reappears late during cell division and is recruited to the mature divisome where it likely contributes to FtsZ-ring disassembly during constriction. Thus, together MipZ and KidO restrict FtsZ-ring formation to the mid-cell of predivisional cells.

Remarkably, not all alphaproteobacterial species lack a Min system. Among the alphaproteobacteria, the MinCDE proteins are found among the Rhodospirallales, Rhodobacterales, and Rhizobiales clades. The *minCDE* cluster is likely regulated by CtrA, the master cell cycle regulator, in several Rhizobiales species including *Brucella abortus* [48], *Prosthecomicrobium hirschii* [49], and *Sinorhizobium meliloti* [50]. In *S. meliloti*, CtrA negatively regulates *minCD* expression [50] and overexpression of MinCD inhibits cell division [51]. Together, these observations suggest that the Min system may contribute to the regulation of cell division in the Rhizobiales. Here, we expand our knowledge about the function of the Min system in Rhizobiales by characterizing its contribution to regulation of cell division in *Agrobacterium tumefaciens*. The *A. tumefaciens* genome reveals the presence of an operon predicted to encode the MinCDE proteins, but there is not an obvious nucleoid occlusion system or MipZ homolog [52]. The MinCDE proteins from *Agrobacterium* share significant sequence similarity with the *E. coli* proteins (percent identities: MinC 31.70%, MinD 61.05%, and MinE 39.29%) suggesting that they may have conserved functions. In this work, we have systematically characterized the role of the Min proteins on cellular morphology, constriction site placement, and chromosome segregation. Our results suggest that the Min system

contributes to the regulation of cell division; however, other FtsZ-positioning proteins likely exist in *A. tumefaciens*.

Materials and Methods

Bacterial strains and culture conditions. A list of all bacterial strains and plasmids used in this study is provided in Table 1. *Agrobacterium tumefaciens* C58 and derived strains were grown in AT minimal medium with 0.5% glucose (ATGN) [53] without exogenous iron at 28°C with shaking. For *sacB* counterselection during construction of deletion mutants 5% sucrose replaced glucose as the sole carbon source (ATSN). *Escherichia. coli* DH5α and S17-1 λ *pir* were routinely cultivated in Luria-Bertani (LB) medium at 37°C with shaking. When appropriate, kanamycin was used at 300 μg/ml for *A. tumefaciens* and 50 μg/ml for *E. coli*. When indicated, IPTG was used as an inducer at a concentration of 1 mM.

Table A.1. Bacterial strains and plasmids used in this study.

Strain or plasmid	Relevant characteristics	Reference/Source
Plasmids		
pNTPS138/139	Km^r; Suicide vector containing *oriT* and *sacB*	D. Alley
pNTPS139Δ*minC*	Km^r Suc^s; deletion plasmid for *minC*	This study
pNTPS139Δ*minD*	Km^r Suc^s; deletion plasmid for *minD*	This study
pNTPS139Δ*minE*	Km^r Suc^s; deletion plasmid for *minE*	This study
pNTPS139Δ*minCDE*	Km^r Suc^s; deletion plasmid for *minCDE*	This study
pRV-Pvan-FtsZ-GFP	Km^r ; replicating plasmid for constitutive expression of FtsZ-GFP	[54]
pSRKKm-Plac-YFP-ParB	Km^r; replicating plasmid for inducible expression of YFP-ParB	[55]
E. coli strains		
DH5α	Cloning strain	Life Technologies
S17-1	Sm^r; RP4-2, Tc::Mu,Km-Tn*7*, for	[56]

	plasmid mobilization	
A. tumefaciens strains		
C58	Nopaline type strain; pTiC58; pAtC58	[57]
C58 Δ*minC*	C58 with deletion of *minC*	This study
C58 Δ*minD*	C58 with deletion of *minD*	This study
C58 Δ*minE*	C58 with deletion of *minE*	This study
C58 Δ*minCDE*	C58 with deletion of *minCDE*	This study

Plasmid construction. PCR was used to amplify approximately 500 bp of flanking sequence upstream (primers 1 and 2) and downstream (primers 3 and 4) of the gene targeted for deletion. Primers used for amplification of regions upstream and downstream of *minC* (Atu 3249), *minD* (Atu3248), *minE* (Atu3247) are shown in Table 2. For regions upstream and downstream of the *minCDE* locus, primers Atu 3249 P1-Spel, Atu 3249 P2, Atu 3247 P3, and Atu 3247 P4-BamHI were used. All PCR reactions contained 10 μM of each primer, 100 ng of genomic DNA purified from wildtype *Agrobacterium tumefaciens* C58, 10 mM deoxynucleotides (dNTPs; New England Biolabs), 0.5 U Phusion DNA Polymerase (Thermo Scientific), 1.5% DMSO, and 5X Phusion GC Buffer (Thermo Scientific). Upstream and downstream DNA fragments were amplified by routine PCR reactions with the following cycling conditions: denaturation 98°C for 30 seconds, annealing 2 degrees higher than the calculated annealing temperature of the primers for 30 seconds, extension 72°C for 30 seconds, and final extension was done at 72°C for five minutes. The PCR ran for 30 cycles. PCR products were run on a 0.8% agarose gel by electrophoresis, stained with DNA SafeStain (Midwest Scientific) and gel purified usinga GeneJet PCR purification kit (Thermo Scientific). A second PCR reaction was done using PCR SOEing (synthesis by overlap extension) to anneal linker sequence from the

500 bp upstream and downstream together as described previously [58]. Briefly, purified PCR products were used as both templates and primers for a five-cycle PCR. A final PCR step with primers 1 and 4, using 2 µl of the second-step reaction mix as the template, generates the full-length spliced product. PCR products were then gel purified. PCR products and the pNTPS139 vector were then digested overnight at 37°C using enzymes SpeI and BamHI (New England Biolabs). Digested products were gel purified and ligated together using T4 DNA ligase (New England Biolabs). Ligations were transformed into *E. coli* DH5α competent cells using the suggested manufacturer protocol (Invitrogen). Transformants were plated on LB-agar plates containing kanamycin. Individual colonies from the transformation were then grown overnight in LB and plasmid extraction was performed using GeneJet plasmid miniprep kit (Thermo Scientific). Plasmid inserts were verified by sequencing and the plasmids were transformed into *E. coli* S-17 by electroporation.

Table A.2. Synthesized DNA primers used in this study

Primers	Sequence
Atu 3249 P1-SpeI	5'-ACA CGT ACT AGT CAG GCC GAT GCG G -3'
Atu 3249 P2	5'-AAG CTT GGT ACC GAAA TTC GCG AAG CTC G -3'
Atu 3249 P3	5'-GAA TTC GGT ACC AAGCTT CGA ACGCTG G -3'
Atu 3249 P4-BamHI	5'-CGC GCG GGA TCC GCA ATC GAA TTG ACC A -3'
Atu 3248 P1-SpeI	5'-ACA CGT ACT AGT TAT GGC CTG ATG CTG C -3'
Atu 3248 P2	5'-AAG CTT GGT ACC GAA TTC AGG AGG GCT G -3'
Atu 3248 P3	5'-GAA TTC GGT ACC AAG CTT TAC AAC GAC TA -3'
Atu 3248 P4-BamHI	5'-CGC GCG GGA TCC GTT CGC CCG TCG ATG A -3'
Atu 3247 P1-SpeI	5'-ACA CGT ACT AGT GCC GAT CTT GCC GGG C -3'
Atu 3247 P2	5'-AAG CTT GGT ACC GAA TTC CTG CGC GCT -3'
Atu 3247 P3	5'-GAA TTC GGT ACC AAG CTT GAT GCT CAT GC -3'
Atu 3247 P4-BamHI	5'-CGC GCG GGA TCC GAA TGG GTC ATC GCC G -3'
MinCDE P5	5'-CAT GGA ATG CGT GGC GAG CAC GAA TAC G -3'
MinCDE P6	5'-GAA GCC CGC ATG CCA TAGG ATA CGT TGC AG -3

Deletion of target genes in *A. tumefaciens*. Nonpolar, markerless deletions of the *A. tumefaciens* individual *minC* (Atu 3249*), minD (*Atu 3248*), and minE* (Atu3247*)* genes and the entire locus were generated using the plasmids pNPTS139Δ*minC*, pNPTS139Δ*minD*, pNPTS139Δ*minE, and* pNTPS139Δ*minCDE* following an established protocol [59]. Deletion of target genes was confirmed by colony PCR using the indicated primer pairs: *ΔminC* (Atu 3249 P1-SpeI and MinCDE P6), *ΔminD* (Atu 3248 P1-SpeI and Atu 3249 P4-BamHI), *ΔminE* (Atu 3247 P1-SpeI and Atu 3248 P4-BamHI), and *ΔminCDE* (MinCDE P5 and Atu 3249 P4-BamHI). PCR products were gel purified and sequence verified to confirm deletion of the target gene.

Growth curve analysis. Strains were grown in ATGN until exponential phase was reached, then back diluted to reach an OD_{600} = 0.1 in 1 ml of ATGN. 200 µl of culture was placed into 3 wells of a 96-well plate. A BioTek Synergy H1 Hybrid Reader was programed to read the optical density at 600 nm every 5 minutes after shaking for one minute. The plate reader was maintained at a temperature of 28°C for a period of 36 h. Growth curve experiments were completed in triplicate and a total of 4 biological replicates were completed.

Cell viability assays. Serial dilutions of *A. tumefaciens* cells were spotted on ATGN plates to assess the viability of the *min* mutants. Exponential cultures (OD_{600} = 0.4 - 0.6) were diluted to OD_{600} 0.05 in ATGN. Cells were then serially diluted and 4 µl of each dilution was spotted onto ATGN plates. Plates were grown for 3 days at 28°C and imaged.

Phase contrast microscopy, cell length analysis, and quantitation of constriction position. Cells were grown in ATGN media until exponential phase was reached. A small volume (0.6 µl-0.8 µl) of live cells was then placed onto a 1% agarose ATGN pad as described previously [60,61]. Phase contrast microscopy was performed with an inverted Nikon Eclipse TiE with a QImaging Rolera em-c^2 1K EMCCD camera and Nikon Elements Imaging Software. Cell length distributions of 948 cells per strain were determined using the longest medial axis measured using MicrobeJ software [62]. Sites of cell constrictions were determined for ~1000 individual cells for each strain using stacked phase contrast images. Sites of constriction were autodetected using a preset MicrobeJ constriction detection function. To determine the polar orientation of each cell, old poles were identified using the lipophilic dye FM4-64 as previously described [61].

Fluorescence microscopy. For DNA staining, 1 ml of cells at an OD_{600} = 0.4 - 0.6 were treated with 1 µl of Sytox Orange (Invitrogen) for 5 minutes in the dark. Cells were pelleted and washed with PBS two times to remove excess dye. Cell pellets were resuspended in PBS and cells were imaged immediately on an agarose pad. Replicating plasmids pRV-Pvan-FtsZ-GFP and pSRKKm-Plac-YFP-ParB were introduced into wildtype cells and *min* mutants via an established electroporation protocol [59]. For imaging of YFP-ParB, exponential phase cells were diluted to OD_{600} = 0.2 and were induced with IPTG for 4 hours until reaching an OD_{600} = 0.4-0.6 and were then imaged on agarose pads. Dual channel images were stacked and cell outlines and YFP-ParB foci were automatically detected using MicrobeJ [62]. Demographs depicting YFP-ParB

localization were created by capturing the fluorescent intensity along the midline of the longitudinal axis of each cell and ordering these images by cell length. Both cell outlines and identified YFP-ParB foci were manually reviewed to ensure that the plots reflect accurate sites of YFP-ParB foci. For imaging of cells expressing constitutive FtsZ-GFP, cells were grown to OD_{600} = 0.4-0.6 and placed on agarose pads. Cells were imaged using phase contrast and epifluorescence microscopy with the appropriate filters. For timelapse microscopy cells were grown on ATGN 1.5% agarose pads with images collected either every 5 minutes or 10 minutes.

Results

Deletion of *min* genes does not have a large impact on cell growth or viability, but causes a broader cell length distribution. Transposons accumulate in the *min* region of *A. tumefaciens* during saturating transposon mutagenesis experiments in *A. tumefaciens* suggesting that the Min system is not required for cell survival [52]. To verify these results, we constructed markerless deletions in each *min* gene and the entire *min* locus. Growth curves of *min* mutants were indistinguishable from the growth curve of the parent strain (Figure A.1A). The *min* mutants are viable (Figure A.1B) with only a slight decrease in viability in Δ*minE*, suggesting that unregulated MinCD is more problematic than loss of the entire *min* locus. Although the *min* mutants are viable, phase contrast images of the cell populations revealed a small but consistent proportion of cells with atypical morphologies, including short cells (Figure A.2A). Quantitative image analysis was used to determine the cell length distributions of the *min* mutants (Figure A.2B).

While the medians of the cell length distributions of the *min* mutants are actually slightly longer than that of the parent strain, the length of the whiskers is significantly increased suggesting that both short and long cells are accumulating in the *min* mutants. Next, we determined the percentage of cells with typical cell lengths (defined as 1.5 - 3.5 μm), cells with branches or bulges, short cells (< 1.5 μm), and cells with visible constrictions (Figure A.3). Indeed, these observations confirm the presence of a small but reproducible proportion of short cells in the *min* mutant cells (Figure A.3, panel iii). Furthermore, although the overall proportion of cells with constrictions is not impacted by the loss of individual *min* genes or the entire locus, we observe an increase in cells with obvious asymmetric constrictions or multiple constrictions (Figure A.3, panel iv).

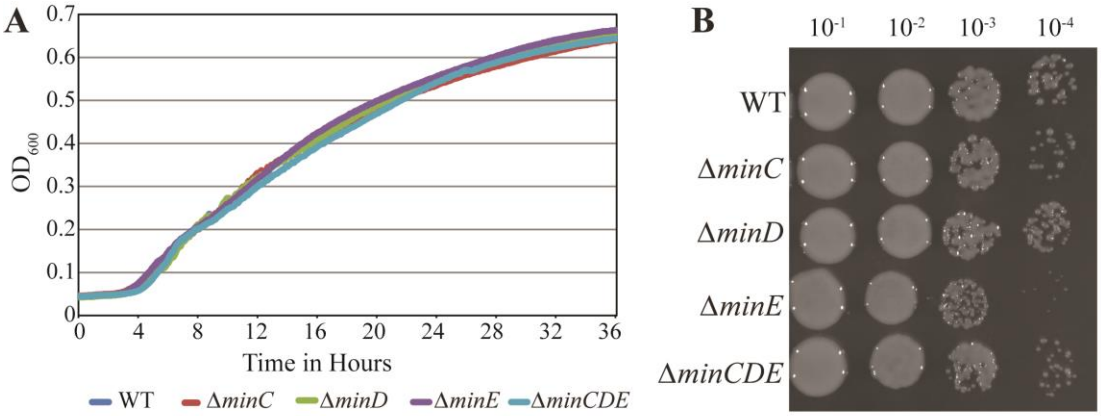

Figure A.1. Growth and viability of *min* mutants is not compromised. (A) Growth of Wildtype *A. tumefaciens* strain C58 and *min* mutants is monitored over 36 hours by observing the increase in cell density. (B) Exponentially growing cells were diluted to OD_{600} = 0.05 and serial dilutions were spotted on nutrient rich medium to observe viability.

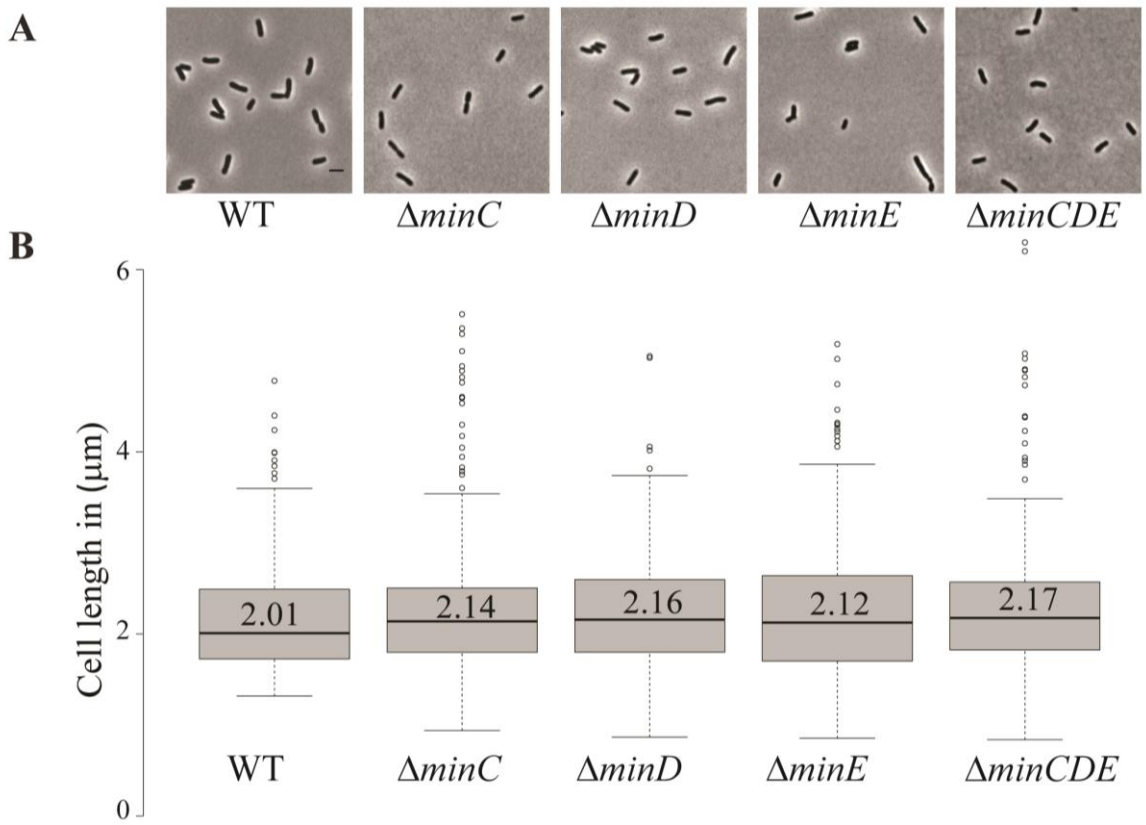

Figure A.2. Short cells accumulate in *min* mutants. (A) Phase contrast images of representative wildtype and *min* mutant cells. Scale bar = 2 μm. (B) Box plots illustrate cell length distributions of wildtype cells and *min* mutants. Medians are shown by the labeled center lines. Box limits indicate the 25th and 75th percentiles as determined by R software; whiskers extend 1.5 times the interquartile range and outliers are represented by dots. Cell lengths measured from 948 cells for each strain.

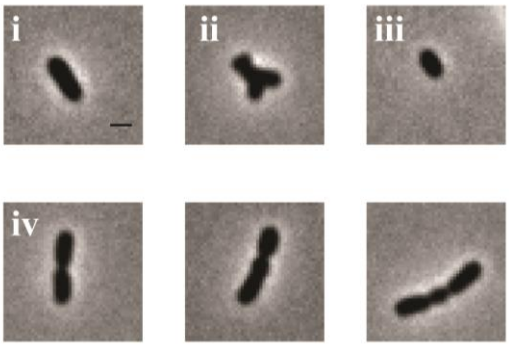

	(i) Rod-shaped	(ii) Branched	(iii) Small <1.5μm	(iv) Constricting
WT	75%	<1%	5%	20%
Δ*minC*	71%	1%	8%	20%
Δ*minD*	70%	1%	8%	21%
Δ*minE*	61%	1%	12%	25%
Δ*minCDE*	71%	1%	8%	20%

Figure A.3. Atypical morphologies are observed in *min* mutants. Phase contrast images of representative morphologies. All images taken from the Δ*minE* cell population. Scale bar = 1 μm. (top) Quantitation of bacterial morphologies. (bottom) The percentage of cells with a rod-shaped morphology (i: 1.5 – 3.5 μm in length), branched morphology (ii), short cell morphology (iii: <1.5 μm in length), and cells with visible constrictions (iv) are shown in the table. Cell morphologies were categorized from at least 948 cells for each strain.

The Min system contributes to precise placement of constriction sites. The previous observations suggest that the Min system may contribute to the proper placement of the site of cell division in *A. tumefaciens*. To better understand the function of the Min system in the establishment of constriction sites, we quantitated the position of constriction sites in wildtype cells (n = 186). In this analysis, the true mid-cell is defined as 0 and negative values indicate positions of constrictions closer to the old pole whereas positive values indicate positions of constrictions closer to the new pole. Using the wildtype data set, we define a typical constriction placement to occur near mid-cell with a bias toward the new pole: 95% of constrictions formed between -0.1 and 0.35 μm from the true mid-cell position (Figure A.4A, left). In addition, constrictions are consistently observed in cells with lengths between 2.5 and 3.5 μm (Figure A.4A, right). These observations indicate that the site of constriction is established well before the cell has completed elongation. Cells longer than 4 μm in length with constrictions are rarely observed, presumably because the cells have successfully completed cell division.

In the *min* mutants, constrictions form in ~20% of the cell population which is similar to what is observed in wildtype (Figure A.3); however, the placement of the constrictions is perturbed. The *min* mutants have a broader distribution of constriction placement (Figure A.4A). The Δ*minE* mutant in particular has lost the ability to maintain the proper bias of constriction site placement near the new pole. In contrast, when the entire *min* locus is absent 82% of constrictions are observed in the typical position and the bias for constriction placement toward the new pole is retained. These observations suggest that the unregulated activity of MinCD results in a more random positioning of constrictions,

but proper positioning of constrictions is frequently retained when the *min* locus is entirely deleted. Although constriction sites form more randomly in *min* mutants, we rarely observe constriction sites immediately adjacent to the cell poles (Figure A.4B) and short cells, rather than minicells are formed. Since constriction sites are not biased only toward the new pole in *min* mutants, this phenotype cannot be readily explained by the continuation of growth at the new pole and may indicate the existence of another mechanism to protect the poles. Furthermore, an increase in long cells (>4 μm) with visible constrictions (Figure A.4B) is observed in *min* mutants. This observation suggests that cell division efficiency is adversely impacted in the *min* mutants. It is possible that the perturbations of the Min system result in a delay in cell division or an increase in the frequency of constrictions that do not lead to a productive cell division event.

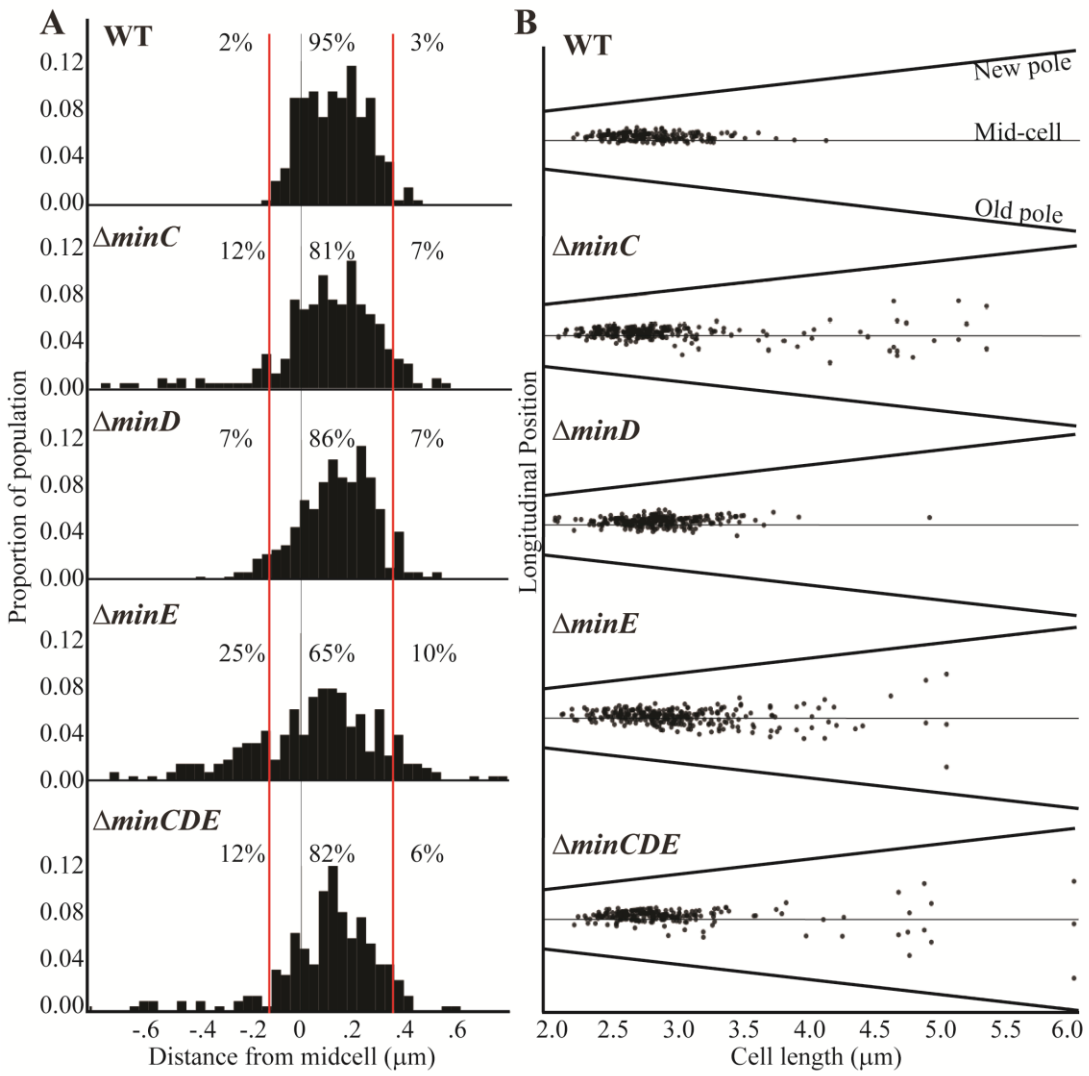

Figure A.4. Cell constriction placement in wildtype and *min* mutant cells. (A) Histograms of constriction position relative to distance from the mid-cell (grey line; relative position = 0). The red lines at -0.1 μm and 0.35 μm mark the region where constrictions typically form in wildtype cells. Negative numbers are closer to the old pole whereas the positive numbers are closer to the new pole. Percentages indicate the proportion of constrictions placed farther than -0.1 μm from mid-cell, placed between -0.1 μm and 0.35 μm, and placed more than 0.35 μm from mid-cell. (B) The longitudinal position of constrictions is plotted against cell length. For this analysis, cells are ordered

by cell length and black dots indicate the position of the constriction. Mid-cell is indicated by the center grey line and the slanted lines indicate the position of the new and old pole for each cell. For these analysis, the pre-divisional cells within a population of ~1000 cells were analyzed (n = 186 for wildtype; n = 242 for Δ*minC*, n = 262 for Δ*minD*, n = 285 for Δ*minE*, and n = 225 for Δ*minCDE*).

FtsZ-rings form in *min* mutants. In order to provide additional insights into the position of constriction placement, we introduced a plasmid which constitutively expresses *ftsZ-gfp* at a low level [54] into wildtype and *min* mutant cells. In wildtype cells, FtsZ-rings initially form at an asymmetric position near the new pole and mark the future site of cell division (Figure A.5A-B). As the cell continues to elongate at the new pole, the FtsZ-ring is ultimately positioned near mid-cell and constriction leads to the appearance of a discrete focus of FtsZ in late predivisional cells. In the *min* mutants, FtsZ-rings are observed at asymmetric positions, near mid-cell and in some cells multiple FtsZ-rings form (Figure A.5A). Unlike the pattern of FtsZ-ring formation in wildtype cells which is very consistent, the pattern of FtsZ-ring formation is variable in the *min* mutants. For example, asymmetric FtsZ-rings form in positions biased toward either the new or old pole in Δ*minE* mutants (Figure A.5C, top two panels). In either case, the establishment of an FtsZ-ring can lead to a cell division event which creates daughter cells of different cell sizes. These observations are consistent with the broader cell length distribution of the *min* mutants which includes both short and long cells (Figure A.2) and with the asymmetric positioning of constrictions (Figure A.4). In addition, Δ*minC*, Δ*minE*, and Δ*minCDE* cells with multiple FtsZ-rings are readily observed (Figure A.5A). In Δ*minE*

cells with two FtsZ-rings, both sites marked with FtsZ undergo constriction leading to the production of a bow-tie morphology and cell division ultimately occurs at either both or a single site marked by an FtsZ-ring (Figure A.5C, bottom two panels).

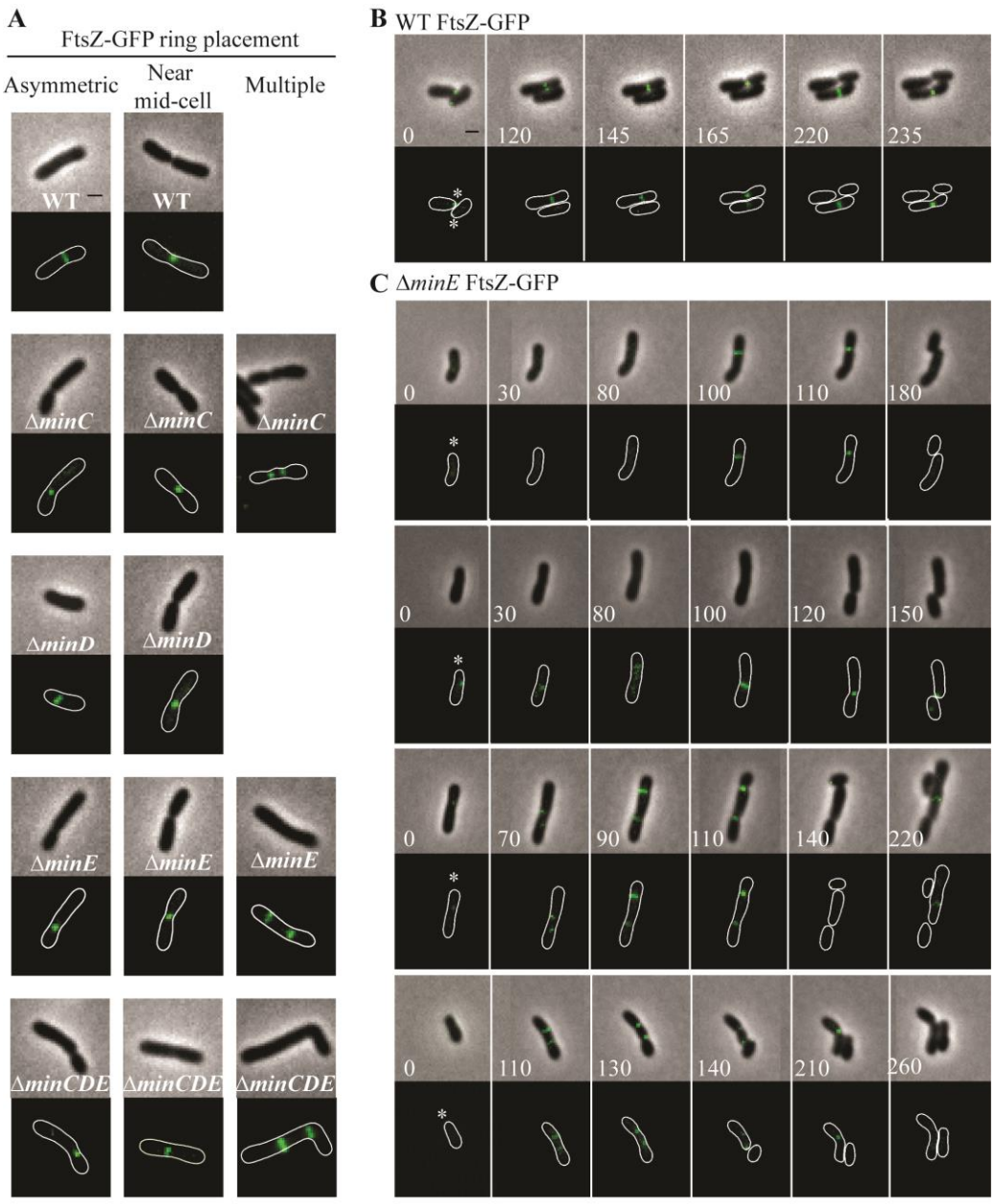

Figure A.5. FtsZ-ring position in wildtype and *min* mutant cells. (A) Representative images of FtsZ-GFP localization patterns in wildtype and *min* mutants including asymmetric localization, near mid-cell localization, and multiple ring formation. The absence of an image indicates that the localization pattern is not observed in the strain. (B) Timelapse microscopy showing typical FtsZ-GFP localization patterns in wildtype

cells. Asterisks mark the growing poles. (C) Timelapse microscopy of FtsZ-GFP localization in Δ*minE* cells. Asterisks mark the growing poles.

Cell division is initiated prior to nucleoid separation. After observing that FtsZ-rings are present in wildtype cells without visible constrictions (Figure A.5B), we next aimed to determine if FtsZ-rings form over DNA (Figure A.6). In elongating wildtype cells, FtsZ is typically observed either at a polar focus or in an asymmetric FtsZ-ring, whereas Sytox Orange labeling indicates that the DNA is diffuse (Figure A.6A, columns 1-2). The DNA remains diffuse in cells with early constrictions (Figure A.6A, column 3) and only forms separated nucleoids in deeply constricted cells (Figure A.6A, column 4). These observations are consistent with the possibility that *A. tumefaciens* does not use a nucleoid occlusion mechanism to position FtsZ at mid-cell. Similar results are observed in the *min* mutants, as exemplified by Δ*minE* (Figure A.6B). Notably, in the *ΔminE* mutant FtsZ-rings form over the top of DNA at asymmetric positions and when multiple FtsZ-rings are present. Finally, we observed that short cells in the Δ*minE* population typically contain diffuse DNA (Figure A.6B, right column).

In the wildtype cells and each of the *min* mutants, 90-95% of the cell population (based on observations of ~230 cells/strain) has diffuse DNA. In the *min* mutants, DNA is diffuse in cells without constrictions irrespective of cell shape (shown for Δ*minE* in Figure A.6C, panel i), including short and branched cells. Two distinct nucleoids are observed in 5-10% of the wildtype and *min* mutant cell populations (shown for Δ*minE* in Figure A.6C, panel ii). As expected due to the formation of asymmetric sites of cell constriction, the *min* mutants contain a higher proportion of cells with asymmetrically separated nucleoids. In less than 1% of the Δ*minC and* Δ*minE* cells, the presence of more than 2 nucleoids is observed (Figure A.6C, panel iii).

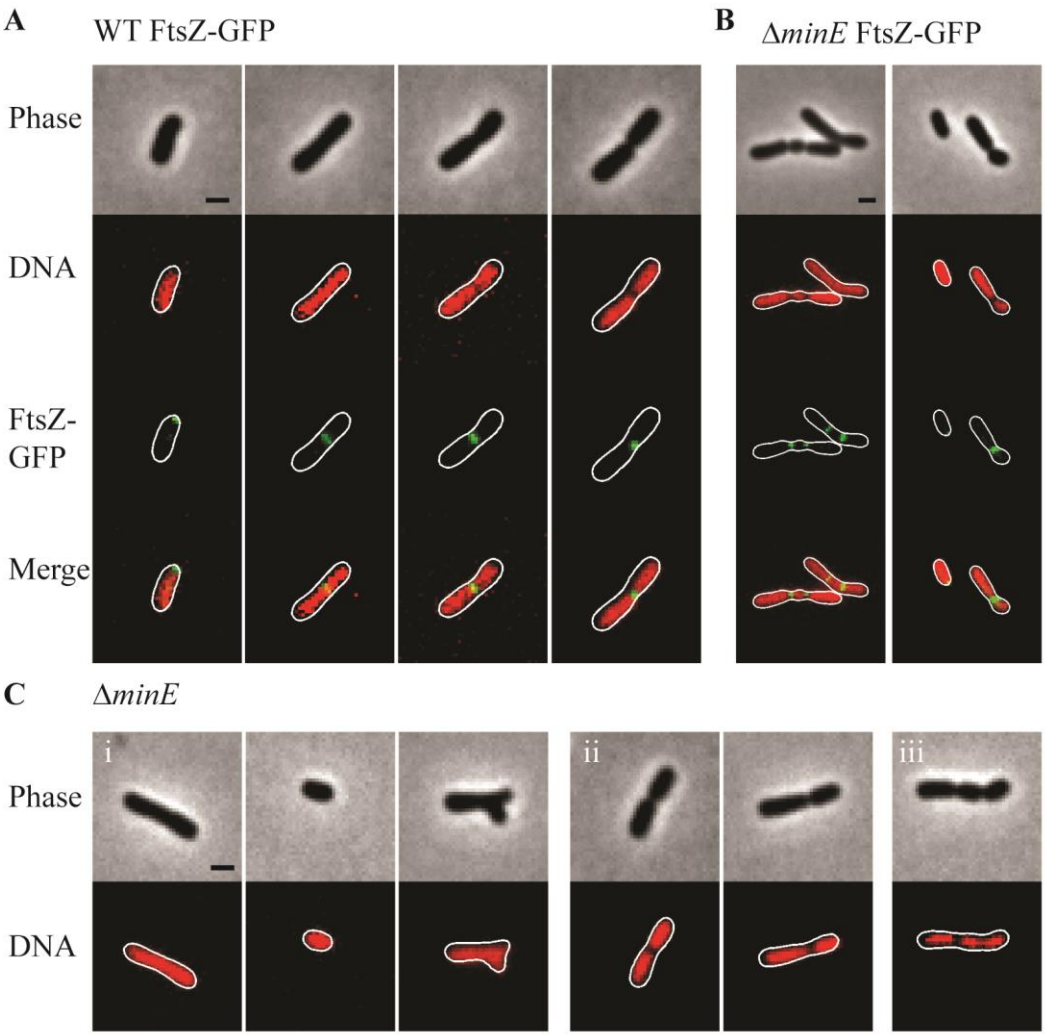

Figure A.6. Nucleoid position in wildtype and *min* mutant cells. (A) Representative images demonstrating FtsZ-GFP localization in wildtype cells with Sytox Orange stained DNA. (B) Representative images of FtsZ-GFP localization in Δ*minE* cells with Sytox Orange stained DNA. (C) Representative images from the Δ*minE* mutant population. Sytox Orange was used to label DNA and observe localization patterns including (i) diffuse, (ii)separated nucleoids, and (iii) other patterns.

Chromosome segregation is delayed in single *min* mutants. Since the inefficiency of cell division in the *min* mutants may cause a delay in chromosome segregation, we next tracked the early stages of chromosome segregation by introducing an IPTG inducible plasmid expressing *yfp-parB* [55] into the *min* mutants. ParB attaches to the *parS* site near the origin of replication, making it suitable to track the movement of newly replicated origin [55]. In *A. tumefaciens* ParB localizes at the old pole and as the cell nears division a second focus appears and rapidly tracks across the cell to the new pole ensuring both cells receive a copy of the chromosome (Figure A.7; [55]). The longitudinal profile of over 500 cells expressing YFP-ParB were aligned in order of cell length to create a demograph depicting the localization of YFP-ParB throughout the cell cycle (Figure A.7A). In wildtype cells, YFP-ParB is observed in three patterns: first, a single focus is observed in short cells, next we observe a brief transition period where a second focus of YFP-ParB appears and transits along the longitudinal axis of the cell, finally in predivisional cells, both foci are anchored at opposite poles. To examine the YFP-ParB localization pattern at the population level, the positions of the YFP-ParB foci were normalized by cell length and plotted along the cell axis (Figure A.7B). In wildtype cells, a larger number of foci are observed at the old pole than at the new pole due to the presence of a single focus in short cells and two foci near the old pole at the onset of DNA replication. Notably, very few YFP-ParB foci are observed transiting from old pole to new pole presumably due to the rapid rate of DNA replication and chromosome segregation.

The deletion of single *min* genes results in less consistent patterns of YFP-ParB localization throughout the cell cycle. In the absence of MinC, MinD, or MinE, YFP-ParB is located at a single focus in short cells; however, not all of the foci are found at the old pole (Figure A.7A). Furthermore, we observe an increase in the number of foci observed between the poles (Figure A.7A-B). This phenotype is due to a combination of cells which accumulate more than 2 YFP-ParB foci and cells in which the duplicated origin is not efficiently transited from pole to pole. Although MinD has been described as a candidate protein to tether DNA to the membrane during chromosome segregation in *E. coli* (Ventura et al 2013), we do not observe a more severe phenotype in the *ΔminD* mutant compared to the *ΔminC* or *ΔminE* mutants. Furthermore, deletion of the entire *min* locus results in a localization pattern of YFP-ParB which is more similar to wildtype. Since the *min* mutants are viable (Figure 1) and even short cells are capable of resuming growth (Figure A.5C, bottom panel), we infer that chromosome segregation is delayed presumably due to inefficient cell division in the *min* mutants.

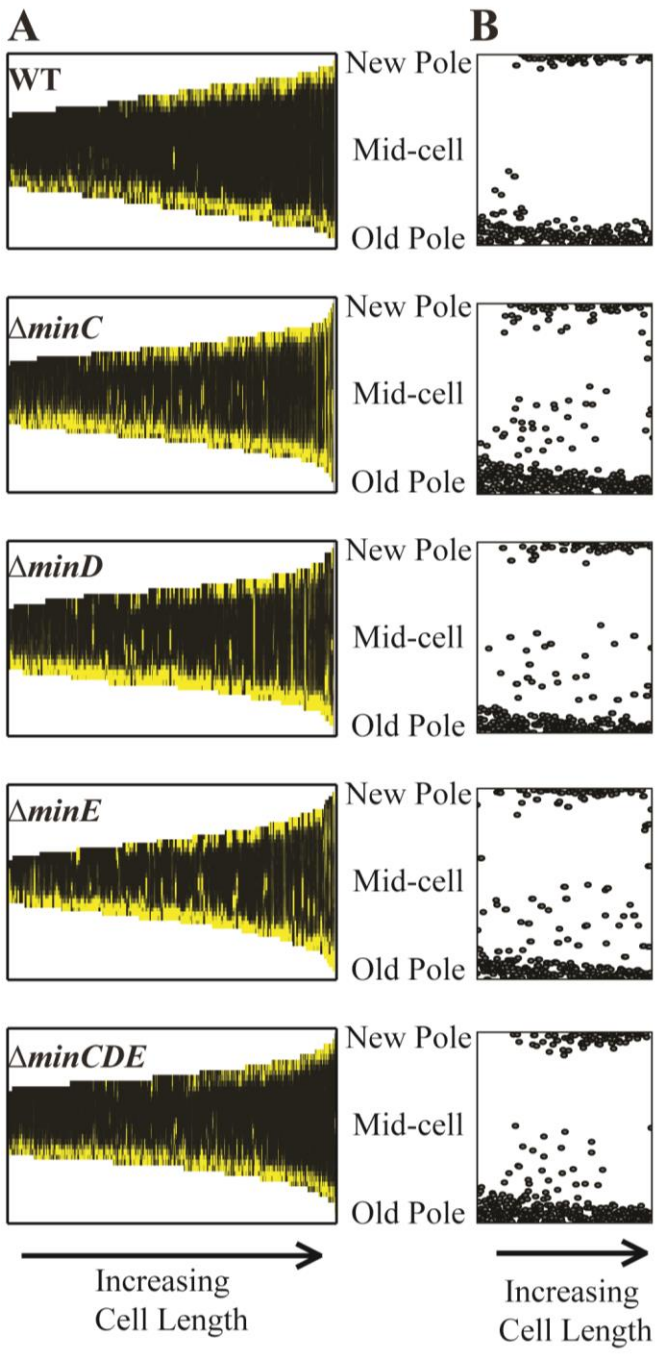

Figure A.7. YFP-ParB localization in wildtype and *min* mutant cells. (A) Demographs of YFP-ParB localization. Cells are ordered according to cell length and positions of the new pole, mid-cell, and old pole are indicated. (B) Position of YFP-ParB foci are plotted relative to longitudinal position in the cells. At least 500 cells were analyzed for each strain.

Discussion

In this work, we have characterized the impact of the Min system on the cell division of *A. tumefaciens*. Similar to findings in *S. meliloti* [51] and consistent with a saturating transposon screen in *A. tumefaciens* suggesting that the *min* genes are not essential [52], we have confirmed that the *min* genes are not required for cell viability (Figure 1). Quantitative image analysis of cell morphology reveals that cell length distributions and placement of sites of cell constrictions are perturbed when single *min* genes are deleted compared to wildtype cells (Figures 2-4). In particular, the absence of MinE leads to the accumulation of both long and short cells suggesting that the placement of the septum is perturbed. Indeed, the sites of cell constriction (Figure A.4) and localization of FtsZ-GFP is more variable in the Δ*minE* strain (Figure A.5) suggesting that the misregulation of MinCD is detrimental to efficient cell division. These observations are consistent with the *E. coli* model of the Min system where MinE regulates the activity of the MinCD complex by driving the oscillation of MinC and MinD from pole-to-pole and preventing the establishment of polar FtsZ-rings [17,63]. In *A. tumefaciens*, the absence of MinE leads to a more random distribution of active of MinCD complexes, allowing the observed misplacement of FtsZ-rings and constriction sites. Remarkably, asymmetric FtsZ-rings are not observed immediately adjacent to the cell poles in *min* mutants (Figure A.5A and C) and can form over DNA in both wildtype cells and *min* mutants (Figure A.6). Finally, the absence of the entire Min system has a relatively mild phenotype enabling most cells to divide near mid-cell (Figures 2 and 4). Together, these results suggest that other mechanisms for proper placement of FtsZ-rings must exist in *A. tumefaciens*.

While the *A. tumefaciens min* mutant phenotypes are generally consistent with the *E. coli* Min model, a key component of this model remains to be tested in *A. tumefaciens*. In *E. coli*, the Min proteins oscillate from pole-to-pole producing a local minimum inhibition zone at mid-cell in which FtsZ-rings can form [22,23,64]. In contrast, in *B. subtilis* the MinCDJ system does not use protein oscillation. DivIVA binds to regions of the membrane with negative curvature [65,66]. Next, MinJ acts as an adaptor protein and enables the recruitment of MinD and subsequently MinC to sites of DivIVA localization [67,68]. Initially, it was thought that the MinCD complexes formed a static bipolar gradient which protects the poles from FtsZ-ring assembly [69,70]; however, DivIVA is recruited to the nascent division site when constriction is initiated leading to the formation of DivIVA-rings on either side of the division site [71]. MinCDJ complexes are assembled at these DivIVA-rings and presumably prevent the formation of additional FtsZ-rings near mid-cell. Based on the presence of *minE* and the absence of *divIVA* and *minJ* in the genome of *A. tumefaciens*, we hypothesize that the MinCD proteins should localize at cell poles and oscillate from pole-to-pole and MinE should exhibit a dynamic localization pattern with enrichment at sub-polar region. Our initial efforts to construct C-terminal fluorescent protein fusions to the *A. tumefaciens* Min proteins have been unsuccessful. A rigorous effort will be needed to observe the localization patterns of the Min proteins in *A. tumefaciens* to determine if pole-to-pole oscillation of the Min proteins contributes to the efficient establishment of constriction sites at the proper position.

In addition to cell division defects, single deletion of *min* genes results in delayed chromosome segregation (Figure A.7). At first glance, this finding appears to be consistent with observations of chromosome partitioning defects in *E. coli min* mutants [72-74]; however, there are notable phenotypic differences. First, in *E. coli*, the production of minicells devoid of DNA due to polar cell division events is a hallmark of *min* mutants [35]. In contrast, short cells arising from misplacement of constriction sites in *A. tumefaciens min* mutants typically contain DNA. This difference may suggest that *A. tumefaciens* does not employ a nucleoid occlusion system to prevent the establishment of FtsZ-rings over unsegregated nucleoids [36,75] and is consistent with the absence of an obvious nucleoid occusion protein in the *A. tumefaciens genome* [76,77] and the formation of FtsZ-rings over DNA in unconstricted cells (Figure A.6A). Second, in *E. coli*, a Δ*minCDE* mutant has a more severe defect in chromosome segregation than a Δ*minC* mutant leading to the hypothesis that MinD may directly contribute to chromosome segregation [74]. The MinD/ParA family of proteins share an evolutionary history and MinD and ParA function in providing positional information for spatial organization of the FtsZ-ring and segregating chromosome, respectively [47]. *E. coli* MinD can nonspecifically bind chromosomal DNA and may provide polar gradients of DNA tethering sites during chromosome segregation [74]. If *A. tumefaciens* MinD is capable of binding DNA and tethering chromosomes to the membrane, the predicted random distribution of MinCD complexes in the absence of MinE may explain why the YFP-ParB foci do not rapidly transit from pole-to-pole. Nevertheless, if *A. tumefaciens* MinD is involved in chromosome segregation we would expect to observe segregation defects in the Δ*minD* and Δ*minCDE* strains. Remarkably, the Δ*minC,* Δ*minD,* and Δ*minE*

strains exhibit a strikingly similar phenotype with a delay in transition of the YFP-ParB focus from the old pole to the new pole (Figure A.7). Furthermore, the Δ*minCDE* strain has a less severe phenotype and YFP-ParB is bipolar in the longest cells. Together, these data suggest that the chromosome segregation defect in the *min* mutants likely arises indirectly as a consequence of less efficient cell division.

Remarkably, in some *C. crescentus* cells lacking MipZ, productive cell division events occur resulting in the production of minicells which contain DNA [45]. Although constrictions form over chromosomes that have not completed segregation, most isolated minicells contain both an origin of replication and a terminus. These observations suggest that cell division is delayed until DNA replication is finished and the complete chromosome is delivered to the minicell compartment [45]. In most bacteria, DNA replication and chromosome segregation occur simultaneously. These processes consist of three major stages: separation and translocation of the duplicated origin, segregation of the bulk chromosome, and separation of the terminus region [78,79]. *C. crescentus* uses the widely distributed ParABS system [80] to segregate the *ori* region of the chromosome. Briefly, ParB binds to DNA at the *parS* site which is proximal to the origin of replication. Following duplication of *ori*, one of the ParB-bound *ori* regions remains at the old pole and the other is translocated across the cell to the opposite pole following a receding cloud of ParA [81-83]. ParB is anchored to the poles through a direct interaction with the polar organizing protein PopZ [84,85]. When PopZ is absent, the chromsomes become untethered from the pole and minicells without DNA are formed [85]. MipZ not only inhibits FtsZ-ring assembly, it also binds to ParB, protecting the *ori* proximal

regions from FtsZ-ring formation [45]. Thus, the processes of cell division and *ori* partitioning are tightly coupled through MipZ. Later stages of cell division and chromosome segregation are also coupled through FtsK. In *C. crescentus,* the N-terminus of FtsK contributes to the stability of FtsZ-rings and the C-terminus of FtsK is responsible for clearing the termini from the division plane [86]

The observation that the *A. tumefaciens min* mutants produce short cells that contain DNA may suggest that *A. tumefaciens* also couples the processes of cell division and chromosome segregation. Indeed, the deletion of *popZ* in *A. tumefaciens* results in untethered chromosomes and the production of cells devoid of DNA [55]. In some *ΔpopZ* cells, DNA appears to be segregated in the wrong direction across the division plane. FtsK functions as a DNA translocase that assists in the completion of cell division by moving DNA across the division plane in the direction of the termini [78,87]. If a terminus is trapped on the wrong side of the division plane in the absence of PopZ, FtsK may pump DNA in the wrong direction leading to the production of cells without DNA. Notably, whereas the deletion of *popZ* leads to the production of minicells in *C. crescentus* [85], the loss of *popZ* results in the production of a broad distribution of cell lengths in *A. tumefaciens* [54] suggesting that the poles are still largely protected from FtsZ-ring formation. Similarly, when the Min system is removed the short cells sometimes arise (Figure 2) and although *ori* partitioning appears to be delayed (Figure A.7), most cells are viable (Figure 1) suggesting that even short cells inherit an intact chromosome. Timelapse microscopy of the *ΔminE* mutant illustrates that short cells are capable of resuming growth following cell division (Figure A.5C, bottom panel).

Together, these observations suggest that *A. tumefaciens* must use another FtsZ-positioning mechanism to protect the poles and that the processes of DNA replication, chromosome segregation, and cell division must be coordinated.

How might DNA replication, chromosome segregation, and cell division be properly coordinated in *A. tumefaciens*? In *S. meliloti,* expression of *minC* and *minD* was upregulated during depletion of CtrA, implicating this master cell cycle regulator as a transcriptional repressor of this operon [50]. Remarkably, *minCD* are the only known cell division genes directly regulated by CtrA; however, introduction of a deletion of *minCDE* into the CtrA depletion strain did not rescue the cell division defect suggesting the Min overexpression is not exclusively responsible for the cell division phenotype. Depletion of CtrA in *A. tumefaciens* leads to a block in cell division [88] and a putative consensus CtrA binding site (TTAA-N_7-TTAA) is present upstream of *minC* in the *A. tumefaciens* genome. Thus, it is tempting to speculate that the transcription of the *min* genes is under the control of CtrA. Cell-cycle regulation of the Min system may ensure that these proteins are functioning as needed when the cells approach cell division. In *C. crescentus* the expression of *ftsZ* is directly regulated by CtrA [89,90] and FtsZ is subject to proteolysis by ClpAP and ClpXP [91] leading to cell-cycle variability of FtsZ levels. Even when *ftsZ* is expressed constitutively, it is subject to post-translational control leading to cell cycle variability of FtsZ levels [91]. The cell cycle variability in FtsZ levels may be a common feature among bacteria with an alphaproteobacterial cell cycle. Thus, in *A. tumefaciens* the cell cycle regulation of the Min system may temporally coordinate the expression levels of the Min and FtsZ proteins. Future studies will be

necessary to determine if FtsZ, other divisome components, and the Min proteins are coordinated through cell-cycle regulation in *A. tumefaciens*. Such studies are necessary to better understand how the processes of DNA replication, chromosome segregation, and cell division are coordinated in *A. tumefaciens*.

Overall these results suggest that while the *A. tumefaciens* Min system contributes to the precise positioning of FtsZ-ring and constriction site near mid-cell, other mechanisms must exist to ensure proper spatial organization during cell division. In *A. tumefaciens,* the phenotype of the Δ*minCDE* strain is milder than that of the individual Δ*minC,* Δ*minD,* or Δ*minE* strains suggesting that this FtsZ positioning system is dispensable for the completion of cell division. There are a number of alternative FtsZ positioning proteins including nucleoid occlusion proteins, MipZ in *Caulobacter crescentus* which forms a bipolar gradient and directly inhibits FtsZ-ring assembly near the poles [45,46], and positive regulators which localize to mid-cell and promote FtsZ-ring assembly [17]. Other than the *min* locus, genes encoding candidate FtsZ-positioning proteins cannot be readily identified in the *A. tumefaciens* genome [76,77]. Since the entire *min* locus can be deleted with minimal effects on cell viability, cell morphology, sites of cell constriction, or FtsZ position, other mechanisms must exist to regulate cell division in *A. tumefaciens*. Thus, further studies of *A. tumefaciens* cell division are likely to reveal novel strategies to ensure proper mid-cell assembly of the divisome.

Conflict of Interest Statement

This research was conducted in the absence of any commercial or financial relationships that could be construed as a potential conflict of interest.

Author Contributions

SF, MH, JD, and PB designed experiments. SF, MH, JD, and RP conducted experiments. SF, MH, RP, and PB analyzed data. All authors contributed to writing and editing of the manuscript.

Funding

Research in the Brown lab on *A. tumefaciens* cell growth and division is supported by the National Science Foundation (IOS1557806).

Acknowledgements

We thank Grant Bowman (University of Wyoming) for the plasmid containing YFP-ParB and members of the Brown lab for feedback during the preparation of this manuscript.
Research in the Brown lab on *A. tumefaciens* cell growth and division is supported by the National Science Foundation (IOS1557806).

References

1. Bi EF, Lutkenhaus J: FtsZ ring structure associated with division in *Escherichia coli*. *Nature* 1991, 354:161-164.

2. Szwedziak P, Wang Q, Bharat TA, Tsim M, Lowe J: Architecture of the ring formed by the tubulin homologue FtsZ in bacterial cell division. *eLife* 2014, 3:e04601.

3. den Blaauwen T, Buddelmeijer N, Aarsman ME, Hameete CM, Nanninga N: Timing of FtsZ assembly in *Escherichia coli*. *J Bacteriol* 1999, 181:5167-5175.

4. Li Z, Trimble MJ, Brun YV, Jensen GJ: The structure of FtsZ filaments in vivo suggests a force-generating role in cell division. *Embo J* 2007, 26:4694-4708.

5. Ma X, Ehrhardt DW, Margolin W: Colocalization of cell division proteins FtsZ and FtsA to cytoskeletal structures in living *Escherichia coli* cells by using green fluorescent protein. *Proc Natl Acad Sci U S A* 1996, 93:12998-13003.

6. Sun Q, Margolin W: FtsZ dynamics during the division cycle of live *Escherichia coli* cells. *J Bacteriol* 1998, 180:2050-2056.

7. Goley ED, Yeh YC, Hong SH, Fero MJ, Abeliuk E, McAdams HH, Shapiro L: Assembly of the *Caulobacter* cell division machine. *Mol Microbiol* 2011, 80:1680-1698.

8. Lutkenhaus J, Du S: *E. coli* cell cycle machinery. *Subcell Biochem* 2017, 84:27-65.

9. Addinall SG, Cao C, Lutkenhaus J: FtsN, a late recruit to the septum in *Escherichia coli*. *Mol Microbiol* 1997, 25:303-309.

10. Muller P, Ewers C, Bertsche U, Anstett M, Kallis T, Breukink E, Fraipont C, Terrak M, Nguyen-Disteche M, Vollmer W: The essential cell division protein FtsN

interacts with the murein (peptidoglycan) synthase PBP1B in *Escherichia coli*. *J Biol Chem* 2007, 282:36394-36402.

11. Moll A, Thanbichler M: FtsN-like proteins are conserved components of the cell division machinery in proteobacteria. *Mol Microbiol* 2009, 72:1037-1053.
12. Cho H, Wivagg CN, Kapoor M, Barry Z, Rohs PD, Suh H, Marto JA, Garner EC, Bernhardt TG: Bacterial cell wall biogenesis is mediated by SEDS and PBP polymerase families functioning semi-autonomously. *Nat Microbiol* 2016 19:16172.
13. Botta GA, Park JT: Evidence for involvement of penicillin-binding protein 3 in murein synthesis during septation but not during cell elongation. *J Bacteriol* 1981, 145:333-340.
14. Bertsche U, Kast T, Wolf B, Fraipont C, Aarsman ME, Kannenberg K, von Rechenberg M, Nguyen-Disteche M, den Blaauwen T, Holtje JV, et al.: Interaction between two murein (peptidoglycan) synthases, PBP3 and PBP1B, in *Escherichia coli*. *Mol Microbiol* 2006, 61:675-690.
15. Bisson-Filho AW, Hsu YP, Squyres GR, Kuru E, Wu F, Jukes C, Sun Y, Dekker C, Holden S, VanNieuwenhze MS, et al.: Treadmilling by FtsZ filaments drives peptidoglycan synthesis and bacterial cell division. *Science* 2017, 355:739-743.
16. Yang X, Lyu Z, Miguel A, McQuillen R, Huang KC, Xiao J: GTPase activity-coupled treadmilling of the bacterial tubulin FtsZ organizes septal cell wall synthesis. *Science* 2017, 355:744-747.
17. Rowlett VW, Margolin W: The Min system and other nucleoid-independent regulators of Z ring positioning. *Front Microbiol* 2015, 6:478.

18. Wu LJ, Errington J: Nucleoid occlusion and bacterial cell division. *Nat Rev Microbiol* 2011, 10:8-12.

19. Fu X, Shih YL, Zhang Y, Rothfield LI: The MinE ring required for proper placement of the division site is a mobile structure that changes its cellular location during the *Escherichia coli* division cycle. *Proc Natl Acad Sci U S A* 2001, 98:980-985.

20. Hale CA, Meinhardt H, de Boer PA: Dynamic localization cycle of the cell division regulator MinE in *Escherichia coli*. *Embo J* 2001, 20:1563-1572.

21. Hu Z, Lutkenhaus J: Topological regulation of cell division in *Escherichia coli* involves rapid pole to pole oscillation of the division inhibitor MinC under the control of MinD and MinE. *Mol Microbiol* 1999, 34:82-90.

22. Raskin DM, de Boer PA: MinDE-dependent pole-to-pole oscillation of division inhibitor MinC in *Escherichia coli*. *J Bacteriol* 1999, 181:6419-6424.

23. Raskin DM, de Boer PA: Rapid pole-to-pole oscillation of a protein required for directing division to the middle of *Escherichia coli*. *Proc Natl Acad Sci U S A* 1999, 96:4971-4976.

24. Dajkovic A, Lan G, Sun SX, Wirtz D, Lutkenhaus J: MinC spatially controls bacterial cytokinesis by antagonizing the scaffolding function of FtsZ. *Curr Biol* 2008, 18:235-244.

25. Hu Z, Lutkenhaus J: Analysis of MinC reveals two independent domains involved in interaction with MinD and FtsZ. *J Bacteriol* 2000, 182:3965-3971.

26. Justice SS, Garcia-Lara J, Rothfield LI: Cell division inhibitors SulA and MinC/MinD block septum formation at different steps in the assembly of the *Escherichia coli* division machinery. *Mol Microbiol* 2000, 37:410-423.

27. Hu Z, Lutkenhaus J: A conserved sequence at the C-terminus of MinD is required for binding to the membrane and targeting MinC to the septum. *Mol Microbiol* 2003, 47:345-355.

28. de Boer PA, Crossley RE, Hand AR, Rothfield LI: The MinD protein is a membrane ATPase required for the correct placement of the *Escherichia coli* division site. *Embo J* 1991, 10:4371-4380.

29. de Boer PA, Crossley RE, Rothfield LI: Roles of MinC and MinD in the site-specific septation block mediated by the MinCDE system of *Escherichia coli*. *J Bacteriol* 1992, 174:63-70.

30. Hu Z, Lutkenhaus J: Topological regulation of cell division in *E. coli.* Spatiotemporal oscillation of MinD requires stimulation of its ATPase by MinE and phospholipid. *Mol Cell* 2001, 7:1337-1343.

31. Loose M, Fischer-Friedrich E, Herold C, Kruse K, Schwille P: Min protein patterns emerge from rapid rebinding and membrane interaction of MinE. *Nat Struct Mol Biol* 2011, 18:577-583.

32. Park KT, Wu W, Battaile KP, Lovell S, Holyoak T, Lutkenhaus J: The Min oscillator uses MinD-dependent conformational changes in MinE to spatially regulate cytokinesis. *Cell* 2011, 146:396-407.

33. Park KT, Villar MT, Artigues A, Lutkenhaus J: MinE conformational dynamics regulate membrane binding, MinD interaction, and Min oscillation. *Proc Natl Acad Sci U S A* 2017, 114:7497-7504.

34. Bonny M, Fischer-Friedrich E, Loose M, Schwille P, Kruse K: Membrane binding of MinE allows for a comprehensive description of Min-protein pattern formation. *PLoS Comput Biol* 2013, 9:e1003347.

35. de Boer PA, Crossley RE, Rothfield LI: A division inhibitor and a topological specificity factor coded for by the minicell locus determine proper placement of the division septum in *E. coli*. *Cell* 1989, 56:641-649.

36. Bernhardt TG, de Boer PA: SlmA, a nucleoid-associated, FtsZ binding protein required for blocking septal ring assembly over chromosomes in *E. coli*. *Mol Cell* 2005, 18:555-564.

37. Cho H, McManus HR, Dove SL, Bernhardt TG: Nucleoid occlusion factor SlmA is a DNA-activated FtsZ polymerization antagonist. *Proc Natl Acad Sci U S A* 2011, 108:3773-3778.

38. Tonthat NK, Arold ST, Pickering BF, Van Dyke MW, Liang S, Lu Y, Beuria TK, Margolin W, Schumacher MA: Molecular mechanism by which the nucleoid occlusion factor, SlmA, keeps cytokinesis in check. *Embo J* 2011, 30:154-164.

39. Du S, Lutkenhaus J: SlmA antagonism of FtsZ assembly employs a two-pronged mechanism like MinCD. *PLoS Genet* 2014, 10:e1004460.

40. Bailey MW, Bisicchia P, Warren BT, Sherratt DJ, Mannik J: Evidence for divisome localization mechanisms independent of the Min system and SlmA in *Escherichia coli*. *PLoS Genet* 2014, 10:e1004504.

41. Cambridge J, Blinkova A, Magnan D, Bates D, Walker JR: A replication-inhibited unsegregated nucleoid at mid-cell blocks Z-ring formation and cell division

independently of SOS and the SlmA nucleoid occlusion protein in *Escherichia coli*. *J Bacteriol* 2014, 196:36-49.

42. Rothfield L, Taghbalout A, Shih YL: Spatial control of bacterial division-site placement. *Nat Rev Microbiol* 2005, 3:959-968.

43. Jensen RB: Coordination between chromosome replication, segregation, and cell division in *Caulobacter crescentus*. *J Bacteriol* 2006, 188:2244-2253.

44. Radhakrishnan SK, Pritchard S, Viollier PH: Coupling prokaryotic cell fate and division control with a bifunctional and oscillating oxidoreductase homolog. *Dev Cell* 2010, 18:90-101.

45. Thanbichler M, Shapiro L: MipZ, a spatial regulator coordinating chromosome segregation with cell division in *Caulobacter*. *Cell* 2006, 126:147-162.

46. Kiekebusch D, Michie KA, Essen LO, Lowe J, Thanbichler M: Localized dimerization and nucleoid binding drive gradient formation by the bacterial cell division inhibitor MipZ. *Mol Cell* 2012, 46:245-259.

47. Lutkenhaus J: The ParA/MinD family puts things in their place. *Trends Microbiol* 2012, 20:411-418.

48. Bellefontaine AF, Pierreux CE, Mertens P, Vandenhaute J, Letesson JJ, De Bolle X: Plasticity of a transcriptional regulation network among alpha-proteobacteria is supported by the identification of CtrA targets in *Brucella abortus*. *Mol Microbiol* 2002, 43:945-960.

49. Williams M, Hoffman MD, Daniel JJ, Madren SM, Dhroso A, Korkin D, Givan SA, Jacobson SC, Brown PJ: Short-stalked *Prosthecomicrobium hirschii* cells have a *Caulobacter*-like cell cycle. *J Bacteriol* 2016, 198:1149-1159.

50. Pini F, De Nisco NJ, Ferri L, Penterman J, Fioravanti A, Brilli M, Mengoni A, Bazzicalupo M, Viollier PH, Walker GC, et al.: Cell cycle control by the master regulator CtrA in *Sinorhizobium meliloti*. *PLoS Genet* 2015, 11:e1005232.

51. Cheng J, Sibley CD, Zaheer R, Finan TM: A *Sinorhizobium meliloti minE* mutant has an altered morphology and exhibits defects in legume symbiosis. *Microbiology* 2007, 153:375-387.

52. Curtis PD, Brun YV: Identification of essential alphaproteobacterial genes reveals operational variability in conserved developmental and cell cycle systems. *Mol Microbiol* 2014, 93:713-735.

53. Morton ER, Fuqua C: Laboratory maintenance of *Agrobacterium*. *Curr Protoc Microbiol* 2012, Chapter 1:Unit 3D. 1.

54. Howell M, Aliashkevich A, Salisbury AK, Cava F, Bowman GR, Brown PJB: Absence of the polar organizing protein PopZ results in reduced and asymmetric cell division in *Agrobacterium tumefaciens*. *J Bacteriol* 2017, 199:e00101-17.

55. Ehrle HM, Guidry JT, Iacovetto R, Salisbury AK, Sandidge DJ, Bowman GR: Polar organizing protein PopZ Is required for chromosome segregation in *Agrobacterium tumefaciens*. *J Bacteriol* 2017, 199:e00111-17.

56. Simon R, Priefer U, Puhler A: A broad host range mobilization system for *in vivo* genetic engineering: transposon mutagenesis in gram negative bacteria. *Nat Biotechnol* 1983, 1:784-791.

57. Watson B, Currier TC, Gordon MP, Chilton MD, Nester EW: Plasmid required for virulence of *Agrobacterium tumefaciens*. *J Bacteriol* 1975, 123:255-264.

58. Merritt PM, Danhorn T, Fuqua C: Motility and chemotaxis in *Agrobacterium tumefaciens* surface attachment and biofilm formation. *J Bacteriol* 2007, 189:8005-8014.

59. Morton ER, Fuqua C: Genetic manipulation of *Agrobacterium*. *Curr Protoc Microbiol* 2012, Chapter 1:Unit 3D 2.

60. Brown PJB, de Pedro MA, Kysela DT, Van der Henst C, Kim J, De Bolle X, Fuqua C, Brun YV: Polar growth in the alphaproteobacterial order Rhizobiales. *Proc Natl Acad Sci USA* 2012, 109:1697-1701.

61. Howell M, Daniel JJ, Brown PJB: Live cell fluorescence microscopy to observe essential processes during microbial cell growth. *J Vis Exp* 2017, 129.

62. Ducret A, Quardokus EM, Brun YV: MicrobeJ, a tool for high throughput bacterial cell detection and quantitative analysis. *Nat Microbiol* 2016, 1:16077.

63. Lutkenhaus J: Assembly dynamics of the bacterial MinCDE system and spatial regulation of the Z ring. *Annu Rev Biochem* 2007, 76:539-562.

64. Meinhardt H, de Boer PA: Pattern formation in *Escherichia coli*: a model for the pole-to-pole oscillations of Min proteins and the localization of the division site. *Proc Natl Acad Sci U S A* 2001, 98:14202-14207.

65. Lenarcic R, Halbedel S, Visser L, Shaw M, Wu LJ, Errington J, Marenduzzo D, Hamoen LW: Localisation of DivIVA by targeting to negatively curved membranes. *EMBO J* 2009, 28:2272-2282.

66. Ramamurthi KS, Losick R: Negative membrane curvature as a cue for subcellular localization of a bacterial protein. *Proc Natl Acad Sci U S A* 2009, 106:13541-13545.

67. Patrick JE, Kearns DB: MinJ (YvjD) is a topological determinant of cell division in *Bacillus subtilis*. *Mol Microbiol* 2008, 70:1166-1179.

68. Bramkamp M, Emmins R, Weston L, Donovan C, Daniel RA, Errington J: A novel component of the division-site selection system of *Bacillus subtilis* and a new mode of action for the division inhibitor MinCD. *Mol Microbiol* 2008, 70:1556-1569.

69. Adams DW, Errington J: Bacterial cell division: assembly, maintenance and disassembly of the Z ring. *Nat Rev Microbiol* 2009, 7:642-653.

70. Bramkamp M, van Baarle S: Division site selection in rod-shaped bacteria. *Curr Opin Microbiol* 2009, 12:683-688.

71. Eswaramoorthy P, Erb ML, Gregory JA, Silverman J, Pogliano K, Pogliano J, Ramamurthi KS: Cellular architecture mediates DivIVA ultrastructure and regulates min activity in *Bacillus subtilis*. *MBio* 2011, 2.

72. Akerlund T, Bernander R, Nordstrom K: Cell division in *Escherichia coli minB* mutants. *Mol Microbiol* 1992, 6:2073-2083.

73. Akerlund T, Gullbrand B, Nordstrom K: Effects of the Min system on nucleoid segregation in *Escherichia coli*. *Microbiology* 2002, 148:3213-3222.

74. Di Ventura B, Knecht B, Andreas H, Godinez WJ, Fritsche M, Rohr K, Nickel W, Heermann DW, Sourjik V: Chromosome segregation by the *Escherichia coli* Min system. *Mol Syst Biol* 2013, 9:686.

75. Wu LJ, Errington J: Coordination of cell division and chromosome segregation by a nucleoid occlusion protein in *Bacillus subtilis*. *Cell* 2004, 117:915-925.

76. Goodner B, Hinkle G, Gattung S, Miller N, Blanchard M, Qurollo B, Goldman BS, Cao Y, Askenazi M, Halling C, et al.: Genome sequence of the plant pathogen and biotechnology agent *Agrobacterium tumefaciens* C58. *Science* 2001, 294:2323-2328.

77. Wood DW, Setubal JC, Kaul R, Monks DE, Kitajima JP, Okura VK, Zhou Y, Chen L, Wood GE, Almeida NF, Jr., et al.: The genome of the natural genetic engineer *Agrobacterium tumefaciens* C58. *Science* 2001, 294:2317-2323.

78. Badrinarayanan A, Le TB, Laub MT: Bacterial chromosome organization and segregation. *Annu Rev Cell Dev Biol* 2015, 31:171-199.

79. Surovtsev IV, Jacobs-Wagner C: Subcellular organization: a critical feature of bacterial cell replication. *Cell* 2018, 172:1271-1293.

80. Livny J, Yamaichi Y, Waldor MK: Distribution of centromere-like *parS* sites in bacteria: insights from comparative genomics. *J Bacteriol* 2007, 189:8693-8703.

81. Ptacin JL, Lee SF, Garner EC, Toro E, Eckart M, Comolli LR, Moerner WE, Shapiro L: A spindle-like apparatus guides bacterial chromosome segregation. *Nat Cell Biol* 2010, 12:791-798.

82. Schofield WB, Lim HC, Jacobs-Wagner C: Cell cycle coordination and regulation of bacterial chromosome segregation dynamics by polarly localized proteins. *Embo J* 2010, 29:3068-3081.

83. Shebelut CW, Jensen RB, Gitai Z: Growth conditions regulate the requirements for *Caulobacter* chromosome segregation. *J Bacteriol* 2009, 191:1097-1100.

84. Bowman GR, Comolli LR, Zhu J, Eckart M, Koenig M, Downing KH, Moerner WE, Earnest T, Shapiro L: A polymeric protein anchors the chromosomal origin/ParB complex at a bacterial cell pole. *Cell* 2008, 134:945-955.

85. Ebersbach G, Briegel A, Jensen GJ, Jacobs-Wagner C: A self-associating protein critical for chromosome attachment, division, and polar organization in caulobacter. *Cell* 2008, 134:956-968.

86. Wang SC, West L, Shapiro L: The bifunctional FtsK protein mediates chromosome partitioning and cell division in *Caulobacter*. *J Bacteriol* 2006, 188:1497-1508.

87. Besprozvannaya M, Burton BM: Do the same traffic rules apply? Directional chromosome segregation by SpoIIIE and FtsK. *Mol Microbiol* 2014, 93:599-608.

88. Figueroa-Cuilan W, Daniel JJ, Howell M, Sulaiman A, Brown PJ: Mini-Tn*7* insertion in an artificial *att*Tn*7* site enables depletion of the essential master regulator CtrA in the phytopathogen *Agrobacterium tumefaciens*. *Appl Environ Microbiol* 2016, 82:5015-5025.

89. Kelly AJ, Sackett MJ, Din N, Quardokus E, Brun YV: Cell cycle-dependent transcriptional and proteolytic regulation of FtsZ in *Caulobacter*. *Genes Dev* 1998, 12:880-893.

90. Laub MT, Chen SL, Shapiro L, McAdams HH: Genes directly controlled by CtrA, a master regulator of the *Caulobacter* cell cycle. *Proc Nat Acad Sci U S A* 2002, 99:4632-4637.

91. Williams B, Bhat N, Chien P, Shapiro L: ClpXP and ClpAP proteolytic activity on divisome substrates is differentially regulated following the *Caulobacter* asymmetric cell division. *Mol Microbiol* 2014, 93:853-866.

Vita

Matthew Howell graduated high school in 2008 from Sullivan High school, located in Sullivan, Missouri. He then attended college at Columbia College in Columbia, Missouri, where he earned his B.S. in Biology with a Chemistry minor in 2012. After graduation, Matthew worked as a quality assurance microbiologist at Unilever Co. in Jefferson City, Missouri.

Matthew began graduate school at the University of Missouri in 2013 and completed his dissertation in 2018. During his time in graduate school Matthew was a teaching assistant for Introductory Biology for non-majors and Microbiology lab. He also had the opportunity to teach Microbiology at Stephens College as an adjunct professor. Matthew attended four research conferences as a graduate student and has presented 1 oral and 7 poster presentations.

Matthew has accepted a post-doctoral position in Dr. John Walker's lab at the University of Missouri, where he will continue research in molecular biology.